Relations between Reggeon and photon couplings

Wright, A.D.M.

RELATIONS BETWEEN REGGEON AND PHOTON COUPLINGS

Relations between Reggeon and Photon Couplings

Thesis submitted to

The University of Durham

by

A.D.M. Wright, B.Sc.(Durham)

for the Degree of Doctor of Philosophy

Department of Physics
Durham University

August 1978

CONTENTS

ACKNOWLEDGEMENTS

I would like to thank my supervisor Peter Collins, without whose help and encouragement this work could not have been completed. I extend my thanks to friends and colleagues of the physics department for suggestions and advice, especially to Dr. F.D. Gault who unveiled to me the mysteries of minimization. I am also grateful to my typist, Mrs. Henderson, who has coped wonderfully with a difficult typescript.

Finally, I acknowledge the S.R.C. for financial support.

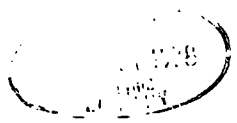

ABSTRACT

We propose (a) "the vector coupling hypothesis" (VCH) that the leading normal parity regge trajectories (P, f, ω, ρ, A_2) couple to quarks like vector particles, and (b) the "gamma analogy hypothesis" (GAH) that the couplings of P, f and ω to any quark are proportional to the isoscalar photon coupling while the ρ and A_2 couple like the isovector photon. These hypotheses are motivated by duality and vector dominance. Within the context of a naive ideally-mixed quark model we specify the spin-dependent nature of our coupling relations using the technique of covariant reggeization.

As a major test of our hypotheses we use the formalism to elucidate the nature of the elastic scattering amplitudes and hence describe all the data on elastic scattering. We also make successful predictions for vector meson-proton cross-sections. Using these elastic scattering amplitudes we extend the formalism to predict (up to one free parameter) diffractive boson and baryon differential cross-sections. We find that our hypotheses successfully describe both the energy and t-dependence of all these cross-sections despite the fact that the helicity structure is much richer than, and the t-dependence quite different from, elastic scattering. We also use the meson couplings determined in our fits to predict the mesonic decay widths of resonances lying on the exchanged trajectories. Good agreement with experiment is found.

FIGURES AND TABLES

We list here all tables, together with those figures to be found at the end of each chapter.

INTRODUCTION

The proposal that the pomeron and photon couplings to particles should be proportional is long-standing. For example, Chou and Yang (1) parametrized elastic scattering in terms of the electromagnetic form factors. Ravandel (1) has suggested that diffractive processes might be controlled by a conserved vector-current pomeron coupling. However, it has been discovered that diffractive differential cross-sections do not vanish in the forward direction (t = 0) as predicted by a conserved vector current coupling. Furthermore, the helicity structure of the pomeron coupling is complicated by s-channel helicity conservation in some processes but not others (2). These features appear to argue against such a simple pomeron-photon coupling analogy.

On the other hand, duality (5) predicts that the pomeron coupling will be related to that of the f, which is in turn exchange degenerate with the ω(6). According to the vector dominance model (4) the isoscalar part of the photon couples to hadrons mainly through the ω pole, and likewise for the isovector photon and the ρ pole. This suggests that there should be some relation between the P, f, ω, ρ and A_2 couplings, and the photon couplings at different vertices. Further, the success of the additive quark model indicates that perhaps this analogy should be between reggeon and photon couplings to individual quarks. The main purpose of this thesis is to suggest a detailed form of this relation, and compare it with what is known about diffractive processes and other natural parity regge exchange reactions.

In Chapter 1 we review the various theoretical arguments favouring such a reggeon-photon coupling hypothesis. Then, within the context of a naive, ideally-mixed quark model we clarify the spin-dependent nature of our hypothesis using the technique of covariant reggeization.

In Chapter 2, as a primary major test of our ideas, we apply our model in detail to the large amount of data on elastic scattering. In principle, we could determine the few free parameters at our disposal by fitting just one process ($pp \to pp$ for example) and then predicting other elastic cross-sections. In practice, in order to arrive at the best compromise for our free parameters, we fit all the data on pp, πp and Kp elastic and total cross-sections. This enables us to predict δ, the ratio Re A(s,t = 0)/Im A(s,t = 0), elastic polarization data and πN charge exchange cross-sections as a good consistency check. Then, in Chapter 3 we make predictions for other processes, $\pi\pi$ and Λp total cross-sections for example. We also predict cross-sections for vector meson-proton differential and total cross-sections and finally the cross-section $\sigma^{tot}_{\gamma p}(s)$, which has recently been measured at high values of s ($\simeq 180$ GeV^2).

In Chapter 4 we extend our model to predict (up to one normalization parameter g_1 (the orbital angular momentum coupling constant)) diffractive boson and baryon differential cross-sections using the elastic scattering amplitudes formulated in Chapter 2. Using our "vector coupling hypothesis" we also make predictions for the t-channel production density matrices. In the particular case of diffractive K^* production our model allows us to make an absolute prediction for $\frac{d\sigma}{dt}(Kp \to K^*p)$. Then, in Chapter 5 we use the meson coupling parameters determined in our fits to estimate the decays of resonances lying on the exchanged trajectories into pseudo scalars. Using a similar technique we can also estimate the values of the normalization parameters g_1^ℓ from resonance decay widths. We find that the fit and decay values of g_1^ℓ agree to within a factor of 2. Finally we present some conclusions.

CHAPTER I

THE REGGEON-PHOTON COUPLING ANALOGY

1.1 Introduction

As we have mentioned in the introduction, the original motivation for the proposal that the diffractive (P) and the electromagnetic (γ) couplings might be related was the argument of Chou and Yang (1) that the matter distribution in a hadron to which the pomeron couples is given by the electromagnetic form factor. Abarbanel et al, (2) later extended the idea to large angle scattering. However, in order to account for the observed rise of the proton-proton total cross-section at I.S.R. energies the intercept of the pomeron must be above 1 (3). Furthermore, the model does not describe the shape of the differential cross-section, nor is its extension to diffractive processes obvious.

Because of these difficulties, we prefer to motivate the analogy via a combination of the vector dominance model (4), the f-dominated pomeron model (5) and exchange degeneracy (6). In the next section we describe briefly these three models and show how they lead us to a relationship between reggeon and photon couplings.

1.2 Motivation

(a) Vector Dominance

The photon couples to hadrons via the vector mesons; or phrased more appropriately for our purposes, the isoscalar part of the photon, g^{γ_S}, couples to quarks mainly via the ω pole (we ignore for the time being the error involved in omitting the other I = 0 vector mesons) and similarly the isovector part of the photon g^{γ_V} via the ρ pole, as shown in Figure 1.2.1.

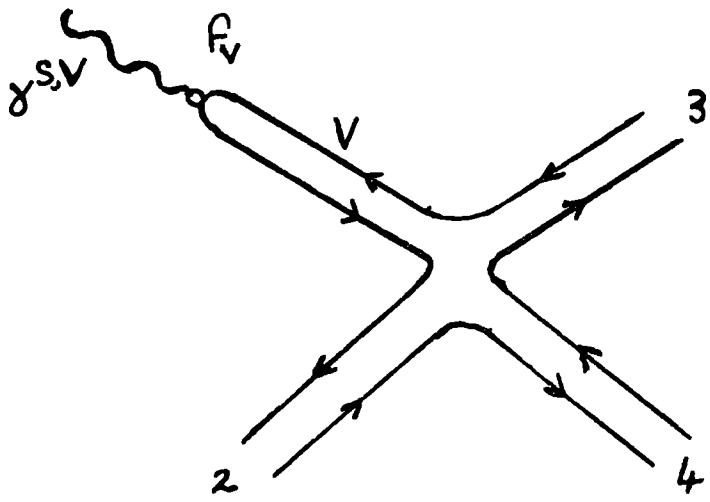

Figure 1.2.1: The Vector Dominance model for the process $\gamma 2 \to 34$.

The VDM hypothesis for the amplitude of Figure 1.2.1 is

$$A_H(\gamma 2 \to 34) = \sum_V \frac{e}{f_V} A_H(V2 \to 34) \qquad (1.2.1)$$

where f_V is the coupling between the photon and the vector meson V. Approximating the isoscalar part of the photon by the lightest $I = 0$ vector meson, the ω, then

$$\frac{g_i^{\gamma_S}}{g_i^{\omega}} = \frac{e}{f_\omega} \qquad (1.2.2)$$

$i = u, d$ quarks

This VDM hypothesis has been extensively tested and seems to be in accord with the photoproduction data (7). The corresponding hypothesis for that of the isovector part of the photon and the ρ meson is also quite successful (8). However, equation (1.2.2) is based on the assumption that the coupling does not vary much during the continuation from $t = 0$ to $t = M_\omega^2$. To extend this hypothesis to vector exchanges (see Figure 1.2.2) we have to assume further that the coupling variation will still be small when we continue back to $t < 0$ down the ω trajectory, where

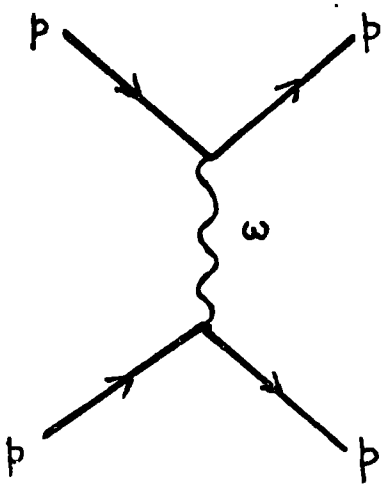

Figure 1.2.2: ω exchange in pp scattering

$\alpha_\omega(t) \lesssim 0.5$. This assumption is supported by the observed "Universality" of the ω trajectory couplings (9).

Of course for real photons where $M_\gamma = 0$, the coupling is a conserved current coupling, and the photon couples only to those vertices which have $\Delta\lambda = \pm 1$ in any channel, while the ω particle has couplings with $\Delta\lambda = 0, \pm 1$. In photoproduction experiments, it is found that equation (1.2.1) works for helicity amplitudes in which the vector mesons are transversely polarized in the s-channel (7). On the other hand the ω trajectory (as opposed to the elementary ω meson) can couple to any amount of helicity flip, although when $\alpha_\omega(t) = \text{integer} < \Delta\lambda_t$, nonsense decoupling must occur. But except at these isolated points, there is no restriction to the number of couplings available to a trajectory in the s-channel scattering region, $t \lesssim 0$ and $\alpha(t) \lesssim 1$.

However, there appear to be some simple empirical rules for reggeon couplings, such as dominantly s-channel helicity non-flip for the ω (and P + f) coupling to $N\bar{N}$ and s-channel helicity flip for the ρ (and A_2) coupling to $N\bar{N}$, which suggests that the effective number of couplings is often less than the maximum available. Although there is little information concerning trajectory couplings to high-spin vertices, the little we do know suggests that, at least to a first approximation, trajectories couple like

the lowest spin particles lying on them. This, together with the exchange degeneracy of the dominant vector and tensor trajectories implies that all trajectories couple like vector particles.

Thus we are led to the "vector coupling hypothesis" (VCH) - that the only important couplings for the ω trajectory (and all other leading natural parity trajectories) are those corresponding to $\Delta\lambda_t = 0, \pm 1$, as for the exchange of a J = 1 particle .

(b) Exchange Degeneracy

The f is exchange degenerate with the ω in both trajectory and residue.

This arises from duality as follows. All resonances so far well established can be considered to be composed of $q\bar{q}$ for mesons and qqq for baryons. This results in the SU(4) multiplets 1 and 15 of mesons and 4, 20 and 20 of baryons. All other sets of quantum numbers are called "exotic". (For a more recent and topical treatment of exotics see, for example, reference (10)). Two-particle scattering with a non-exotic s-channel, like $K^-p \to K^-p$ for example, can be represented by a duality diagram (see Figure 1.2.3(A)) obeying Zweigs rule (11). Zweigs rule says that the only permitted diagrams are those which are planar with no quark beginning and ending on the same particle. According to the two-component duality hypothesis (12), in the above example the imaginary part of the non-diffractive amplitude is given by the dominant t-channel exchanges f + ω, which are dual to the s-channel resonances.

However, for exotic $K^+p \to K^+p$ (Figure 1.2.3(B)) we cannot draw a planar diagram , s-channel resonances are not allowed, and so the dominant non-diffractive regge exchanges f - ω must cancel. Hence the contributions of f and ω must be exchange degenerate. (Note that the ω is odd under change conjugation).

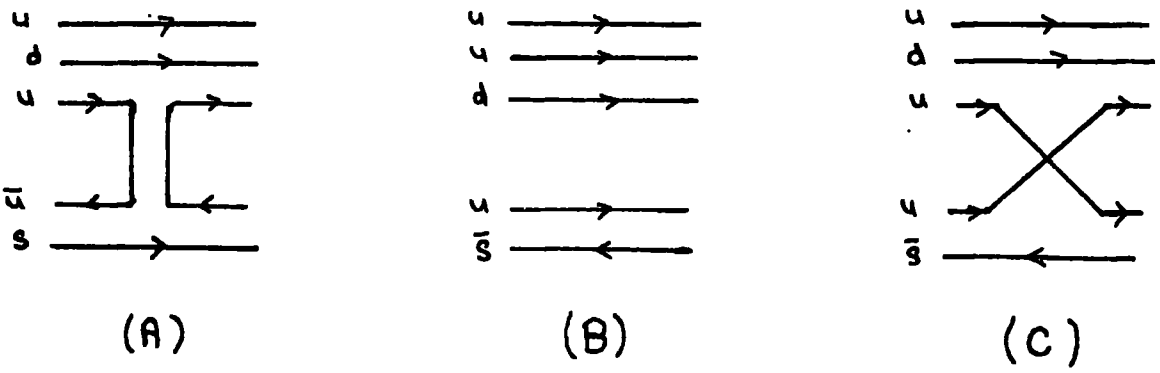

Figure 1.2.3: (A) Zweig allowed diagram for $K^-p \to K^-p$ scattering with f, ω exchange.
(B) Diagram for $K^+p \to K^+p$ scattering. Here only exotic $qqqq\bar{q}$ resonances can be formed in the s-channel and hence the regge exchanges f, ω must be exchange degenerate.
(C) Zweig violating diagram for $K^+p \to K^+p$

This exchange degeneracy-hypothesis (6) is supported by the flatness of the K^+p and pp total cross-sections when compared with K^-p and $\bar{p}p$. However, the degeneracy cannot be exact since, for instance, $\sigma_{pp}^{tot}(s)$ falls with s at low energies indicating that the f - ω cancellation is not perfect. Allowing for the exchange degeneracy breaking in the most simple way leads us to the following hypothesis:

$$\begin{aligned} g_{pp}^{f}(t) &= g_{pp}^{\omega}(t)\ (1 + \varepsilon_B) \\ g_{KK}^{f}(t) &= g_{KK}^{\omega}(t)\ (1 + \varepsilon_B) \end{aligned} \qquad (1.2.3)$$

where ε_B is assumed to be independent of t, and the subscript B = | Baryon number | of the external particles.

We shall find in chapter two that the value of ε_B is zero at a meson vertex, B = 0, giving exact exchange degeneracy, and small (≈ 0.1) at a baryon vertex, B = 1, implying approximate exchange degeneracy.

(c) Duality and the f-Dominated Pomeron

Since the pomeron carries the quantum numbers of the vacuum, we can always extend the duality diagrams in Figure 1.2.3 to include the diagrams 1.2.4 shown below.

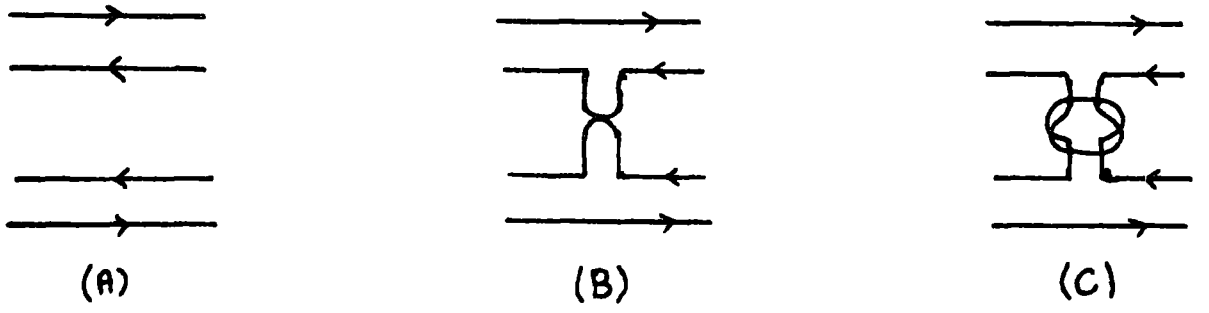

Figure 1.2.4: Pomeron exchange according to the dual unitarization scheme.

The diagram 1.2.4(C) has been distorted to produce a dual cylinder term (13) which corresponds to the pomeron. However, the coupling to external particles is always via the f-meson for particles with zero strangeness (that is, u, d quarks only). For particles containing strange quarks, the f' meson can also be exchanged, and likewise the f_c, f_b .... for "charmed" or "beautiful" (!) particles, if we assume ideal mixing (see Chapter 2, Section 2). Hence the quark content of the external particles will dictate the allowed f, f', f_c, f_b.... meson exchanges and hence the strength of the pomeron coupling. For example, in πp scattering we have only u and d quarks and so only the f meson can couple, whereas for Kp scattering, we have s quarks at the KK vertex, and hence the pomeron can couple via the f' meson, although an f' meson cannot be exchanged across the diagram. Similar arguments should apply if the target particles contain charmed or even top and bottom quarks. Thus we employ the f-dominated pomeron hypothesis (FDP) of Carlitz, Green and Zee (5) that the pomeron couples to a given vertex via the f, f'... mesons depending upon the quark content of

the target. That is:

$$g^P \propto \frac{g^f}{\alpha_P(t) - \alpha_f(t)} + \frac{g^{f'}}{\alpha_P(t) - \alpha_{f'}(t)} + \ldots \qquad (1.2.4)$$

or, in a more convenient form

$$\frac{g_i^P(t)}{g_i^f(t)} = \rho_F(t) \qquad (1.2.5)$$

where i runs over u and d quarks, and $\rho_F(t)$ is given by

$$\rho_F(t) = \rho_0(t)\ (1 + r_F(t)) \qquad (1.2.6)$$

$\rho_0(t)$ is a "universal" function of t, independent of the nature of the vertex, and $r_F(t)$ (F = flavour) is a function of the f, f', f_c, f_b ..... trajectory parameters, to be discussed more fully in the next chapter. This FDP hypothesis has been extensively tested in both elastic scattering and inclusive processes (14) and given the inevitable uncertainties involved in separating the P and f contributions (assumptions of ideal mixing etc.) (15) appears to work well.

By combining equations (1.2.2), (1.2.3) and (1.2.5), we obtain the relation:

$$g_i^P(t) = \rho_F(t)\, g_i^f(t) = \rho_F(t)(1+\varepsilon_B)\, g_i^\omega(t) = \frac{f_\omega(t)}{e}(1+\varepsilon_B)\ \rho_F(t)\, g_i^{\gamma_S}(t) \qquad (1.2.7)$$

which gives us a relation not only between the pomeron and photon couplings but also for the f and ω. We expect a similar relation to hold for the isovector ρ and A_2 exchanges and the isovector photon γ_V, viz:-

$$g_i^{A_2}(t) = g_i^\rho(t)(1+\varepsilon_B') = \frac{f_\rho(t)}{e}(1+\varepsilon_B')\ g_i^{\gamma_V}(t) \qquad (1.2.8)$$

Thus we have the "gamma analogy hypothesis" (GAH) that the couplings of the dominant I = 0 regge exchanges, the P, f and ω, to quarks are proportional to the isoscalar photon coupling, while the I = 1 ρ and A_2 exchanges couple like the isovector photon. We summarize the continuations in the J - t plane involved in applying the GAH in Figure 1.2.5.

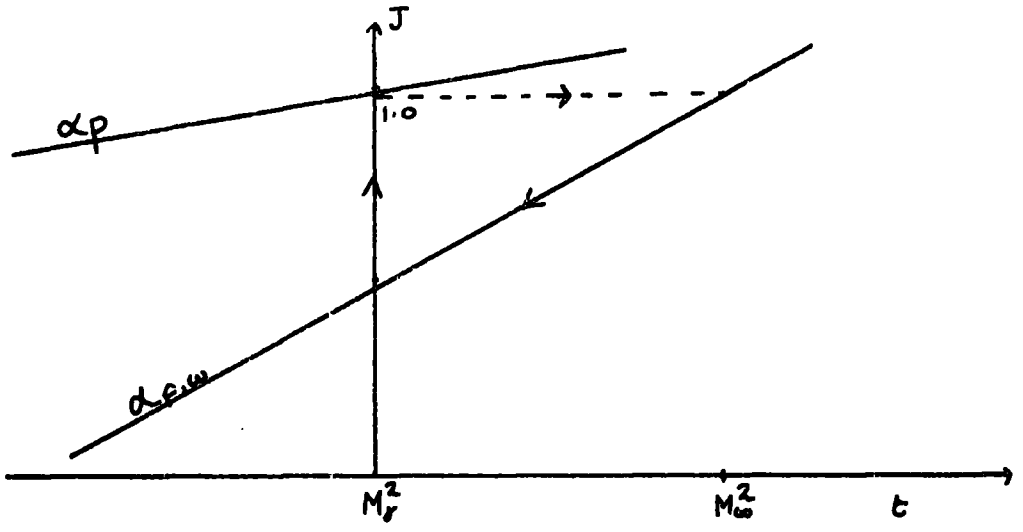

Figure 1.2.5: VDM takes us from $\gamma \to \omega$ at fixed J = 1. Then the GAH allows us to continue down the ω trajectory, which is approximately exchange degenerate with the f. Finally the FDP hypothesis allows us to jump from the f to the P trajectory and hence back to $J \simeq 1$ for $t \simeq 0$.

Although we have not been able to maintain our assumption of exact f - ω exchange degeneracy, the breaking is only $\simeq 10\%$, and once we have fixed the ratios of P : f : ω : ρ : A_2 couplings in one process, the ratio should be fixed for all vertices.

And so we can see from equation (1.2.7) that the pomeron coupling to any vertex should be related to the photon coupling at that vertex by a universal t-dependent function. This t-dependence makes our hypothesis quite different from that of Chou and Yang (1) since the matter and charge distributions need no longer be identical.

However, before we can confront equations (1.2.7) and (1.2.8) with experimental data, we need to clarify their spin-dependence. In order to maintain crossing symmetry, it is most simple to assume that they are relations for covariant couplings (that is, the couplings appropriate for invariant amplitudes), and thus it will be desirable to invoke the technique of covariant reggeization in order to specify this spin-dependence.

In the remaining sections of this chapter, we develop the formalism necessary to clarify the spin-dependent nature of our hypothesis 1.2.7.

1.3 The Quark Coupling

In order to describe external particle wave-functions we choose to use a naive additive quark model, rather than the more usual Rarita-Schwinger formalism. This choice is motivated by the fact that the quark model successfully predicts particle spectroscopy, radiative decay widths etc., and thus we expect will give a more direct physical interpretation of the necessarily rather involved calculations on which we are to embark. The "end product" will automatically give us, for example, the result that the isoscalar flip couplings of the P, f and ω exchanges at the $N\bar{N}$ vertex are zero.

In this model, quark spins are arranged to give $j = 0$ or 1 for bosons and $j = \frac{1}{2}$ or $\frac{3}{2}$ for fermions, any additional angular momentum being accounted for by orbital excitation of the $q\bar{q}$ or qqq system. We assume that both the mass M and the four-momentum P of the particle are shared by the constituent quarks. Thus, for a boson containing u and d quarks only, then $m_u = m_d = M/2$, $k_u = k_d = P/2$. From the above we can see that

$$\frac{k_u}{m_u} = \frac{k_d}{m_d} = \frac{P}{M} \tag{1.3.1}$$

In a similar fashion, we assume that for particles containing strange, charmed, top ... etc. quarks, similar relations will hold, that is

$$\frac{k_s}{m_s} = \frac{k_u}{m_u} \qquad (1.3.2)$$

or, generally

$$\frac{k_i}{m_i} = \frac{P}{M} \qquad (1.3.3)$$

where m_i = mass of quark, flavour i, and k_i four-momentum of quark i. However, the strange and other quarks need not have the same mass as the u, d quarks, although their combined mass must be equal to that of the particle they constitute.

We further assume that in a particle scattering process each quark is scattered individually through reggeon exchange, and invoke confinement to constrain the spectator quark (or quarks) to move off with the struck quark, as shown in Figure 1.3.1. In so doing they must share the transferred momentum. This is of course a very naive picture since the quarks inside a hadron have a momentum distribution which depends upon the binding energy. But as only the particle momenta appear finally in our calculation of helicity amplitudes (which are, of course, related to experimental observables) we need not concern ourselves with this momentum distribution in the weak binding limit.

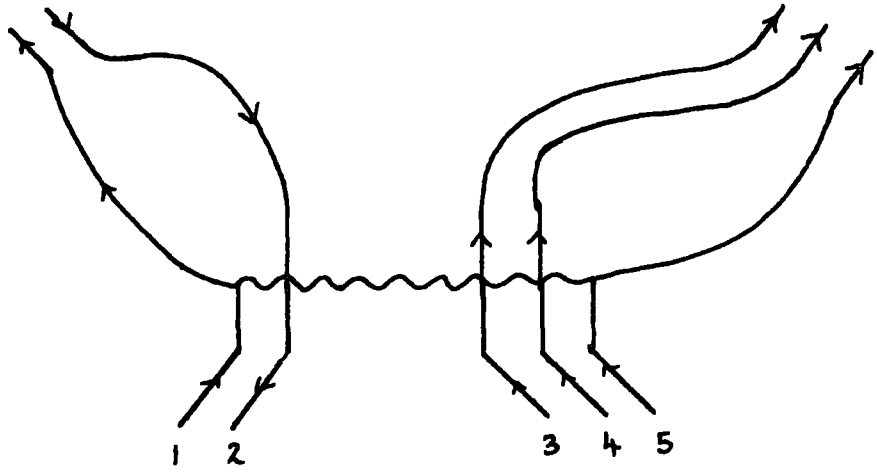

Figure 1.3.1: Exclusive meson-baryon scattering. Quark 1 is struck by quark 5 via reggeon exchange. Confinement then constrains the quarks not directly taking part in the interaction (2, 3 and 4) to move off with the struck quark.

This cavalier dismissal of the problems of quark momentum distribution, quark binding energy etc., also circumvents the problems of Lorentz invariance of the ℓ-excitation quark model (see, for example reference (16), C15 p.362, ff.). We argue that the precise form of any input quark model should not seriously affect our conclusions provided the input is capable of giving a reasonable description of physical particles in the weak binding limit.

Having thus very briefly outlined the manner in which we describe particles, we construct the particle wave-functions in the following way:- In Figure 1.3.2 we shown the reggeon exchange diagram for the s-channel process 1 + 2 → 3 + 4, which serves to introduce our notation.

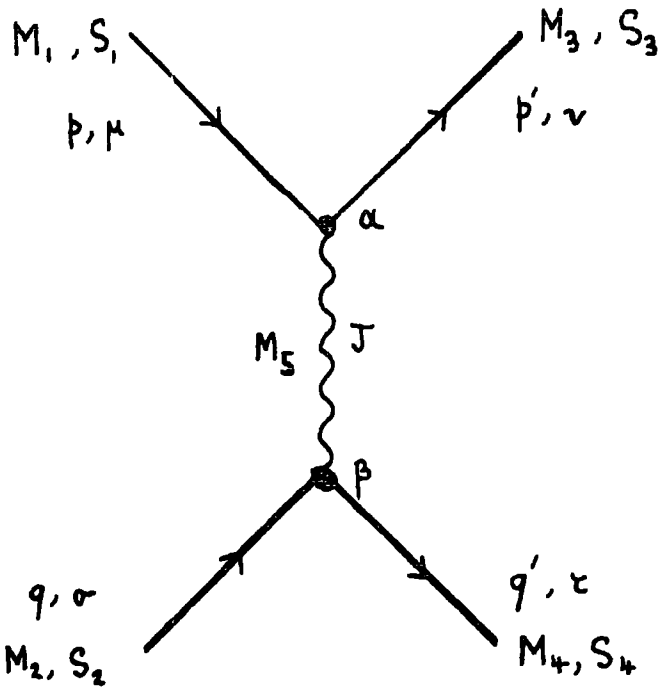

Figure 1.3.2: The reggeon exchange diagram for the s-channel process 1 + 2 → 3 + 4, showing the notation used.

Particle 1, the initial state particle has mass M_1, spin S_1, 4-momentum p_α and wave-function labels $\mu_1 \ldots \mu_{\ell_1}$, and similarly for the other particles as in Figure 1.3.2. The coupling labels for the exchanged

particle 5, spin = J and mass M_5 are denoted by α and β at the upper and lower vertices respectively. The momenta p_α, p'_α are related by:-

$$\begin{aligned} P_\alpha &= \tfrac{1}{2}(p + p')_\alpha \,, \quad Q_\beta = \tfrac{1}{2}(q + q')_\beta \\ s &= (p_\alpha + q_\beta)^2 = (P_\alpha + Q_\beta)^2 \\ \Delta_\alpha &= (p'_\alpha - p_\alpha) = (q_\alpha - q'_\alpha) \,, \quad t = (p'_\alpha - p_\alpha)^2 = \Delta^2 \\ \nu &= P_\alpha \cdot Q_\alpha = \frac{s-u}{4} \,, \quad z_t = \frac{\underline{P}\cdot\underline{Q}}{|\underline{P}||\underline{Q}|} \end{aligned} \tag{1.3.4}$$

Using the results (1.3.1) to (1.3.4) inclusively, then

$$\frac{k_{i\alpha}}{m_i} = \frac{P_\alpha}{M} \,, \quad \frac{k_{i\beta}}{m_i} = \frac{Q_\beta}{M} \tag{1.3.5}$$

where $k_{i\alpha}$, $k_{i\beta}$ are the quark i 4-momenta and thus relations (1.3.4) hold equally for quark momenta, viz

$$K_{i\alpha} = \tfrac{1}{2}(k_i + k'_i)_\alpha \,, \quad Q_{i\beta} = \tfrac{1}{2}(k_i + k'_i)_\beta \tag{1.3.6}$$

etc.

We represent each u quark by a Dirac spinor (17)

$$u^\delta(k_u) = \frac{1}{\sqrt{2m_u}}(k_{ou} + m_u)^{\frac{1}{2}}\left(1 + i\frac{\gamma_5 \cdot \underline{\sigma}\cdot\underline{k}_u}{k_{ou}+m_u}\right)\phi^\delta \tag{1.3.7}$$

where $\delta\,(= \pm\frac{1}{2})$ is the z-component of the spin, with

$$\phi^{\frac{1}{2}} = \begin{pmatrix}1\\0\end{pmatrix} \,, \quad \phi^{-\frac{1}{2}} = \begin{pmatrix}0\\1\end{pmatrix} \tag{1.3.8}$$

and

$$\gamma_0 = \begin{pmatrix}\underline{1} & 0\\ 0 & -\underline{1}\end{pmatrix} \,, \quad \gamma = \begin{pmatrix}0 & \underline{\sigma}\\ -\underline{\sigma} & 0\end{pmatrix} \,, \quad i\gamma_5 = \begin{pmatrix}0 & \underline{1}\\ \underline{1} & 0\end{pmatrix}$$

The $\underline{\sigma}$'s are the usual Pauli matrices, defined in Appendix 1, and $\underline{1}$ is the

2 x 2 unit matrix. Corresponding expressions for $d^{\delta}(k_d)$, $s^{\delta}(k_s)$... the down, strange ... quark spinors follow in a similar way. These spinors satisfy the Dirac equation

$$(\gamma \cdot k - m_u)\, u(k) = 0 \tag{1.3.10}$$

where, with our normalization,

$$\bar{u}(k)\, u(k) = 1 \tag{1.3.11}$$

However, for vertices involving unequal mass particles the normalization condition (1.3.7) would yield

$$\bar{u}(k')\, u(k) \to \frac{2m_+}{\sqrt{2m_1}\,\sqrt{2m_3}} \quad , \quad m_+ = \frac{m_1 + m_3}{2} \tag{1.3.12}$$

where we have anticipated the results of equation (1.5.10). In order to maintain unit normalization for unequal masses we will substitute $\sqrt{2m_+}$ for $\sqrt{2m_u}$ in (1.3.7) for all our vertex calculations. With this representation we tabulate in Appendix 2, following reference (18), fermion and boson SU(6) wave-functions.

In order to construct high-spin particle wave-functions we describe the orbital angular momentum ℓ by covariant spin = 1 polarization vectors $\varepsilon_{\mu}^{\lambda}(p)$, $\lambda = \pm 1, 0$, $\mu = 0, 1, 2, 3$ where (19) λ is the helicity, $\mu_1 \ldots \mu_{\ell}$ are the spin polarization labels and

$$\begin{aligned} \varepsilon_{\mu}^{\pm 1}(p) &= \frac{1}{\sqrt{2}}\,(0, \mp 1, -i, 0) \\ \varepsilon_{\mu}^{0}(p) &= \frac{1}{M}\,(p_z, 0, 0, p_0) \end{aligned} \tag{1.3.13}$$

which satisfy the subsidiary condition

$$p_{\mu} \cdot \varepsilon_{\mu}(p) = 0 \tag{1.3.14}$$

where the arguments of the ε's are the particle masses and momenta as defined in Figure 1.3.2.

A spin = S particle is then represented by

$$\psi^{\lambda}_{\mu_1..\mu_\ell}(p) = \sum_{\lambda_1..\lambda_{\ell-j},m} \langle \lambda_1..\lambda_{\ell-j};\ j\ m \,|\, S\lambda \rangle |j,m\rangle \varepsilon^{\lambda_1}_{\mu_1}(p)...\varepsilon^{\lambda_{\ell-j}}_{\mu_\ell}(p) \tag{1.3.15}$$

where $|j,m\rangle$ represents a general quark wave-function, as tabulated in Appendix 2, with j = total quark spin of the state (that is, $0\ \pm\frac{1}{2}, \pm 1, \pm\frac{3}{2}$) and m its helicity.

$\langle \lambda_1...\lambda_{\ell-j};\ j\ m \,|\, S\lambda\rangle$ are the usual Clebsch-Gordan coefficients with S = total spin of the particle and ℓ = the orbital angular momentum.

For simplicity we shall denote the spin labels in 1.3.14, 1.3.15 collectively by μ, so

$$\psi^{\lambda}_{\mu_1..\mu_\ell}(p) \equiv \psi^{\lambda}_{\mu}(p) \tag{1.3.16}$$

As an example, the $N^*(\frac{3}{2}^-, 1520)$ $\lambda = \frac{1}{2}$ wave-function (where the $N^*\ \frac{3}{2}^-$ is an $\ell = 1$, $S = \frac{3}{2}$, $j = \frac{1}{2}$ state) is given by

$$\psi^{\frac{1}{2}}_{\mu}(p) = \sqrt{\frac{2}{3}}\, P\uparrow(p)\ \varepsilon^{0}_{\mu}(p) + \sqrt{\frac{1}{3}}\, P\downarrow(p)\ \varepsilon^{+1}_{\mu}(p) \ ... \tag{1.3.17}$$

where P↑(p), P↓(p) is a shorthand notation for the proton wave-function given by (see Appendix 2).

$$\begin{aligned} P\uparrow(p) = P^{+\frac{1}{2}}(p) = \frac{1}{\sqrt{18}} \Big[& 2u^+(k_u)d^-(k_d)u^+(k_u) + 2u^+(k_u)u^+(k_u)d^-(k_d) \\ & + 2d^-(k_d)u^+(k_u)u^+(k_u) - u^+(k_u)u^-(k_u)d^+(k_d) - u^+(k_u)d^+(k_d)u^-(k_u) \\ & - u^-(k_u)d^+(k_d)u^+(k_u) - d^+(k_d)u^-(k_u)u^+(k_u) - d^+(k_d)u^+(k_u)u^-(k_u) \\ & - u^-(k_u)u^+(k_u)d^+(k_d) \Big] \end{aligned} \tag{1.3.18}$$

Hence, with the above notation we can describe particle wave-function for particles with arbitrarily high spin.

Next, we consider the covariant particle coupling, built by combining the coupling to the quarks, and to the orbital angular momentum.

The photon coupling to a free quark with no anomalous magnetic moment may be written in the form

$$\bar{u}\ 2\frac{m_i}{M_o}\ e_q\ \gamma_\alpha u = \bar{u}\left[2\frac{m_i}{M_o}\ k_{i\alpha} \quad + \quad 2\,e_q\ \frac{\sigma_{\alpha\beta}\ \Delta_\beta}{2M_o}\right] u \tag{1.3.19}$$

where e_q is the quark charge, γ_α the gamma matrices, defined in (1.3.9) $k_{i\alpha}$ is the momentum of quark i, and m_i the quark mass. $\sigma_{\alpha\beta}$ is the anti-symmetric tensor matrix (see reference (17), page 70 ff.) and $\Delta_\alpha = (k' - k)_\alpha$, defined above. Since we have chosen to normalize our spinors to unity (see equation (1.3.11)) rather than to $2m_i$, as is more usual (see, for example, reference (17)), and measure our momenta in units of M_o, we have multiplied (1.3.19) by $2\frac{m_i}{M_o}$ in order to retain the usual definition of the electromagnetic current, that is

$$2\frac{m_i}{M_o}\ e_q\ \gamma_\alpha \underset{s\to\infty}{\to} 2\frac{m_i}{M_o}\ e_q\ \frac{(p'+p)_\alpha}{2m_i} = e_q\ \frac{(p'+p)_\alpha}{M_o}$$

The factor M_o is a scale factor, and sets the scale in which we wish to measure the $k_{i\alpha}$'s, and is introduced to render the momenta factors dimensionless (see Section 4). To check that equation (1.3.19) holds for free particles, the reader is referred to reference (17), page 248 ff.

For a spin = $\frac{1}{2}$ particle of mass M, the particle coupling is given by (see reference (17), page 253)

$$\frac{2M}{M_o}\ \left[G_E\ \frac{P_\alpha}{M} + G_M\ \frac{\sigma_{\alpha\beta}\Delta_\beta}{2M}\right] \tag{1.3.20}$$

where G_E and $\frac{G_M}{2M}$ are the fermion electric and magnetic couplings respectively.

Hence from (1.3.18),

$G_E^q = G_M^q = e_q$, the quark charge, where G_E^q and $\frac{G_m^q}{2m}$ are the quark electric and magnetic couplings. However, for a quark confined in a particle of mass M, the effective coupling must take the more general form

$$\frac{M}{M_o}\left[g_1\frac{k_{i\alpha}}{m_i} + g_2\gamma_\alpha\right] = \frac{M}{M_o}\left[(g_1+g_2)\frac{k_{i\alpha}}{m_i} + g_2\frac{\sigma_{\alpha\beta}\Delta_\beta}{2m_i}\right] \tag{1.3.21}$$

where now $2G_E^q = g_1 + g_2 = 2e_q$ (1.3.22)

and $2G_m^q = g_2 = 2e_q(1+\kappa_q)$ (1.3.23)

where κ_q is the quark's effective anomalous magnetic moment.

We assume that the static properties of a particle (20), that is the charge and the magnetic moment, are the sum of those of the quarks. Thus, for the charge,

$$G_E = e = \sum_{q_i} G_E^q = \sum_{q_i} e_{q_i} \tag{1.3.24}$$

The particle magnetic moment is

$$\frac{G_M}{2M} = \frac{2}{2M}(1+\kappa) \tag{1.3.25}$$

where κ is the particle anomalous magnetic moment. In terms of the quark magnetic moments, this is given by

$$\frac{G_M}{2M} = \sum_{q_i} \langle e_{q_i} \cdot \underline{S}_z \rangle \frac{1}{m_i} \tag{1.3.26}$$

where $\underline{S}_i$ is the spin of quark i. Using $S_z = \pm\frac{1}{2}$, the effective magnetic moment of a quark confined in a particle is

$$2G_M^q = g_2 = 2\frac{M}{m_i}e_q \tag{1.3.27}$$

Combining (1.3.23) with (1.3.27), we deduce that

$$\kappa_q = \frac{M}{m_i} - 1 \qquad (1.3.28)$$

That is, the quarks' effective anomalous magnetic moment depends upon the mass of the particle in which it is confined. From(1.3.22) and (1.3.27)

$$g_1 = 2\, e_q \left(1 - \frac{M}{m_i}\right) \qquad (1.3.29)$$

while (1.3.27) and (1.3.29) inserted into (1.3.21) gives

$$2e_q\left(1 - \frac{M}{m}\right) \frac{k_{i\alpha} M}{m_i M_o} + 2\, e_q \cdot \frac{M}{m_i}\, \gamma_{i\alpha} \frac{M}{M_o} = 2\, e_q \frac{k_{i\alpha}}{m_i} \frac{M}{M_o} + 2\, e_q \frac{M}{m_i} \frac{\sigma_{\alpha\beta}\Delta_\beta}{2m_i} \frac{M}{M_o} \qquad (1.3.30)$$

for the confined quark coupling.

With our assumption that for a meson, $M = 2m_i$, and for a baryon $M = 3m_i$, (and thus $M_+ = 2m_+$, $M_+ = 3m_+$ respectively) and using equation (1.3.5), then (1.3.30) becomes

$$- 2e_q \frac{P_\alpha}{M_o} + 4e_q\, \gamma_\alpha \frac{M}{M_o} \quad \text{(mesons)} \qquad (1.3.31)$$

and

$$- 4e_q \frac{P_\alpha}{M_o} + 6e_q\, \gamma_\alpha \frac{M}{M_o} \quad \text{(baryons)} \qquad (1.3.32)$$

Inserting in equations (1.3.31) and (1.3.32) the appropriate quark charges, $e_u = \frac{2}{3}$, $e_d = -\frac{1}{3}$, $e_s = -\frac{1}{3}$ ..... etc. and constructing the combinations $\frac{u+d}{2}$ and $\frac{u-d}{2}$ allows us to write down the photon isoscalar and isovector couplings to u and d quarks in mesons and baryons as:- (s,c,t ... quarks have zero isovector photon couplings)

$$\left.\begin{array}{ll} -\frac{e}{3}\frac{P_\alpha}{M_o} + \frac{2e}{3}\gamma_\alpha\frac{M}{M_o} & I = 0 \\ \pm\left(-e\frac{P_\alpha}{M_o} + 2e\,\gamma_\alpha\frac{M}{M_o}\right) & I = 1 \end{array}\right\} \text{mesons} \qquad (1.3.33)$$

and

$$\left.\begin{array}{ll} -\frac{2e}{3}\frac{P_\alpha}{M_o} + e\,\gamma_\alpha\frac{M}{M_o} & I = 0 \\ \pm\left(-2e\frac{P_\alpha}{M_o} + 3e\,\gamma_\alpha\frac{M}{M_o}\right) & I = 1 \end{array}\right\} \text{baryons} \qquad (1.3.34)$$

Using these results, and equation (1.3.30) we can identify the values of $g^i_{1,2}$, the isoscalar, isovector, strange, charm ... etc. photon couplings to quarks of any flavour (i) in mesons and baryons, and are given in Table 1.3.1 below.

	BOSONS		FERMIONS	
quark flavour i	g^i_1	g^i_2	g^i_1	g^i_2
isoscalar $(u+d)/2$ (S)	$-\frac{1}{3}$	$\frac{2}{3}$	$-\frac{2}{3}$	1
Isovector $(u-d)/2$ (V)	-1	2	-2	3
s	$\frac{2}{3}$	$-\frac{4}{3}$	$\frac{4}{3}$	-2
c	$-\frac{4}{3}$	$\frac{8}{3}$	$-\frac{8}{3}$	4
t	$-\frac{4}{3}$	$\frac{8}{3}$	$-\frac{8}{3}$	4
b	$\frac{2}{3}$	$-\frac{4}{3}$	$\frac{4}{3}$	-2

Table 1.3.1: The photon coupling to quark i, where the superfix i refers to isoscalar, isovector, strange, charmed, top or beautiful quarks.

Having thus defined our particle wave-functions and the quark coupling, the coupling appropriate for a particle of any spin may be written as follows:-

$$C_{\nu_1 \ldots \nu_{\ell_3};\ \alpha_1 \ldots \alpha_J}(S_1,S_3,J) \equiv \sum_i \left(g_1^i \frac{P_\alpha}{M_o} + g_2^i \gamma_{i\alpha} \frac{M_+}{M_o} \right) g_1^{\ell_3} \frac{P_{\alpha_2}}{M_o} \cdots \frac{P_{\alpha_J}}{M_o}$$

$$\times \frac{P_{\nu_1}}{M_o} \ldots \frac{P_{\nu\ell_3}}{M_o} + \sum_i g_1^i \, g_2^{\ell_3} \, g_{\nu_1\alpha_1} \frac{P_{\alpha_2}}{M_o} \ldots \frac{P_{\alpha_J}}{M_o} \frac{P_{\nu_2}}{M_o} \ldots \frac{P_{\nu\ell_3}}{M_o} \tag{1.3.35}$$

Since we will only consider incoming (beam) particles with $\ell_1 = 0$ we have suppressed the spin label μ on the coupling $C_{\nu\alpha}$. The first term in brackets ( ) appearing in (1.3.35) is the photon-quark coupling of (1.3.30). However, since the coupling is now referring to particles at a vertex rather than a single particle as in the discussion above (see equations (1.3.11), (1.3.12)), we have introduced M_+, where $M_+ = (M_1 + M_3)/2$. (Furthermore, with the reggeon-photon coupling analogy (see equation (1.2.7)), the photon-quark coupling $g^i_{1,2} \to g^i_{1,2} f_{\omega,\rho}$ (the reggeon coupling). Thus, unless specified, the constants $g^i_{1,2}$ will henceforth refer to the reggeon coupling to quark i). This term is multiplied by $g_1^{\ell_3} \frac{P_{\alpha_2}}{M_o} \ldots \frac{P_{\alpha_J}}{M_o} \frac{P_{\nu_1}}{M_o} \ldots \frac{P_{\nu\ell_3}}{M_o}$, where $g_1^{\ell_3}$ is a covariant orbital angular momentum (ℓ) coupling constant. The P_α's, P_ν's are the particle momenta, as defined in (1.3.4) and $g_{\nu\alpha}$ is the metric tensor. The combination of these two pieces has the effect of leaving the orbital angular momentum in the t-channel unchanged, but allowing the quark spin to be flipped. The second term in (1.3.35) is made up of a quark non-flip piece multiplied by an orbital angular momentum flip term, where $g_2^{\ell_3}$ is a second covariant orbital angular momentum coupling constant. Thus in the t-channel, the coupling (1.3.35) can flip the quark spin (j) but not ℓ , flip ℓ but

leave j unchanged, or change neither ℓ or j.

The form of this coupling is a direct consequence of the VCH which limits J (the spin of the exchange) to 1. Thus we can immediately re-write (1.3.35) to read.

$$C_{\nu,\alpha}(S_1,S_3,J) = C^{\alpha}_{qNF}\, g_1^{\ell_3}\, \frac{P_{\nu_1}}{M_o} \cdot\cdot \frac{P_{\nu\ell_3}}{M_o} + C_{qN}\, g_2^{\ell_3}\, g_{\nu_1\alpha_1} \frac{P_{\nu_2}}{M_o} \cdot\cdot \frac{P_{\nu\ell_3}}{M_o} \tag{1.3.36}$$

where we have shortened $\nu_1 \cdot\cdot \nu_{\ell_3}$, $\alpha_1 \cdot\cdot \alpha_J$ to ν,α and defined

$$C^{\alpha}_{qNF} = \sum_i g_1^i \frac{P_\alpha}{M_o} + g_2^i \gamma_{i\alpha} \frac{M_+}{M_o} \tag{1.3.37}$$

$$C_{qN} = \sum_i g_1^i$$

If we consider $\frac{1}{2},\frac{1}{2}$ scattering (that is with $\ell = 0$), then

$$C_{\nu\alpha}(S_1,S_3,J) = C_{\nu\alpha}(\tfrac{1}{2},\tfrac{1}{2},J) = C^{\alpha}_{qNF} \tag{1.3.38}$$

In general, for integral $J > S_1 + S_3$, the number of couplings of a spin = J exchange to spins S_1 and S_3 would be $(2S_1 + 1)(2S_3 + 1)$ (see reference (21)). However, for integral $J < S_1 + S_3$, the number of couplings is reduced by $g(g + 1)$, where $g = S_1 + S_3 - J$ With the VCH we never have to consider $J > 1$ so there are only two couplings . In a regge amplitude, this reduction is achieved by nonsense decoupling. Our prescription for this will be (see reference (22)) that those couplings which involve more projection operator labels than are available at a given nonsense point vanish there. Thus, in the above example J = 0 corresponds to a nonsense point at the $\frac{1}{2},\frac{1}{2}$ vertex and so, using the above rule, there will be only a single coupling allowed, without a label. In order for us to use equation (1.3.38) we must, therefore, "continue" to J = 1 and then remove the unwanted factor of $\frac{P_\alpha}{M_o}$.

In the next two sections, we demonstrate how the couplings and wave-function introduced above are incorporated into a covariant reggeization

procedure, enabling to write down leading order regge pole contributions to s-channel helicity amplitudes.

1.4 Covariant Reggeization

The technique of covariant reggeization was originally developed in references (21-26) and subsequently used by the authors of references (27-33). Since we will need to make use of the detailed properties of covariant couplings, we give here a brief description of the formalism, drawing appropriate results from references (21-33) where necessary.

We consider the s-channel process 1 + 2 → 3 + 4, as shown in Figure 1.3.2. Following reference (33), we introduce m functions for the process in terms of helicity amplitudes by

$$\langle \lambda_3\lambda_4|A|\lambda_1\lambda_2\rangle = \bar{\psi}_\nu^{\lambda_3}(p')\,\bar{\psi}_\tau^{\lambda_4}(q')\,m_{\mu\nu\sigma\tau}(P,Q)\,\psi_\mu^{\lambda_1}(p)\,\psi_\sigma^{\lambda_2}(q) \qquad (1.4.1)$$

where $\bar{\psi}$ is the adjoint wave-function to ψ, and these m functions for any spin combination can be expressed in the form

$$m_{\mu\nu\sigma\tau}(P,Q) = \sum_j A^j(s,t)\,\kappa^j_{\mu\nu\sigma\tau}(P,Q) \qquad (1.4.2)$$

where the $A^j(s,t)$ are invariant amplitudes, free of kinematical singularities, and the κ^j are the dimensionless kinematical covariants, constructed from the momenta and γ matrices. But unlike reference (21), we require these covariants to be of a dimensionless nature in order that the various covariant coupling constants appearing finally in our results for helicity vertex functions (see Table 1.5.1) will also be dimensionless. The m functions defined in (1.4.2) above are, in fact, channel independent, but we have expressed them in terms of t-channel covariants for future use.

The covariant three-particle coupling is given by (see equation (1.3.35))

$$C_{\mu\nu\alpha}(S_1,S_3J) = C^{\alpha}_{qNF}\, g_1^{\ell_3} \frac{P_{\mu_1}}{M_o}\cdot\cdot\frac{P_{\mu_{\ell_1}}}{M_o}\frac{P_{\nu_1}}{M_o}\cdot\cdot\frac{P_{\nu_{\ell_3}}}{M_o} + C_{qN}\, g_{\mu_1\alpha_1}\frac{P_{\mu_2}}{M_o}\cdot\cdot\frac{P_{\mu_{\ell_1}}}{M_o}\, g_2^{\ell_3}\frac{P_{\nu_1}}{M_o}\cdot\cdot\frac{P_{\nu_{\ell_3}}}{M_o} \tag{1.4.3}$$

where we have included the spin label μ for completeness although in practice $\ell = 0$ for the beam particles (π's, K's or p's) and hence $\mu = 0$. This is, of course, not the most general three particle coupling (see references (21), (33)), but is the most general coupling we allow given our assumptions, that is the VCH, which restricts helicity change in the t-channel to be ≤ 1 unit and hence suppresses all propagator labels α, β greater than α_1 or β_1. We define the scale factor $M_o \equiv \sqrt{s_o}$, where s_o is the regge scale factor and is discussed in reference (34), equation (6.2.9) ff. In Table 1.4.1 (given at the end of this chapter), we give expressions for $C_{\mu,\nu,\alpha}(S_1,S_3,J)$ for the vertices we will consider in this thesis.

Next, we introduce the propagator function for a particle of spin = J denoted by $\bar{P}^{J}_{\alpha_1..\alpha_J;\beta_1..\beta_J}(P,-Q;\Delta)$ and tabulated in equation (7) of reference (21). Following reference (21) equation (8), we may write the propagator function in terms of solid Legendre functions in the form

$$\frac{P_{\alpha_1}}{M_o}\cdot\cdot\frac{P_{\alpha_J}}{M_o}\;\bar{P}^{J}_{\alpha;\beta}(P,-Q;\Delta)\;\frac{Q_{\beta_1}}{M_o}\cdot\cdot\frac{Q_{\beta_J}}{M_o} = C_J\,\underline{P}_J\,(P\cdot Q) \tag{1.4.4}$$

where the sum over the β and α labels is implicit, and

$$C_J = 2^J\frac{(J!)^2}{(2J)!} \tag{1.4.5}$$

The Solid Legendre polynomial $\underline{P}_J\,(P\cdot Q)$ is defined by

$$P_J(P\cdot Q) = \left|\frac{P}{M_o}\right|^J \left|\frac{Q}{M_o}\right|^J P_J(z_t)\;,\quad z_t = \frac{P\cdot Q}{|P|\,|Q|} \tag{1.4.6}$$

However, with the VCH, $J \leq 1$ and hence the propagator function carries at most 1 β or 1 α label. This has the effect of "contracting" the propagator (see reference (33)),

since all other propagator labels have been suppressed. Thus $\bar{P}^{J}_{\alpha;\beta}(P,-Q;\Delta)$ is notationally similar to equation (22) of reference (21). However, the appearance of the factors M_o in (1.4.4) ensures that our propagators are dimensionless.

In terms of these propagators and couplings, the t-channel partial-wave series for the m function (see (1.4.1)) may be written as

$$m_{\mu\nu\sigma\tau}(P,Q) = \sum_{J}(2J+1)\, A_J\, C_{\mu\nu\alpha}(S_1,S_3,J)\, \bar{P}^{J}_{\alpha;\beta}(P,-Q;\Delta)\quad C_{\sigma\tau\beta}(S_2,S_4,J) \tag{1.4.7}$$

This expression (1.4.7) gives the m function in a dimensionless form since the propagators and couplings have been arranged to be dimensionless and A_J, the partial-wave amplitude is just $\frac{2q_s}{\sqrt{s}} \sin\delta_\ell(s)\, e^{i\delta_\ell(s)}$, where $\delta_\ell(s)$ is the phase shift (see, for example, reference (34), p.51) and hence dimensionless. Thus the contribution of a resonance pole of spin = J and mass M_5 exchanged in the t-channel (see Figure 1.3.2) is

$$m(P,Q) = \frac{2J+1}{\alpha'(t-M_5^2)}\, C_{\mu\nu\alpha}(S_1,S_3,J)\, \bar{P}^{J}_{\alpha;\beta}(P,-Q;\Delta)\quad C_{\sigma\tau\beta}(S_2,S_4,J) \tag{1.4.8}$$

where we have assumed a linear trajectory $\alpha(t) = \alpha_o + \alpha' t$ and a pole at $t = M_5^2 = \frac{J-\alpha_o}{\alpha'}$

In order to reggeize (1.4.8), one must first decompose it into partial-wave amplitudes for the various invariant amplitudes $A^j(s,t)$ of (1.4.2) (see, for example, reference 34)). The partial-wave series which result contain just Legendre polynomials and their derivations, and hence each series may be inverted to yield the Froissart-Gribov projections for the partial-wave amplitudes (34). Re-writing each partial-wave series as a Sommerfeld-Watson contour integral in J and deforming the contour to expose the leading J-plane regge poles at $J = \alpha(t)$ leads to

$$m^{R_u}_{\mu\nu\sigma\tau}(P,Q) = 2(\alpha(t)+1)S^{\pm} C_{\mu\nu\alpha}(S_1,S_3,\alpha(t))\bar{P}^{\alpha(t)}_{\alpha;\beta}(P,-Q;\Delta) \quad C_{\sigma\tau\beta}(S_2,S_4,\alpha(t)) \tag{1.4.9}$$

for the regge pole contribution to the m function (22), where

$$S^{\pm} \equiv \frac{1 \pm e^{-i\pi\alpha(t)}}{2\sin\pi\alpha(t)} \tag{1.4.10}$$

the usual signature factor and $C_{\mu\nu\alpha}(S_1,S_3,\alpha(t))$ etc. is obtained by substituting regge residues $g_i(t)$ for the orbital angular momentum coupling constants $g_i^{\ell}(i = 1,2)$ in the expressions for the covariant couplings in Table 1.4.1. To obtain $\bar{P}^{\alpha(t)}_{\alpha;\beta}(P,-Q;\Delta)$ we simply replace J by $\alpha(t)$ in (1.4.5) and (1.4.6).

The appearance of the momentum factors in (1.4.6) ensures that the regge residues have the correct threshold behaviour. However, the appropriate nonsense factors must be inserted by hand. Since it will be sufficient for our purposes to work to leading order in s/s_o we need not concern ourselves with the fact that for unequal masses $\bar{P}^{J}_{\alpha;\beta}(P,-Q;\Delta)$ will contain terms in 1/t etc. which would produce singularities in the $A^j(s,t)$ were they not cancelled by daughter trajectories or some other similar mechanism (22,23).

In working to leading order in s/s_o it was shown in references (24,26) that one can replace $P^{\alpha(t)}_{\alpha;\beta}(P,-Q;\Delta)$ in (1.4.9) by derivatives of the solid Legendre polynomial, viz.

$$M_o^{\alpha_1..\alpha_J} M_o^{\beta_1..\beta_J} \left(\frac{\partial}{\partial P_{\alpha_1}} \cdots \frac{\partial}{\partial P_{\alpha_J}}\right) \left(\frac{\partial}{\partial Q_{\beta_1}} \cdots \frac{\partial}{\partial Q_{\beta_J}}\right) \underline{P}_{\alpha(t)}(P.Q) \tag{1.4.11}$$

(where, for the sake of generality, we have summed from P_{α_1} up to P_{α_J}, although setting J = 1 in no way affects the argument). This is so because, for example, from (1.4.4)

$$\frac{\partial}{\partial P_{\alpha_1}} \left(P_{\alpha_1} \cdots P_{\alpha_J}\right) \bar{P}^{J}_{\alpha_1 \cdots \alpha_J ; \beta_1 \cdots \beta_J}(P,-Q;\Delta)\, Q_{\beta_1} \cdots Q_{\beta_J}\, M_o^{-2J+1}$$

$$= J\, P_{\alpha_2} \cdots P_{\alpha_J}\, \bar{P}^{J}_{\alpha_1 \cdots \alpha_J ; \beta_1 \cdots \beta_J}(P,-Q;\Delta)\, Q_{\beta_1} \cdots Q_{\beta_J}\, M_o^{-2J+1}$$

(since $\partial P_{\alpha_i} / \partial P_{\alpha_1} = g_{\alpha_1 \alpha_i}$ (the metric tensor))

$$= J\, \bar{P}^{J}_{\alpha_1}(P,-Q;\Delta) \tag{1.4.12}$$

If we then replace $P_{\alpha(t)}(P.Q)$ in (1.4.11) by its assymptotic form $\left(\frac{P.Q}{s_o}\right)^{\alpha(t)}$, we finally get for (1.4.9) (see reference (28)) (absorbing all the necessary nonsense factors $\alpha(t)$ into $g_i(t)$)

$$m^{R}_{\mu\nu\sigma\tau}(P,Q) = S^{\pm} C_{\mu\nu\alpha}(S_1,S_3,\alpha(t))\, C_{\sigma\tau\beta}(S_2,S_4,\alpha(t))$$

$$\times M_o^{\alpha_1 \cdots \alpha_J} M_o^{\beta_1 \cdots \beta_J} \left(\frac{\partial}{\partial P_{\alpha_1}} \cdots \frac{\partial}{\partial P_{\alpha_J}}\right)\left(\frac{\partial}{\partial Q_{\beta_1}} \cdots \frac{\partial}{\partial Q_{\beta_J}}\right) \left(\frac{P.Q}{s_o}\right)^{\alpha(t)} \tag{1.4.13}$$

Thus, with this dimensionless form of m function we may read off the leading order regge pole contributions to the invariant amplitudes, after insertion of the $C_{\mu\nu\alpha}$'s... etc. appropriate for the process (see, for example, reference (22)).

1.5 Helicity Vertices

Since invariant amplitudes have a rather complicated relation to experimental observables such as cross-sections and density matrices, it is obviously desirable to be able to relate the $A^J(s,t)$ to helicity amplitudes. As equation (1.4.13) has been obtained in a factorized form it is possible to work, at least to leading order in s/s_o, with s-channel helicity vertices instead (28).

To calculate an s-channel helicity amplitude one sandwiches the m functions between particle wave-functions of the appropriate helicity and obtains (28)

$$\langle\lambda_3\lambda_4|A|\lambda_1\lambda_2\rangle = c_\alpha^{\lambda_1\lambda_3}(S_1,S_3)\; c_\beta^{\lambda_2\lambda_4}(S_2,S_4)\; S^{\pm}\left(\frac{\partial}{\partial P_\alpha}\right)\left(\frac{\partial}{\partial Q_\beta}\right)\left(\frac{P\cdot Q}{s_o}\right)^{\alpha(t)} M_o^n \tag{1.5.1}$$

where the product over the α and β labels is understood, and n = number of differentiations of $\left(\frac{P\cdot Q}{s_o}\right)^{\alpha(t)}$. Since each differentiation of $\left(\frac{P\cdot Q}{s_o}\right)^{\alpha(t)}\left[\equiv\left(\frac{\nu}{s_o}\right)^{\alpha(t)}\right]$ lowers the power of $\frac{\nu}{s_o}$ by one, only those parts of the helicity coupling $c_\alpha^{\lambda_1\lambda_3}(S_1,S_3)$ and $c_\beta^{\lambda_2\lambda_4}(S_2,S_4)$ which are effectively proportional to the required number of $\frac{P_\alpha\text{'s}}{M_o}$ and $\frac{Q_\beta\text{'s}}{M_o}$ respectively give leading order contributions. This is so because the $\frac{P_\alpha\text{'s}}{M_o}$ and $\frac{Q_\beta\text{'s}}{M_o}$ in the c's can then restore $\left(\frac{\nu}{s_o}\right)^{\alpha(t)-n}$, obtained after differentiation of the leading power, which is always $\left(\frac{\nu}{s_o}\right)^{\alpha(t)}$. Therefore it is useful to introduce (28) helicity vertices $V_{\lambda_1\lambda_3}(S_1,S_3)$ and $V_{\lambda_2\lambda_4}(S_2,S_4)$ defined in terms of helicity couplings, and having these momenta, as well as the kinematical t-dependence extracted. That is, we put

$$c_\alpha^{\lambda_1\lambda_3} \equiv \left(\frac{-t}{s_o}\right)^{\frac{1}{2}|\lambda_1-\lambda_3|} \frac{P_\alpha}{M_o}\, V_{\lambda_1\lambda_3}(S_1,S_3)$$

$$c_\beta^{\lambda_2\lambda_4} \equiv \left(\frac{-t}{s_o}\right)^{\frac{1}{2}|\lambda_2-\lambda_4|} \frac{Q_\beta}{M_o}\, V_{\lambda_2\lambda_4}(S_2,S_4) \tag{1.5.2}$$

To obtain these V's, which are given in Table 1.5.1 (at the end of this chapter) we need to find the expectation values of the momenta and

γ-matrices between helicity wave-functions. In order to perform the calculation, we require the following results:-

The matrix elements of the unit operator between two Dirac spinors (see equation (1.3.7)) are given by

$$\bar{u}^{\lambda_3}(k'_u)\,\underline{1}\,u^{\lambda_1}(k_u) = \frac{1}{\sqrt{2m_+}}\,(k'_{ou}+m_u)^{\frac{1}{2}}\,\phi^{\lambda_3\dagger}\left(1-\frac{i\gamma_5\,\underline{\sigma}\cdot\underline{k}'_u}{(k'_{ou}+m_u)}\right)\underline{1}$$

$$\times\ \frac{1}{\sqrt{2m_+}}\,(k_{ou}+m_u)^{\frac{1}{2}}\,\phi^{\lambda_1}\left(1+\frac{i\gamma_5\,\underline{\sigma}\cdot\underline{k}_u}{(k_{ou}+m_u)}\right) \qquad (1.5.3)$$

$$= \frac{1}{2m_+}\,\phi^{\lambda_3\dagger}\left[(k'_{ou}+m_u)^{\frac{1}{2}}\,(k_{ou}+m_u)^{\frac{1}{2}} - (\underline{\sigma}\cdot\hat{\underline{k}}'_u)\,(\underline{\sigma}\cdot\hat{\underline{k}}_u)\,(k'_{ou}-m_u)^{\frac{1}{2}}\,(k_{ou}-m_u)^{\frac{1}{2}}\right]\phi^{\lambda_1} \qquad (1.5.4)$$

where m_u, k_{ou} etc. refer to the quark mass and momenta and are defined in equations (1.3.1) to (1.3.6) inclusively and

$$m_+ \equiv \frac{m_1+m_3}{2} = \frac{m_u+m_u}{2} = m_u \qquad (1.5.5)$$

as defined in Section 3 above. In equation (1.5.4) we have used the result that $k_o^2 = \underline{k}^2 + m^2$ etc., and $\hat{\underline{k}} = \frac{\underline{k}}{|\underline{k}|}$, and $\bar{u}$ is the adjoint spinor and not the anti-quark.

Then we write

$$\phi^{\lambda_3}(\theta) = \sum_m D^{\frac{1}{2}}_{m\lambda_3}(\theta)\,\phi^m(o) \qquad (1.5.6)$$

(m is the z-component of the angular momentum ≡ helicity) where θ is the s-channel c.m.s. scattering angle (that is, the angle between the direction of motion of quark 3(say) and quark 1, which is the z-axis) and the rotation matrix (34) is

$$D^{\frac{1}{2}}_{mm'}(\theta) = \begin{pmatrix} \cos\theta/2 & -\sin\theta/2 \\ \sin\theta/2 & \cos\theta/2 \end{pmatrix} \tag{1.5.7}$$

(since we have set ϕ, the azimuthal angle about the z-axis equal to zero).

Hence, for $\lambda_1 = \lambda_3 = \pm\frac{1}{2}$, we have

$$\phi^{\lambda_3\dagger}(\theta)\ \phi^{\lambda_1}(o) = \cos\theta/2 \to 1 \qquad s \to \infty \tag{1.5.8}$$

while for $\lambda_1 \neq \lambda_3$

$$\phi^{\lambda_3\dagger}(\theta)\ \phi^{\lambda_1}(o) = \pm\sin\frac{\theta}{2} \to \pm\sqrt{\frac{-t}{s}} \qquad s \to \infty \tag{1.5.9}$$

So expanding the square bracket in (1.5.4) for large energies, we find for the diagonal elements

$$\frac{1}{2m_+}(k_{ou}\,k'_{ou})^{\frac{1}{2}}\left[1+\frac{1}{2}\left(\frac{m_u}{k'_{ou}}+\frac{m_u}{k_{ou}}\right)+\ldots-1+\frac{1}{2}\left(\frac{m_u}{k'_{ou}}+\frac{m_u}{k_{ou}}\right)+\ldots\right]$$

$$=\frac{1}{2m_+}\left[m_u\left(\frac{k_{ou}}{k'_{ou}}\right)^{\frac{1}{2}}+\ m_u\left(\frac{k'_{ou}}{k_{ou}}\right)^{\frac{1}{2}}+\ldots\right]\to\frac{m_u+m_u}{2m_+}=1 \tag{1.5.10}$$

while the off-diagonal elements (using (1.5.9) $\to \pm\sqrt{\frac{-t}{s}}$

So the result is

$$\bar{u}^{\lambda_3}(k'_u)\ \underline{1}\ u^{\lambda_1}(k_u) \to \begin{pmatrix} 1 & \frac{\sqrt{-t_u}}{2m_+} \\ \frac{-\sqrt{-t_u}}{2m_+} & 1 \end{pmatrix} \qquad s \to \infty \tag{1.5.11}$$

valid for $s \gg t, m^2$

Similarly, by using the algebra of the Dirac matrices (17), it is possible to show that

$$\bar{u}^{\lambda_3}(k'_u)\ \gamma_\alpha\ u^{\lambda_1}(k_u) \rightarrow \begin{pmatrix} \frac{k_{u\alpha}}{m_+} & 0 \\ 0 & \frac{k_{u\alpha}}{m_+} \end{pmatrix} \tag{1.5.12}$$

With our assumptions in Section 3, then

$$\frac{k_{u\alpha}}{m_+} \equiv \frac{P_\alpha}{M_+}\ , \quad \frac{\sqrt{-t_u}}{2m_+} \equiv \frac{\sqrt{-t}}{2M_+} \tag{1.5.13}$$

For vertices involving higher spin particles, that is particles with $\ell \neq 0$, we also need matrix elements involving the polarization vectors. Because of the subsidiary condition $P_\mu\ \epsilon^\lambda_\mu(p) = 0$ for the incoming particle 1 (referring to Figure 1.3.2) we have

$$\frac{P_\mu}{M_o}\ \epsilon^{\pm 1}_\mu(p) = \frac{1}{2M_o}(p + p')_\mu\ \epsilon^{\pm 1}_\mu(p) = \frac{1}{2M_o}\ p'_\mu\ \epsilon^{\pm 1}_\mu(p)$$

$$= \pm\frac{1}{2}\sqrt{\frac{1}{2}}\ \frac{|p'|}{M_o}\ \sin\theta \rightarrow \pm\frac{1}{2}\sqrt{\frac{1}{2}}\ \frac{\sqrt{-t}}{M_o} \tag{1.5.14}$$

from equation (1.5.9) (since the scattering is in the x-z plane) while

$$\frac{P_\mu}{M_o}\ \epsilon^0_\mu(p) \rightarrow \frac{1}{M_1 M_o}\ (M_+ M_- - \frac{1}{4}\ t) \tag{1.5.15}$$

$$g_{\mu\alpha}\ \epsilon^{\pm 1}_\mu(p) = \epsilon^{\pm 1}_\alpha(p)\ , \quad \frac{P_\alpha}{M_o}\ \epsilon^{\pm 1}_\alpha(q) \rightarrow 0$$

$$g_{\mu\alpha}\ \epsilon^0_\mu(p) \rightarrow \frac{P_\alpha}{M_1}$$

where $$M_{\pm} \equiv \frac{1}{2}(M_3 \pm M_1) \qquad (1.5.16)$$

Similarly, for the outgoing particle 3:-

$$\varepsilon_\nu^{\pm 1*}(p')\frac{P_\nu}{M_o} \to \pm\frac{1}{2}\sqrt{\frac{1}{2}}\frac{\sqrt{-t}}{M_o}, \quad \varepsilon_\nu^{o*}(p')\frac{P_\nu}{M_o} \to \frac{1}{M_3 M_o}(M_+M_- + \frac{1}{4}t)$$

$$\varepsilon_\nu^{\pm 1*}(p')\, g_{\nu\alpha} = \varepsilon_\alpha^{\pm 1*}(p'), \quad \frac{P_\alpha}{M_o}\varepsilon_\alpha^{\pm 1*}(p') \to 0$$

$$\varepsilon_\nu^{o*}(p')\, g_{\nu\alpha} \to \frac{P_\alpha}{M_3} \qquad (1.5.17)$$

with the obvious substitutions for $\frac{Q}{M_o}$, β, σ, τ, M_2 and M_4 at the lower vertex in Figure 1.3.2.

The above results ensure that the appropriate momentum and $\frac{\sqrt{-t}}{M_o}$ factors always appear in the couplings in the assymptotic limit, as in equation (1.5.2) and, with the aid of a specific example given below, should enable Table 1.5.1 to be checked.

We consider in detail the πA_2 vertex. The allowed natural parity regge exchanges are the I = 0 P and f (isoscalar photon) and the I = 1 ρ (isovector photon). In the quark model, parity P of a $q\bar{q}$ state is given by

$$P = -(-1)^{\ell} \qquad (1.5.18)$$

and since the A_2 is a spin = 2 + ve parity state, then ℓ = 1. That is, it is in an ℓ = s = 1, J = 2, λ = ± 2, ± 1,0 state. The normality of a particle $\eta(=\pm 1)$ is defined to be

$$\eta = P(-1)^{J-\nu} \qquad (1.5.19)$$

where ν = 0 for bosons

= $\frac{1}{2}$ for fermions

Likewise the normality of a vertex (5 → 1 + 3) in the language of Figure 1.3.2) is

$$\eta_\nu = \eta_1\eta_3\eta_5 = \pm 1 \text{ for normal/abnormal vertices} \quad (1.5.20)$$

As we will always be considering natural parity regge exchanges, the normality of each vertex will be defined accordingly. Thus, in the above example, the $\pi A_2 f$ and $\pi A_2 \rho$ are abnormal, and denoted by $V^-_{\lambda_1\lambda_3}(\pi A_2)$ in Table 1.5.1.

The π^+ wave-function (see Appendix (2)) is given by

$$\psi^o_o(p) = \frac{1}{\sqrt{2}} (\bar{d}^+(k_{\bar{d}})\, u^-(k_u) - \bar{d}^-(k_{\bar{d}})\, u^+(k_u) \quad (1.5.21)$$

while for the A_2 in a $\lambda = 2$ state

$$\bar{\psi}^2_\nu(p') = \bar{d}^+(k'_{\bar{d}})\, u^+(k'_u)\, \varepsilon^{+1*}_\nu(p') \quad (1.5.22)$$

(The Clebsch-Gordan coefficient = 1 and henceforth we delete the arguments of the spinors $\frac{k_u}{m_u}\left(=\frac{k_{\bar{d}}}{m_{\bar{d}}}\right)$ and $\frac{k'_u}{m_u}\left(=\frac{k'_{\bar{d}}}{m_{\bar{d}}}\right)$).

Referring to Table 1.4.1, we see that for this vertex, the coupling $C_{\mu\nu\alpha}(S_1,S_3\mathcal{J})$ is given by

$$C_{\nu\alpha}(\pi A_2) = C^\alpha_{qNF}\, g^1_1 \frac{P_{\nu_1}}{M_o} + C^\alpha_{qN}\, g^1_2\, g_{\nu_1\alpha_1} \quad (1.5.23)$$

$$= \sum_i \left(g^i_1 \frac{P_\alpha}{M_o} + g^i_2 \gamma_{\perp\alpha} \frac{M_+}{M_o}\right) g^1_1 \frac{P_{\nu_1}}{M_o} + \sum_i^{S/V} g^i_1\, g^1_2\, g_{\nu_1\alpha_1} \quad (1.5.24)$$

where $\frac{P_{\nu_1}}{M_o} = \frac{1}{M_o}\left(\frac{(p+p')_\nu}{2}\right)$ and $g_{\nu_1\alpha_1}$ is the metric tensor.

Thus

$$c^{-02}_{\alpha_1}(\pi A_2) = \overline{\bar{d}^+ u^+}\, \varepsilon^{+*}_{\nu_1}(p') C_{\nu_1\alpha_1}(\pi A_2)\, \frac{1}{\sqrt{2}}\, (\bar{d}^+ u^- - \bar{d}^- u^+) \qquad (1.5.25)$$

Considering firstly isoscalar exchange and specifically + ve c parity (but remembering that the A_2 has $\ell = 1$), then

$$\begin{aligned} c^{-02}_{\alpha_1}(\pi A_2) = {} & \frac{1}{\sqrt{2}} \varepsilon^{+1*}_{\nu_1}(p')\, g^1_1 \frac{P_{\nu_1}}{M_o}\, g^S_1 \Big[\overline{\bar{d}^+ u^+}\, \frac{P_{\alpha_1}}{M_o}\, \bar{d}^+ u^- + \overline{\bar{d}^+ u^+} \frac{P_{\alpha_1}}{M_o}\, \bar{d}^+ u^- \\ & - \overline{\bar{d}^+ u^+}\, \frac{P_{\alpha_1}}{M_o}\, \bar{d}^- u^+ - \overline{\bar{d}^+ u^+}\, \frac{P_{\alpha_1}}{M_o}\, \bar{d}^- u^+ \Big] \\ & + \frac{1}{\sqrt{2}} \varepsilon^{+1*}_{\nu_1}(p')\, g^1_1 \frac{P_{\nu_1}}{M_o}\, g^S_2 \Big[\overline{\bar{d}^+ u^+}\, \gamma_{d\alpha_1}\, \bar{d}^+ u^- - \overline{\bar{d}^+ u^+}\, \gamma_{u\alpha_1}\, \bar{d}^- u^+ \Big] \frac{M_+}{M_o} \\ & + \frac{1}{\sqrt{2}} \varepsilon^{+1*}_{\nu_1}(p')\, g^1_2 g_{\nu_1\alpha_1} g^S_1 \Big[\overline{\bar{d}^+ u^+}\, \underline{1}\, \bar{d}^+ u^- + \overline{\bar{d}^+ u^+}\, \underline{1}\, \bar{d}^+ u^- - \overline{\bar{d}^+ u^+}\, \underline{1}\, \bar{d}^- u^+ \\ & - \overline{\bar{d}^+ u^+}\, \underline{1}\, \bar{d}^- u^+ \Big] \end{aligned} \qquad (1.5.26)$$

where for the second term in square brackets in (1.5.26) above we have used (1.5.12) to set the off-diagonal elements to zero, that is $\bar{u}^+ \gamma_{\alpha_1} u^- = 0$. Inspecting the first and third terms we see that the terms inside the square brackets cancel for either c-parity, leaving

$$c^{-02}_{\alpha_1}(\pi A_2) = \frac{1}{\sqrt{2}} \varepsilon^{+1*}_{\nu_1}(p')\, \frac{P_{\nu_1}}{M_o}\, g^1_1 \frac{M_+}{M_o}\, g^S_2 \Big[\overline{\bar{d}^+ u^+}\, \gamma_{d\alpha_1}\, \bar{d}^+ u^- - \overline{\bar{d}^+ u^+}\, \gamma_{u\alpha_1}\, \bar{d}^- u^+ \Big] \qquad (1.5.27)$$

Using equations (1.5.11), (1.5.12) and (1.5.13)

$$c^{-02}_{\alpha_1}(\pi A_2) = -\frac{1}{\sqrt{2}}\ \varepsilon^{+1*}_{\nu_1}(p')\ \frac{P_{\nu_1}}{M_o}\ 2\frac{P_{\alpha_1}}{M_+}\ \frac{\sqrt{-t}}{2M_+}\ \frac{M_+}{M_o}\ g_1^1\ g_2^S \qquad (1.5.28)$$

Using equation (1.5.15)

$$c^{-02}_{\alpha_1}(\pi A_2) = -\frac{1}{\sqrt{2}}\frac{P_{\alpha_1}}{M_o}\ \frac{\sqrt{-t}}{M_+}\ g_1\ g_2^S\left[-\frac{1}{2}\sqrt{\frac{1}{2}}\ \frac{\sqrt{-t}}{M_o}\right] \qquad (1.5.29)$$

Comparing (1.5.29) with equation (1.5.2), that is

$$a^{\lambda_1\lambda_3}_{\alpha} = \left(\frac{-t}{s_o}\right)^{\frac{1}{2}|\lambda_1 - \lambda_3|}\ \frac{P_\alpha}{M_o}\ V_{\lambda_1\lambda_3}(S_1,S_3) \qquad (1.5.30)$$

and remembering that $\frac{1}{2}|\lambda_1 - \lambda_3| = 1$ gives

$$V^-_{02}(\pi A_2) = \frac{g_2^S\ g_1^1\ M_o}{4M_+} \qquad (1.5.31)$$

the isoscalar coupling to the πA_2 vertex. Similarly for the isovector coupling, it is easy to show that

$$V^-_{02}(\pi A_2) = \frac{g_2^V\ g_1^1\ M_o}{4M_+} \qquad (1.5.32)$$

where the values of $g^i_{1,2}$ are given in Table 1.3.1.

<u>The $N\bar{N}$ vertex</u>

We consider here the vertex $c^{+\frac{1}{2},\frac{1}{2}}_{\beta}$(pp). Referring to Appendix 2 we write to proton wave-function in the shorthand notation P↑(k_u) (referring to the lower vertex in Figure 1.3.2). The coupling appropriate for $\frac{1}{2}\ \frac{1}{2}$ scattering is, from Table 1.4.1 ,

$$C^{\alpha}_{qNF} = \sum_{i} \left(g_1^{i\,S/V} \frac{Q_\beta}{M_o} + g_2^{i\,S/V} \gamma_{i\beta} \frac{M_+}{M_o} \right) \tag{1.5.33}$$

Thus, $c^{+\frac{1}{2},\frac{1}{2}}_{\beta}(pp) = \bar{P}\uparrow(q')\, C^{\alpha}_{qNF}\, P\uparrow(q)$ (1.5.34)

Sparing the reader the tedious details the result is (for isoscalar exchange)

$$3(g_1^S + g_2^S) \frac{Q_\beta}{M_o} \tag{1.5.35}$$

Comparing (1.5.35) with (1.5.2) ,

$$V^{+}_{\frac{1}{2},\frac{1}{2}}(pp) = 3(g_1^S + g_2^S) \tag{1.5.36}$$

Inserting the values of g_1^S , g_2^S from Table 1.3.1, then

$$V^{+}_{\frac{1}{2},\frac{1}{2}}(pp) = 1(f_\omega) \tag{1.5.37}$$

That is, the isoscalar photon coupling to $N\bar{N}$ at t = 0 is given just by the charge, e, as expected.

Following the two examples given above should enable all other results in Table 1.5.1 to be deduced. Although we include all factors of M_o ($\equiv \sqrt{s_o}$) to clarify the dimensionless nature of our helicity vertex functions, in practice we make the usual assumption that $s_o = 1\ GeV^2$.

Having thus established our covariant formalism, we are in a position to test relation (1.2.7) and (1.2.8) since we may now write down specific relations between each coupling. It is the purpose of the following chapters to explore the combined consequences of the vector coupling hypothesis and the gamma analogy hypothesis within the framework outlined above.

TABLE 1.4.1

From equation (1.3.37) we have defined the quark non-flip and flip coupling C^{α}_{qNF} by

$$C^{\alpha}_{qNF} = \sum_i \left(g^i_1 \frac{P_\alpha}{M_o} + g^i_2 \gamma_{i\alpha} \frac{M_+}{M_o} \right)$$

and the quark non-flip coupling

$$C_{qN} = \sum_i g^i_1$$

For the lower vertex in Figure 1.3.2, make the substitution $\frac{P_\alpha}{M_o} \to \frac{Q_\beta}{M_o}$, $\gamma_\alpha \to \gamma_\beta$ in the above. $g_{\mu\nu}$ is the metric tensor and g^1_1 , g^1_2 , g^2_1 , g^2_2 .... etc. are the covariant dimensionless orbital angular momentum coupling constants. In order to implement our formalism without the constraint of the VCH (which is, of course, built in to our couplings given below) we refer the reader to Table1(b) of reference (33) where he will find the 'reduced' couplings appropriate for an exchange of arbitrarily high spin.

To specify the spins S_1, S_3 (or S_2, S_4) of the external particles we will use the usual J^{PC_n} notation where $J = \ell + j$ and, for $q\bar{q}$ states,

$$P = (-1)^{\ell+1} \quad , \quad C_n = (-1)^{\ell+j}$$

$$C_{\alpha}(0^{-+},\ 0^{-+}) = C^{\alpha}_{qNF}$$

$$C_{\nu_1,\alpha_1}(0^{-+},\ 0^{++}) = C^{\alpha}_{qNF}\, g^1_1 \frac{P_{\nu_1}}{M_o} + C_{qN}\, g^1_2\, g_{\nu_1\alpha_1}$$

$$C_{\alpha}(0^{-+},\ 1^{--}) = C^{\alpha}_{qNF}$$

$$C_{\nu_1,\alpha_1}(0^{-+},\ 1^{++}) = C^{\alpha}_{qNF}\, g^1_1 \frac{P_{\nu_1}}{M_o} + C_{qN}\, g^1_2\, g_{\nu_1\alpha_1}$$

$$C_{\nu_1,\alpha_1}(0^{-+},\ 1^{+-}) = C^{\alpha}_{qNF}\, g^1_1 \frac{P_{\nu_1}}{M_o} + C_{qN}\, g^1_2\, g_{\nu_1\alpha_1}$$

$$C_{\nu_1,\alpha_1}(0^{-+},\ 2^{++}) = C^{\alpha}_{qNF}\, g^1_1 \frac{P_{\nu_1}}{M_o} + C_{qN}\, g^1_2\, g_{\nu_1\alpha_1}$$

$$C_{\nu_1\nu_2,\alpha_1}(0^{-+},\ 2^{-+}) = C^{\alpha}_{qNF}\, g^2_1 \frac{P_{\nu_1}}{M_o} \frac{P_{\nu_2}}{M_o} + C_{qN}\, g^2_2\, g_{\nu_1\alpha_1} \frac{P_{\nu_2}}{M_o}$$

$$C_{\nu_1\nu_2,\alpha_1}(0^{-+},\ 2^{--}) = C^{\alpha}_{qNF}\, g^2_1 \frac{P_{\nu_1}}{M_o} \frac{P_{\nu_2}}{M_o} + C_{qN}\, g^2_2\, g_{\nu_1\alpha_1} \frac{P_{\nu_2}}{M_o}$$

$$C_{\nu_1\nu_2,\alpha_1}(0^{-+},\ 3^{--}) = C^{\alpha}_{qNF}\, g^2_1 \frac{P_{\nu_1}}{M_o} \frac{P_{\nu_2}}{M_o} + C_{qN}\, g^2_2\, g_{\nu_1\alpha_1} \frac{P_{\nu_2}}{M_o}$$

$$C_{\nu_1\nu_2\nu_3,\alpha_1}(0^{-+},\ 3^{+-}) = C^{\alpha}_{qNF}\, g^3_1 \frac{P_{\nu_1}}{M_o} \frac{P_{\nu_2}}{M_o} \frac{P_{\nu_3}}{M_o} + C_{qN}\, g^3_2\, g_{\nu_1\alpha_1} \frac{P_{\nu_2}}{M_o} \frac{P_{\nu_3}}{M_o}$$

$$C_{\alpha}\left(\tfrac{1}{2}^{+}, \tfrac{1}{2}^{+}\right) = C^{\alpha}_{qNF}$$

$$C_{\alpha}\left(\tfrac{1}{2}^{+}, \tfrac{3}{2}^{+}\right) = C^{\alpha}_{qNF}$$

$$C_{\nu_1,\alpha_1}\left(\tfrac{1}{2}^{+}, \tfrac{3}{2}^{-}\right) = C^{\alpha}_{qNF}\, g^{1}_{1}\, \frac{P_{\nu_1}}{M_o} + C_{qN}\, g^{1}_{2}\, g_{\nu_1\alpha_1}$$

$$C_{\nu_1,\alpha_1}\left(\tfrac{1}{2}^{+}, \tfrac{5}{2}^{-}\right) = C^{\alpha}_{qNF}\, g^{1}_{1}\, \frac{P_{\nu_1}}{M_o} + C_{qN}\, g^{1}_{2}\, g_{\nu_1\alpha_1}$$

$$C_{\nu_1\nu_2,\alpha_1}\left(\tfrac{1}{2}^{+}, \tfrac{5}{2}^{+}\right) = C^{\alpha}_{qNF}\, g^{2}_{1}\, \frac{P_{\nu_1}}{M_o}\, \frac{P_{\nu_1}}{M_o} + C_{qN}\, g^{2}_{2}\, g_{\nu_1\alpha_1}\, \frac{P_{\nu_2}}{M_o}$$

$$C_{\nu_1\nu_2,\alpha_1}\left(\tfrac{1}{2}^{+}, \tfrac{7}{2}^{+}\right) = C^{\alpha}_{qNF}\, g^{2}_{1}\, \frac{P_{\nu_1}}{M_o}\, \frac{P_{\nu_2}}{M_o} + C_{qN}\, g^{2}_{2}\, g_{\nu_1\alpha_1}\, \frac{P_{\nu_2}}{M_o}$$

$$C_{\nu_1\nu_2\nu_3,\alpha_1}\left(\tfrac{1}{2}^{+}, \tfrac{7}{2}^{-}\right) = C^{\alpha}_{qNF}\, g^{3}_{1}\, \frac{P_{\nu_1}}{M_o}\, \frac{P_{\nu_2}}{M_o}\, \frac{P_{\nu_3}}{M_o}$$

$$+ C_{qN}\, g^{3}_{2}\, g_{\nu_1\alpha_1}\, \frac{P_{\nu_2}}{M_o}\, \frac{P_{\nu_3}}{M_o}$$

Fermion Helicity Vertices

$$V^{+}_{\frac{1}{2},\frac{1}{2}}(pp) = 3(g_1^S + g_2^S)$$

$$V^{+}_{\frac{1}{2},-\frac{1}{2}}(pp) = \frac{(3g_1^S + 2g_2^S)\,M_o}{2M_+}$$

$$V^{+}_{\frac{1}{2},\frac{1}{2}}(p\Delta^+) = V^{-}_{\frac{1}{2},-\frac{1}{2}}(p\Delta^+) = 0$$

$$V^{-}_{\frac{1}{2},\frac{3}{2}}(p\Delta^+) = V^{-}_{\frac{1}{2},-\frac{3}{2}}(p\Delta^+) = 0$$

$$V^{+}_{\frac{1}{2},\frac{1}{2}}(pN^*_{1520}) = \sqrt{\frac{2}{3}}\,\frac{1}{M_3}\left[3g_1^S\,g_2^1\,M_o - 3(g_1^S + g_2^S)\,\frac{Tg_1^1}{M_o}\right] - \frac{(3g_1^S + 2g_2^S)}{2M_+}\,\frac{g_1^1\,t}{2\sqrt{6}\,M_o}$$

$$V^{+}_{\frac{1}{2},\frac{3}{2}}(pN^*_{1520}) = -3(g_1^S + g_2^S)\,\frac{g_1^1}{2\sqrt{2}}$$

$$V^{+}_{\frac{1}{2},-\frac{1}{2}}(pN^*_{1520}) = 3(g_1^S + g_2^S)\,\frac{g_1^1}{2\sqrt{6}} + \frac{(3g_1^S + 2g_2^S)}{2M_+}\sqrt{\frac{2}{3}}\,\frac{1}{M_3}\,T\,g_1^1 - \frac{3g_1^S}{2M_+}\,\frac{g_2^1\,M_o^2}{M_3}\sqrt{\frac{2}{3}}$$

$$V^{+}_{\frac{1}{2},-\frac{3}{2}}(pN^*_{1520}) = \frac{-(3g_1^S + 2g_2^S)}{2M_+}\,\frac{g_1^1\,M_o}{2\sqrt{2}}$$

$$V^{+}_{\frac{1}{2},\frac{1}{2}}(pN^*_{1688}) = \frac{3(g_1^S + g_2^S)}{\sqrt{10}}\left[\frac{g_1^2\,t}{4M_o^2} + \frac{2T^2\,g_1^2}{M_o^2\,M_3^2}\right] - \frac{2T\,g_2^2}{M_3^2}\,\frac{3g_1^S}{\sqrt{10}}$$

$$+ \frac{(3g_1^S + 2g_2^S)}{2M_+}\,\frac{t}{\sqrt{10}\,M_3}\,\frac{T\,g_1^2}{M_o^2} - \frac{3g_1^S}{2M_+}\,\frac{g_2^2\,t}{2\sqrt{10}\,M_3}$$

$$V^{+}_{\frac{1}{2},\frac{3}{2}}(pN^{*}_{1688}) = 3(g_1^S + g_2^S)\frac{T g_1^2}{\sqrt{5}\, M_3 M_o} - \frac{3g_1^S g_2^2 M_o}{2\sqrt{5}\, M_3} + \frac{(3g_1^S + 2g_2^S)}{2M_+}\frac{g_1^2 t}{8\sqrt{5}\, M_o}$$

$$V^{+}_{\frac{1}{2},\frac{5}{2}}(pN^{*}_{1688}) = 3(g_1^S + g_2^S)\frac{g_1^2}{8}$$

$$V^{+}_{\frac{1}{2},-\frac{1}{2}}(pN^{*}_{1688}) = \frac{3g_1^S g_2^2 M_o}{2\sqrt{10}\, M_3} + \frac{3(g_1^S + g_2^S) T g_1^2}{\sqrt{10}\, M_3 M_o} - \frac{(3g_1^S + 2g_2^S)}{2M_o M_+}\frac{1}{\sqrt{10}}\left[\frac{g_1^2 t}{4} + \frac{2T^2 g_1^2}{M_3^2}\right]$$

$$+ \frac{3g_1^S}{M_+}\frac{T g_2^2 M_o}{\sqrt{10}\, M_3^2}$$

$$V^{+}_{\frac{1}{2},-\frac{3}{2}}(pN^{*}_{1688}) = 3(g_1^S + g_2^S)\frac{g_1^2}{8\sqrt{5}} + \frac{(3g_1^S + 2g_2^S)}{2M_+}\frac{T g_1^2}{\sqrt{5}\, M_3} - \frac{3g_1^S}{2M_+}\frac{g_2^2 M_o^2}{2\sqrt{5}\, M_3}$$

$$V^{+}_{\frac{1}{2},-\frac{5}{2}}(pN^{*}_{1688}) = -\frac{(3g_1^S + 2g_2^S)}{2M_+}\frac{g_1^2 M_o}{8}$$

$$V^{+}_{\frac{1}{2},\frac{1}{2}}(pN^{*}_{2190}) = 3(g_1^S + g_2^S)\frac{t}{2\sqrt{70}\, M_3}\frac{3g_1^3 T}{M_o^3} - \frac{3g_1^S t}{2\sqrt{70}\, M_3}\frac{g_2^3}{M_o}$$

$$- 3(g_1^S + g_2^S)\frac{4}{\sqrt{70}\, M_3^2}\frac{T^3 g_1^3}{M_3 M_o^3} + 3g_1^S T^2 g_2^3 \frac{4}{\sqrt{70}\, M_3^2 M_o^2}$$

$$- \frac{1}{\sqrt{70}}\frac{(3g_1^S + 2g_2^S)}{2M_+}\left[\frac{3g_1^3 t}{16 M_o} + \frac{3T^2 t g_1^3}{M_3^2 M_o^3}\right] + \frac{3g_1^S}{2M_+\sqrt{70}}\frac{2g_2^3 T t}{M_o M_3^2}$$

$$V^{+}_{\frac{1}{2},\frac{3}{2}}(pN^{*}_{2190}) = -\frac{3(g_1^S+g_2^S)}{\sqrt{42}}\left[\frac{3g_1^3 t}{16 M_o^2}+\frac{3g_1^3 T^2}{M_3^2 M_o^2}\right]+\frac{3g_1^S}{\sqrt{42}}\cdot\frac{2g_2^3 T}{M_3^2}$$

$$-\frac{(3g_1^S+2g_2^S)}{2M_+}\frac{3g_1^3 tT}{4\sqrt{42}\,M_3 M_o^2}+\frac{3g_1^S}{2M_+}\cdot\frac{t g_2^3}{4\sqrt{42}\,M_3}$$

$$V^{+}_{\frac{1}{2},\frac{5}{2}}(pN^{*}_{2190}) = -\frac{(3g_1^S+2g_2^S)}{2M_+}\frac{t g_1^3}{16\sqrt{14}\,M_o}-\frac{3(g_1^S+g_2^S)}{4\sqrt{14}\,M_o}\frac{3g_1^3 T}{M_3}+\frac{3g_1^S M_o g_2^3}{4\sqrt{14}\,M_3}$$

$$V^{+}_{\frac{1}{2},\frac{7}{2}}(pN^{*}_{2190}) = -3(g_1^S+g_2^S)\frac{g_1^3}{16\sqrt{2}}$$

$$V^{+}_{\frac{1}{2},-\frac{1}{2}}(pN^{*}_{2190}) = \frac{3(g_1^S+g_2^S)}{\sqrt{70}\,M_o^2}\left[\frac{3g_1^3 t}{16}+\frac{3g_1^3 T^2}{M_3^2}\right]-\frac{3g_1^S}{\sqrt{70}}\frac{2g_2^3}{M_3^2}M_o^2$$

$$+\frac{(3g_1^S+2g_2^S)}{2M_+}\frac{1}{\sqrt{70}\,M_3 M_o^2}\left[\frac{3g_1^3 tT}{2}+\frac{2g_1^3 T^3}{M_3^2}\right]-\frac{3g_1^S}{2M_+\sqrt{70}\,M_3}\left[\frac{g_2^3 t}{2}-\frac{4g_2^3 T^2}{M_3^2}\right]$$

$$V^{+}_{\frac{1}{2},-\frac{3}{2}}(pN^{*}_{2190}) = -3(g_1^S+g_2^S)\frac{1}{\sqrt{42}\,M_3 M_o}\frac{3g_1^3 T}{4}+\frac{3g_1^S M_o}{\sqrt{42}\,M_3}\frac{g_2^3}{4}$$

$$-\frac{(3g_1^S+2g_2^S)}{2M_+}\frac{1}{\sqrt{42}\,M_o}\left[\frac{3g_1^3 t}{16}+\frac{3g_1^3 T^2}{M_3^2}\right]+\frac{3g_1^S}{2M_+}\frac{M_o}{\sqrt{42}\,M_3^2}2g_2^3 T$$

$$V^{+}_{\frac{1}{2},-\frac{5}{2}}(pN^{*}_{2190}) = \frac{3(g_1^S+g_2^S)}{16\sqrt{14}}g_1^3+\frac{(3g_1^S+2g_2^S)}{2M_+}\frac{3g_1^3 T}{4\sqrt{14}\,M_3}$$

$$-\frac{3g_1^S}{2M_+}\frac{g_2^3 M_o^2}{4\sqrt{14}\,M_3}$$

$$V^{+}_{\frac{1}{2},-\frac{7}{2}}(pN^{*}_{2190}) = -\frac{(3g_1^S+2g_2^S)}{2M_+}\frac{g_1^3 M_o}{16\sqrt{2}}$$

Table 1.5.1(a)

Here $T \equiv \frac{1}{4}(M_3^2 - M_1^2 + t)$

Parity:- $V^{\pm}_{-\lambda_1,-\lambda_3} = \pm(-1)^{\lambda_1-\lambda_3} V^{\pm}_{\lambda_1,\lambda_3}$

I = 1 exhcange:- make the following substitutions

$$3(g_1^S + g_2^S) \rightarrow (g_1^V + g_2^V) \qquad \text{(non-flip)}$$

$$\frac{(3g_1^S + 2g_2^S)}{2} \qquad \left(\frac{g_1^V}{2} - \frac{g_2^V}{3}\right) \qquad \text{(flip)}$$

and

$$3g_1^S \rightarrow g_1^V$$

except at the following vertices:-

$$V^{-}_{\frac{1}{2},\frac{3}{2}}(p\Delta^+) = -\left(\frac{g_1^V}{2} - \frac{g_2^V}{3}\right)\frac{M_o}{M_+}\sqrt{\frac{2}{3}}$$

$$V^{-}_{\frac{1}{2},-\frac{3}{2}}(p\Delta^+) = -\left(\frac{g_1^V}{2} - \frac{g_2^V}{2}\right)\frac{\sqrt{3}\,M_o^2}{2\sqrt{2}\,M_+^2}$$

Boson Helicity Vertices

I = 0 exchange

$$V^{+}_{00}(\pi\pi) = 2(g^{S}_{1} + g^{S}_{2})$$

$$V^{+}_{00}(\rho\rho) = 2(g^{S}_{1} + g^{S}_{2})$$

$$V^{+}_{01}(\rho\rho) = 4g^{S}_{1} + 2g^{S}_{2}$$

$$V^{-}_{00}(\pi\rho) \quad 0$$

$$V^{-}_{01}(\pi\rho) = -\frac{g^{S}_{2} M_{o}}{\sqrt{2} M_{+}}$$

$$V^{+}_{00}(\pi B) = 2g^{S}_{1} g^{1}_{2} \frac{M_{o}}{M_{4}} - 2(g^{S}_{1} + g^{S}_{2}) T \frac{g^{1}_{1}}{M_{4} M_{o}}$$

$$V^{+}_{01}(\pi B) = -2(g^{S}_{1} + g^{S}_{2}) \frac{g^{1}_{1}}{2\sqrt{2}}$$

$$V^{+}_{00}(\pi A_{1}) \equiv 0$$

$$V^{+}_{01}(\pi A_{1}) = g^{S}_{2} \frac{g^{1}_{1}}{\sqrt{2}} \frac{T}{M_{4} M_{+}}$$

$$V^{-}_{02}(\pi A_{2}) = g^{S}_{2} \frac{g^{1}_{1} M_{o}}{4M_{+}}$$

$$V^{-}_{01}(\pi A_{2}) = g^{S}_{2} \frac{g^{1}_{1} T}{2M_{+} M_{4}}$$

$$V^{-}_{00}(\pi A_{2}) \equiv 0$$

$$V_{02}^{+}(\pi A_3) = 2(g_1^S + g_2^S)\frac{g_1^2}{8}$$

$$V_{01}^{+}(\pi A_3) = 2(g_1^S + g_2^S)\frac{T g_1^2}{2M_4 M_o} - \frac{g_1^S g_2^2 M_o}{2M_4}$$

$$V_{00}^{+}(\pi A_3) = 2(g_1^S + g_2^S)\left[\frac{t g_1^2}{4\sqrt{6} M_o^2} + \frac{2}{\sqrt{6}}\frac{T^2 g_1^2}{M_4^2 M_o^2}\right] - \frac{4g_1^S}{\sqrt{6}}\frac{T g_2^2}{M_4^2}$$

$$V_{03}^{-}(\pi g) = -\frac{g_2^S}{4\sqrt{2}}\frac{g_1^2 M_o}{M_+}$$

$$V_{02}^{-}(\pi g) = -\frac{g_2^S}{2\sqrt{3}}\frac{g_1^2 T}{M_+ M_4}$$

$$V_{01}^{-}(\pi g) = \frac{g_2^S}{M_+}\left[\frac{t g_1^2}{4\sqrt{30} M_o} + \frac{4}{\sqrt{30}} T^2 \frac{g_1^2}{M_4^2 M_o}\right]$$

$$V_{00}^{-}(\pi g) \equiv 0$$

$$V_{00}^{+}(KK) = (g_1^s + g_2^s) + (g_1^S + g_2^S)$$

$$V_{01}^{-}(KK^*) = -\frac{M_o}{2\sqrt{2} M_+}\left[g_2^s + g_2^S\right]$$

$$V_{00}^{-}(KK^*) = 0$$

$$V_{02}^{-}(KK^{**}) = \frac{M_o}{8M_+}\left[g_2^s + g_2^S\right] g_1^1$$

$$V_{01}^{-}(KK^{**}) = \frac{T g_1^1}{4 M_+ M_4}\left[g_2^s + g_2^S\right]$$

$$V_{00}^{-}(KK^{**}) = 0$$

Table 1.5.1(b)

Here, $T \equiv \frac{1}{4}(M_4^2 - M_2^2 + t)$. For isovector exchange make the substitutions $g_1^S \to g_1^V$, $g_2^S \to g_2^V$ using the values of $g_{1,2}^i$ given in Table 1.3.1 appropriate for the flavour of the particles at that vertex.

The helicity phase conventions used here are those of Jacob and Wick [35] except that we take $\phi = 0$ and do not include a factor $(-)^{s-\lambda_2}$ for "particle 2".

We have included the factor M_o ($\equiv \sqrt{s_o}$, the regge scale factor) in order to demonstrate explicitly the dimensionless nature of our covariant couplings g_i ($i \leq 2$), although in practice we set $s_o \equiv 1$ GeV^2.

CHAPTER 2

ELASTIC SCATTERING

2.1 Introduction

In Chapter 1, we introduced the reggeon-photon coupling analogy (RPCA) and proceeded to describe a detailed formalism with which the hypothesis could be tested. In this chapter, as a primary test of our ideas, we apply the model in detail to elastic scattering processes including pp, $\bar{p}p$, $K^{\pm}p$, demonstrating that the RPCA can account in a simple and natural way for all the elastic and total cross-section data.

2.2 Parametrization of elastic scattering amplitudes

The reggeon exchanges occurring in elastic scattering are shown in Table 2.2.1, in which the signs displayed are those of the imaginary part of the amplitude at small t required by duality; the relative signs from one charge state to another being fixed by the isospin and charge-conjugation properties of the trajectories.

PROCESS	EXCHANGE
$pp \to pp$	$P + f - \omega + A_2 - \rho$
$\bar{p}p \to \bar{p}p$	$P + f + \omega + A_2 + \rho$
$pn \to pn$	$P + f - \omega - A_2 + \rho$
$\bar{p}n \to \bar{p}n$	$P + f + \omega - A_2 - \rho$
$K^+p \to K^+p$	$P + f - \omega + A_2 - \rho$
$K^-p \to K^-p$	$P + f + \omega + A_2 + \rho$
$K^+n \to K^+n$	$P + f - \omega - A_2 + \rho$
$K^-n \to K^-n$	$P + f + \omega - A_2 - \rho$
$\pi^+p \to \pi^+p$	$P + f - \rho$
$\pi^-p \to \pi^-p$	$P + f + \rho$

Table 2.2.1: The regge exchanges occurring in elastic scattering.

From equations (1.5.1) and (1.5.2) in Chapter 1, the contribution of a reggeon R to the s-channel amplitude for $1 + 2 \to 3 + 4$ may be written in the form

$$A^{R}_{\lambda_1\lambda_2\lambda_3\lambda_4}(s,t) = -\left(-t\right)^{\frac{1}{2}|\lambda_1-\lambda_3| + |\lambda_2-\lambda_4|} V^{\pm}_{\lambda_1\lambda_3}(t)\, V^{\pm}_{\lambda_2\lambda_4}(t)\, R(s,\alpha(t)) \qquad (2.2.1)$$

where

$$R(s,\alpha(t)) = \frac{\alpha(t)}{\alpha(t)!}\left[\frac{e^{-i\pi\alpha(t)} + S}{2\sin\pi\alpha(t)}\right] s^{\alpha(t)} \qquad (2.2.2)$$

S is the signature and the λ_i $(i = 1,4)$ are the helicities. We assume, unless otherwise stated, nonsense decoupling at $\alpha(t) = 0$. In order to write down the contribution of any specific regge pole to the s-channel scattering amplitude, we need to know the form of $V^{\pm}_{\lambda_1\lambda_3}(t)$. The reggeon photon coupling analogy allows us to make specific statements about the regge coupling at any vertex in terms of the photon coupling to that vertex in the following way:-

The photon couplings to meson-meson and baryon-baryon vertices may be written as follows:

For mesons,

$$g^{\gamma}_{i}(t) = eF(t) \qquad (2.2.3)$$

where the form factor $F(t) \underset{t\to 0}{\to} 1$ by definition. At the $N\bar{N}$ vertex, following reference (33), we may write the nucleon electromagnetic current as

$$\bar{u}^{\pm}(p')\left(g_1 P_\beta + g_2 \gamma_\beta\right) u^{\pm}(p) = 2\left(M g^{\gamma}_{1}(t) + g^{\gamma}_{2}(t)\right) \qquad (2.2.4)$$

or, in the notation of reference (17), page 251

$$\bar{u}(p')\left[\left(G_V(t) + G_T(t)\right)\gamma_\beta - \frac{G_T(t) P_\beta}{M}\right] u(p) \qquad (2.2.5)$$

where p,p' are the nucleon momenta, defined in Figure 1.4.1, and $G_V(t)$, $G_T(t)$ are the vector and tensor couplings.

Evidently,

$$g_1^\gamma(t) = -\frac{G_T(t)}{M} \quad , \quad g_2^\gamma(t) = G_V(t) + G_T(t) \tag{2.2.6}$$

and are related to the nucleon electric and magnetic form factors $G_E(t)$, $G_M(t)$, by (see reference (17)

$$eG_E(t) = \left[(Mg_1^\gamma(t) + g_2^\gamma(t)) - \frac{t}{4M} g_1^\gamma(t)\right] \tag{2.2.7}$$

$$eG_M(t) = g_2^\gamma(t) \tag{2.2.8}$$

which obey the threshold constraint $G_E(4M^2) = G_M(4M^2)$. For the isoscalar coupling at $t = 0$, we know that

$$G_E^S(0) = \frac{1}{2} \quad , \quad G_M^S(0) = \frac{1}{2} + \frac{1}{2}(\kappa_p + \kappa_n) = 0.44 \tag{2.2.9}$$

while for the isovector coupling,

$$G_E^V(0) = \frac{1}{2} \quad , \quad G_M^V(0) = \frac{1}{2} + \frac{1}{2}(\kappa_p - \kappa_n) = 2.35 \tag{2.2.10}$$

where κ_p and κ_n are the proton and neutron anomalous magnetic moments. Thus from equations (2.2.4), (2.2.7) and (2.2.8) we can see that the isoscalar and isovector photon non-flip couplings to $N\bar{N}$ at $t = 0$ are given just by the charge (e) and, away from $t = 0$, by rearranging (2.2.7) and (2.2.8) by,

$$Mg_1^\gamma(t) + g_2^\gamma(t) = \frac{e\left[G_E(t) - \frac{t}{4M^2} G_M(t)\right]}{1 - \frac{t}{4M^2}} \tag{2.2.11}$$

The apparent singularity at $t = 4M^2$ is removed by the threshold constraint $G_E(4M^2) = G_M(4M^2)$. Similarly, for the isoscalar and isovector flip couplings, using the result

$$\bar{u}^{\pm}(p')\ (g_1 P_\beta + g_2 \gamma_\beta)\ u^{\mp}(p) = g_1^{\gamma}(t) \qquad (2.2.12)$$

it is easy to show that

$$Mg_1^{\gamma}(t) = \frac{e\left[G_E(t) - G_M(t)\right]}{1 - \frac{t}{4M^2}} \qquad (2.2.13)$$

Referring to Table 1.5.1, the helicity vertex functions at the $N\bar{N}$ vertex are:-

$$V^{+}_{\frac{1}{2},\frac{1}{2}}(0) = 3(g_1^S + g_2^S) = (g_1^V + g_2^V) \qquad \text{Helicity non-flip isoscalar and isovector couplings} \qquad (2.2.14)$$

$$V^{+}_{\frac{1}{2},-\frac{1}{2}}(0) = 0 = \frac{(3g_1^V + 2g_2^V)}{2M_p} \qquad \text{Helicity flip isoscalar and isovector couplings} \qquad (2.2.15)$$

while at the spinless meson vertex

$$V^{+}_{oo}(0) = 2(g_1^S + g_2^S) \quad 2(g_1^V + g_2^V) \qquad \text{Isoscalar and isovector couplings} \qquad (2.2.16)$$

where the $g_i^{S,V}$ $(i = 1,2)$ are the photon isoscalar and isovector quark couplings at $t = 0$ from Table 1.3.1. Inserting these g_i's into (2.2.14) - (2.2.16) above gives, at the meson vertex

$$V^{+}_{oo}(0) = \frac{2e}{3}\left(\frac{e}{3}\right)_{\pi\pi\,(KK)} \quad I = 0$$

$$2e\ \ (e)_{\pi\pi\,(KK)} \quad I = 1 \qquad (2.2.17)$$

and at the baryon vertex

$$V^{+}_{\frac{1}{2},\frac{1}{2}}(0) \quad = \quad e \ (I = 0) = V^{+}_{\frac{1}{2},\frac{1}{2}}(0) \ (I = 1)$$

(2.2.18)

$$V^{+}_{\frac{1}{2},-\frac{1}{2}}(0) \quad = \quad (I = 0) \equiv 0 \ , \quad V^{+}_{\frac{1}{2},-\frac{1}{2}}(0) \ (I = 1) = \frac{-2e}{M_p}$$

Thus we may write the photon coupling generally as

$$V_{\substack{\lambda_1\lambda_3 \\ \lambda_2\lambda_4}}(0) \quad \bar{F}_B(t) \tag{2.2.19}$$

(with our hypothesis (the GAH) that the couplings corresponding to $\Delta\lambda_t = \pm 1$ (the maximum allowed by the VCH) are related to the electromagnetic form factors, that is to say, the dominant I = 0 natural parity regge trajectories (the P,f and ω) couple like the isoscalar part of the photon, while the I = 1 natural parity regge trajectories (the ρ and A_2) couple like the isovector photon, then using (2.2.18) and (2.2.19), we see immediately that the I = 0 flip: non-flip ratio = 0, and the I = 1 flip: non flip ratio = $2/M_p$. Hence the P,f and ω have only non-flip couplings to $N\bar{N}$, while the ρ and A_2 have predominantly flip couplings to $N\bar{N}$) where the factor $\bar{F}_B(t)$ (B = |baryon number|) is given by the t-dependence of the electromagnetic form factor (since we assume the same form for $G_E(t)$ and $G_M(t)$):

$$F_B(t) \quad = \quad \left(1 - \frac{t}{M_\rho^2}\right)^{-1} \quad \bar{F}_B(t) \tag{2.2.20}$$

where the form of (2.2.20) above is demanded by our ρ,ω-photon coupling analogy, that is we require the reggeized ρ pole to be incorporated into our regge pole exchanges.

Empirically, the factor $\bar{F}_B(t) = 1$ for B = 0. That is, the pion and kaon form factors are given reasonably well by the rho pole alone (36).

For B = 1, in order to describe $G_E(t)$ and $G_M(t)$ for nucleons (the p and n electromagnetic form factors) we require

$$\bar{F}_1(t) = \left(1 - \frac{t}{0.9}\right)^{-1} \qquad (2.2.21)$$

Shown in Figure 2.2.1 is a fit to the proton magnetic (= electric in our model) form factor using this parametrization, where we note, that the above description is at least as good as the more usual dipole fit, even out to quite large $|t|$.

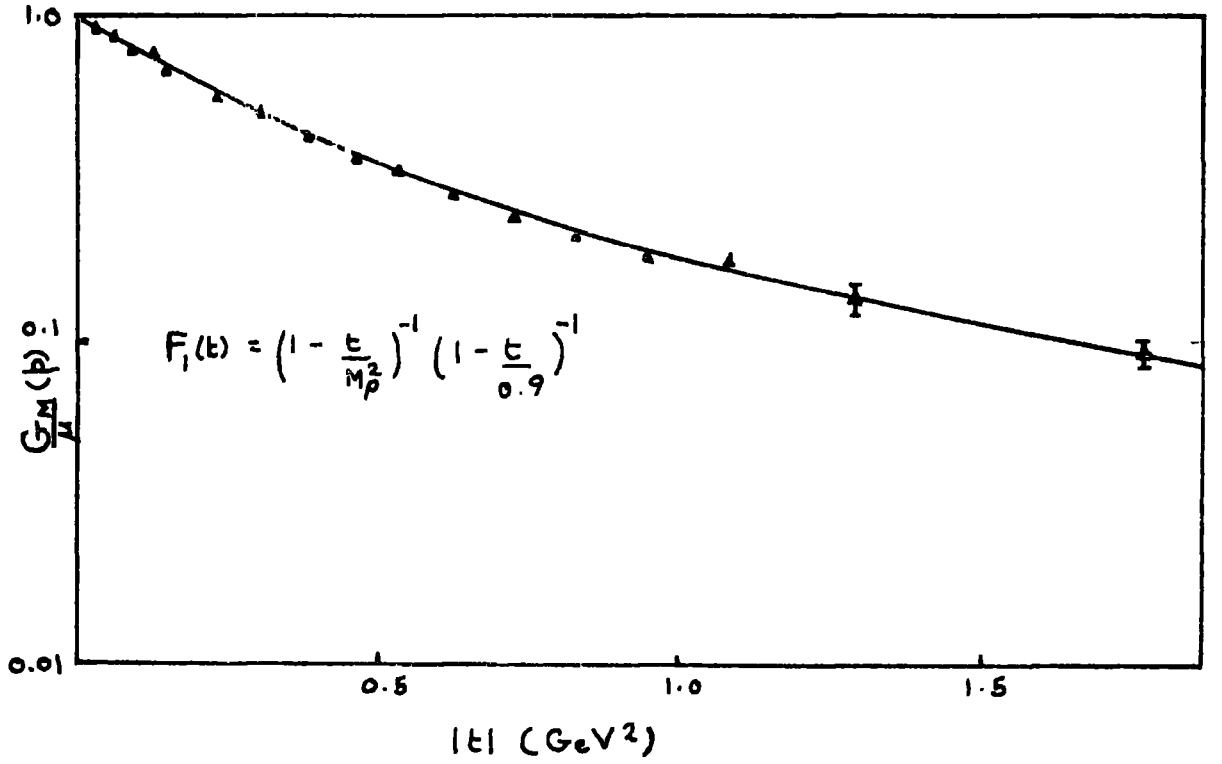

Figure 2.2.1: The proton magnetic form factor data (37) compared with $F_1(t)$ given in equation (2.2.20)

Using equations (1.2.7) and (1.2.8), we can relate the photon-particle coupling, written generally in (2.2.19) as $V^{\pm}_{\lambda,\lambda'}(0)\ \bar{F}_B(t)$, which we have determined in terms of the g_i's, the photon-quark couplings, and $\bar{F}_B(t)$ from (2.2.20), to the leading natural parity regge exchanges in the following way:-

Equations (1.2.7) and (1.2.8) are

$$g_i^P(t) = \rho_F(t)\ g_i^f(t) = \rho_F(t)(1+\varepsilon_B)\ g_i^\omega(t) = \frac{f_\omega(t)}{e}(1+\varepsilon_B)\ \rho_F(t)\ g_i^{\gamma_S}(t) \tag{2.2.22}$$

and

$$g_i^{A_2}(t) = (1+\varepsilon_B')\ g_i^\rho(t) = \frac{f_\rho(t)}{e}(1+\varepsilon_B')\ g_i^{\gamma_V}(t) \tag{2.2.23}$$

The constants f_ω and f_ρ are the $\omega-\gamma$ and $\rho-\gamma$ coupling constants respectively. f_ω is defined by

$$\Gamma_{\omega\to e^+e^-} = \frac{4\pi\alpha^2}{3}\ \frac{M_\omega}{f_\omega^2} \tag{2.2.24}$$

and from the ideally mixed quark model (20), $f_\rho = \frac{f_\omega}{3}$ (which in fact gives the ratio $\Gamma_{\rho\to e^+e^-} : \Gamma_{\omega\to e^+e^-} = 9$, c.f. the experimental result (38) of $8.42 \pm .7$). In order for us to maintain the above definition of f_ω and f_ρ, when inserted in the regge residues, we must multiply by $\sqrt{\frac{\pi\alpha'_{\rho,\omega}}{2}}$ (see, for example, Collins and Squires (39), page 62 ff.)

Thus, from equations (2.2.22) and (2.2.20), the ω coupling at the $N\bar{N}$ vertex is given by

$$V^+_{\frac{1}{2},\frac{1}{2}}(pp\omega) = \frac{f_\omega}{e}\sqrt{\frac{\pi\alpha'_\omega}{2}}\ V^+_{\frac{1}{2},\frac{1}{2}}(0)\ \bar{F}_1(t) \tag{2.2.25}$$

$$= \frac{f_\omega}{e}\sqrt{\frac{\pi\alpha'_\omega}{2}}\ e\ \bar{F}_1(t) \tag{2.2.26}$$

from (2.2.18), while for the f coupling,

$$V^+_{\frac{1}{2},\frac{1}{2}}(ppf) = \frac{f_\omega}{e}\sqrt{\frac{\pi\alpha'_\omega}{2}}\ (1+\varepsilon_1)\ e\ \bar{F}_1(t) \tag{2.2.27}$$

The pomeron (P) coupling to any allowed vertex is

$$V^{\pm}_{\lambda_1\lambda_3}(P) = e(1+\varepsilon_B)\frac{f_\omega}{e}\sqrt{\frac{\pi\alpha'_\omega}{2}}\ \bar{F}_B(t)\ \rho_F(t) \qquad (2.2.28)$$

(where $\lambda_1 = \lambda_3$)

while the isovector non-flip couplings to $N\bar{N}$ are given by

$$\left.\begin{aligned} V^{+}_{\frac{1}{2}\frac{1}{2}}(pp\rho) &= \frac{f_\omega}{3e}\sqrt{\frac{\pi\alpha'_\rho}{2}}\ e\,\bar{F}_1(t)\ , \\ V^{+}_{\frac{1}{2}\frac{1}{2}}(ppA_2) &= \frac{f_\omega}{3e}\sqrt{\frac{\pi\alpha'_\rho}{2}}\ e\,\bar{F}_1(t)\ (1+\varepsilon'_1) \end{aligned}\right\} \qquad (2.2.29)$$

The isovector flip couplings to $N\bar{N}$ are ,

$$\left.\begin{aligned} V^{\pm}_{\frac{1}{2}-\frac{1}{2}}(pp\rho) &= \frac{f_\omega}{3e}\sqrt{\frac{\pi\alpha'_\rho}{2}}\ \frac{2e}{M_p}\ \bar{F}_1(t) \\ V^{+}_{\frac{1}{2}-\frac{1}{2}}(ppA_2) &= \frac{f_\omega}{3e}\sqrt{\frac{\pi\alpha'_\rho}{2}}\ \frac{2e}{M_p}\ \bar{F}_1(t)\ (1+\varepsilon'_1) \end{aligned}\right\} \qquad (2.2.30)$$

At the spinless meson vertex, the relations are very similar, viz:

$$\left.\begin{aligned} V^{+}_{oo}(\pi\pi f) = V^{+}_{oo}(KKf) &= \frac{2e}{3}(1+\varepsilon_o)\frac{f_\omega}{e}\sqrt{\frac{\pi\alpha'_\omega}{2}}\ \bar{F}_o(t) \\ V^{+}_{oo}(\pi\pi\rho) = V^{+}_{oo}(KK\rho) &= 2e\,(1+\varepsilon_o)\frac{f_\omega}{3e}\sqrt{\frac{\pi\alpha'_\omega}{2}}\ \bar{F}_o(t) \end{aligned}\right\} \qquad (2.2.31)$$

From inspection of the above coupling formulae it is clear that the difference in t-dependence of the reggeon couplings at meson-meson (MM) and baryon-baryon (BB) vertices is given just by $\bar{F}_1(t)$ (since $\bar{F}_o(t) \equiv 1$). Thus we predict that the ratio $\frac{d\sigma}{dt}(pp) : \frac{d\sigma}{dt}(\pi p)$ will be given by $\left(\frac{3}{2}(1+\varepsilon_1)\bar{F}_1(t)\right)^2$. In Figure 2.2.2 we display our prediction against the ratio $\frac{d\sigma}{dt}(pp/\pi p)$, using ε_1 - the exchange degeneracy breaking factor

(to be discussed shortly) = 0.14. We note that for $|t| \gtrsim 0.6$, the data falls beneath the predicted curve. This might have been anticipated from the fact that P⊗P cuts are known (40) to be present in pp, but not πp, scattering in order to account for the diffractive minimum at $|t| = 1.4$ GeV^2. However, at small $|t|$, where any cut contribution should be small, our prediction describes the data quite well.

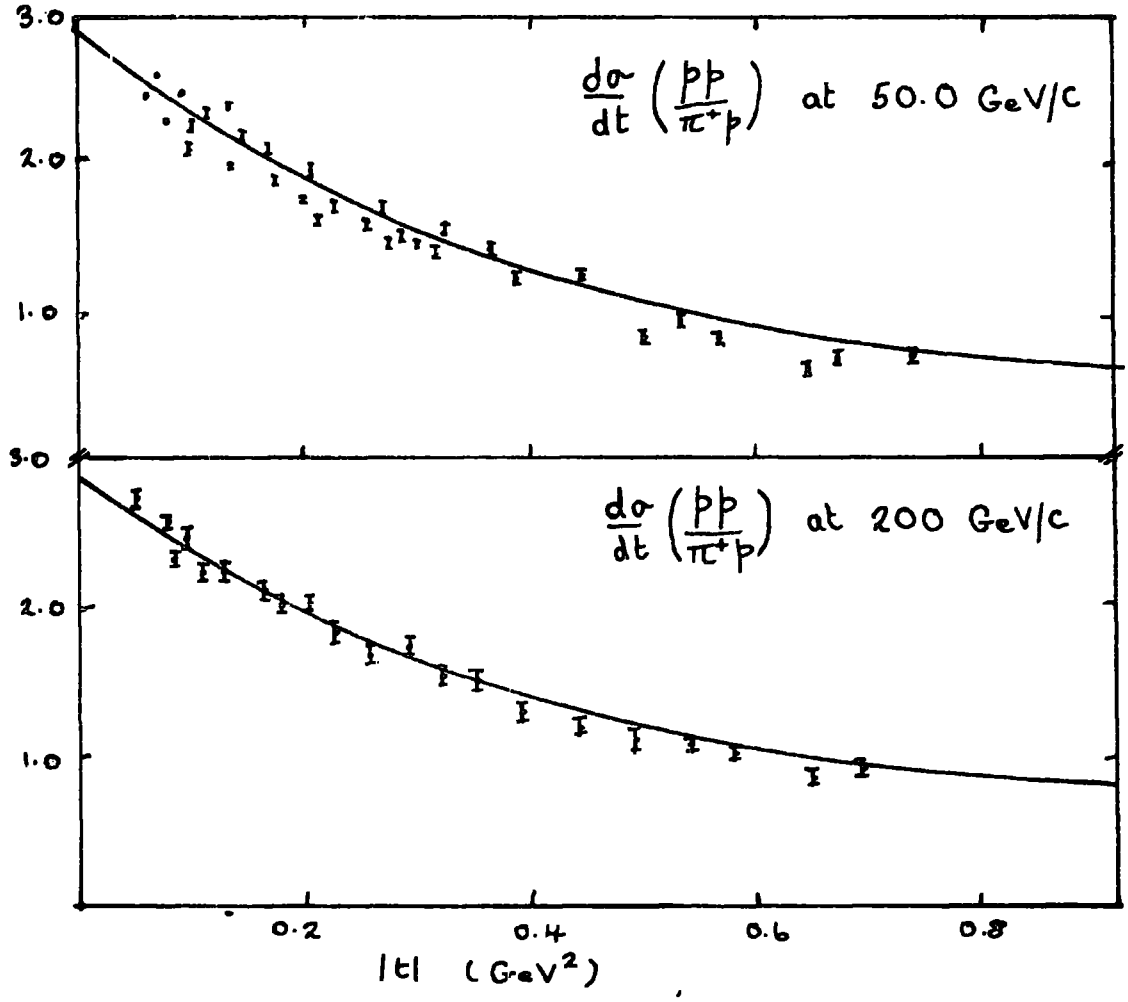

Figure 2.2.2: The ratio of $\frac{d\sigma}{dt}(pp) : \frac{d\sigma}{dt}(\pi^+p)$ compared with $(1.7\ \bar{F}_1(t))^2$ which should at high energies, where the pomeron dominates, given the cross-section ratio. Data from reference (41).

The factor ε_B appearing in equation (2.2.22) ff. is the exchange degeneracy breaking factor and is set equal to zero for isovector exchanges at any vertex, that is $\varepsilon'_{0,1} \equiv 0$. ε_B is also found to be zero for isoscalar

exchanges at meson vertices, leaving the value of $c_B \neq 0$ only at baryon vertices. In a recent analysis by Roberts et al. (42) it has been suggested that the $K^{\pm}p$ and $\pi^{\pm}p$ data are compatible with exact $f - \omega$ exchange degeneracy provided that the pomeron contribution is non-monotonic. After a similar analysis we have found the πp and Kp total cross-section data to be compatible with approximate exchange degeneracy, that is the degeneracy is broken in trajectory but not in residue, in which case a simple monotonic pomeron with $\alpha_P(0) > 1$ describes the data very well. We also note that the same condition applies to the ρ and A_2, where $\alpha_\rho(0) = 0.51$ in order to describe the πN charge exchange data.

However, if we now demand factorization, we insist on the same approximate exchange degeneracy in pp scattering, which is incompatible with the $\sigma_{pp}^{tot}(s)$ data, which falls sharply at low s. Hence we conclude that meson vertices have exchange degenerate $f - \omega$ and $\rho - A_2$ couplings, but at baryon vertices, the exchange degeneracy is broken for isoscalar exchange. This result is, however, not completely surprising, since duality (12) requires exotic resonances in BB scattering, an example of which is shown in Figure 2.2.3.

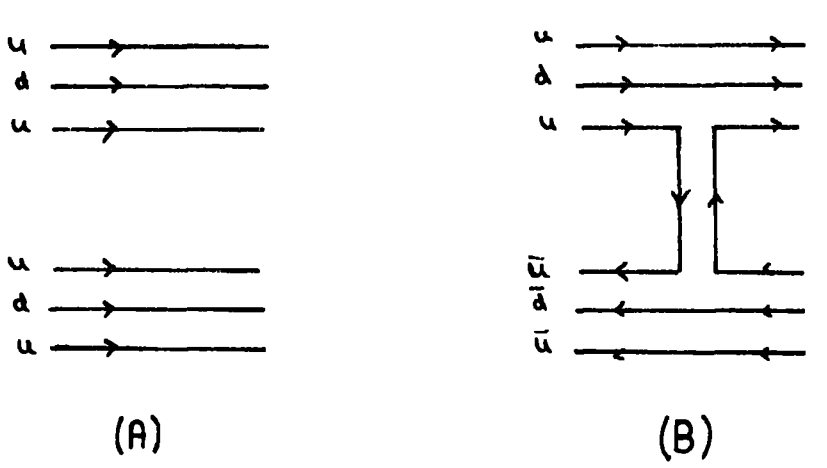

Figure 2.2.3: (A) pp scattering with exotic s-channel and
(B) $\bar{p}p$ scattering, where s-channel resonances may be formed.

Thus, in the case of pp scattering, as in Figure 2.2.3A, the duality requirement of exotic resonances implies that the t-channel non-diffractive regge exchanges must vanish, giving a completely flat pp total cross-section (rising slowly if $\alpha_p(0) > 1$). The fact that $\sigma_{pp}^{tot}(s)$ is not flat implies $f \neq \omega$ and hence our value of $\varepsilon_1 = 0.14$ reflects the failure of simple duality (Figure 2.2.3A) for processes involving baryons.

Although we might hope that the coupling relations (2.2.25) - (2.2.31) will hold without further modification there is, of course, the well-known complication of rather strong absorption in the ρ and ω non-flip amplitudes, producing a cross-over zero in the imaginary part of these amplitudes at $|t| \sim 0.1$ GeV^2 (0.13 GeV^2 at 6.0 GeV/C (43) for the ρ) and not at $\alpha(t) = 0$ as it would be in a nonsense decoupling regge pole model. In order to take account of this rather strong absorption we make the following replacements in equation (2.2.2).

$$\text{In} \quad \mathrm{ImA}^{\omega}_{0\frac{1}{2}0\frac{1}{2},\frac{1}{2}\frac{1}{2}\frac{1}{2}\frac{1}{2}} \qquad \alpha_\omega(t) \to \alpha_\omega(0)(1 + t/t_o)$$

$$\text{in} \quad \mathrm{ImA}^{\rho}_{0\frac{1}{2}0\frac{1}{2},\frac{1}{2}\frac{1}{2}\frac{1}{2}\frac{1}{2}} \qquad \alpha_\rho(t) \to \alpha_\rho(0) \times (1 + t/t_o)\, e^{C_\rho t} \qquad (2.2.32)$$

$$\text{in} \quad \mathrm{ImA}^{A_2}_{0\frac{1}{2}0\frac{1}{2},\frac{1}{2}\frac{1}{2}\frac{1}{2}\frac{1}{2}} \qquad \alpha_{A_2}(t) \to x\, \alpha_{A_2}(t)$$

where we have anticipated absorption in the A_2 non-flip amplitude. In (2.2.32), t_o is the observed position of the cross-over zero which for simplicity we take to be equal in both the ρ and the ω , and set equal to 0.19, while x represents the effective change in magnitude of the ρ and A_2 couplings produced by the absorptive cut correction. The factor C_ρ gives the t-dependence induced in the ρ pole coupling, and is required to reduce the otherwise large negative magnitude of the ρ non-flip amplitude at $0.25 < |t| < 0.6$ GeV^2 which would fill in the dip at $|t| \approx 0.6$ GeV^2 in the

πN charge exchange differential cross-section. In Figure 2.2.4 we show a plot of $ImA_{++}(\rho)$ taken from Barger and Halzen (44) against our ρ pole as prescribed by (2.2. 2) and the ρ pole with absorptive corrections. While our amplitude is not a perfect description of the data, the representation is quite good bearing in mind the over-simplified form of our absorptive corrections. However, the other ρ amplitudes are in reasonable agreement with the data from reference (44).

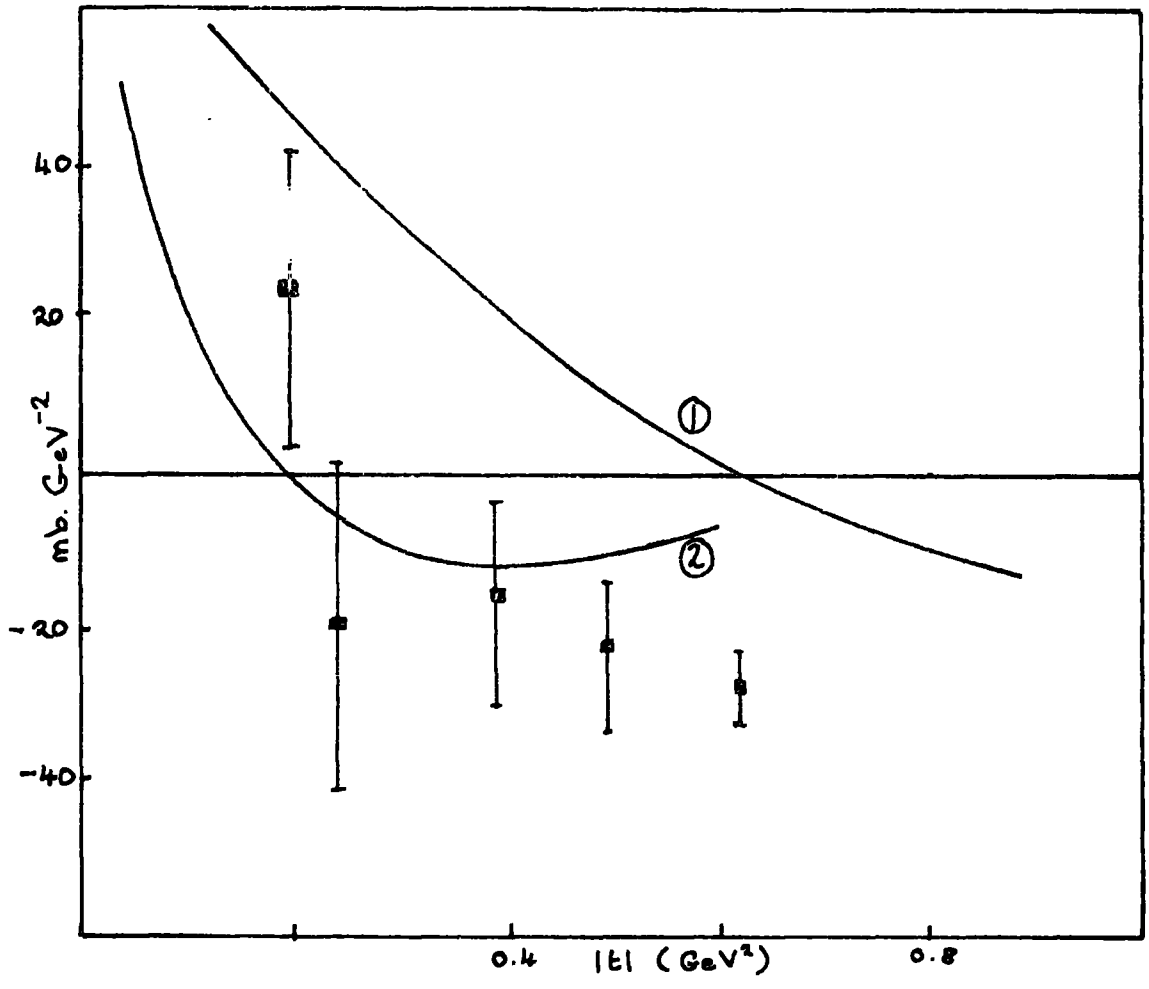

Figure 2.2.4: The imaginary part of the s-channel ρ non-flip helicity amplitude from reference (44). Curve (1) is our unabsorbed ρ pole. Curve (2) is our ρ pole absorbed as in equation (2.2.32).

This, along with the large $|t|$ pp differential cross-section data (see, for example, reference (40)) is the only feature in all of the elastic scattering data which requires us to take explicit account of the

exchange of regge cuts. In the latter case, however, we will include the cut explicitly, as will be demonstrated in the next section. For all the other amplitudes, we may rely on the fact that there is little difference between a nonsense zero and an absorptive correction, and that most amplitudes appear to have regge-pole energy dependences, even out to large $|t|$ (46).

Finally, the pomeron : f ratio is written in the form

$$\rho_F(t) = \rho(0)\, e^{at}\, (1 - \frac{t}{\bar{t}})^{-1}\, r_F(t) \qquad (2.2.33)$$

The parameters $\rho(0)$, a and $\bar{t}$ are arbitrary constants to be determined by fits to the data, but their arrangement in (2.2.33) above motivated by the overall shape of the elastic MB and BB cross-sections at small $|t|$. The factor $r_F(t)$ depends upon the flavour, F, of the quarks at a vertex, and through the FDP model is given by the trajectory function of the $f,f',f_{c...}$ mesons as follows.

Assuming ideal mixing (see, for example, Kokkadee, reference (20)), we have

$$f = \frac{1}{\sqrt{3}}\, f_8 + \frac{2}{\sqrt{3}}\, f_1$$

$$f' = \frac{2}{\sqrt{3}}\, f_8 - \frac{1}{\sqrt{3}}\, f_1 \qquad (2.2.34)$$

where f_1 and f_8 are the SU(3) singlet and octet isosinglets respectively. Referring to Figure 2.2.5, which is presented in a way analogous to that of Carlitz, Green and Zee (5), (see also Chapter 1, Figure 1.2.4),

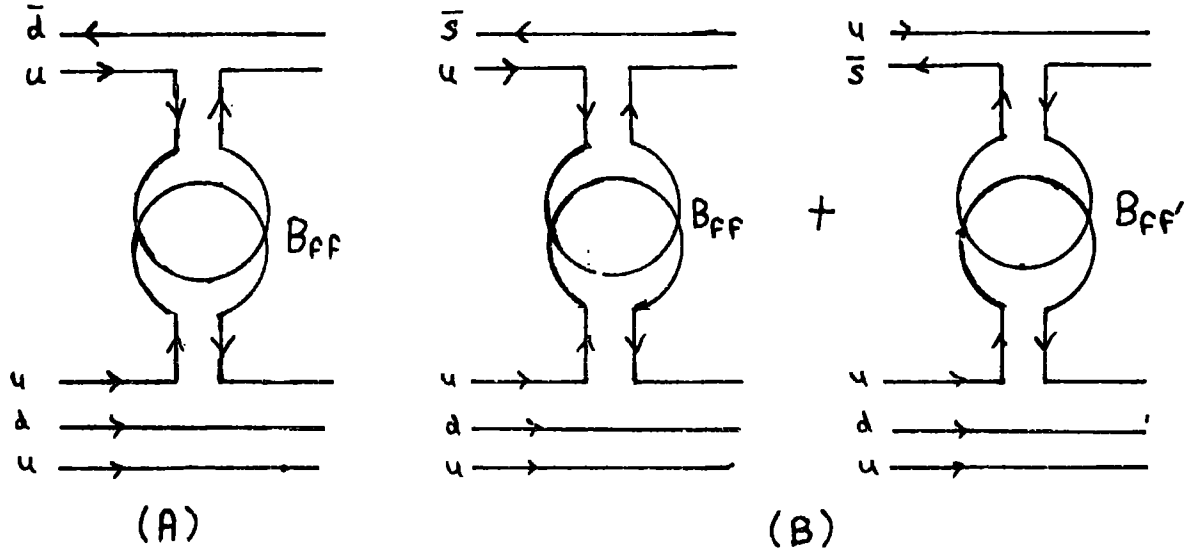

Figure 2.2.5: The f-dominated pomeron coupling for (A) πp and (B) Kp elastic scattering, with ideal mixing so the f' decouples from any vertex containing only non-strange quarks. B_{ff} and $B_{ff'}$ represent the central loop and its couplings to f and f'.

We see that the f' is decoupled from the $\pi\pi$ vertex, and so that P:f coupling ratio is

$$\frac{g^{P_{\pi\pi}}}{g^{f_{\pi\pi}}} = \frac{B_{ff}^{\frac{1}{2}}}{\alpha_P(0) - \alpha_f(0)} \equiv \rho(0) \qquad (2.2.35)$$

where $\rho(0)$ is the P : f ratio at $t = 0$ for non-strange vertices, and B_{ff} represents the f couplings to the pomeron loop, while at the $K\bar{K}$ vertex (Figure 2.2.5(B))

$$\frac{g^{PKK}}{g^{fKK}} = \frac{B_{ff}^{\frac{1}{2}}}{\alpha_P(0) - \alpha_f(0)} + \frac{g^{f'KK}}{g^{fKK}} \frac{B_{ff'}^{\frac{1}{2}}}{\alpha_P(0) - \alpha_{f'}(0)} \qquad (2.2.36)$$

In the limit of exact SU(3) (n) symmetry, the pomeron would couple through degenerate f and f' (and f_c, f_b ...) trajectories. When SU(3) (n) is broken, the f', f_c... masses become greater than the f mass,

and hence the trajectories lie lower than the f. It is traditional to assume that this is the only manifestation of the broken symmetry, that is the masses shift, but the couplings remain SU(3) (n) symmetric. Thus, $B_{ff}, B_{ff'}, \ldots$ remain singlets (that is, $B_{ff}\ldots$ etc. contain an equal mixture of u,d,s,c,t... quarks), coupling with relative strengths 1 and 1/2 to the f and f'(f_c,f_b...) trajectories. Thus,

$$g^{f'PP} = \frac{-1}{\sqrt{2}}\, g^{fPP} \qquad (2.2.37)$$

and for the symmetric (D-type) coupling,

$$g^{f'KK} = -\sqrt{2}\; g^{fKK} \qquad (2.2.38)$$

Hence at t = 0, (2.2.36) becomes

$$\frac{g^{PKK}}{g^{fKK}} = \frac{B_{ff}^{\frac{1}{2}}}{\alpha_P(0) - \alpha_f(0)} \; -\sqrt{2}\left(-\frac{1}{\sqrt{2}}\right) \frac{B_{ff'}^{\frac{1}{2}}}{\alpha_P(0) - \alpha_{f'}(0)} \qquad (2.2.39)$$

and remembering that $\rho(0) = \dfrac{B_{ff}^{\frac{1}{2}}}{\alpha_P(0) - \alpha_f(0)}$,

$$\frac{g^{PKK}}{g^{fKK}} = \rho(0)\left[1 + r_s(0)\right] \qquad (2.2.40)$$

where

$$r_s(0) = \frac{\alpha_P(0) - \alpha_f(0)}{\alpha_P(0) - \alpha_{f'}(0)} \qquad (2.2.41)$$

with obvious extensions to vertices containing charmed, top, bottom etc. quarks. Hence for $t \neq 0$, we may write our "universal" P:f ratio $\rho_F(t)$ as in equation (2.2.33), where $\rho_F(t)$ represents B_{ff} $B_{ff'}$ ... and the factors $r_F(t)$ are given in Table 2.2.2.

quark	u	d	s	c	b
$r_F(t)$	1	1	$\frac{\alpha_p(t) - \alpha_f(t)}{\alpha_p(t) - \alpha_{f'}(t)}$	$\frac{\alpha_p(t) - \alpha_f(t)}{\alpha_p(t) - \alpha_{f_c}(t)}$	$\frac{\alpha_p(t) - \alpha_f(t)}{\alpha_p(t) - \alpha_{f_b}(t)}$

Table 2.2.2: The f-dominated pomeron coupling coefficients as used in equation (2.2.33).

Having thus described the terms appearing in equations (2.2.23) to (2.2.31) inclusively we have, in principle, determined our scattering amplitudes. However, a roll-call of free parameters tells us that we have in all 22 arbitrary parameters which the data should determine. In fact, we are in a position to determine 14 of the 22 parameters by constraining all our regge trajectories to be linear and pass through (or lie within 50 MeV of) the particles lying on them. The results of this constraint are given in Table 2.2.3. In order to determine the T trajectory, we first fitted the I = 0 trajectories (the ω, ϕ and ψ) with a function quadratic in M, that is we set

$$AM^2 + BM + C = \alpha_o \qquad (2.2.42)$$

inserting the values of α_o and M for the ω, ϕ and ψ respectively from Table 2.2.3 and then solving the simultaneous equations. We have found that A = -0.166, B = -0.156 and C = 0.667 and, using M_T = 9.4 GeV, gave the T trajectory parameters as shown below.

In the next section we determine the 8 residual free parameters and describe our fit to the data.

Trajectory	α(t)	Theory (MeV)	Experiment (MeV)	Theory (MeV)	Experiment (MeV)
P	1.068+ 0.1 t				
f	0.49 + 0.95 t	f(1260)	1271 ± 5	h(1992)	2040 ± 20
f'	0.27 + 0.72 t	φ(1007)	1020 ± 3	f'(1550)	1516 ± 10
f_c	-2.10 + 0.33 t	ψ(3065)	3097 ± 2	χ(3524)	3554 ± 5
f_b	-15.45 + 0.19 t	Υ(9400)	[9400]		
ω	0.40 + 0.96 t	ω(790)	783 ± 3	ω*(1645)	1668 ± 10
ρ	0.51 + 0.85 t	ρ(759)	776 ± 3	ϒ(1711)	1688 ± 20
A_2	0.42 + 0.85 t	A_2(1363)	1312 ± 5	A_2^*(2052)	⩾1900†

Table 2.2.3: Trajectory functions used in all our fits to the data. All data from reference (38) except † (reference (45)). The [ ] denotes input (see text), and the P parameters are fitted.

2.3 Fit to the Data

(a) Total cross-sections

As a preliminary exercise we isolate, using Table 2.2.1, the ω, ρ and A_2 trajectory contributions to the total cross-sections by forming cross-section differences as follows:

$$\sigma_{pp}(\omega) = \tfrac{1}{4}(\sigma(\bar{p}p) + \sigma(\bar{p}n) - \sigma(pp) - \sigma(pn))$$

$$\sigma_{Kp}(\omega) = \tfrac{1}{4}(\sigma(K^-p) + \sigma(K^-n) - \sigma(K^+p) - \sigma(K^+n))$$

$$\sigma_{pp}(A_2) = \tfrac{1}{4}(\sigma(\bar{p}p) - \sigma(\bar{p}n) + \sigma(pp) - \sigma(pn))$$

$$\sigma_{Kp}(A_2) = \tfrac{1}{4}(\sigma(K^-p) - \sigma(K^-n) + \sigma(K^+p) - \sigma(K^+n))$$

$$\sigma_{pp}(\rho) = \tfrac{1}{4}(\sigma(\bar{p}p) - \sigma(\bar{p}n) - \sigma(pp) + \sigma(pn))$$

$$\sigma_{Kp}(\rho) = \tfrac{1}{4}(\sigma(K^-p) - \sigma(K^-n) - \sigma(K^+p) + \sigma(K^+n))$$

$$\sigma_{\pi p}(\rho) = \tfrac{1}{2}(\sigma(\pi^-p) - \sigma(\pi^+p))$$

where $\sigma(pp)$ etc. $\equiv \sigma_{pp}^{tot}(s)$

The fits shown in Figure 2.3.1 (at the end of this chapter) determine the trajectory intercepts α_o which, of course, serve as a consistency check of Table 2.2.3, and also the effective couplings in equations (2.2.25) - (2.2.31), that is f_ω and xf_ρ ($\equiv x\frac{f_\omega}{3}$), where f_ω is found to be 17.1, in accord with the value of 15.1 ± 2 deduced from the decay $\omega \to e^+e^-$ (see equation (2.2.24). The value of x is found to be equal to 0.435, which implies strong absorption of the ρ and A_2 at t = 0. Of course such absorption is to be anticipated given our discussion of the πN charge exchange data at 6.0 GeV/C (43) in the preceding section. However, the fact that no such reduction is required for the ω at t = 0 is surprising in view of the similar amount by which the ρ and ω zeroes in the non-flip imaginary part of the amplitude have been moved towards t = 0.

Inspection of Figure 2.3.1 shows that the combination of the total cross-section data giving $\sigma_{pp}(A_2)$ (from 2.3.1) is negative at low and medium values of s. Given the difficulty of extracting accurate data from neutron targets, we conclude that the errors have been under-estimated, and therefore attach less significance to these particular points.

Having determined the ρ, ω and A_2 regge pole contributions we proceed to fit the total cross-section data (47) on pp, $\bar{p}p$, pn, $\bar{p}n$, K^+p, K^-p, K^-n, π^+p and π^-p from a p_{LAB} of 4.0 GeV/C up to the highest available energy (I.S.R. energies in the case of pp, ≈ 280 GeV/C for the other processes). A fit to high energy $\sigma_{pp}^{tot}(s)$ alone determines the pomeron intercept to be 1.0688, while a fit to the whole data set determines ϵ_1, the isoscalar exchange degeneracy breaking factor at baryon vertices, to be 0.14 and ρ(0), the P:f ratio at t = 0, equal to 0.47. The resulting economical fit is presented in Figure 2.3.2. (We give a complete list of all coupling parameters in Table 2.3.1).

It is perhaps worth noting that with our value of $\alpha_P(0) > 1$, the actual value of the P:f ratio at t = 0 is rather different from earlier

fits (14) using $\alpha_p(0) \leq 1$. However, we find that our parametrization strongly supports the f-dominated pomeron hypothesis. In fact, allowing a different P:f ratio for BB and MB processes made no significant change to the overall χ^2/pt, while the global value of $\rho(0) = 0.47268$ moved to 0.46921 for baryon-baryon processes and remained the same for meson-baryon scattering.

The only minor difficulty encountered with the above description of total cross-sections was one of slightly ($\approx 5\%$) under-fitting $\sigma_{pp}^{tot}(s)$ and $\sigma_{\bar{p}p}^{tot}(s)$ at low s. As we have confidence in the magnitude of the ρ, ω and A_2 contributions (see Figure 2.3.1), we conclude that this extra contribution must come from another exchange lower lying in the J plane, that is a daughter to the f or to the f'. The f' exchange was ruled out on the grounds that (a) if present, it must couple strongly to $K\bar{K}$, and inclusion thereof significantly worsened the fit to $\sigma_{Kp}^{tot}(s)$, despite dramatic alteration to the other coupling parameters; and (b) the f' exchange when included in $\sigma_{pp}^{tot}(s)$ interfered with the other amplitudes in such a way as to destroy the previously reasonable description of δ , the ratio ReA :ImA at t = 0.

On the other hand, recent analysis (48) of low energy ($\leq$11.8 GeV/C) pp elastic polarization data has concluded that the I = 0 amplitude at these energies is best described by a pole of intercept $\simeq$ -0.5. Guided by this information, we have included in our fit to pp and $\bar{p}p$ a daughter to the f, the S*, with intercept $\alpha_{S^*}(0) = \alpha_f(0) - 1$ and parametrized in an otherwise identical way to the f (apart from an arbitrary coupling magnitude) We refer the reader to Figure 2.3.2 where we display our fit to $\sigma_{MB,BB}^{tot}(s)$. In Figure 2.3.3 we show our successful prediction of δ($\delta \equiv$ ReA/ImA at t = 0) for πp, pp and Kp scattering (49).

At high energies, where the pomeron dominates, the ratios of the total cross-sections are given by

$$\sigma_{pp}^{tot}(s) : \sigma_{\pi p}^{tot}(s) = \frac{3}{2}(1 + \varepsilon_1) = 1.71 \qquad (2.3.2)$$

$$\sigma_{Kp}^{tot}(s) : \sigma_{\pi p}^{tot}(s) = \frac{1 + r_s(0)}{2} = 0.87 \qquad (2.3.3)$$

So the quark model ratio (20) for pp : πp is modified by the fact that f - ω exchange degeneracy is broken at the pp vertex but not at the ππ vertex. The Kp : πp ratio is the standard result of the FDP hypothesis but with $\alpha_p(0) > 1$, our value is slightly different from some previous estimates (14).

Before continuing our parametrization away from t = 0 we mention, by way of a brief aside, the cosmic ray pp total cross-section data (50), displayed in Figure 2.3.2. Using this data, we attempted to distinguish between a power, logs or $\log^2 s$ behaviour of the total cross-section. In a recent paper Lipkin(51) has fitted the $\sigma_{pp}^{tot}(s)$ with a combination of regge pole terms at low s, and two power terms $s^{\delta} + s^{\varepsilon}$, where $\delta = 0.185$ and $\varepsilon = 0.13$, at higher energies. However, after a similar analysis of the data, we conclude that it is not possible to make a clear distinction between a simple power of s, that is s^{α_o}, $\alpha_o > 1$, and more complicated $\log s/s_o$, $\log^2 s/s_o$, $(\log s/s_o)^{\gamma}$.... etc. terms since, although the data reported by Yodh (50) matches on to the I.S.R. data quite well, the errors involved are rather large.

(b) Charge exchange differential cross-sections

Since the regge trajectory slopes are determined by the particle masses (see Table 2.2.3), and the value of f_ρ ($\equiv \frac{f_\omega}{3}$) and x have been determined by the total cross-section fits, the A_2 amplitudes in $\pi^- p \to \eta n$ and the ρ amplitudes in $\pi^- p \to \pi^o n$ are completely determined, except for the single free parameter c_ρ in the imaginary part of the ρ non-flip amplitude (see equation (2.2.32). We present in Figure 2.3.4 our prediction of the

$\pi^- p \to \eta n$ differential cross-section, against the data from reference (52) and our prediction/fit of the $\pi^- p \to \pi^o n$ cross-section, with data from reference (53). We can also predict the KN charge exchange reactions with these exchanges, but it is well known (54) that they obey the SU(3) sum rule very well, so nothing new is learned. As we have mentioned previously, our πN amplitudes are in good agreement with those determined by Halzen and Michael (43) at 6.0 GeV/C although, as displayed in Figure 2.2.4, our simple exponential $e^{c\rho t}$ in equation (2.2.26) is a barely adequate parametrization of the absorption, and for more accurate work a more sophisticated parametrization would be required.

c. Elastic Scattering

Having determined our few t = 0 free parameters and the t-dependent nature of the ρ and A_2 amplitudes, we next examine elastic scattering differential cross-sections. The only new arbitrary parameters at our disposal are α'_P , the slope of the pomeron trajectory, and a and $\bar{t}$ from equation (2.2.33). The value of α'_P has previously been well determined by Collins and Gault (55) in fits to pp α-effective, and is found to be = 0.1.

Since $\frac{d\sigma}{dt}$(pp) exhibits a minimum at $|t| = 1.4$ GeV^2 we have included in our amplitudes for pp scattering a P⊗P cut taken directly from reference (40). The motivation for its inclusion is twofold: (1) we can economically describe the pp large $|t|$ data that has recently become available and (2) more importantly, by including such a cut, we are freeing the pomeron pole to give a simultaneous description of the πp and Kp $\frac{d\sigma}{dt}$'s out to $|t| \approx 2.0$ GeV^2 (there appear to be no cuts present in elastic meson-baryon scattering) and pp $\frac{d\sigma}{dt}$ at small $|t|$ (< 0.8 GeV^2) where the effect of the cut should be small. (In fact, referring to Figure 2.2.2 we can see the P⊗P cut contribution making a small effect even at $|t| = 0.6$ GeV^2).

Obviously it is possible within our model to fit the small $|t|$ data without such a cut (56) but we feel that in doing so, we are not arriving at the best description of the pomeron pole alone.

Given our complete set of amplitudes, and remembering that the only difference between $\frac{d\sigma}{dt}(pp)$ and $\frac{d\sigma}{dt}(\pi p)$ at high energies and small $|t|$ stems from the factor $\bar{F}_1(t)$ (see Figure 2.2.2), we fit the data (57) as shown in Figure 2.3.5, and in doing so determine a and $\bar{t}$. The only modification to the pomeron ⊗ pomeron cut required by our parametrization is the addition of an extra $\lambda' e^{dt}$ term in the small $|t|$ term in equation (8) of reference (40). This modification is required presumably because the authors of reference (40) use a two exponential pomeron pole, which curves in $|t|$ more sharply than the one used by ourselves. In Table 2.3.1 we present all our coupling parameters.

f_ω	$\rho(o)$	x	ε_1	G_{fD}	C_ρ	a	$\bar{t}$	λ'	d
17.10	0.47	0.435	0.14	-8.10	1.20	0.60	0.74	-0.5o	0.88

Table 2.3.1: The coupling parameters used in all our fits. All cut parameters are as in reference (40), except λ' and $d (\equiv \lambda' e^{dt}$ inserted into the small $|t|$ term of equation (8), reference (40)). The parameter G_{fD} is the f daughter coupling over and above f_ω, the coupling of the f.

In Figure 2.3.6 we show our prediction of the polarization in elastic scattering, which arises from the interference of our ρ and A_2 flip amplitudes with the P, f and ω non-flip amplitudes. Evidently we have a good description of the main features of the data (58), although in order to give a complete description of the complicated dip and double zero structure of the pp polarization data, a more careful and prolonged analysis would be required. For further discussion of the topic, see, for example, reference (59).

So, our strong assumptions of

(1) Universality for the ρ and ω couplings

(2) ρ - A_2 exchange degenerate couplings

(3) A small breaking of exchange degeneracy in the f - ω couplings at $N\bar{N}$ vertices, but none at $M\bar{M}$ vertices

(4) A universal function $\rho(t)$ (see equation 2.2.33) for the P : f coupling ratio

all seem to have worked amazingly well, given the wide range of elastic and total cross-section data we have attempted to describe. The parametrization of Section 2.2 and the values of the parameters given in Table 2.3.1 provide a universal prescription for all the natural parity regge exchanges, and should, if the hypothesis is correct, be applicable in any reaction.

In the next chapter, we use this parametrization to predict total cross-sections $\sigma^{tot}_{\Lambda p}(s)$ for example, and also cross-sections for the process $\gamma p \to Vp$, V = any vector meson.

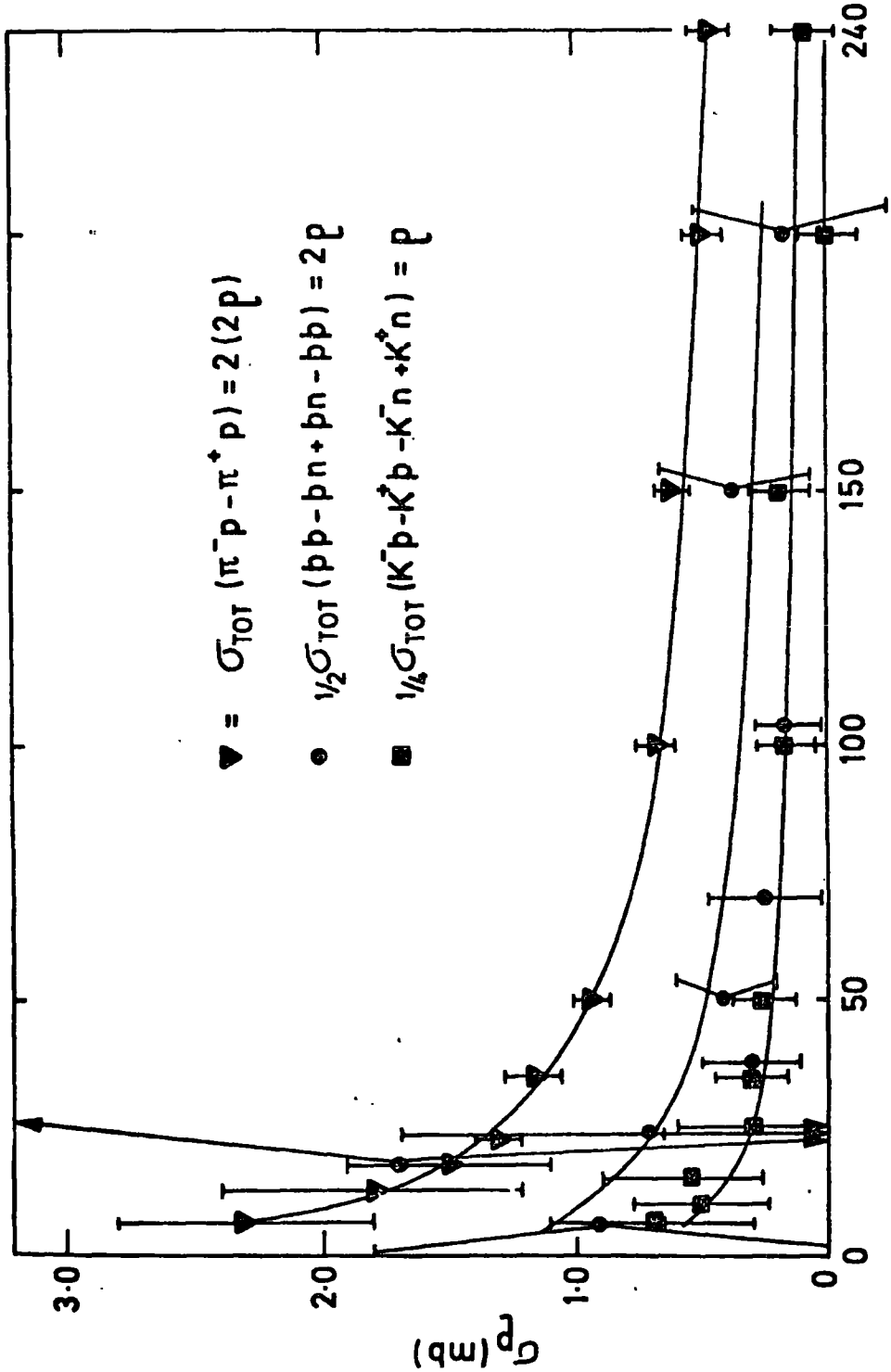

Figure 2.3.1(a): The total cross-section differences of equation 2.3.1 obtained from the data of reference (47) with our parametrization - rho cross-section.

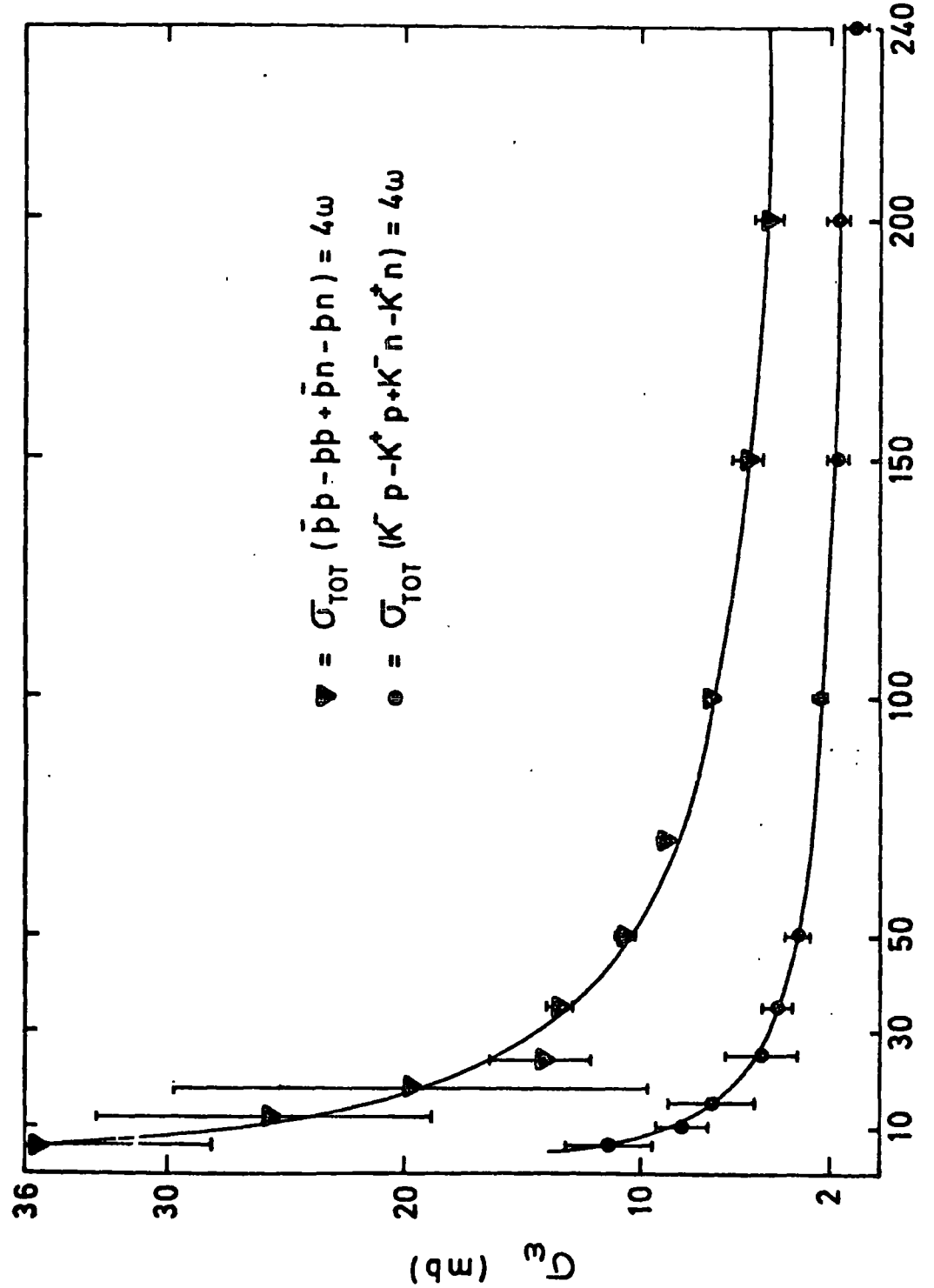

Figure 2.3.1(b) The total cross-section differences of equation 2.3.1 obtained from the data of reference (47) with our parametrization - ω-cross-section

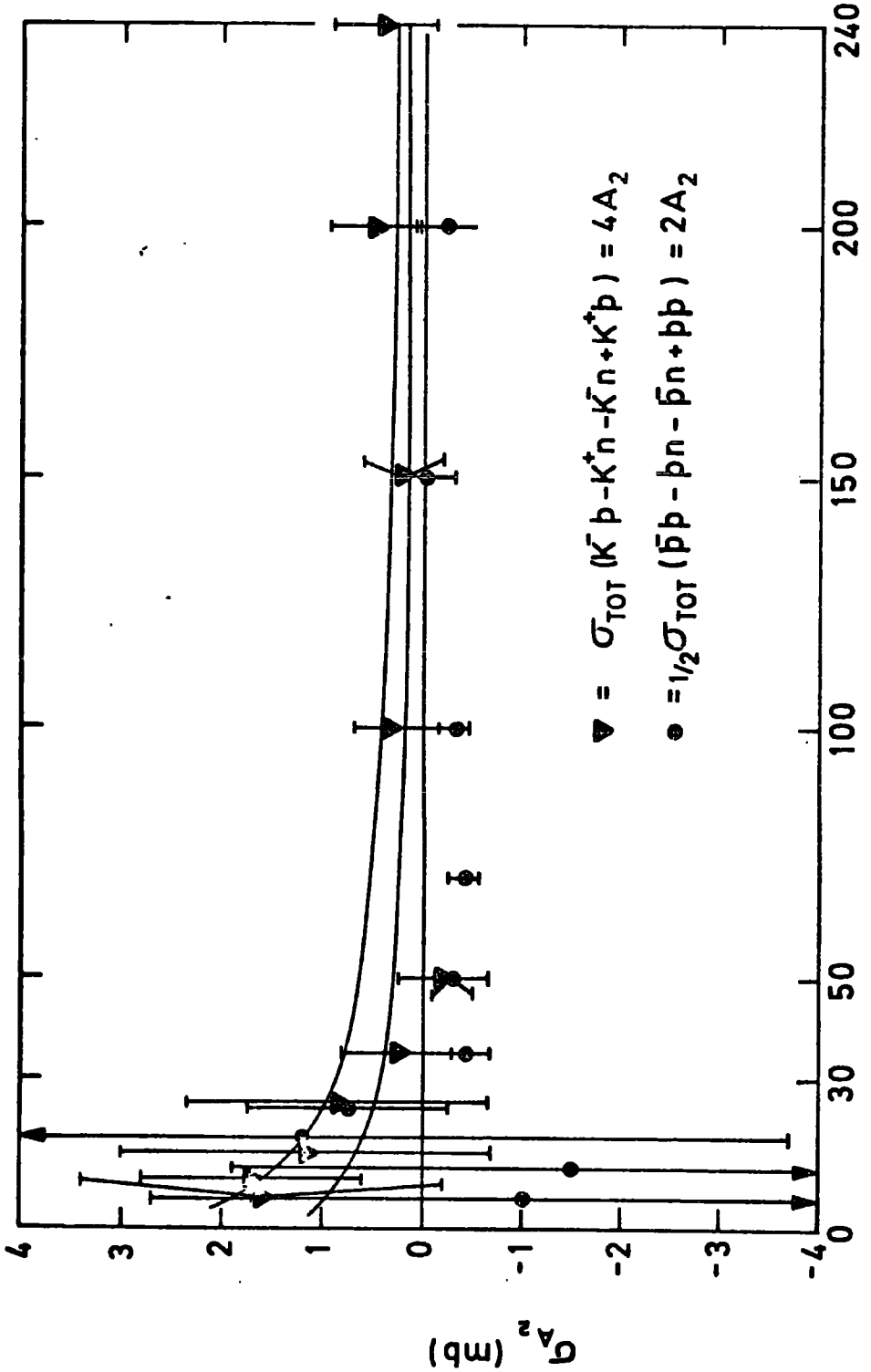

Figure 2.3.1(c): The total cross-section differences of equation 2.3.1 obtained from the data of reference (47) with our parametrization - A_2 cross-section.

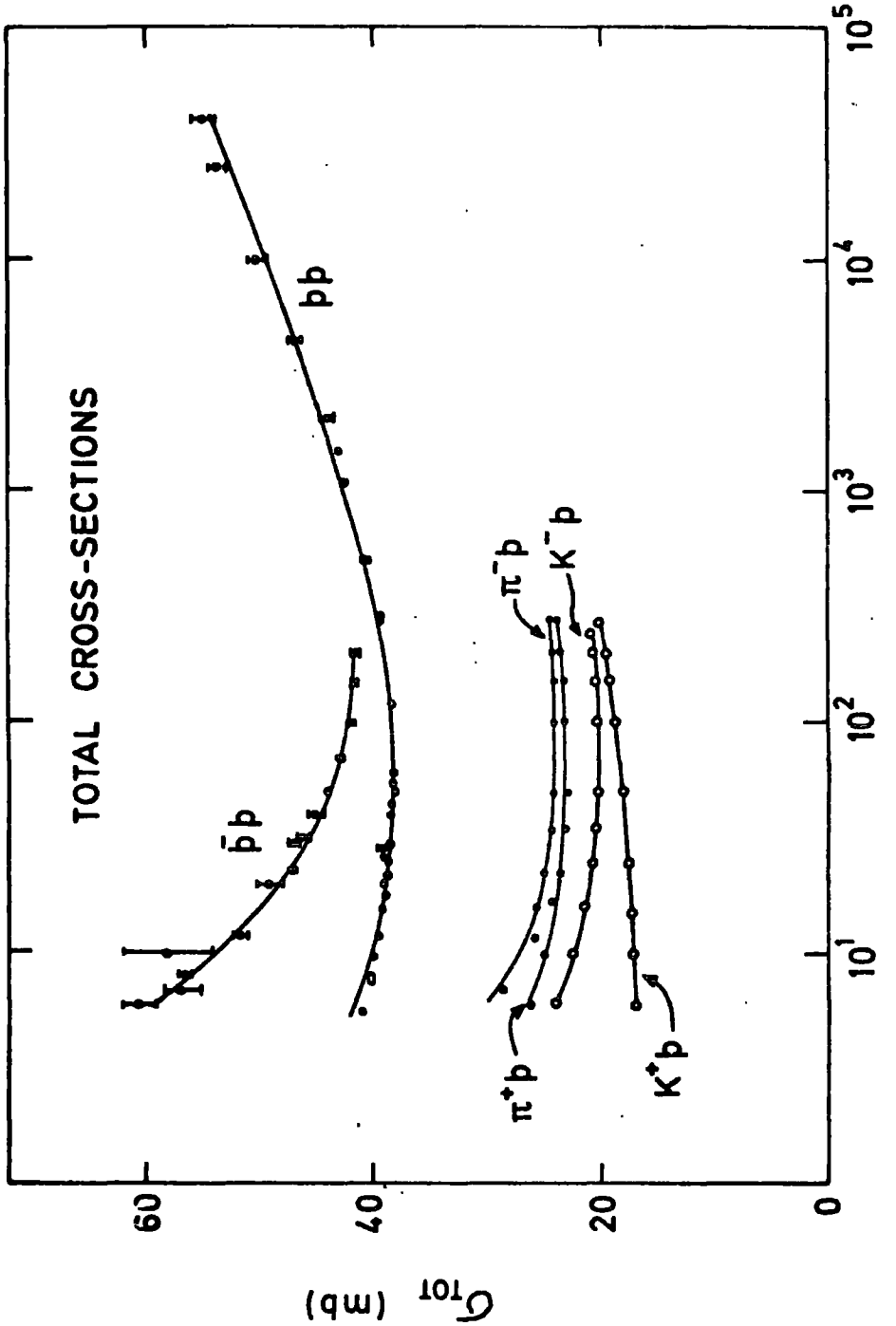

Figure 2.3.2(a): The pp, $\bar{p}p$, $\pi^{\pm}p$, $K^{\pm}p$ total cross-section data from reference (47) and, in the case of $\bar{p}p$, the cosmic ray data from reference (50) fitted by our parametrization.

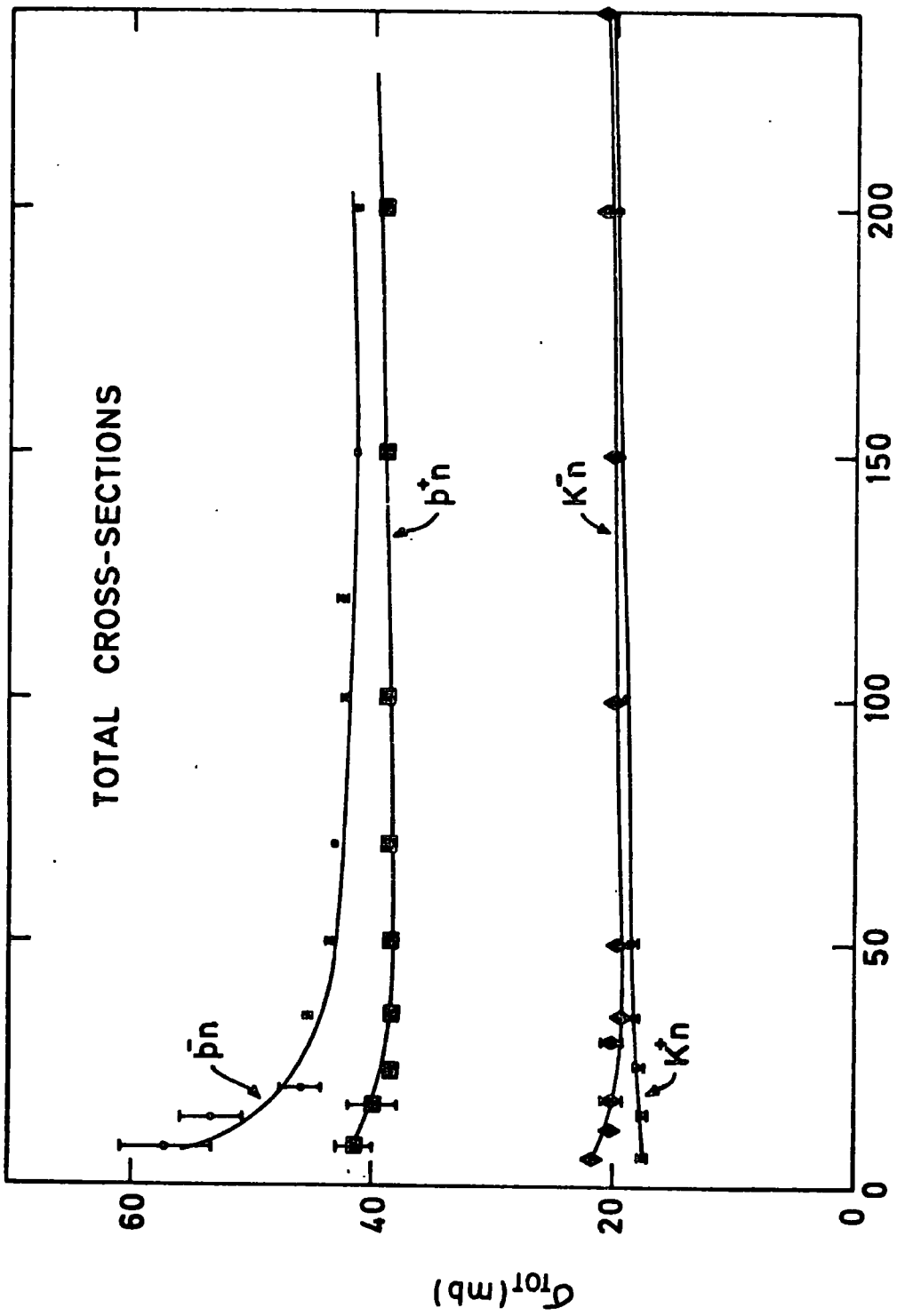

Figure 2.3.2(b): The pn, $\bar{p}n$, $K^{\pm}n$ total cross-section data from reference (47) fitted by our parametrization.

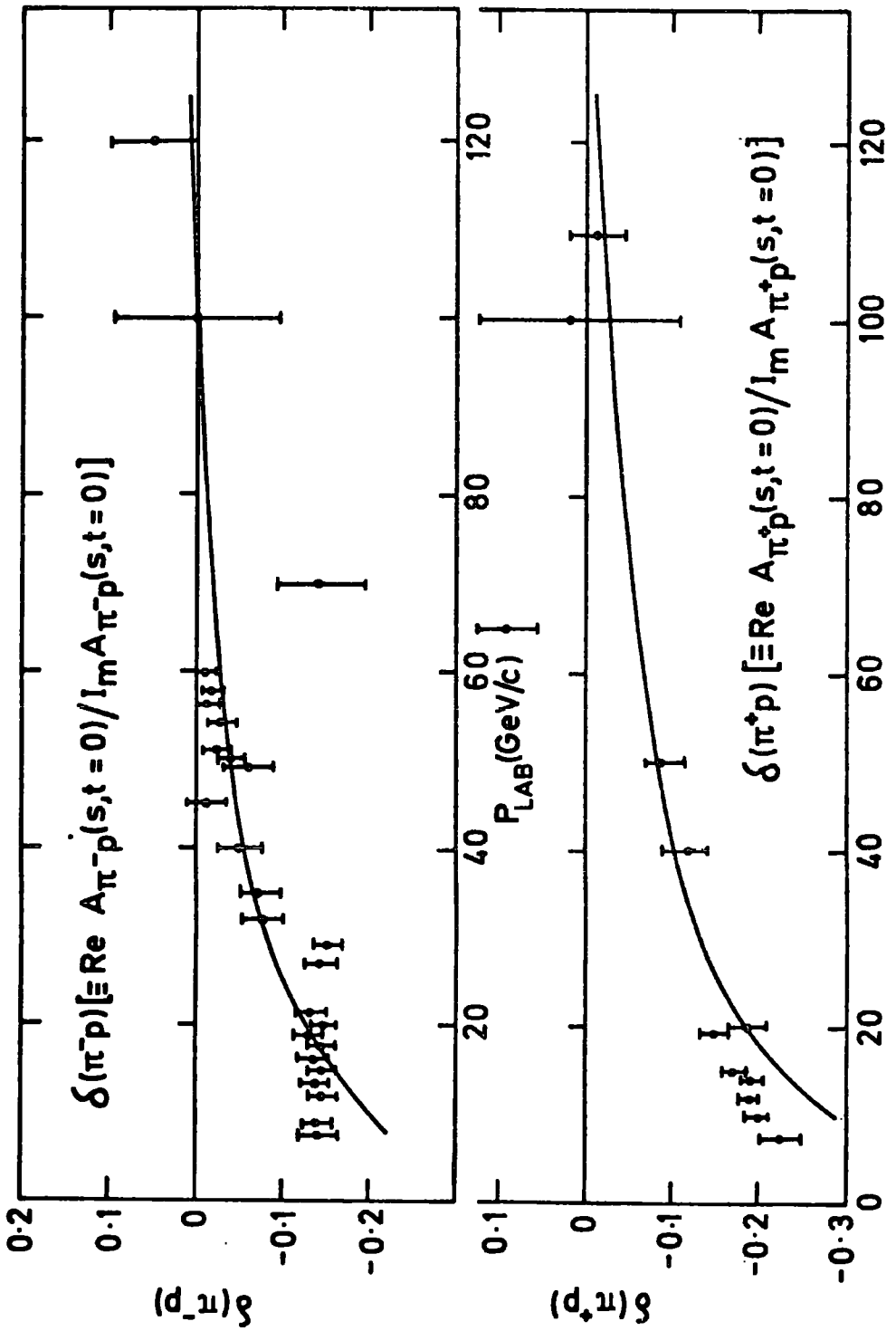

Figure 2.3.3(a): Our prediction of δ ($\equiv$ ReA:ImA) data (49) for $\pi^{\pm}p$

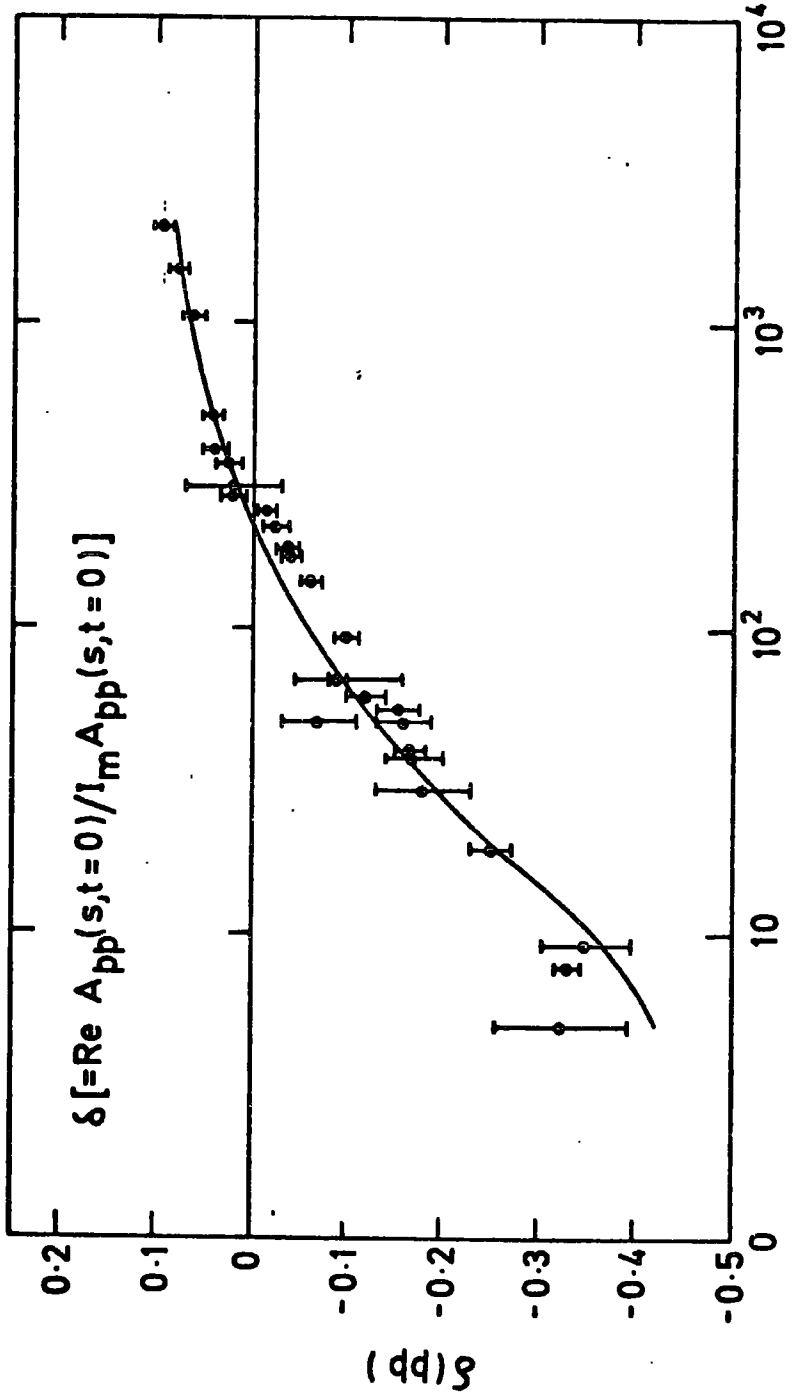

Figure 2.3.3(b): Our prediction of δ ($\equiv$ ReA:ImA) data (49) for pp.

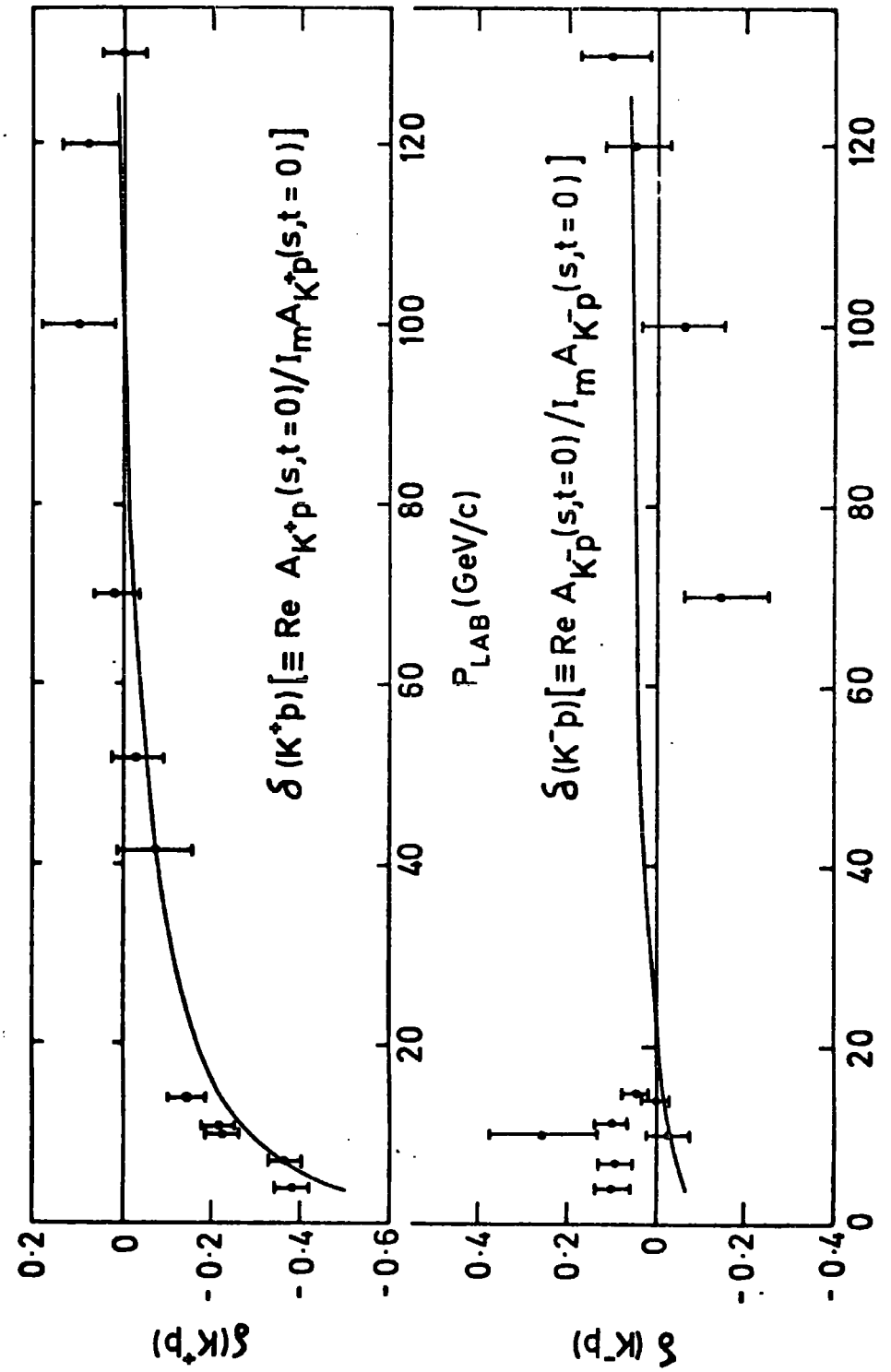

Figure 2.3.3(c): Our prediction of δ ($\equiv$ ReA:ImA) data (49) for $K^{\pm}p$.

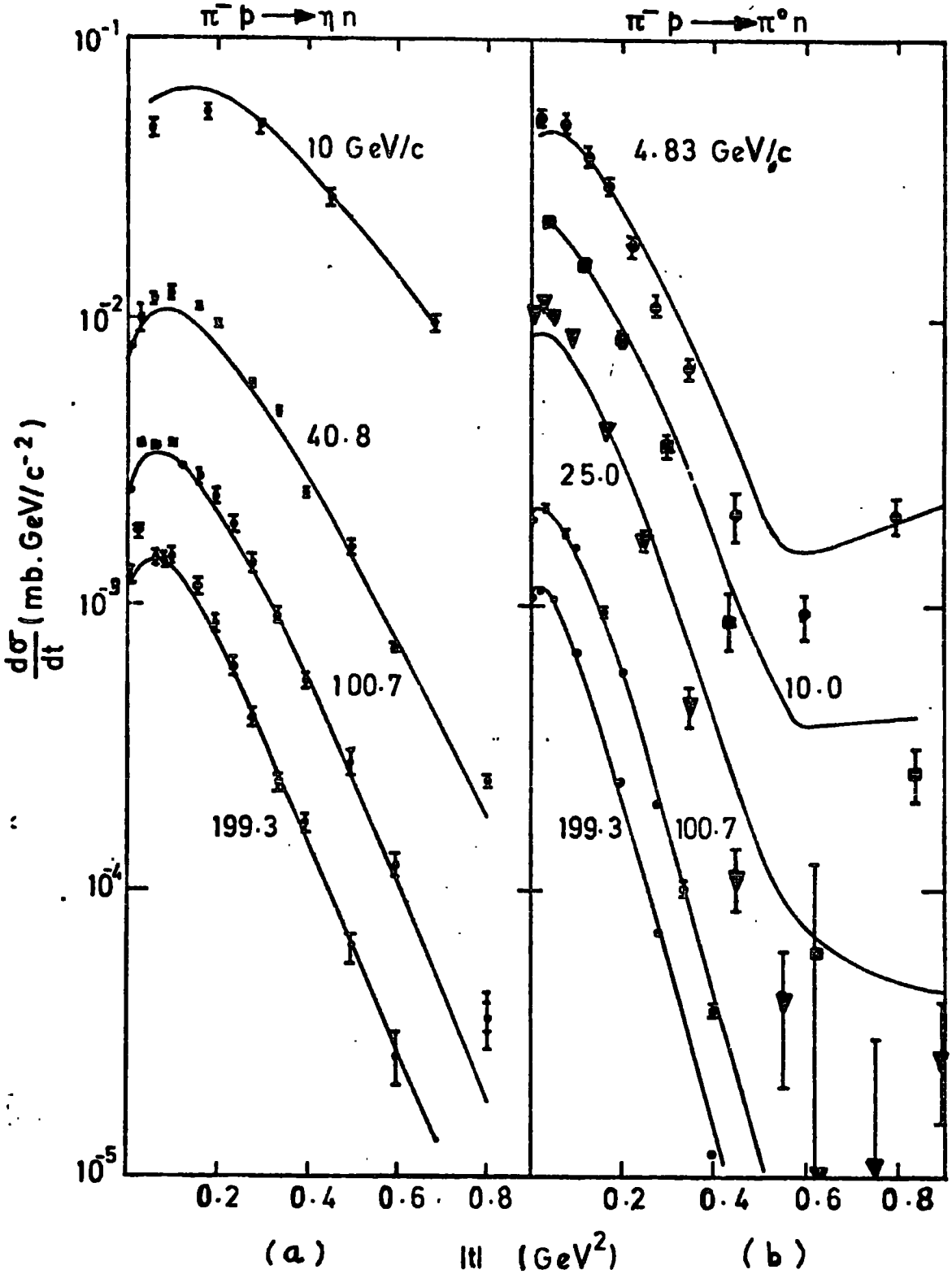

Figure 2.3.4: (a) Our prediction of $\frac{d\sigma}{dt}$ ($\pi^- p \to \eta n$) against the data of reference (52), and
(b) our fit of $\frac{d\sigma}{dt}$ ($\pi^- p \to \pi^0 n$) against the data of reference (53).

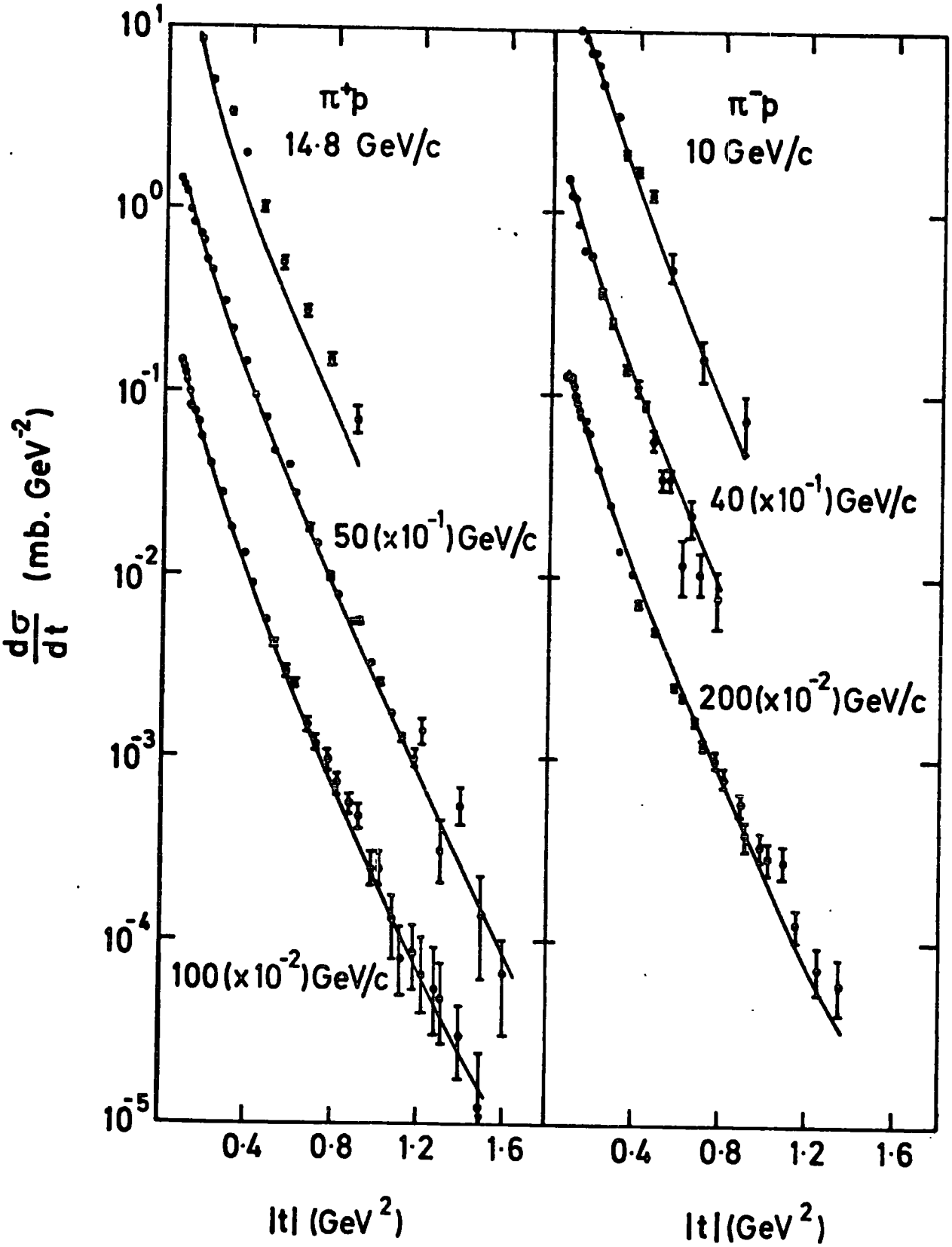

Figure 2.3.5(a) Fit of $\frac{d\sigma}{dt}$ ($\pi^{\pm}p \rightarrow \pi^{\pm}p$) using the data of reference (57).

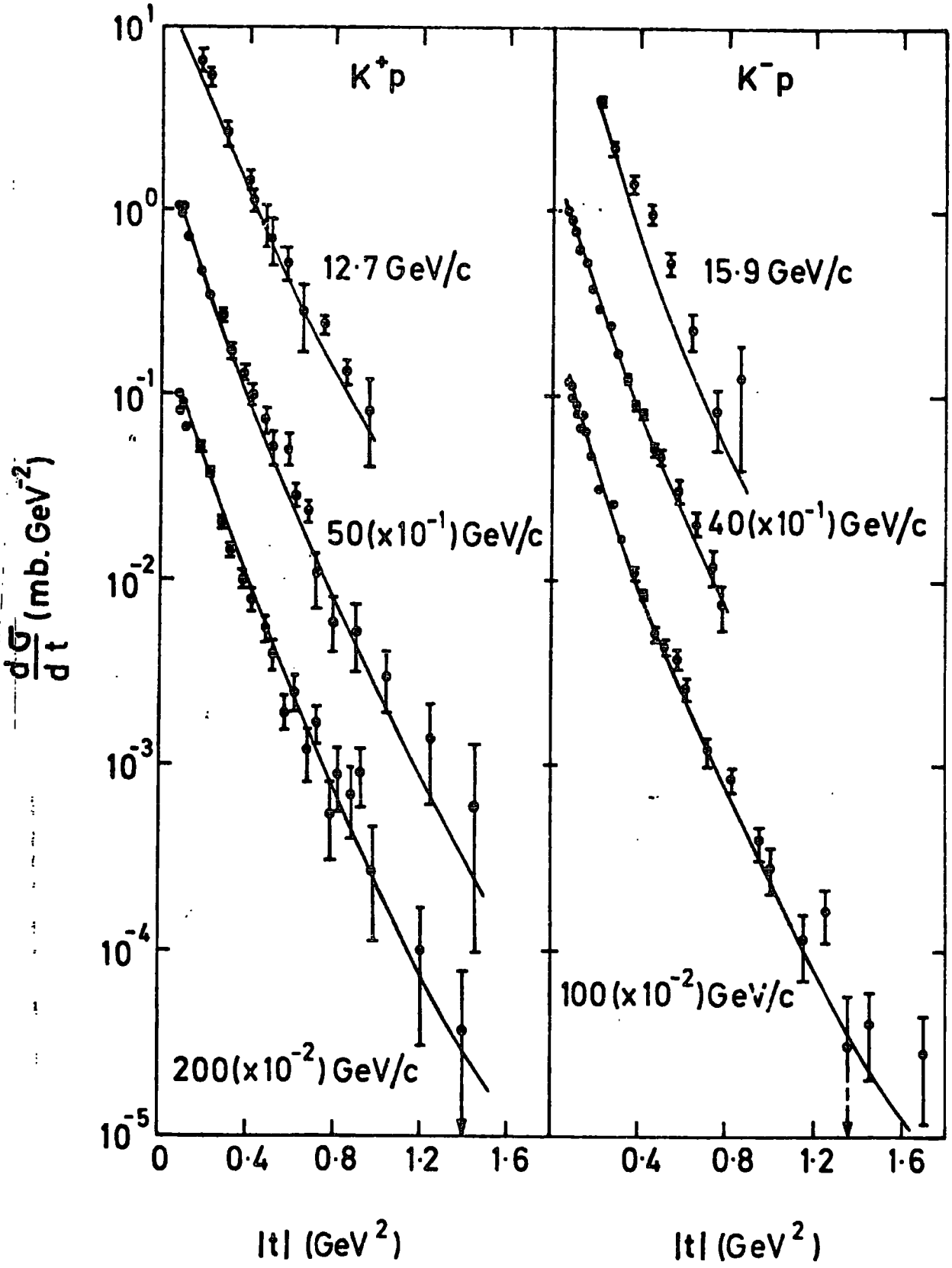

Figure 2.3.5(b): Fit of $\frac{d\sigma}{dt}$ ($K^{\pm}p \rightarrow K^{\pm}p$) using the data of reference (57).

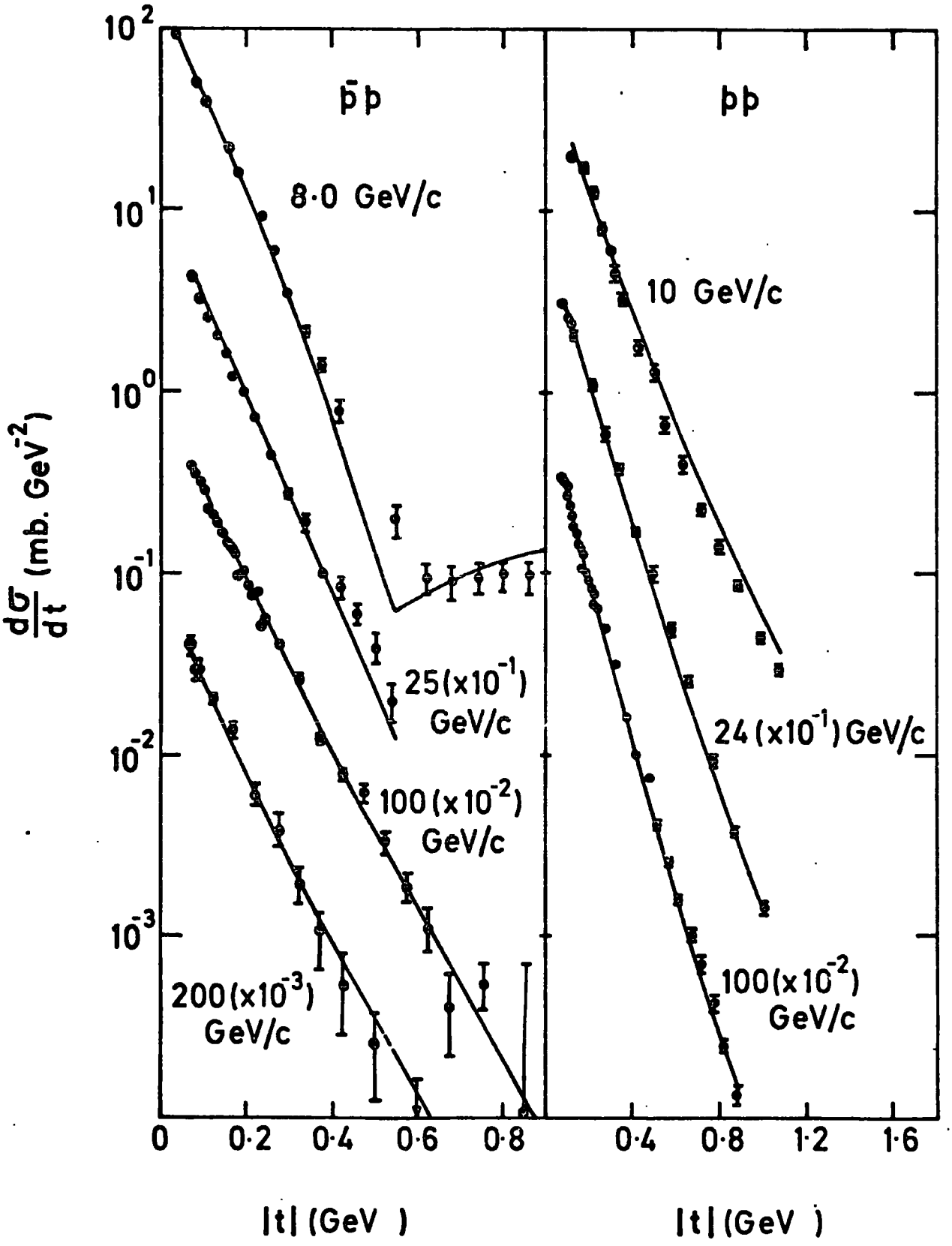

Figure 2.3.5(c): Fit of low and medium energy small $|t|$ $\frac{d\sigma}{dt}$ ($pp \to pp$) and $\frac{d\sigma}{dt}$ ($\bar{p}p \to \bar{p}p$) using the data of reference (57).

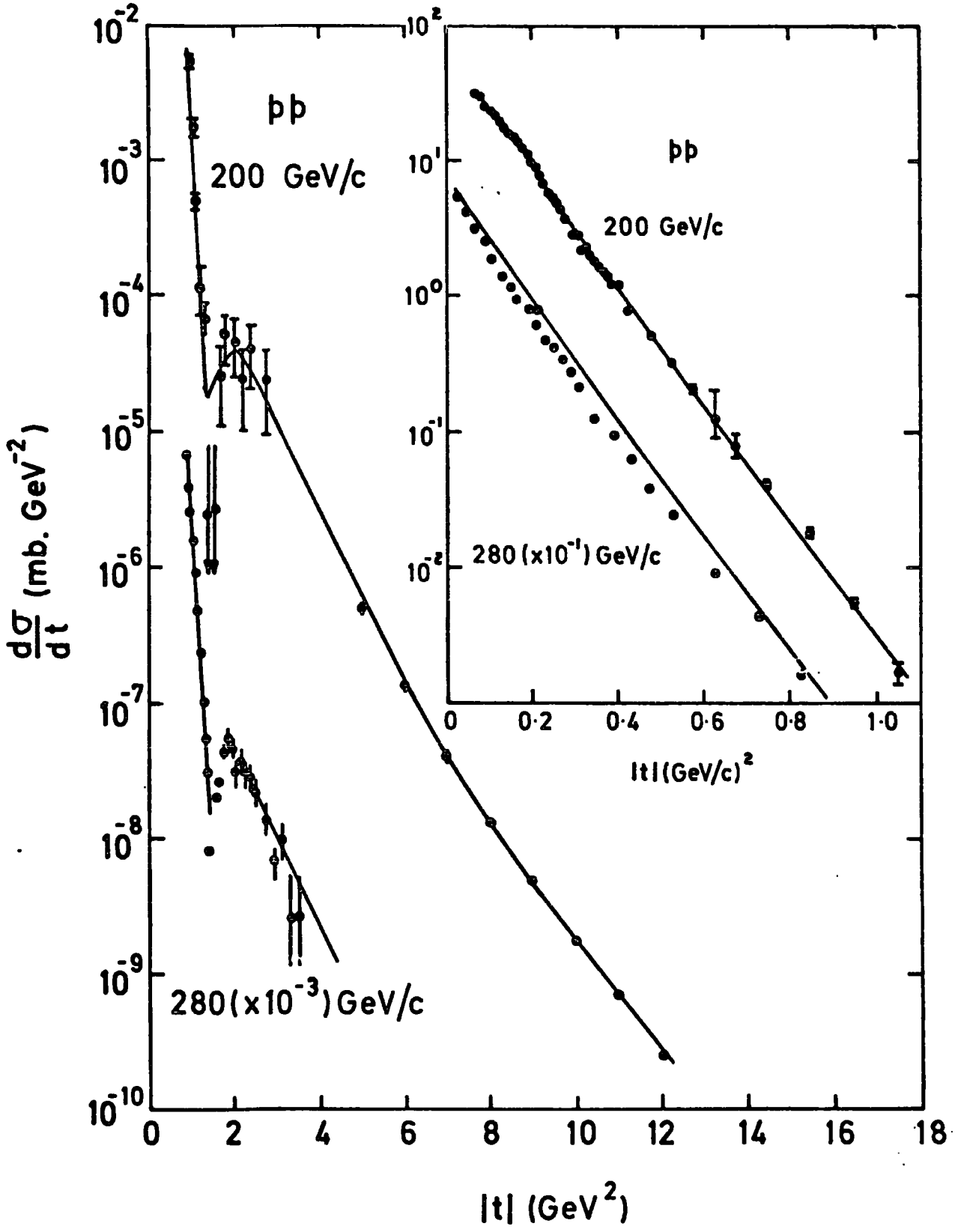

Figure 2.3.5(d): Fit of medium energy small and large $|t|$ $\frac{d\sigma}{dt}$ (pp → pp) using the data of reference (57).

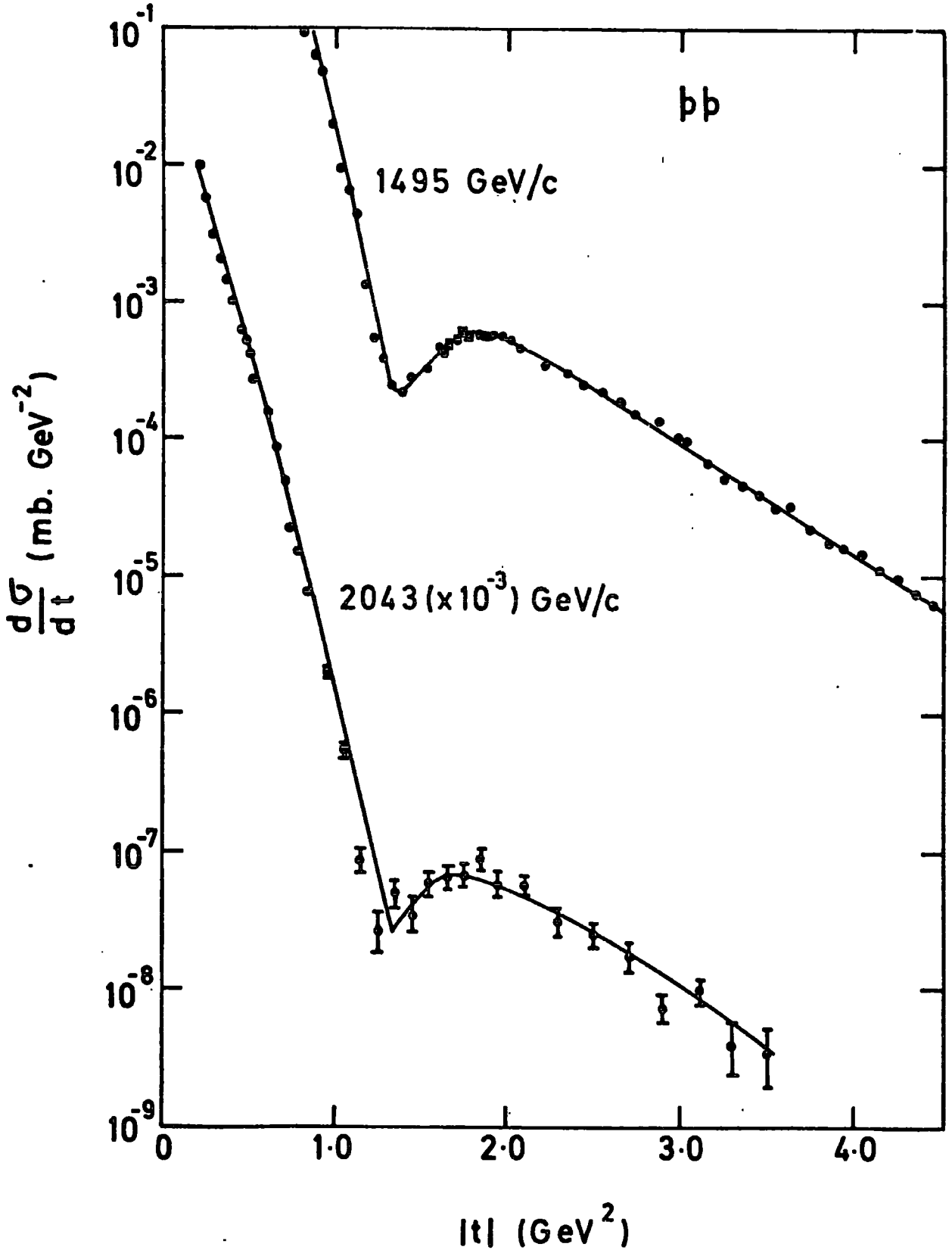

Figure 2.3.5(e): Fit of high energy small and large $|t|$ $\frac{d\sigma}{dt}$ ($pp \to pp$) using the data of reference (57).

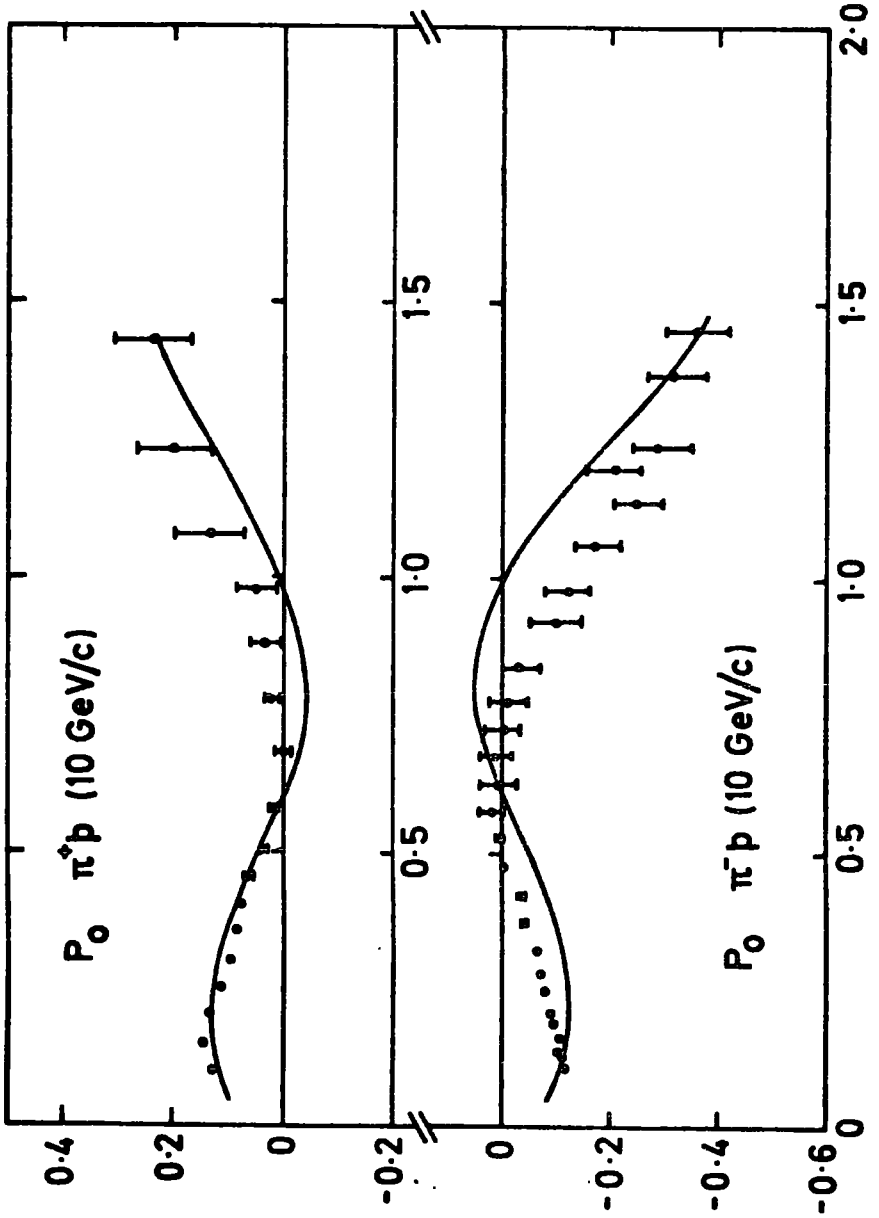

Figure 2.3.6(a): Our prediction of $\pi^{\pm} p$ elastic polarization compared with the data of reference (58).

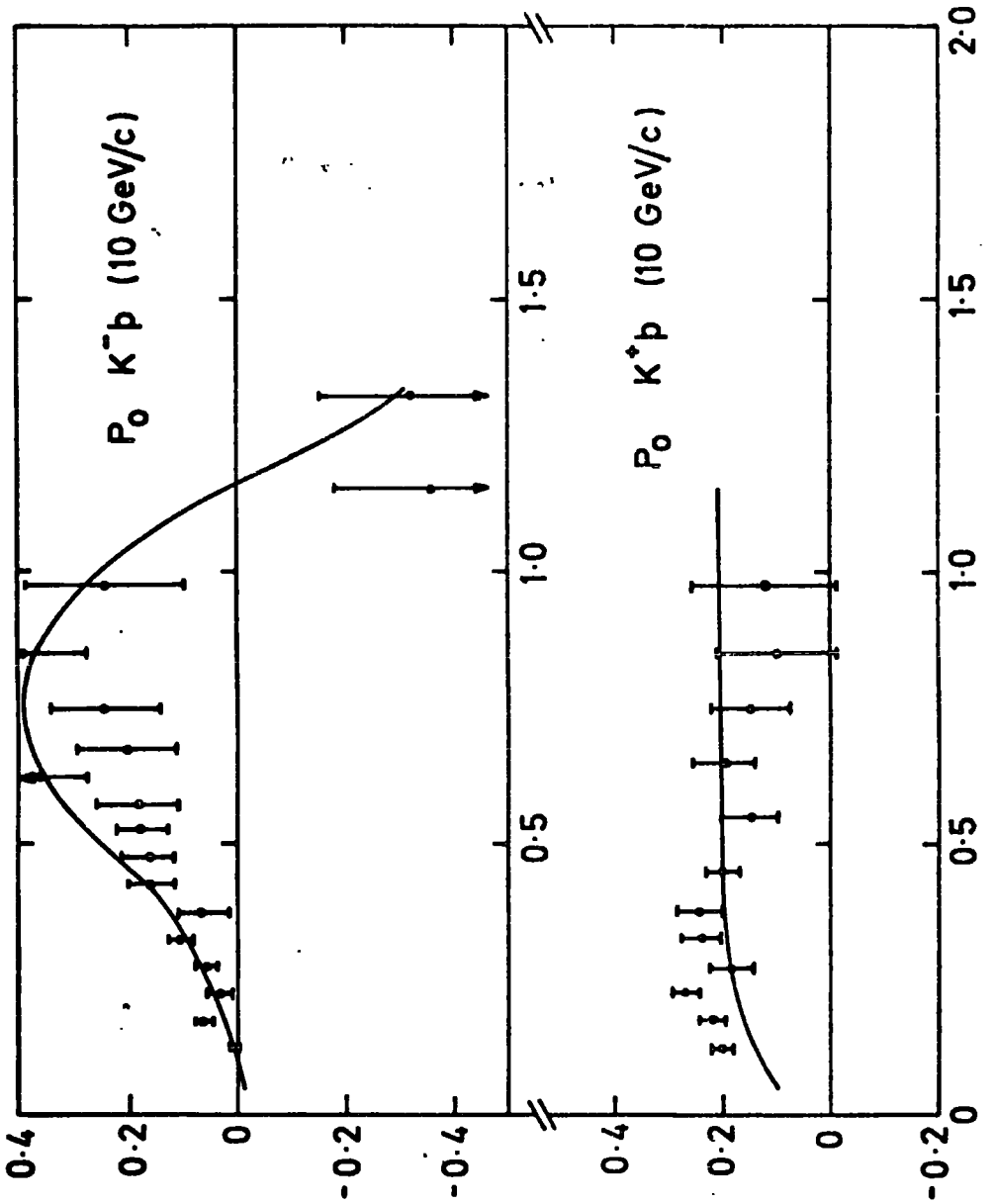

Figure 2.3.6(b): Our prediction of $K^{\pm}p$ elastic polarization compared with the data of reference (58).

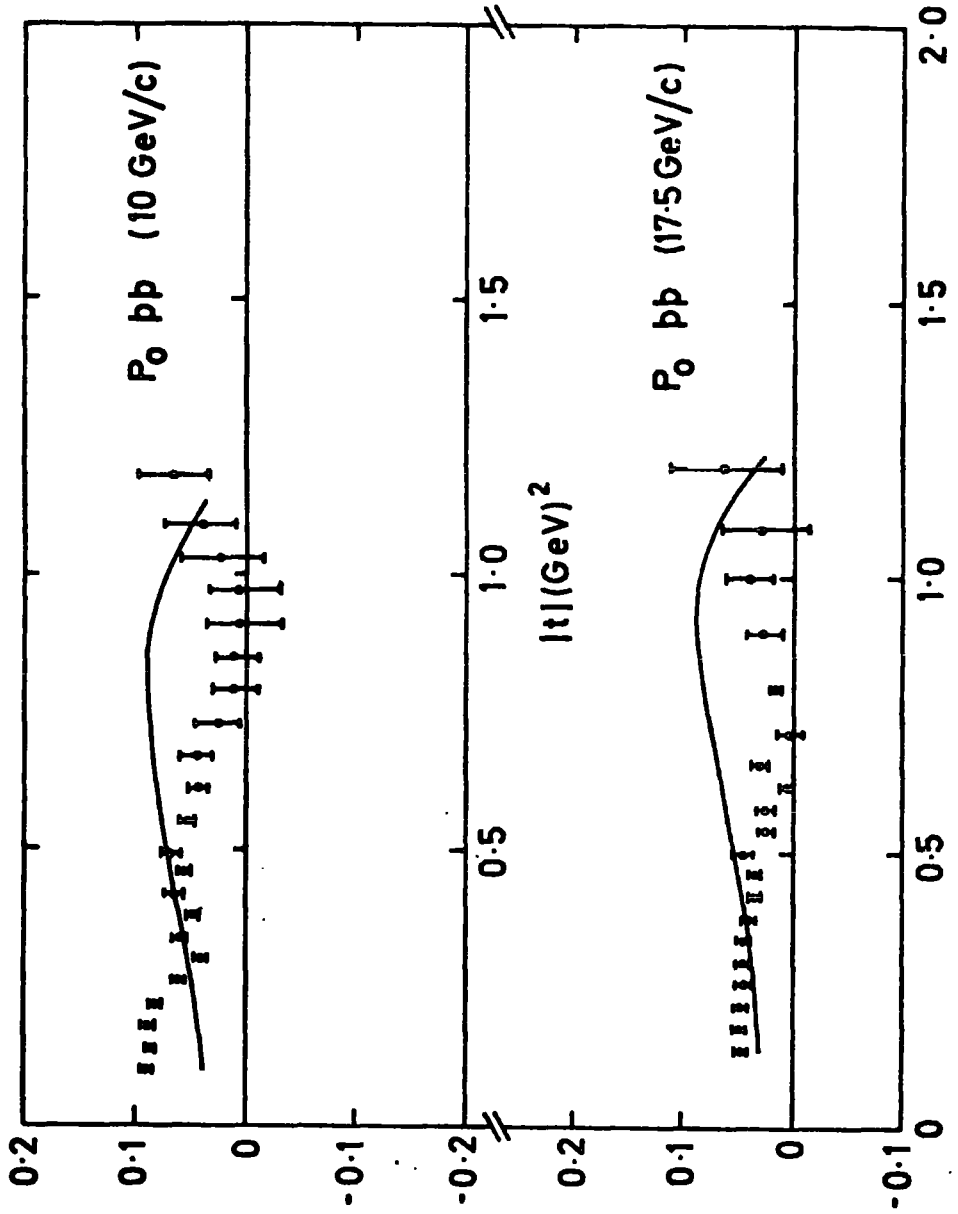

Figure 2.3.6(c): Our prediction of $\vec{p}p$ elastic polarization compared with the data of reference (58).

CHAPTER 3

SOME CROSS-SECTION PREDICTIONS

3.1 Introduction

In the previous chapter, we have given in detail the form of our parametrization of elastic scattering, which results from our reggeon-photon coupling analogy. As the primary test, we have fitted the data on elastic scattering and total cross-sections, and in so doing determined the few free parameters available to us.

In this chapter, we use the parametrization so determined to give predictions of other total cross-sections, viz. $\sigma^{tot}_{\Lambda p}(s)$, $\sigma^{tot}_{\pi^+\pi^-}(s)$, $\sigma^{tot}_{\pi^-\pi^-}(s)$, the vector meson-proton total cross-sections such as $\sigma^{tot}_{\rho p}(s)$, $\sigma^{tot}_{\phi p}(s)$ ... etc. and also $\sigma^{tot}_{\gamma p}(s)$, data on which at high energy has recently become available (60).

3.2 Total Cross-Sections

In our model, $\sigma^{tot}_{\Lambda p}(s)$ and $\sigma^{tot}_{\pi\pi}(s)$ are given by

$$\sigma^{tot}_{\Lambda p}(s) = \sigma^{tot}_{pp}(s) \left(\frac{2 + r_s(o)}{3}\right) \qquad (3.2.1)$$

$$\sigma^{tot}_{\pi^+\pi^-}(s) = \frac{2}{3}\left(\frac{1}{1+\varepsilon_1}\right)\left[\sigma^{P}_{\pi^+p} + \sigma^{f}_{\pi^+p}\right] + \frac{2}{3}\sigma^{\rho}_{\pi^+p} \qquad (3.2.2)$$

$$\sigma^{tot}_{\pi^-\pi^-}(s) = \frac{2}{3}\left(\frac{1}{1+\varepsilon_1}\right)\left[\sigma^{P}_{\pi^+p} + \sigma^{f}_{\pi^+p}\right] - \frac{2}{3}\sigma^{\rho}_{\pi^+p} \qquad (3.2.3)$$

where $r_s(o)$ can be deduced from Tables 2.2.2 and 2.2.3 and is equal to 0.72, and $\sigma^{P,f,\rho}_{\pi^+p}$ denotes the pomeron/f/ρ contribution to the total cross-section in π^+p scattering. Hence, in Figure 3.2.1, we show our predictions for these total cross-sections. In the case of $\sigma^{tot}_{\pi\pi}(s)$, the data (61) is

obtained by extrapolation to the pion exchange pole in inclusive $\pi^{\pm}n \to xp$, so there will necessarily be some theoretical uncertainties in addition to the large experimental errors. However, our predictions, particularly of the rising exotic $\pi^-\pi^-$ cross-section dominated by pomeron exchange seem quite satisfactory.

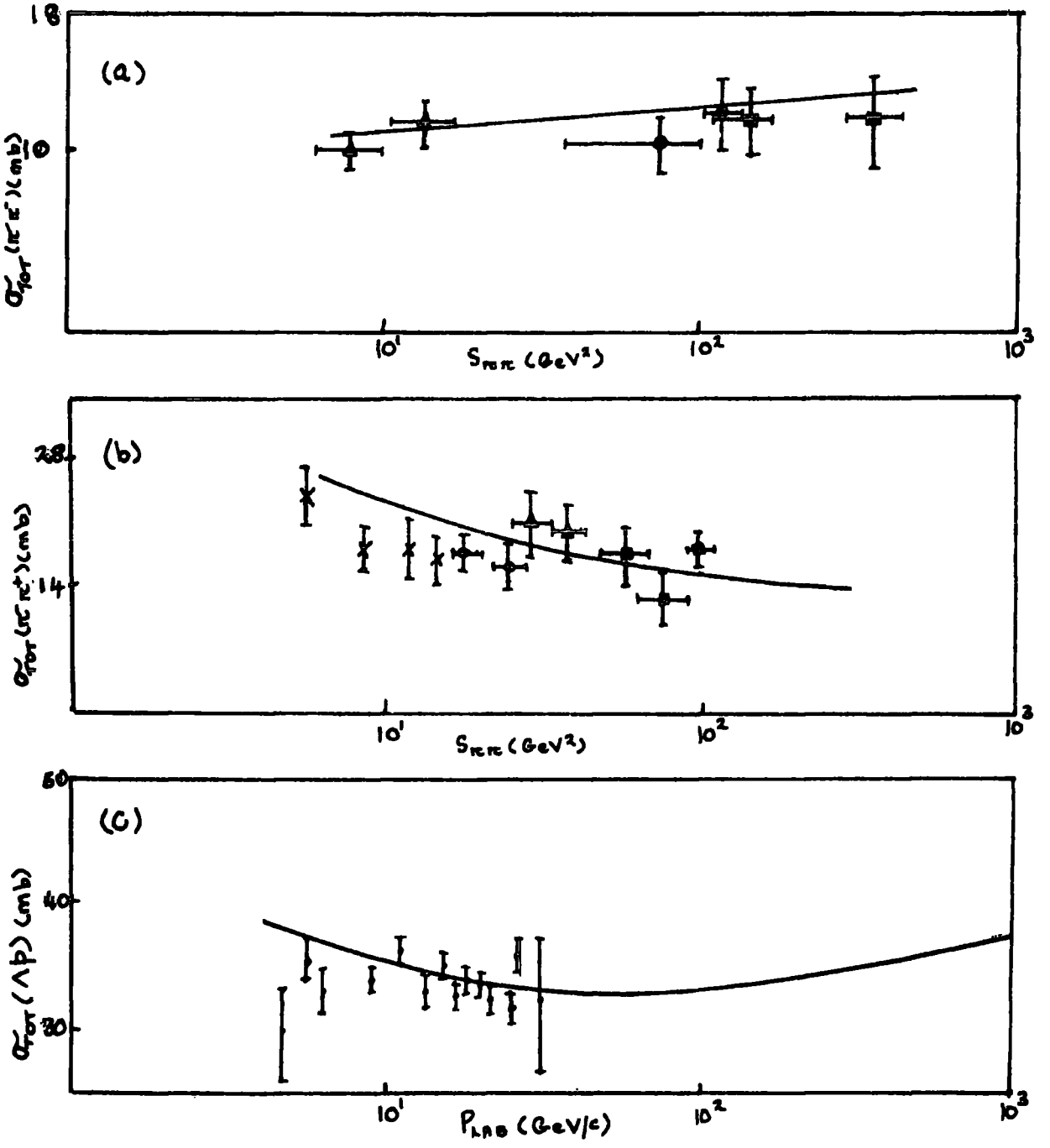

Figure 3.2.1: (a) Prediction of $\sigma^{tot}_{\pi^-\pi^-}(s)$ with data from reference (61);
(b) Prediction of $\sigma^{tot}_{\pi^-\pi^+}(s)$ with data from reference (61);
(c) Prediction of $\sigma^{tot}_{\Lambda p}(s)$ with data from reference (62).

3.3 Vector meson-proton cross-sections

According to the vector dominance model, the total cross-sections for Vp scattering (V ≡ any vector meson) may be obtained from the corresponding vector meson photoproduction differential cross-section at t = 0, since

$$\sigma^{tot}_{Vp}(s) = \frac{0.3893}{s} \text{ ImA } (Vp \to Vp) \tag{3.3.1}$$

and

$$\frac{d\sigma}{dt}(\gamma p \to Vp) = \frac{e^2}{f_V^2} \frac{d\sigma}{dt} (Vp \to Vp) \tag{3.3.2}$$

but

$$\frac{d\sigma}{dt}(Vp \to Vp)\Big|_{t=0} = \frac{0.3893}{16\pi s^2} \left[(\text{ImA } (Vp \to Vp))^2 (1 + \delta^2) \right] \tag{3.3.3}$$

where δ is the ratio ReA/ImA at t = 0.

Therefore, after a little algebra, (3.3.1) (3.3.2) and (3.3.3) lead to

$$\sigma^{tot}_{Vp}(s) = \left[\frac{16\pi \alpha M_V \cdot 0.3893}{3\Gamma_{V\to e^+e^-} (1 + \delta^2)} \frac{d\sigma}{dt} (\gamma p \to Vp)\Big|_{t=0} \right]^{\frac{1}{2}} \tag{3.3.4}$$

Since

$$\Gamma_{V\to e^+e^-} = \frac{4\pi \alpha^2 M_V}{3 f_V^2} \tag{3.3.5}$$

and

$$\alpha = \frac{e^2}{4\pi} \tag{3.3.6}$$

In our model, these cross-sections are predicted to be

$$\begin{aligned}
\sigma^{tot}_{\rho p}(s) &= \sigma^{tot}_{\omega p}(s) = \frac{1}{2}\left[\sigma^{tot}_{\pi^+ p}(s) + \sigma^{tot}_{\pi^- p}(s)\right] P_I(s) \underset{s\to\infty}{=} \sigma^{P}_{\pi p}(s) \\
\sigma^{tot}_{\phi p}(s) &= r_s(o)\, \sigma^{P}_{\pi p}(s)\, P_s(s) \\
\sigma^{tot}_{\psi p}(s) &= r_c(o)\, \sigma^{P}_{\pi p}(s)\, P_c(s) \\
\sigma^{tot}_{Tp}(s) &= r_b(o)\, \sigma^{P}_{\pi p}(s)\, P_b(s)
\end{aligned} \tag{3.3.7}$$

where the superscript P denotes pomeron exchange only, as defined in the previous section, $r_s(o)$, $r_c(o)$, ... ($\equiv r_F(o)$) are defined in equation (2.2.33) and given in Table 2.2.2, and the factor $P_F(s)$ represents the opening of the given flavour (F) channels. We have rather arbitrarily used

$$P_F(s) = \begin{cases} 0, & s < s_F \\ \sin\left(\left(\frac{s - s_F}{s - 2}\right)\pi\right), & s_F < s < 2s_F - 2 \\ 1, & s \geq 2s_F - 2 \end{cases} \qquad (3.3.8)$$

where $s_F = (M_V + M_p)^2$. In fact, a little substitution will demonstrate that for the ρ,ω $P_I(s) = 1$ for $s \geq 3.86$ GeV^2, for the ϕ, $P_s(s) = 1$ for $s \geq 5.67$ GeV^2, for the ψ, $P_c(s) = 1$ for $s \geq 30.5$ GeV^2 and for the T, $P_b(s) = 1$ for $s \geq 211.8$ GeV^2. Thus, for our purposes, the effect of $P_F(s)$ is only seen for $\sigma^{tot}_{\psi p}(s)$. Shown in Figure 3.3.1 is our prediction of $\sigma^{tot}_{\rho p}(s)$, $\sigma^{tot}_{\phi p}(s)$ and $\sigma^{tot}_{\psi p}(s)$, where the effect of $P_c(s)$ is clearly seen. The data (63) has been plotted using relation (3.3.4) and where possible, we have included information (63) on δ, although setting $\delta^2 = 0$ has a negligible effect on $\sigma^{tot}_{Vp}(s)$.

In Figure 3.3.2 we give predictions for $\frac{d\sigma}{dt}(\rho p \to \rho p)$, $\frac{d\sigma}{dt}(\phi p \to \phi p)$, $\frac{d\sigma}{dt}(\psi p \to \psi p)$ and $\frac{d\sigma}{dt}(Tp \to Tp)$ at 9.3 GeV/c. Evidently the model has given a rather good description of the data (64)

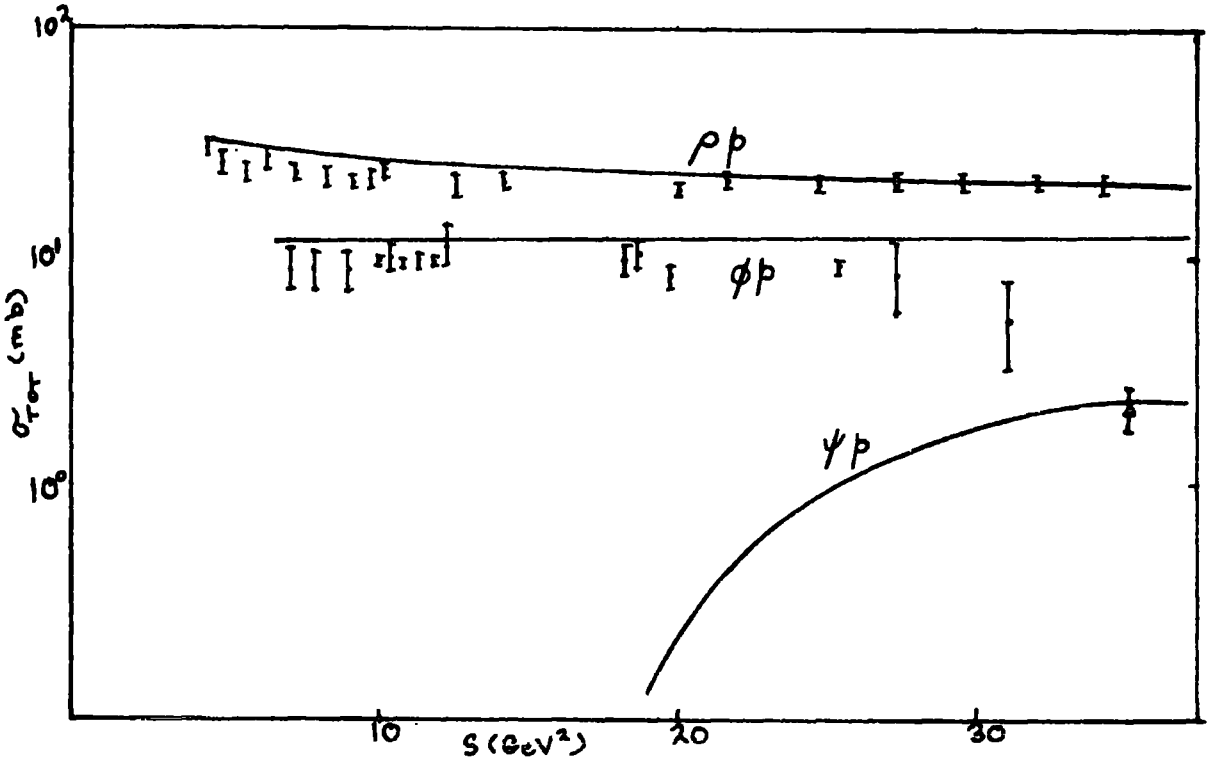

Figure 3.3.1: Our prediction of $\sigma_{Vp}^{tot}(s)$ against the data of reference (63).

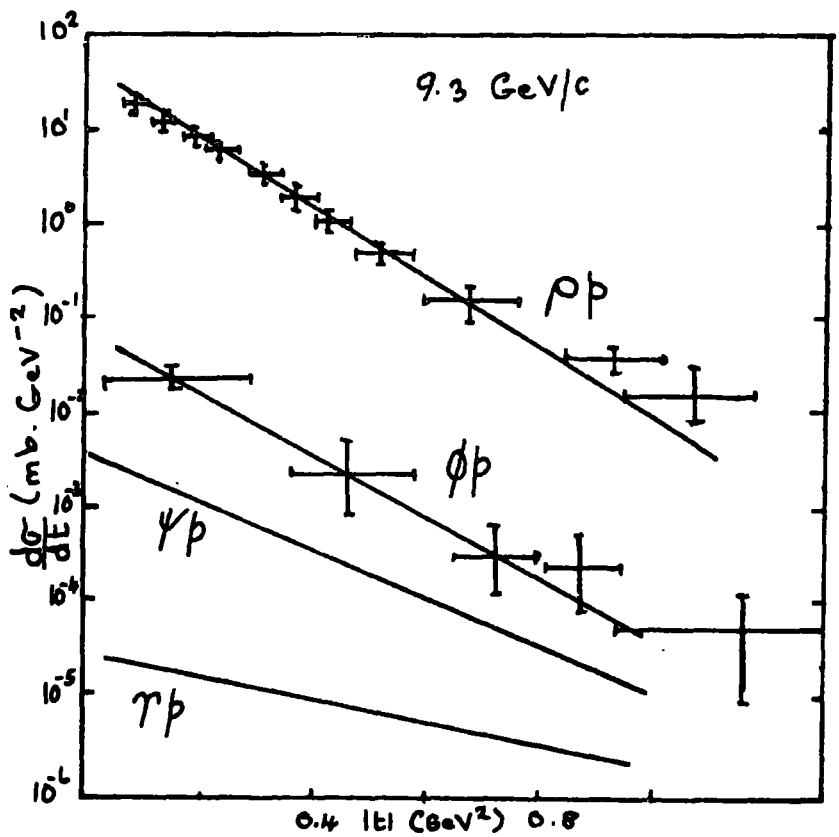

Figure 3.3.2: Our prediction of the vector meson differential cross-section against the data of reference (64). The change in shape is given solely by the variation in t of $r_s(t)$, $r_c(t)$ and $r_b(t)$ from Table 2.2.2

3.4 The photon-proton total cross-section

Using generalized vector dominance (4) we can predict $\sigma^{tot}_{\gamma p}(s)$, that is we put

$$\sigma^{tot}_{\gamma p}(s) = \sum_{V} \frac{3\Gamma_{V \to e^+e^-}}{\alpha M_V} \sigma^{tot}_{Vp}(s) \qquad (3.4.1)$$

(using equations (3.3.1) to (3.3.6) inclusively)

However, it is well known that it is necessary to include not just the leading vector mesons V = $\rho,\omega,\phi,\psi,\Upsilon$ ... but also their daughters (radial excitations) the ρ',ρ'' ..., ω',ω'' ... etc. So we require to know how $\sigma^{tot}_{V'p}(s)$ and $\Gamma_{V' \to e^+e^-}$ vary along a given equally spaced daughter sequence.

Silverman (65) has reported that $\frac{d\sigma}{dt}(\gamma p \to \rho'' p)\Big|_{t=0} = 15 \pm 5$ μb. This result implies, from equation (3.3.4), that $\sigma^{tot}_{\rho'' p}(s) = 21 \pm 12$ mb, compared with $\sigma^{tot}_{\rho p}(s) \simeq 26$ mb. Hence for simplicity, we assume

$$\sigma^{tot}_{V'p}(s) = \sigma^{tot}_{Vp}(s) \qquad (3.4.2)$$

(The above relation is not in complete accord with the data (66) on $\frac{d\sigma}{dt}(\gamma p \to \psi p)$ and $\frac{d\sigma}{dt}(\gamma p \to \psi' p)$ since in this case $\sigma^{tot}_{\psi p}(s) > \sigma^{tot}_{\psi' p}(s)$. However, as pointed out by the authors of reference (67), in order to extract the total cross-section from the data, one has to make assumptions which may not be valid at such high values of q^2).

For the leptonic decays of the vector mesons we used for the parents, the relation

$$\Gamma_{V \to e^+e^-} = \frac{4\pi\alpha^2}{3} \frac{M}{f_\omega^2} C_V \qquad (3.4.3)$$

where $C_V = 9\Sigma e_q^2 = 9, 1, 2, 8, 2$ for V = $\rho, \omega, \phi, \psi, \Upsilon$ (see Gournaris (68) for a similar approach based on the "New Duality" of Sakurai (69)). Equation (3.4.3) is the so-called Yennies formula (70,71) and despite its simplicity

appears to describe the decay widths adequately for our purposes. For the daughter sequence we use

$$\Gamma_{V' \to e^+e^-} = \frac{4\pi\alpha^2}{3} \frac{M_\omega}{F_\omega^2} C_V \frac{1}{(1+1.4(M_{V'} - M_V))^2} \qquad (3.4.4)$$

(We have tried other (68) more complicated expressions for $\Gamma_{V' \to e^+e^-}$ but within the spirit of our approach, we have found the empirical relation (3.4.4) to be the most satisfactory). In Table 3.4.1 (at the end of this chapter) we give our predictions of $\Gamma_{V \to e^+e^-}$ using (3.4.3), and also the integrally spaced daughter leptonic decay widths, $\Gamma_{V' \to e^+e^-}$ from equation (3.4.4).

Combining equations (3.4.1) to (3.4.4) inclusively we find

$$\sigma_{\gamma p}^{tot}(s) = \frac{e^2}{f_\omega^2} \sum_{V,V'} \sigma_{Vp}^{tot}(s)\, M_\omega\, C_V \frac{1}{(1+1.4\ (M_{V'} - M_V)^2} \qquad (3.4.5)$$

which gives the prediction of $\sigma_{\gamma p}^{tot}(s)$ shown in Figure 3.4.1 below.

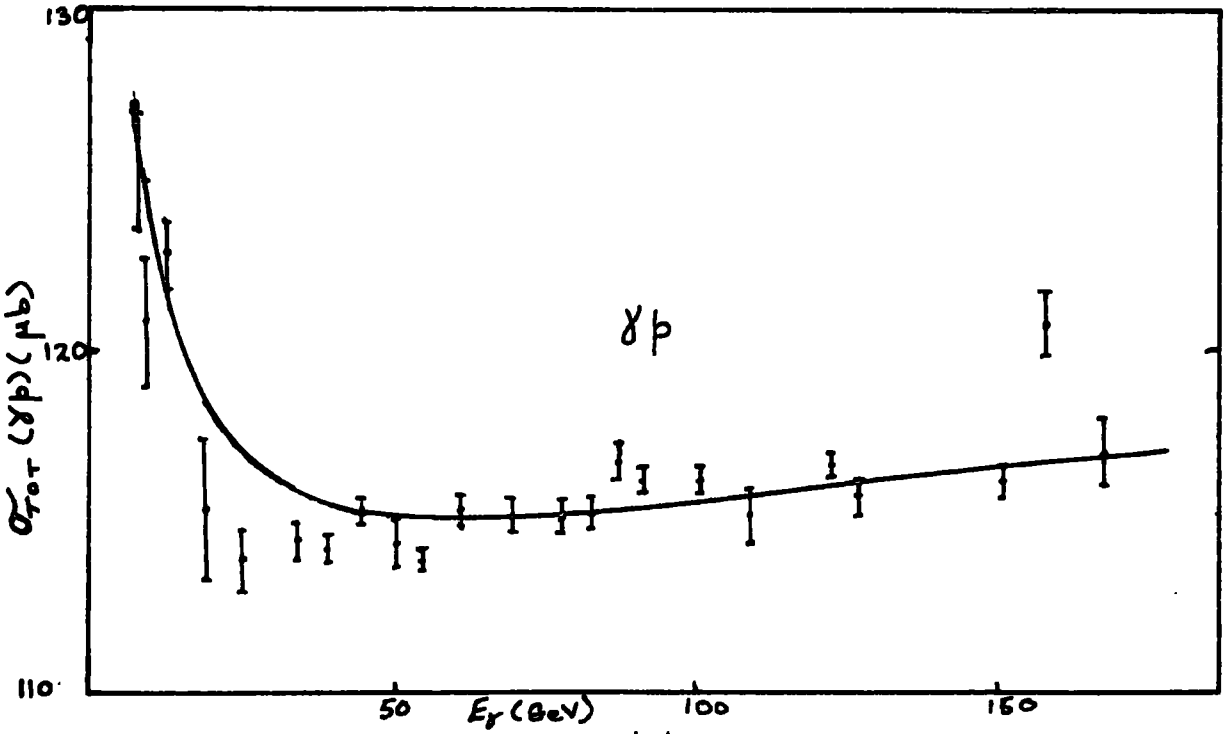

Figure 3.4.1: Our prediction of $\sigma_{\gamma p}^{tot}(s)$ against the data of reference (60).

Shown in Table 3.4.2 is $\sigma_V^{tot}(\gamma p)$, where the suffix V refers to the contribution of the vector meson V to the photon-proton total cross-section. As can be seen, the ψ makes a significant contribution to $\sigma_{\gamma p}^{tot}(s)$, while with our assumptions, the T makes a negligible contribution, certainly much smaller than estimates by other authors (72).

So, as we have demonstrated, the parametrization detailed in the previous chapter has enabled us to make accurate predictions of total cross-sections and vector meson differential cross-sections. In the following chapter, we extend the range of applicability of our model by attempting to describe the diffractive production of high spin meson and baryon resonances.

Vector (MeV)	Experimental Width (KeV)	Predicted Width (KeV)
ρ (759)	6.4 ± .8	5.43
ρ' (1323)	2	1.7
ρ'' (1711)	1.8 ± .4	1.0
ρ''' (2026)	1.7	0.7
ω (790)	0.76 ± 0.17	0.6
ω' (1250)	-	0.22
ω'' (1645)	0.18	0.12
ω''' (1935)	0.19	0.09
ϕ (1006)	1.31 ± .1	1.21
ϕ' (1550)	-	0.39
ϕ'' (1947)	-	0.22
ϕ''' (2276)	-	0.16
ψ (3064)	4.8 ± .6	4.8
ψ' (3525)	2.1 ± .3	1.78
ψ'' (3931)	-	0.98
ψ''' (4399)	0.44 ± 0.14	0.58
T (9455)	- 1.3 ±	1.2
T' (9760)	-	0.59
T'' (10050)	-	0.36

Table 3.4.1: Leptonic decay widths predicted from equations (3.4.3) amd (3.4.4). The particle masses are determined from the trajectory parameters of Table 2.2.2. All data from reference (73).

s	E_γ	ρ	ω	φ	ψ	T	ρ'	ρ''	ρ'''	ω'	ω''	ω'''	φ'	φ''	φ'''	ψ'	ψ''	ψ'''	T'	T''	$\sigma^{tot}_{\gamma p}(s)$
12.15	6.00	81.71	8.67	6.14			14.67	6.68	3.95	1.95	0.83	0.53	1.30	0.58	0.36						127.37
19.66	9.99	76.74	8.14	6.34	1.16		13.78	6.26	3.70	1.82	0.78	0.50	1.33	0.60	0.37						121.52
30.55	14.36	73.8	7.83	6.53	2.10		13.26	6.02	3.56	1.75	0.75	0.48	1.37	0.62	0.38	0.68	0.34	0.18			119.65
47.83	24.99	71.45	7.58	6.74	2.17		12.83	5.83	3.44	1.70	0.73	0.46	1.41	0.64	0.4	0.70	0.35	0.18			116.61
66.62	35.00	70.51	7.48	6.90	2.22		12.66	5.75	3.40	1.67	0.72	0.46	1.45	0.65	0.41	0.71	0.36	0.18			115.53
94.78	49.99	69.83	7.41	7.08	2.29		12.54	5.70	3.37	1.66	0.71	0.45	1.49	0.67	0.42	0.74	0.36	0.18			114.91
188.68	100.00	69.54	7.37	7.41	2.39	0.04	12.48	5.68	3.35	1.65	0.71	0.45	1.56	0.70	0.44	0.76	0.38	0.20	0.	0.01	115.15
282.56	150	69.86	7.41	7.61	2.45	0.04	12.55	5.70	3.37	1.66	0.71	0.45	1.60	0.72	0.45	0.79	0.39	0.20	0.02	0.01	116.0
376.48	200	70.27	7.45	7.76	2.51	0.04	12.62	5.73	3.39	1.67	0.72	0.46	1.63	0.74	0.46	0.80	0.40	0.21	0.02	0.01	116.89
451.6	240	70.68	7.50	7.87	2.54	0.04	12.69	5.77	3.41	1.68	0.72	0.46	1.65	0.75	0.46	0.81	0.41	0.21	0.02	0.01	117.68

Table 3.4.2: Our prediction of $\sigma^{tot}_{\gamma p}(s)$ and $\sigma^{tot}_{V}(\gamma p)$, where the suffix V refers to the contribution of the vector meson V to the γ-p total cross-section.

CHAPTER 4

DIFFRACTIVE RESONANCE PRODUCTION

4.1 Introduction

In this chapter, we apply the reggeon-photon coupling analogy to diffractive meson and baryon production. Since the RPCA gives a relation between covariant couplings, once the reggeon couplings at one selected vertex have been determined, as in Chapter 2, the form of the couplings in all the amplitudes in all other processes can be predicted (up to the unknown orbital angular momentum coupling constants g_1, g_2 if one or both of the particles at that vertex has $\ell > 0$).

In the following sections, we apply this hypothesis to the data on A_2, K*, K** and N* production.

4.2 Diffractive Boson Production

We apply our model to the reactions $\pi^{\pm}p \to A_2^{\pm} p$, $K^{\pm}p \to K^{*\pm}p$ and $K^{\pm}p \to K^{**\pm}p$. These processes are particularly interesting because (a) the data are adequate for a quantitative test (in contrast to $\pi p \to A_1 p$, $Kp \to Qp$ for example), (b) the meson vertices have unnatural parity and so there is only a single covariant coupling g_1^{ℓ} if the vector coupling hypothesis is correct and (c) at the meson vertex in each of these processes

$$P_i P_j \neq (-1)^{S_i - S_j} \qquad (4.2.1)$$

where P_i refers to the parity and S_i the spin of particle i, and so according to the Gribov-Morrison rule (74) pomeron exchange is not allowed, whereas our model demands that P exchange should occur (although it will be suppressed at the KK* vertex due to R-parity - see later). Hence this set of processes should provide a stringent test for our hypothesis.

(Kisslinger (75) has proposed a somewhat related model which has been applied to non-diffractive processes in reference (76)).

4.2(a) $\pi^{\pm} p \to A_2^{\pm} p$

At the π - A_2 vertex, G-parity allows only the following regge pole exchanges: I = O, P, f, η, D; I = 1, ρ, B. The η and D exchanges are very low lying trajectories, and the smallness of the charge exchange $\pi^- p \to A_2^o n$ process relative to elastic scattering indicates that the ρ and B exchanges will be fairly small, although the unnatural parity B exchange does make a significant contribution at low energies. However, we will find when discussing the data that it is possible to make simple corrections for the unnatural parity exchange in both this process and in K* production. Thus we are left with just the P, f and ρ exchanges as in elastic πp scattering.

Since we have helicity conservation at the $N\bar{N}$ vertex (the P and f exchanges have no flip couplings) we can write for $\pi p \to A_2 p$ (that is, 1 + 2 → 3 + 4, see Figure 4.2.1)

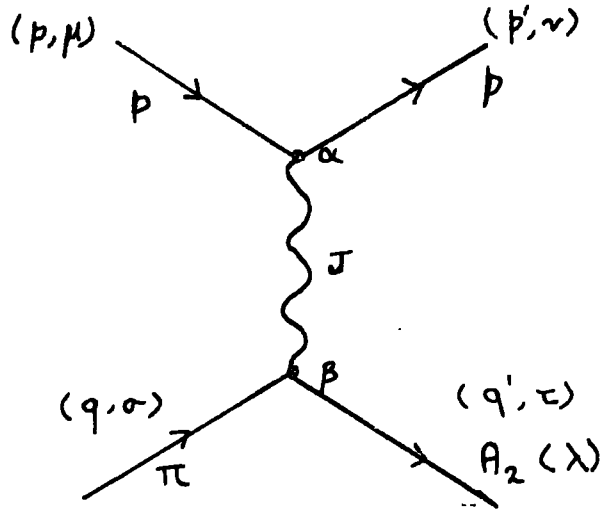

Figure 4.2.1: Reggeon exchange in $\pi p \to A_2 p$. λ is the A_2 helicity and the notation is as in Figure 1.3.2.

$$\frac{d\sigma}{dt} = \frac{0.3893}{16\pi s^2} \sum_{\lambda} |A_{\lambda}(s,t)|^2 \qquad (4.2.2)$$

where the s-channel helicity amplitudes are

$$A_{\lambda}(s,t) = A_{0\frac{1}{2}\lambda\frac{1}{2}}(s,t) \qquad (4.2.3)$$

λ being the helicity in the s-channel of the A_2 produced ($\lambda = 2,1,0,-1,-2$). From equations (1.5.1) and (1.5.2) the contribution of a reggeon to these amplitudes may be written in the form

$$A^R_{\lambda}(s,t) = -\left(\frac{-t}{s_o}\right)^{\frac{1}{2}|\lambda_1-\lambda_3|}\left(\frac{-t}{s_o}\right)^{\frac{1}{2}|\lambda_2-\lambda_4|} V^-_{\lambda_1\lambda_3}(\pi A_2)\, V^+_{\lambda_2\lambda_4}(pp)\, x$$

$$R(s,\alpha(t)) \qquad (4.2.4)$$

$$= -\left(\frac{-t}{s_o}\right)^{\lambda/2} V^-_{o\lambda}(\pi A_2)\, V^+_{\frac{1}{2},\frac{1}{2}}(pp)\, R(s,\alpha(t)) \qquad (4.2.5)$$

where $t' = t - t_{min}$ and $R(s, \alpha(t))$ is defined in equation (2.2.2).

The helicity vertex functions at the $N\bar{N}$ vertex are as in Chapter 2 (see Table 1.5.1). At the π-A_2 vertex we find from Table 1.5.1 that at $t = 0$

$$V^-_{0,2}(\pi A_2) = -V^-_{0,-2}(\pi A_2) = \frac{g_2^S g_1^1 M_o}{4M_+} \qquad (I = 0) \qquad (4.2.6)$$

$$= \frac{g_2^V g_1^1 M_o}{4M_+} \qquad (I = 1) \qquad (4.2.7)$$

$$V^-_{0,1}(\pi A_2) = V^-_{0,-1}(\pi A_2) = \frac{g_2^S T g_1^1}{2M_{A_2} M_+} \qquad (I = 0) \qquad (4.2.8)$$

$$= \frac{g_2^V T g_1^1}{2M_{A_2} M_+} \qquad (I = 1) \qquad (4.2.9)$$

and

$$V^-_{00}(A_2) \equiv 0, \quad I = 0, 1 \qquad (4.2.10)$$

where

$$T \equiv \frac{1}{4}\,(M_{A_2}^2 - M_\pi^2 + t) \quad \text{and} \quad M_+ = \frac{(M_{A_2} + M_\pi)}{2}$$

Substituting for $g_2^{S/V}$ from Table 1.3.1 in the above gives

$$\left.\begin{aligned} \bar{V}_{O,2}(\pi A_2) &= -\bar{V}_{O,-2}(\pi A_2) = \frac{2}{3}\,\frac{g_1^1 M_O}{4M_+} \qquad I = 0 \\ &= 2\,\frac{g_1^1 M_O}{4M_+} \qquad I = 1 \end{aligned}\right\} \qquad (4.2.11)$$

$$\left.\begin{aligned} \bar{V}_{O,1}(\pi A_2) &= \bar{V}_{O,-1}(\pi A_2) = \frac{2}{3}\,\frac{T\, g_1^1}{2M_{A_2} M_+} \qquad I = 0 \\ &= 2\,\frac{T\, g_1^1}{2M_{A_2} M_+} \qquad I = 1 \end{aligned}\right\} \qquad (4.2.12)$$

while at the elastic $\pi\pi$ vertex, the coupling is

$$2(g_1^{S/V} + g_2^{S/V}) = \frac{2}{3}\,,\ 2 \text{ for } I = 0, 1 \text{ exchange respectively.}$$

Thus equations (4.2.11) and (4.2.12) are just the coupling at the $\pi\pi$ vertex $t = 0$ times the kinematical factors for $\bar{V}_{O\pm1}(\pi A_2)$ and $\bar{V}_{O,\pm2}(\pi A_2)$. Hence the scattering amplitudes are built just from the elastic non-flip scattering amplitudes explained in Chapter 2, but multiplied by the kinematical factors we call $F_\lambda(t)$ and our one free parameter g_1^1 (the orbital angular momentum coupling constant) which will serve only to adjust the overall normalization - the shape of the differential cross-section will be absolutely predicted. Thus

$$A_\lambda^R(\pi p \to A_2 p) = g_1^1\, F_\lambda(t)\, A^R(\pi p \to \pi p) \text{ for P, f and } \rho \text{ exchange} \qquad (4.2.13)$$

From (4.2.11), (4.2.12) and (4.2.4), then

$$F_2(t') = -F_{-2}(t') = \frac{(-t')}{4M_+ M_o}$$

$$F_1(t') = F_{-1}(t') = \frac{T\sqrt{-t'}}{2M_{A_2} M_+ M_o} \qquad (4.2.14)$$

$$F_o(t') \equiv 0$$

(remembering that λ is the helicity of the A_2 in the s-channel) where we have set M_o = 1 GeV.

Shown in Figure 4.2.2 is our fit to the data (77) on $\frac{d\sigma}{dt}(\pi^{\pm}p \to A_2^{\pm}p)$, where we find that the best fit value is $g_1^1 = 1.10$ (all other parameters are as in Table 2.3.1). In Figure 4.2.3 we show our prediction of the integrated cross-section, and evidently we have obtained a good description of both the s and t-dependence of the data, despite the fact that only the overall normalization is free. The difference between the two charge states is given by the ρ contribution only (in our model), and we predict a cross-over zero at $|t| \simeq 0.16$ GeV^2, compared with $\simeq 0.19$ in elastic scattering. (See equation (2.2.32) and Figure 2.2.4). However, the error bars on the data are generally larger than the difference between the two charge states, indicating that the ρ contribution is rather small.

At low energies, we have corrected for unnatural parity exchange, as shown in Figure 4.2.3. In order to make this correction, we have used the data given in Figure 13 of reference (78) to multiply our prediction at each energy by the ratio (natural + unnatural)/natural. However, above a p_{LAB} of 10 GeV/C, this correction is almost irrelevant.

In a recent paper, Irving (79) has found that the P:f ratio required by this data is smaller ($\simeq \frac{1}{2}$) than that of the ratio in elastic scattering. Of course, such a result would be rather unfortunate for our model, of which the f-dominated pomeron is an important ingredient.

However, the conclusion of a suppressed P:f ratio is at least partially based on the assumption that the f contribution is determined by the decay coupling, and hence Irving's model has a much larger f contribution, leading naturally to a reduced pomeron coupling. Nevertheless, some new high statistics data (80) on $\pi^- p \to A_2^- p$ at 10.0 GeV/C suggest that the f contribution should indeed be larger than that predicted by our model. On the other hand, data at 22.4 GeV/C and 23.9 GeV/C (81) indicates that a sizeable P contribution is required in order to account for the integrated cross-section of $\simeq$ 60 μb at these energies. Furthermore, data (82) and preliminary data (83) at 50.0 GeV/C suggests that the integrated cross-section has only fallen by $\simeq$ 8 μb in the range $25 < p_{LAB} < 50$ GeV/C, implying that the P:f ratio must be of the order of, if not the same as, that required by elastic scattering.

Complicating the issue still further is the fact that in addition to the large statistical errors on the differential cross-section data, there is also a normalization error, sometimes as large as 30%, to be taken into account. Given all the ambiguities outlined in the foregoing discussion, we feel that the RPCA has given a satisfactory account of the data, while realizing that the fit is not unique. Certainly the Gribov-Morrison prediction of no pomeron coupling is in direct contradiction with the data, which shows a marked flattening at large s.

The density matrices for A_2 production are also predicted by the model. Since the reggeon contributions to each amplitude differ just by the kinematical factors $F_\lambda(t)$ of (4.2.14), the s-channel helicity frame density matrices are given by

$$\rho^H_{mm'} = \frac{F_m(t')\, F^*_{m'}(t')}{\sum_\lambda F_\lambda(t')\, F^*_\lambda(t')} \qquad (4.2.15)$$

that is, they are independent of both g_1^1 and the regge pole parameters.

So we find

$$\rho^H_{00} = \rho^H_{10} = \rho^H_{01} = \rho^H_{20} = \rho^H_{02} = 0 \qquad (4.2.16)$$

(since $F_0(t) = 0$)

and

$$\rho^H_{11} = \rho^H_{1-1} = \rho^H_{-1-1} = \frac{T^2}{2\left(T^2 - \frac{t' M^2_{A_2}}{4}\right)}$$

$$\rho^H_{22} = \rho^H_{2-2} = \rho^H_{-2-2} = \frac{(-t') M^2_{A_2}}{8\left(T^2 - \frac{t' M^2_{A_2}}{4}\right)} \qquad (4.2.17)$$

$$\rho^H_{21} = \rho^H_{2-1} = \frac{(-t')^{\frac{1}{2}} M_{A_2} T}{4\left(T^2 - \frac{t' M^2_{A_2}}{4}\right)}$$

As the bulk of the data (77) is presented in the t-channel (Gottfried-Jackson) frame, it is more convenient for us to consider our predictions in this frame. Since the VCH forbids $\Delta\lambda_t \geq 2$, we predict that in the G.J. frame

$$\rho^t_{22} = \rho^t_{2-2} = \rho^t_{-2-2} = \rho^t_{21} = \rho^t_{2-1} = \rho^t_{20} = \rho^t_{02} = 0 \qquad (4.2.18)$$

while the assumed dominance of natural parity exchange demands

$$\rho^t_{00} = \rho^t_{10} = \rho^t_{01} = 0 \qquad (4.2.19)$$

(that is, the parity constraint of a natural parity exchange at an abnormal parity vertex - see Table 1.5.1).

and

$$\rho^t_{11} = \rho^t_{1-1} = \rho^t_{-1-1} \qquad (4.2.20)$$

From the trace condition $\sum_m \rho_{mm} = 1$ we deduce that

$$\rho^t_{11} + \rho^t_{1-1} = 1 \qquad (4.2.21)$$

A comparison of these predictions with the data (77) at various energies is given in Figure 4.2.4 where we see that all density matrices $\rho_{\lambda 2}$ are negligibly small,vindicating the VCH. At low energies there is a significant fraction of unnatural parity exchange (see reference (78)), which is probably due to B exchange, so ρ_{00} does not vanish as we expect. However, at higher energies, all the relations are satisfied.

Of course, we may deduce the results (4.2.17) directly from (4.2.21) and the crossing relations for helicity states (84) in the limit $s \to \infty$. Because of (4.2.18), the crossing relation

$$\rho^H_{mm'} = \sum_{\mu\mu'} d^J_{m\mu}(\beta)\, \rho^t_{\mu\mu'}\, d^J_{\mu' m'}(-\beta) \qquad (4.2.22)$$

(where m,μ etc. are helicity labels, $d^J_{m\mu}(\beta)$ are the rotation matrices (see reference (85)) and β is the crossing angle given by (84)

$$\sin\beta = \frac{q_s}{a_3} \sin\theta_s \to \frac{\sqrt{-t}}{a_3} \qquad (4.2.23)$$

θ being the centre-of-mass scattering angle, q_s the three-momentum and

$$a_3^2 \equiv \left[t - (M_\pi - M_{A_2})^2\right]\left[t - (M_\pi + M_{A_2})^2\right] / 4M^2_{A_2} \qquad (4.2.24)$$

reduces to the following

$$\rho^H_{22} - \rho^H_{2-2} = \sin^2\beta\,(\rho^t_{11} + \rho^t_{1-1}) = \sin^2\beta$$

$$\rho^H_{11} + \rho^H_{1-1} = \cos^2\beta\,(\rho^t_{11} + \rho^t_{1-1}) = \cos^2\beta \qquad (4.2.25)$$

$$\rho^H_{21} + \rho^H_{2-1} = -\sin\beta\cos\beta\,(\rho^t_{11} + \rho^t_{1-1}) = -\sin\beta\cos\beta$$

Substitution of (4.2.23) into (4.2.25) leads, after a little algebra, to the results (4.2.17) for the helicity frame density matrices. In Appendix 3 we give an example of the calculation of the relations (4.2.25).

4.2(b) $\underline{K^{\pm}p \quad K^{*\pm}p}$

For this process the allowed exchanges are the I = O, P, f, ω, η, H and D and the I = 1 ρ, A_2, B π and A_1. The η, H and D are low-lying trajectories and thus will be ignored, leaving us with just the natural parity P, f, ω, ρ and A_2 as in elastic $K^{\pm}p$ scattering. The major error is the neglect of π exchange which we expect to be important near the forward direction. We expect the ρ and A_2 contributions to be small since the natural parity contribution to $K^{\pm}p \to K^{*o}n$ is small (87) compared to $K^{\pm}p \to K^{*\pm}p$.

Referring to Table 1.5.1 we find that the helicity vertex functions at the KK^* vertex are

$$V^-_{O1}(KK^*) = V^-_{O-1}(KK^*) = -\frac{(g^S_2 + g^S_2)M_o}{2\sqrt{2}M_+} \qquad (I = O)$$

$$= \frac{-g^V_2 M_o}{2\sqrt{2}M_+} \qquad (I = 1) \qquad (4.2.26)$$

$$V^-_{OO}(KK^*) \equiv O$$

For elastic scattering, the $K\bar{K}$ vertex functions are, from Table 1.5.1

$$(g_1^S + g_2^S + g_1^S + g_2^S) = -\frac{1}{3} \quad (I = 0)$$

$$= -1 \quad (I = 1) \quad (S \to V) \tag{4.2.27}$$

(using Table 1.3.1 for $g^i_{1,2}$ etc.) and

$$(g_2^S + g_2^S) = -\frac{1}{3}(-1) \quad \text{for} \quad I = 0 \ (1) \quad (S \to V) \tag{4.2.28}$$

Thus, from (4.2.26), the functions $F_\lambda(t)$ are given by

$$F_1(t) = F_{-1}(t) = \frac{1}{\sqrt{2}} \frac{\sqrt{-t'}}{M_+} \tag{4.2.29}$$

where λ is the helicity of the K^* (in the s-channel) and $M_+ = \frac{M_{K^*} + M_K}{2}$.

We can see from (4.2.28) that we are in a position to make an absolute prediction for the process $K^{\pm}p \to K^{*\pm}p$ since the exchanges are as in elastic $K^{\pm}p$ scattering and the vertex functions do not contain factors of g_1^1, since the K^* is a $j = 1$, $\ell = 0$, $S = 1$ state. Thus, our model for the process predicts

$$A^R_\lambda (Kp \to K^*p) = F_\lambda(t)\, A^R (Kp \to Kp) \tag{4.2.30}$$

However, for the pomeron coupling, we must take into account the effect of R parity (that is, G-parity generalized to SU(3) multiplets, see for example, page 282 of reference (86)) which changes the P:f ratio at the KK^* vertex with respect to the $K\bar{K}$ vertex.

As we have demonstrated in Chapter 2, under the assumption of ideal mixing (20) the P coupling at the $K\bar{K}$ vertex is (see Figure 2.2.5)

$$\frac{g^{PKK}(t)}{g^{fKK}(t)} = \frac{B_{ff}^{\frac{1}{2}}}{(\alpha_P(t) - \alpha_f(t))} + \frac{g^{f'KK}}{g^{fKK}} \frac{B_{ff'}^{\frac{1}{2}}}{(\alpha_P(t) - \alpha_{f'}(t)} \tag{4.2.31}$$

which reduces to

$$\frac{g^{PKK}(t)}{g^{fKK}(t)} = \rho(t)\ (1 + r_s(t)) \qquad (4.2.32)$$

where B_{ff}, $B_{ff'}$ represent the pomeron and its couplings to f and f', $\rho(t)$ is the P:f ratio for non-strange vertices (see Table 2.3.1) and

$$r_s(t) = \frac{\alpha_p(t) - \alpha_f(t)}{\alpha_p(t) - \alpha_{f'}(t)} \qquad (4.2.33)$$

and is given in Table 2.2.2. At the KK^* vertex, there is no coupling of the singlet (f_1) part of the f and f' due to R-parity.

(where $f = \frac{f_8}{\sqrt{3}} + \sqrt{\frac{2}{3}} f_1$

$f' = \sqrt{\frac{2}{3}} f_8 - \sqrt{\frac{1}{3}} f_1$) (4.2.34)

because an antisymmetric (F-type) coupling is necessary, and this is only available for f_8. Hence we find

$$g^{f'KK^*} = \sqrt{2}\, g^{fKK^*} \qquad (4.2.35)$$

c.f. $g^{f'KK} = -\sqrt{2}\, g^{fKK}$)

and so

$$g^{PKK^*}(t) = g^{fKK^*}\, \rho(t)(1 - r_s(t)) \qquad (4.2.36)$$

giving

$$\frac{g^{PKK^*}(t)}{g^{PKK}(t)} = \frac{g^{PKK^*}(t)}{g^{fKK^*}} \frac{g^{fKK^*}}{g^{fKK}} \frac{g^{fKK}}{g^{PKK}(t)}$$

$$= \frac{1 - r_s(t)}{1 + r_s(t)} = 0.163 \quad (\text{at } t = 0) \qquad (4.2.37)$$

where we have deduced the value 0.163 from Table 2.2.3.

So the pomeron coupling in the process $K^{\pm}p \to K^{*\pm}p$ is suppressed relative to the f and ω couplings, and thus equation (4.2.30) becomes

$$A_\lambda(K^{\pm}p \to K^{*\pm}p) = F_\lambda(t)\left[\left(\frac{1 - r_s(t)}{1 + r_s(t)}\right)A^P(Kp) + A^f(Kp) + A^{A_2}(Kp) \mp A^\omega(Kp) \mp A^\rho(Kp)\right] \quad (4.2.38)$$

where the right hand side contains the elastic scattering amplitudes. From the above we see that the pomeron contribution is suppressed quite substantially, and thus the process comes much closer to fulfilling the Gribov-Morrison requirement of no pomeron exchange.

The resulting predictions of the differential and integrated cross-section data (87) are shown in Figures 4.2.5 and 4.2.6, where we see that despite the fact that we have no free parameters, the overall normalization and shape of the data is predicted with remarkable accuracy. The difference between the two charge states is given by the ρ and ω contributions (which are, of course, odd under charge conjugation) and we predict a cross-over at $|t| \simeq 0.15$ GeV^2 which appears to be vinidcated by the data (88), although new data (89) at 13.0 GeV/C suggest that the cross-over is further out in $|t|$, possibly as far as $|t| \simeq 0.4$ GeV^2. However, all the data possess overall normalization errors rendering discussion of such fine details somewhat academic. Nevertheless, the difference between the data for the two charge states is rather larger than anticipated.

The kinematical factors (4.2.29) substituted into (4.2.15) give the density matrix predictions

$$\rho^t_{00} = \rho^t_{01} = \rho^t_{10} = 0 \quad (4.2.39)$$

(since we only allow natural parity exchange).

and

$$\rho^t_{11} = \rho^t_{1-1} = \frac{1}{2} \qquad (4.2.40)$$

where it can be shown (see Appendix (3)) that for spin = 1 particles, (4.2.40) holds in either the helicity or the G.J. frame. A comparison with the data (90) is given in Figure 4.2.7, which confirm the dominance of natural parity exchange except near t = 0.

4.2(c) $\underline{K^{\pm}p \to K^{**\pm}p}$

Here the same exchanges as for K^* production are allowed in principle, and again we restrict ourselves to the I = 0, P, f and ω and the I = 1 ρ, and A_2 exchanges in practice. Since there is no suppression of the pomeron at the KK^{**} vertex due to R-parity, we may write, following the example of A_2 production given above,

$$A^R_\lambda(Kp \to K^{**}p) = g^1_1 F_\lambda(t') A^R(Kp \to Kp) \qquad (4.2.41)$$

with $\lambda = \pm 2, \pm 1, 0$. From Table 1.5.1 the helicity vertex functions at the KK^{**} vertex are

$$V^-_{02}(KK^{**}) = -V^-_{0-2}(KK^{**}) = \frac{1}{8M_+}\left(g^s_2 + g^S_2\right) g^1_1 M_o$$

$$V^-_{01}(KK^{**}) = V^-_{0-1}(KK^{**}) = \frac{Tg^1_1}{4M_+ M_{K^{**}}}\left(g^s_2 + g^S_2\right) \qquad (4.2.42)$$

$$V^-_{00}(KK^{**}) \equiv 0$$

for I = 0 exchange, with g^s_2, $g^S_2 \to g^V_2$ for I = 1 exchange. The vertex functions for the $K\bar{K}$ vertex are as in equations (4.2.27) and (4.2.28), and thus, making the usual substitutions for $g^i_{1,2}$ from Table 1.3.1, the kinematical factors $F_\lambda(t)$ are given by

$$F_2(t') = -F_{-2}(t') = \frac{-t'}{4M_+ M_o}$$

$$F_1(t') = F_{-1}(t) = \frac{T\sqrt{-t'}}{2M_+ M_{K^{**}} M_o} \qquad (4.2.43)$$

where

$$T \equiv \frac{1}{4}(M^2_{K^{**}} - M^2_K + t')$$

The resulting fits to the differential and integrated cross-section data (91) are shown in Figures 4.2.8 and 4.2.9 where in Figure 4.2.9 we have used the data (92) on the ratio (unnatural + natural)/ natural to make the correction for unnatural parity exchange to our prediction of the integrated cross-section. We find the best fit value of g_1^1 to be 1.16, and evidently a satisfactory account of the data is obtained.

The density matrices should obey the relations (4.2.18) - (4.2.21), viz.

$$\rho^t_{22} = \rho^t_{2-2} = \rho^t_{-2-2} = \rho^t_{21} = \rho^t_{2-1} = \rho^t_{20} = \rho^t_{02} = 0. \qquad (4.2.44)$$

$$\rho^t_{00} = \rho^t_{01} = \rho^t_{10} = 0 \qquad (4.2.45)$$

and

$$\rho^t_{11} + \rho^t_{1-1} = 1$$

where the above obviously obey the transformation relations (4.2.25). In Figure 4.2.10 we display our prediction of the data (93) where we see that the agreement is fairly satisfactory. However, even at the higher s and $|t|$ values, $(\rho^t_{11} + \rho^t_{1-1})$ is still less than one. This is due partly to the non-vanishing of ρ_{00}, indicating the occurrence of unnatural parity exchange event at high ($\simeq$ 16 GeV/C) p_{LAB} and $|t|$, and partly due to the inequality

of ρ_{11} and ρ_{1-1}. However, as the data are obtained simply by making a mass cut in the K^{**} mass region (see, for example, reference (94)), there may well be a significant unnatural parity exchange contribution to the background underlying the resonance.

From the foregoing analysis of the diffractive production of A_2, K^* and K^{**}, we see that the reggeon-photon coupling analogy has given a satisfactory account of the available data, especially the data on density matrices, which give a remarkable vindication of the vector coupling hypothesis, which forbids $\Delta\lambda_t \geqslant 2$ and hence requires that the t-channel production density matrices $\rho_{mm'}$ with $|m|$ or $|m'| = 2$ should be negligible. However, as we have mentioned in 4.2(a), there is some debate on the value of the P:f ratio for these processes (see reference (79)). Very high statistics data (80) on $K^+p \to K^{**+}p$ at 10.0 GeV/C gives a value of 131 ± 23 μb GeV^{-2} for $\frac{d\sigma}{dt}$ (MAX) to be compared with our value of $\simeq 86$ μb GeV^{-2}. Thus our cross-section would appear to be a little too small at this energy. Furthermore, as shown in Figure 4.2.9, our account of the energy dependence of the integrated cross-section for this process is only moderate. Nevertheless, at higher energies our fit is in good agreement with the data, indicating that the pomeron contribution is approximately correct, and thus giving us some confidence in the FDP hypothesis (which says that the P:f ratio in $K^{\pm}p \to K^{**\pm}p$ should be the same as in $K^{\pm}p$ elastic scattering).

In the case of K^* production, R-parity strongly suppresses the pomeron coupling, and thus the energy dependence is predicted to be quite steep (see Figure 4.2.6). For A_2 production, the data appear to be inconsistent, even when the normalization errors are taken into account.

Irving has argued that in fact one should reduce the P:f ratio in all three processes to $\simeq \frac{1}{2}$ its value in elastic scattering. In the case

of K^* production, we disagree with this hypothesis, but in K^{**} and A_2 production, it is arguable that our P:f ratio is too big. However, given the large statistical errors, the inconsistencies which are manifest when going to an adjacent energy and the rather large normalization errors, we suggest that it is dangerous to drawn a hard and fast conclusion concerning the ratio of the P and f contributions. The present data are not adequate for such tests. What is required are more high statistics data, as in reference (80), at various energies, including some in the region 50 → 100 GeV/C, which would allow one to make decisive tests between the various models.

4.3 Diffractive Baryon Production

In this section we apply the RPCA to the diffractive production of baryons, in particular to the processes $pp \to pN^*(\frac{3}{2}^-, 1520)$, $pp \to pN^*(\frac{5}{2}, 1688)$ and $pp \to pN^*(\frac{7}{2}^-, 2190)$. Since the results we will obtain have been reported in detail by Collins and Gault (95) we will only briefly outline the procedure. (In fact, the work of reference (95) was the first major test of the RPCA hypothesis). Furthermore, we will restrict our analysis of the data to small $|t|$ (< 1 GeV^2) in order to circumvent the need to insert the $P \otimes P$ cut in our amplitudes. However, Collins and Gault (95) have demonstrated that with the inclusion of the $P \otimes P$ cut, the model is capable of giving an extremely good fit to all the data on the above processes. In fact, the RPCA takes the shape of the pp differential cross-section, multiplies the elastic amplitudes by the factors $F_\lambda(t)$ and predicts, up to a normalization parameter (the covariant orbital angular momentum coupling constant g_1^1) the pN^* differential cross-section. To extend the fit to large $|t|$ one merely includes the $P \otimes P$ cut as determined from elastic scattering (40) and allows oneself one further normalization parameter which determines the pole:cut strength in N^* production.

4.3(a) $pp \to pN^*\ (\frac{3}{2}^-, 1520)$

We assume for simplicity that the dominant exchanges occurring in both this process and in the other two N^* processes we are considering (that is, $N^*\ (\frac{5}{2}^+, 1688)$ and $N^+\ (\frac{7}{2}^-, 2190)$) are the I = 0, P f and ω and the I = 1 ρ and A_2. However, in our model the $\rho - A_2$ degeneracy is broken only in trajectory (see equation (2.2.29) with $\epsilon_1' \equiv 0$) and thus we expect that to a very good approximation the neglect of the ρ and A_2 exchanges will have a negligible effect. Nevertheless, we have checked that their inclusion makes no significant difference. Thus we are left just with the dominant I = 0 P, f and ω exchanges. Referring to Table 1.5.1(a) we see that the helicity vertex functions for isoscalar exchange at the pN^* vertex are

$$V^+_{\frac{1}{2},\frac{1}{2}}(pN^*_{1520}) = \sqrt{\tfrac{2}{3}}\,\frac{1}{M_{N^*}}\left[3g_1^S\, g_2^1\, M_o - 3(g_1^S + g_2^S)\, T\,\frac{g_1^1}{M_o}\right]$$

$$- \frac{(3g_1^S + 2g_2^S)}{2M_+}\,\frac{g_1^1\, t}{2\sqrt{6}\, M_o}$$

$$V^+_{\frac{1}{2},-\frac{1}{2}}(pN^*_{1520}) = 3(g_1^S + g_2^S)\,\frac{g_1^1}{2\sqrt{6}} + \frac{(3g_1^S + 2g_2^S)}{2M_+}\,\frac{T\, g_1^1}{M_{N^*}}\sqrt{\tfrac{2}{3}}$$

$$-\sqrt{\tfrac{2}{3}}\,\frac{1}{M_{N^*}}\,\frac{3g_1^S\, g_2^1}{2M_+}\, M_o^2 \qquad (4.3.1)$$

$$V^+_{\frac{1}{2},\frac{3}{2}}(pN^*_{1520}) = -3(g_1^S + g_2^S)\,\frac{g_1^1}{2\sqrt{2}}$$

$$V^+_{\frac{1}{2},-\frac{3}{2}}(pN^*_{1520}) = -\frac{(3g_1^S - 2g_2^S)}{2M_+}\,\frac{g_1^1\, M_o}{2\sqrt{2}}$$

where $M_+ = \frac{M_{N^*} + M_N}{2}$ and $T \equiv \frac{1}{4}(M^2_{N^*} - M^2_N + t)$

while at the pp vertex

$$V^{+}_{\frac{1}{2},\frac{1}{2}}(pp) = 3(g_1^S + g_2^S)$$

$$V^{+}_{\frac{1}{2},-\frac{1}{2}}(pp) = \frac{3g_1^S + 2g_2^S}{2M_p} M_o \qquad (4.3.2)$$

(as in elastic scattering).

Substituting the values of $g^S_{1,2}$ from Table 1.3.1 we see that the isoscalar P, f and ω non-flip exchanges (the flip coupling is predicted to vanish) in the process $pp \to pN^*_{1520}$ are as in $pp \to pp$ scattering except for the kinetmatical factors $F_\lambda(t)$, with $\lambda \equiv N^*$ helicity in the s-channel, where the factors $F_\lambda(t)$ are deduced from (4.3.1), viz:

$$F_{\frac{1}{2}}(t) = -\sqrt{\frac{2}{3}} \frac{M_o}{M_{N^*_{1520}}} \left[2g_2^1 + \frac{T\, g_1^1}{M_o^2} \right]$$

$$F_{-\frac{1}{2}}(t) = \frac{g_1^1}{2\sqrt{6}} + \sqrt{\frac{2}{3}} \frac{g_2^1}{M_+ M_{N^*}} M_o^2 \qquad (4.3.3)$$

$$F_{\frac{3}{2}}(t) = -\frac{g_1^1}{2\sqrt{2}}$$

$$F_{-\frac{3}{2}}(t) = 0$$

where we have as usual set M_o = 1 GeV.

Using the observed smallness of the $\lambda = \frac{1}{2}$ radiative decay amplitude for $N^* \to N\gamma$, we deduce (see Appendix 4)

$$g_2^1 \simeq - \frac{(M_{N^*_{1520}} - M_N)^2}{2M_{N^*_{1520}}} \frac{(M_{N^*_{1520}} + M_N)}{4M_o^2} g_1^1 \qquad (4.3.4)$$

Substituting (4.3.4) into (4.3.3) we may write

$$A_\lambda(pp \to pN^*_{1520}) = g_1^1 F_\lambda(t) A(pp \to pp) \qquad (4.3.5)$$

where in the right hand side of equation (4.3.5) we are using only the isoscalar exchanges as derived in Chapter 2. Thus the differential cross-section for the process $pp \to pN^*_{1520}$ is predicted to be just the pp differential cross-section times the factors $F_\lambda(t)$ which are regge parameter independent, as in the case of diffractive boson production, and the coupling constant g_1^1, which is the coupling to the orbital angular momentum of the $\ell = 1$ $N^* \frac{3}{2}^-$ state.

In Figure 4.3.1 we display our fit to the data (96) for $|t| < 1.0$ GeV^2, with a best fit value of $g_1^1 = 0.86$. As can be seen we appear to account for both the s and t-dependence of the data extremely well, despite the fact that the t-dependences of the pp and pN^*_{1520} $\frac{d\sigma}{dt}$'s are very different. Furthermore we obtain the correct energy dependence, vindicating the FDP hypothesis, which implies that the P:f coupling ratio is the same in both processes.

4.3(b) $pp \to pN^*_{1688}$

Following the example of Section 4.3(a), from the helicity vertex function of Table 1.5.1(a), the kinematical factors $F_\lambda(t)$ are given by:-

$$F_{\frac{1}{2}}(t) = \frac{1}{\sqrt{10}}\left[\frac{g_1^2 t}{4M_o^2} + \frac{2T^2 g_1^2}{M_{N^*}^2 M_o^2} + \frac{4Tg_2^2}{M_{N^*}^2} + \frac{t g_2^2}{2M_{N^*}M_+}\right]$$

$$F_{-\frac{1}{2}}(t) = \frac{-1}{\sqrt{10}\, M_{N^*}}\left[g_2^2 M_o + \frac{T g_1^2}{M_o} + \frac{2T g_2^2 M_o}{M_+ M_{N^*}}\right]$$

$$F_{\frac{3}{2}}(t) = \frac{1}{\sqrt{5}\, M_{N^*}}\left[\frac{T g_1^2}{M_o} + M_o g_2^2\right] \qquad (4.3.6)$$

$$F_{-\frac{3}{2}}(t) = \frac{g_1^2}{8\sqrt{5}} + \frac{g_2^2 M_o^2}{2\sqrt{5}\, M_{N^*} M_+}$$

$$F_{\frac{5}{2}}(t) = \frac{g_1^2}{8}$$

$$F_{-\frac{5}{2}}(t) = 0$$

From Appendix (4) we use the relation

$$g_2^2 = -\frac{(M_{N^*_{1688}} - M_N)^2}{2M_{N^*_{1688}}} \quad \frac{(M_{N^*_{1688}} + M_N)}{4M_o^2} \quad g_1^2 \qquad (4.3.7)$$

obtained from the radiative decay (c.f. 4.3.4) $N^*_{1688} \to N\gamma = 0$ for the $\lambda = \frac{1}{2}$ decay amplitude.

Inserting (4.3.7) into (4.3.6) we may write

$$A_\lambda(pp \to pN^*_{1688}) = g_1^2 F_\lambda(t)\, A\,(pp \to pp) \qquad (4.3.8)$$

where the right hand side again refers only to the P, f and ω exchanges in elastic scattering and λ is the helicity of the N^*_{1688} in the s-channel.

With this parametrization we fit the data (96) on diffractive N^*_{1688} production as shown in Figure 4.3.2, with a best fit value of $g_1^2 = 3.97$. Again we obtain a good description of both the s and t-dependence of the data, all the more remarkable bearing in mind that our only free parameter g_1^2 serves merely to adjust the overall normalization. Thus the difference in shape of $\frac{d\sigma}{dt}$ (pp) ($\sim e^{11t}$) and $\frac{d\sigma}{dt}$ (pN^*_{1688}) ($\sim e^{6t}$) for $0.2 < |t| < 1$ GeV^2 is given solely by the factors $F_\lambda(t)$. Furthermore, referring to Collins and Gault (95), we see that at large $|t|$, we predict no diffractive minimum (which appears in elastic pp scattering at $|t| \simeq 1.4$ GeV^2 due to destructive pole-cut interference) because of the more complicated helicity structure of the processes $pp \to pN^*$.

4.3(c) $\underline{pp \to pN^*_{2190}}$

Following the two previous example we see, from Table 1.5.1(a), that the functions $F_\lambda(t)$ for I = 0 exchange (the I = 0 flip coupling ≡ 0) are given by (where λ ≡ s-channel N^*_{2190} helicity).

$$F_{\frac{1}{2}}(t) = \frac{t}{2\sqrt{70}\, M_{N^*} M_o}\left[\frac{3g_1^3\, T}{M_o^2} + 2g_2^3 - \frac{4g_2^3\, T}{M_+ M_{N^*}}\right]$$

$$- \frac{4}{\sqrt{70}\, M_{N^*}^2}\left[\frac{T^3 g_1^3}{M_o^3 M_{N^*}} + \frac{2T^2 g_2^3}{M_o^2}\right]$$

$$F_{-\frac{1}{2}}(t) = \frac{t}{\sqrt{70}}\left[\frac{3g_1^3}{16 M_o^2} - \frac{g_2^3}{2M_+ M_{N^*}}\right]$$

$$+ \frac{T}{\sqrt{70}\, M_{N^*}^2}\left[\frac{4g_2^3 M_o}{M_{N^*}} + \frac{3 T g_1^3}{M_o^2} + \frac{4g_2^3}{M_+ M_{N^*}^2}\, T M_o\right]$$

$$F_{\frac{3}{2}}(t) = \frac{1}{\sqrt{42}}\left[-\frac{3g_1^3 t}{16M_o^2} - \frac{3g_1^3 T^2}{M_o^2 M_{N^*}^2} - \frac{4g_2^3 T}{M_{N^*}^2}\right] - \frac{1}{4\sqrt{42}}\frac{t g_2^3}{M_+ M_{N^*}}$$

$$F_{-\frac{3}{2}}(t) = -\frac{1}{\sqrt{42}\,M_{N^*}}\left[\frac{M_o g_2^3}{2} + \frac{3g_1^3 T}{4M_o}\right] - \frac{2g_2^3 T M_o}{\sqrt{42}\,M_+ M_{N^*}^2}$$

$$F_{\frac{5}{2}}(t) = -\frac{1}{4\sqrt{14}\,M_{N^*}}\left[3g_1^3\frac{T}{M_o} + 2g_2^3 M_o\right] \qquad (4.3.9)$$

$$F_{-\frac{5}{2}}(t) = \frac{g_1^3}{16\sqrt{14}} + \frac{g_2^3 M_o^2}{4\sqrt{14}\,M_+ M_{N^*}}$$

$$F_{\frac{7}{2}}(t) = -\frac{g_1^3}{16\sqrt{2}} \qquad F_{-\frac{7}{2}}(t) = 0$$

Assuming that the $\lambda = \frac{1}{2}$ radiative decay amplitude for the decay $N^*_{2190} \to N\gamma = 0$, we may write (from Appendix 4)

$$g_2^3 = \frac{-\left(M_{N^*_{2190}} - M_N\right)^2}{2M_{N^*_{2190}}}\,\frac{\left(M_{N^*_{2190}} + M_N\right)}{4M_o^2}\,g_1^3 \qquad (4.3.10)$$

Substituting for g_2^3 in equations (4.3.9) allows us to write

$$A_\lambda(pp \to pN^*_{2190}) = g_1^3 F_\lambda(t)\, A\,(pp \to pp) \qquad (4.3.11)$$

in direct analogy with the previous examples. With this parametrization we fit the limited quantity of data (96) on $pp \to pN^*_{2190}$ as shown in Figure 4.3.3 and again we arrive at a good description of the data. Our

best fit value of g_1^3 is found to be 2.19.

4.4 Discussion of Results

In the two previous sections we have demonstrated how the RPCA has given a remarkably simple and accurate account of the data on diffractive boson and baryon resonance production. The only free parameters we have had at our disposal have been the dimensionless orbital angular momentum coupling constants $g_i^{1,2,3}$ $(i = 1,2)$. With our assumptions about the smallness of the $\lambda = \frac{1}{2}$ radiative decays of the N^*'s, we have be been able to constrain all our fits to the data discussed above to just one-parameter fits, the one parameter serving only to adjust the overall normalization. Thus the shape of the differential cross-sections for the processes under consideration has been absolutely predicted. However it is to these parameters $g_i^{1,2,3}$ that we now turn our attention.

In Table 4.4.1 we give a list of our best fit values of g_1^1, g_1^2, g_1^3 for the boson and baryon processes considered in the last two sections. According to our model, these g_i's are orbital angular momentum coupling constants and thus one might expect that g_i^1 (say) should be equal for πA_2, KK^{**} and $pN^*(\frac{3}{2}^-, 1520)$ production since all three resonances have $\ell = 1$. As we can see from Table 4.4.1, this condition is approximately fulfilled for πA_2 and KK^{**} but for pN^*_{1520} the coupling is somewhat lower. There are of course significant normalization errors to be taken into account, (see Section 4.2 above) sometimes as much as 30%.

Moreover, one might expect some rationalization of the g_i's when going from $\ell = 1$ to $\ell = 2$, then to $\ell = 3$. Instead the value of g_i jumps from 0.86 to 3.97 in going from $\ell = 1$ to $\ell = 2$ and then falls to 2.19 for $\ell = 3$. Furthermore, g_1^1 does not compare favourably between πA_2 and $pN^*(\frac{3}{2}^-)$ as one might expect given that meson and baryon regge trajectories

Process	ℓ	j	g_1^{ℓ}
$\pi^{\pm}p \to A_2^{\pm}p$	1	1	1.10
$K^{\pm}p \to K^{**\pm}p$	1	1	1.16
$pp \to pN^* \frac{3}{2}^-$	1	$\frac{1}{2}$	0.86
$pp \to pN^* \frac{5}{2}^+$	2	$\frac{1}{2}$	3.97
$pp \to pN^* \frac{7}{2}^-$	3	$\frac{1}{2}$	2.19

Table 4.4.1: The best fit values for g_1^{ℓ}, the orbital angular momentum coupling constants.

share approximately the same slope. Nevertheless, the agreement between πA_2 and KK^{**} is encouraging, certainly well within the inaccuracies of the data.

The results of Table 4.4.1 are perhaps a little disappointing. However, bearing in mind the simplicity of the quark model we have used as input, it is not too surprising that the agreement is not exact. Of course the RPCA itself does not require us to attach any particular significance to the g_i^{ℓ}'s. In the more usual formulation (21) of covariant reggeization the g_i^{ℓ}'s are just covariant coupling constants of an arbitrary value, to be determined by the data (see references (95), (97)), so the fact that they are all of the same order of magnitude is not without significance.

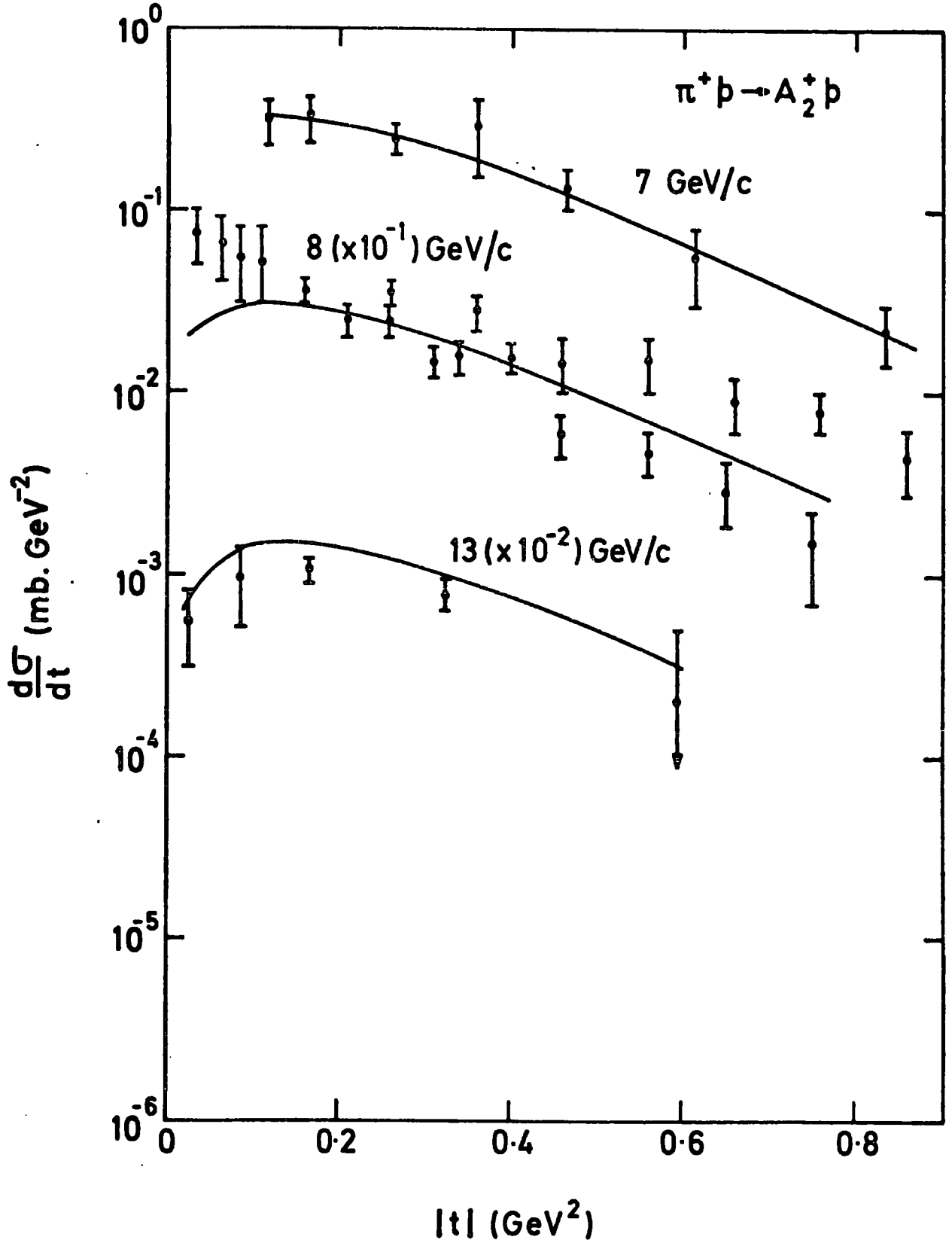

Figure 4.2.2(a) Fit to the differential cross-section $\pi^+ p \rightarrow A_2^+ p$ with data from reference (77).

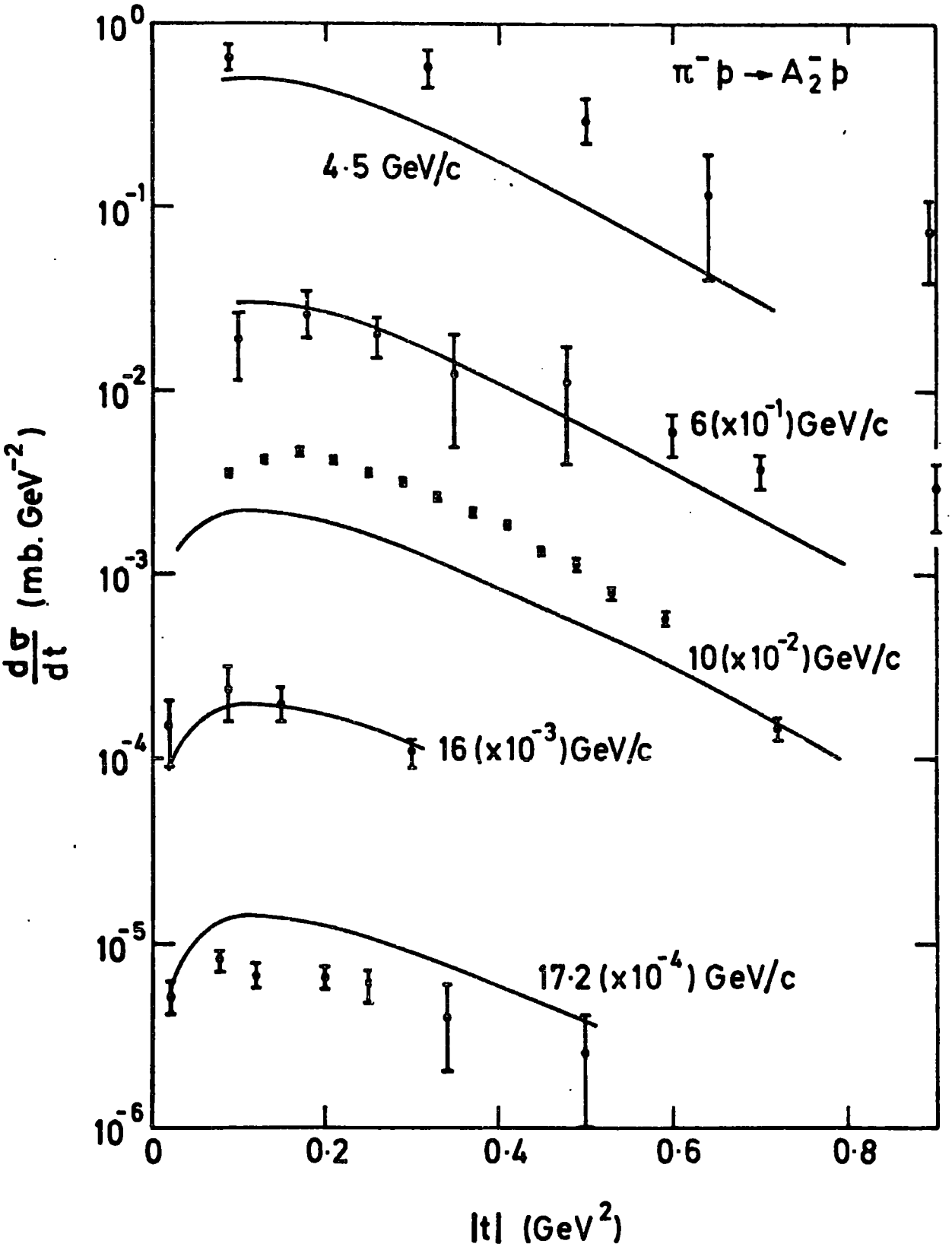

Figure 4.2.2(b) Fit to the differential cross-section $\pi^- p \to A_2^- p$ with data from reference (77).

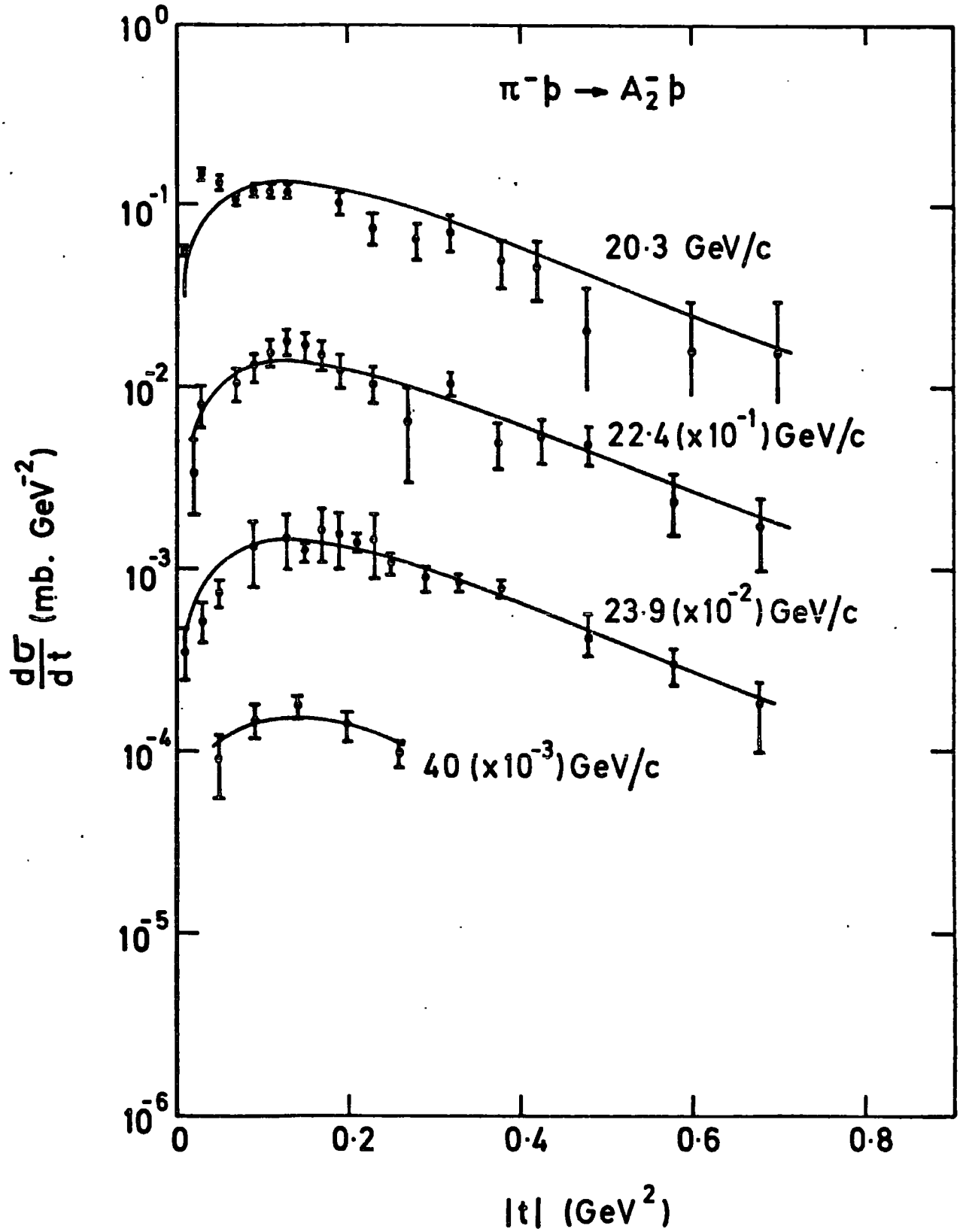

Figure 4.2.2(♣): Fit to the differential cross-section $\pi^- p \rightarrow A_2^- p$ with data from reference (77).

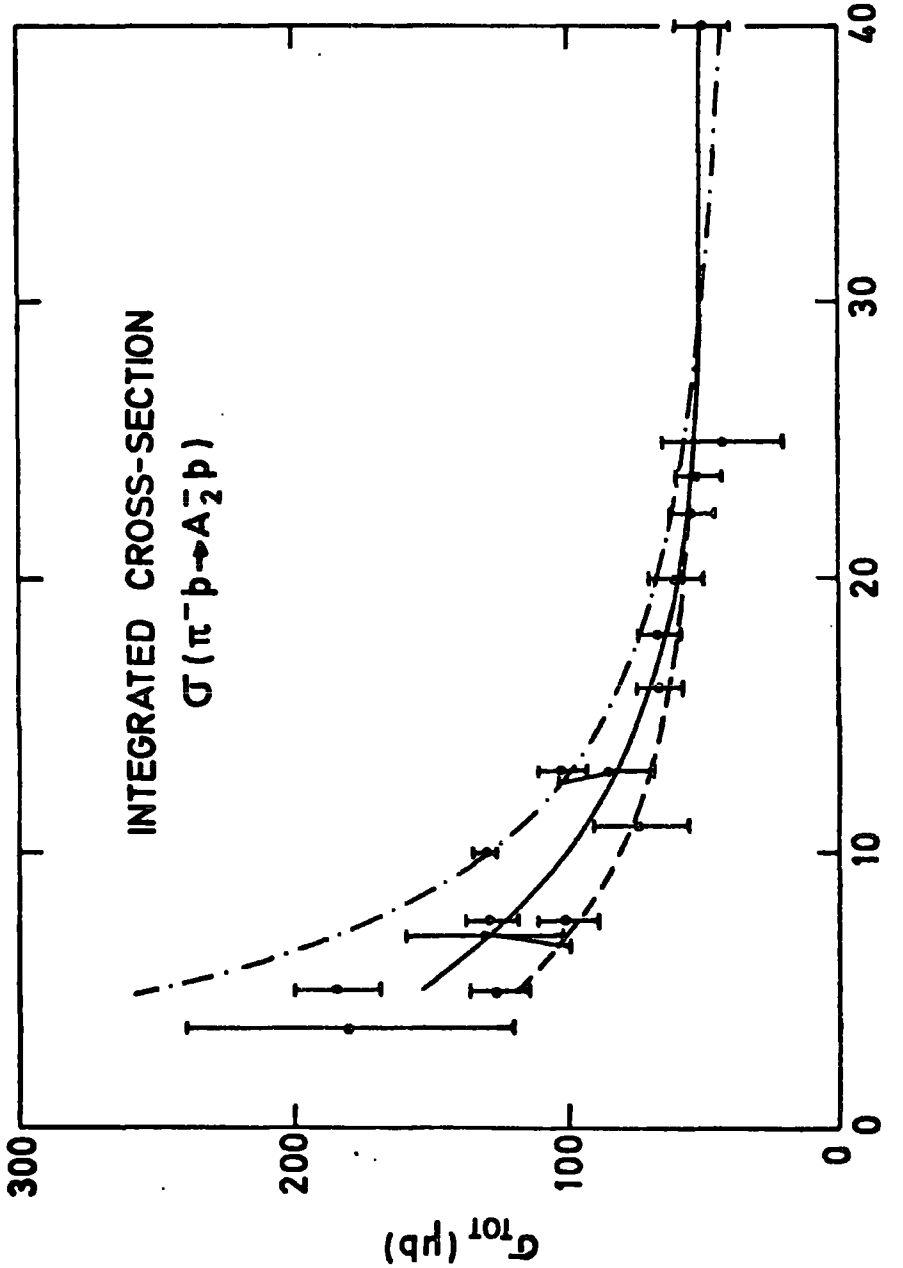

Figure 4.2.3: Prediction for the integrated cross-section $\sigma(\pi^- p \to A_2^- p)$ compared with the data of reference (77). The chain curve is the prediction of Irving (79); broken curve, uncorrected prediction of the GAH and the full curve, the prediction of the GAH for natural parity exchange corrected by ((natural + unnatural)/natural) (see reference (78)).

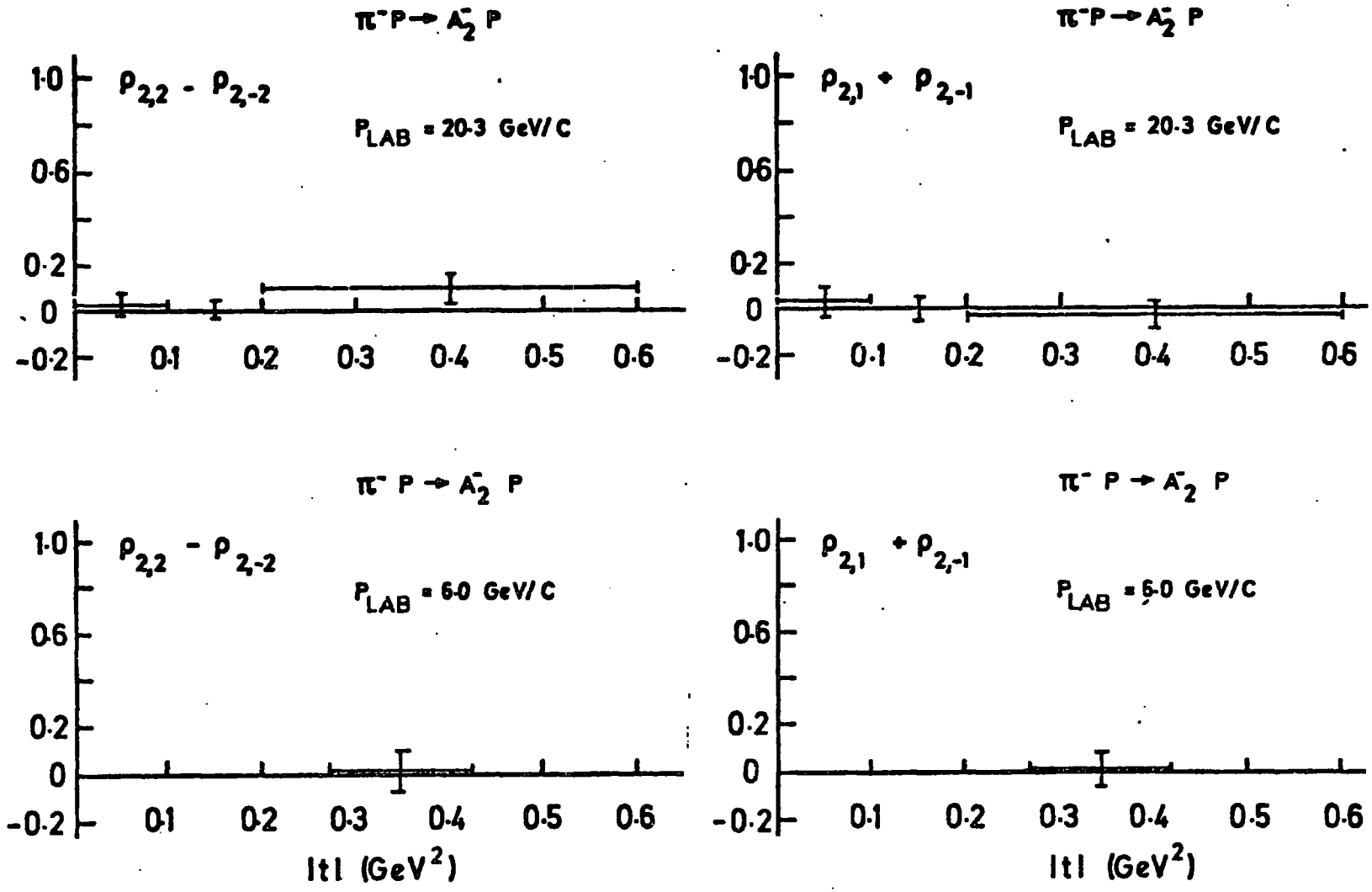

Figure 4.2.4(a): Predictions of the t-channel (Gottfried-Jackson) frame density matrices for $\pi^{\pm}p \to A_2^{\pm}p$ given in equations (4.2.18), (4.2.19), (4.2.20) and (4.2.21) compared with the data from reference (77).

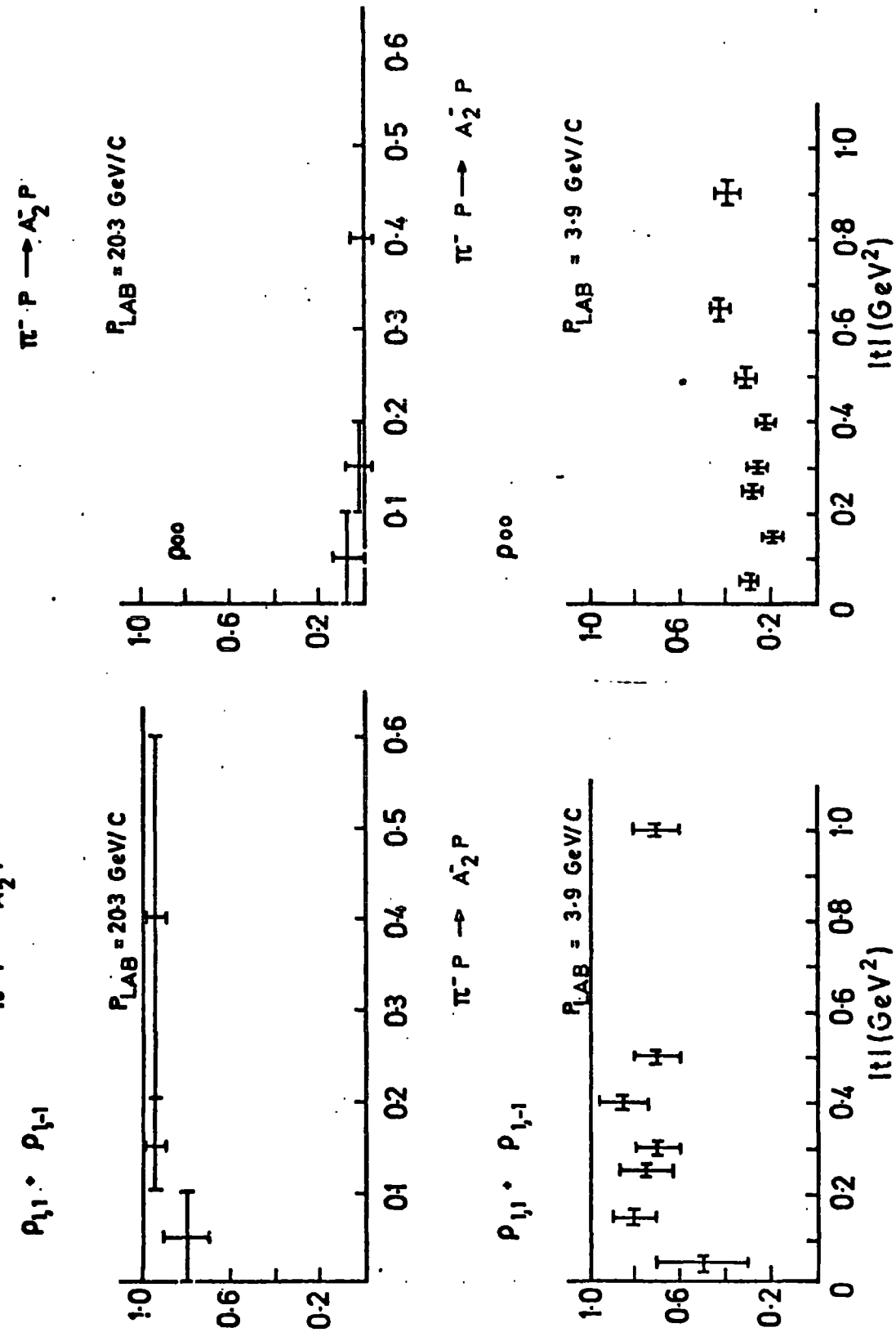

Figure 4.2.4(b): Predictions of the t-channel (Gottfried-Jackson) frame density matrices for $\pi^{\pm} p \rightarrow A_2^{\pm} p$ given in equations (4.2.18), (4.2.19), (4.2.20) and (4.2.21) compared with the data from reference (77).

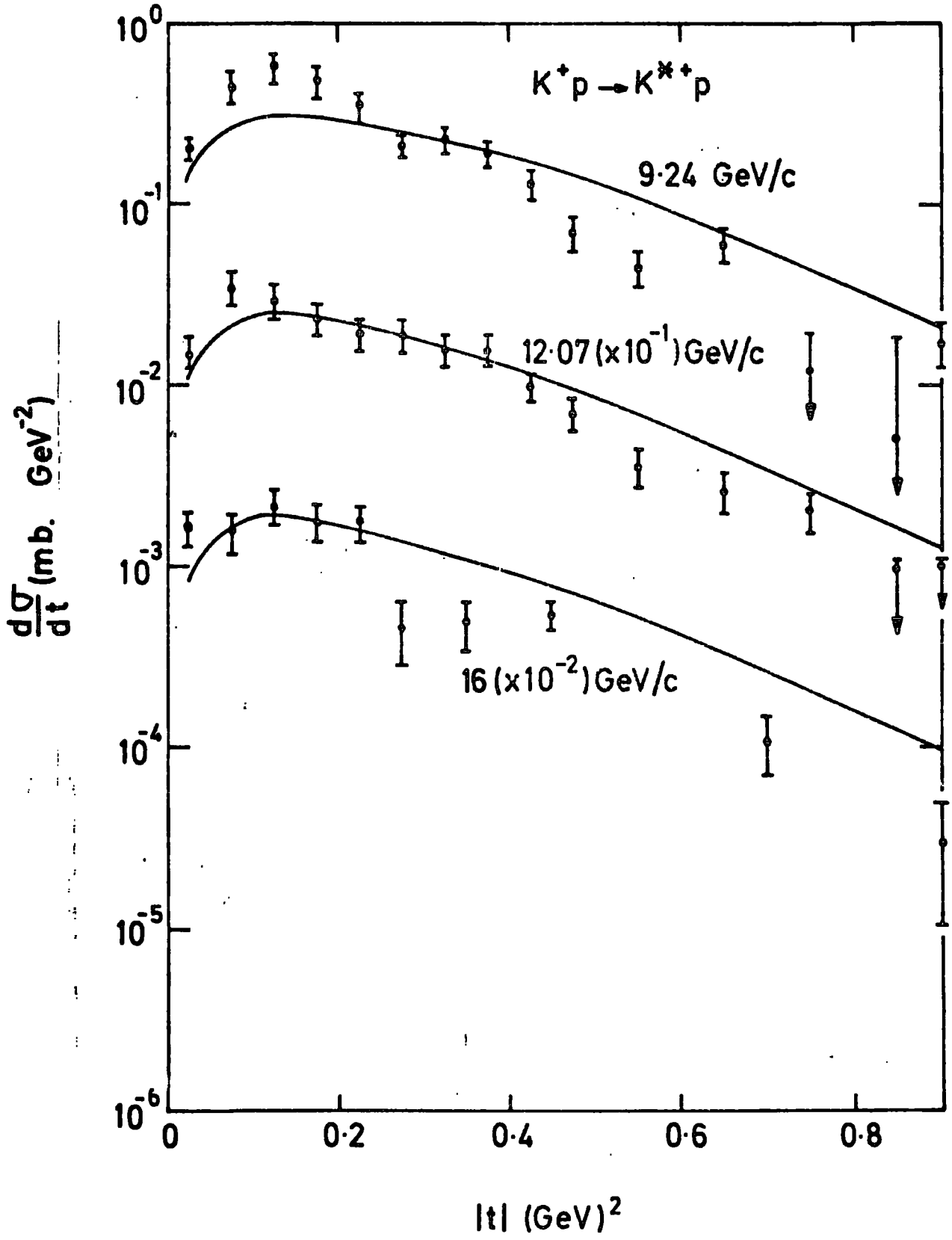

Figure 4.2.5(a): Our prediction of the differential cross-section $K^+p \rightarrow K^{*+}p$ with data from reference (87).

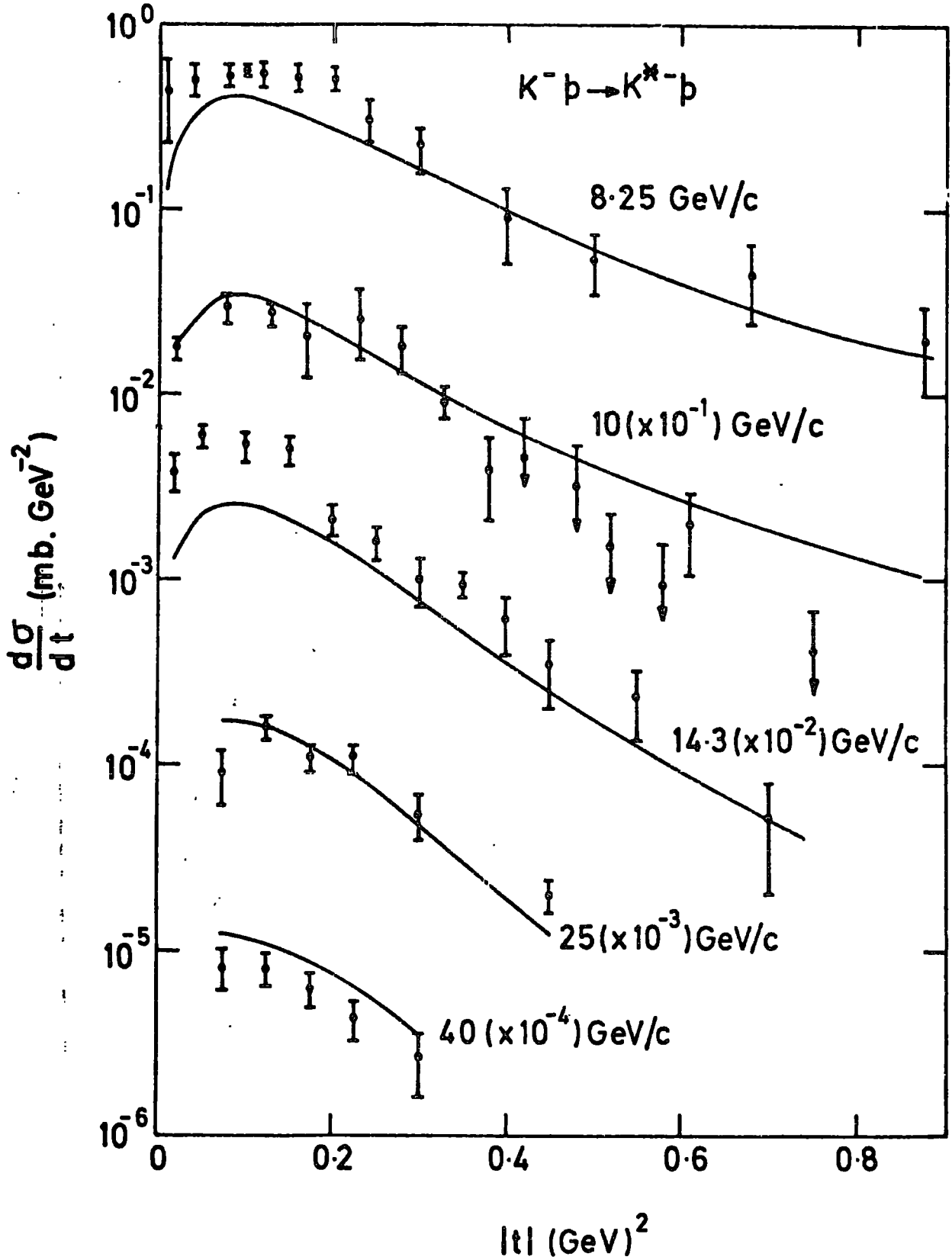

Figure 4.2.5(b): Our prediction of the differential cross-section $K^- p \to K^{*-} p$ with data from reference (87).

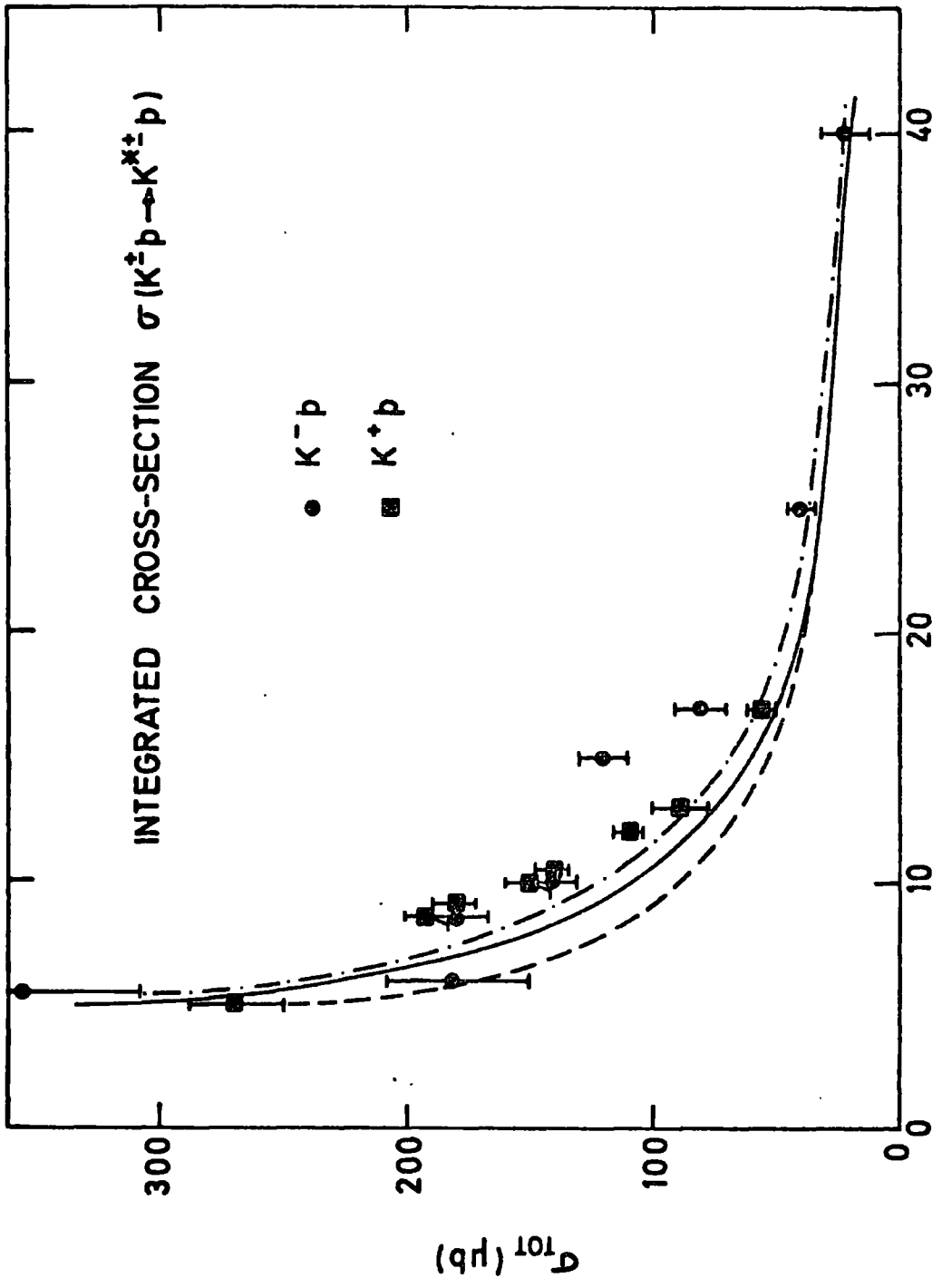

Figure 4.2.6: Our prediction of the integrated cross-section $\sigma(K^{\pm}p \rightarrow K^{*\pm}p)$ compared with the data from reference (87). The curves correspond to the conventions of Figure 4.2.3.

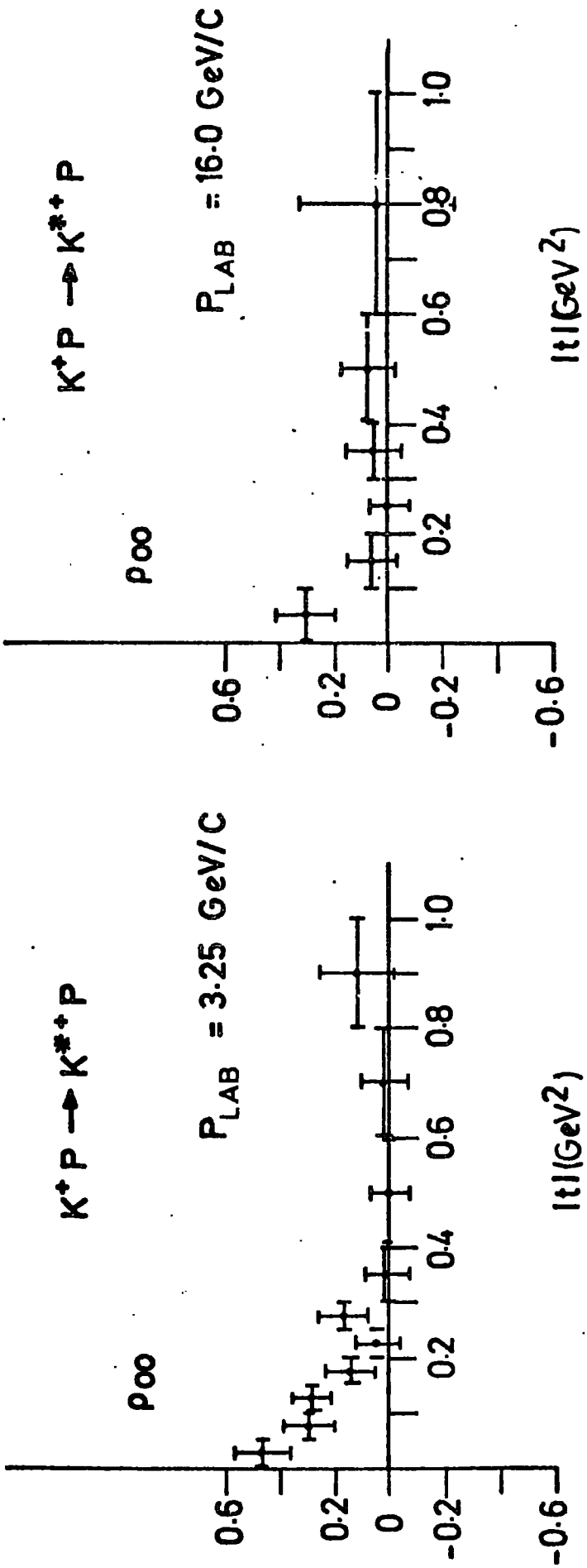

Figure 4.2.7(a): Predictions of the t-channel frame density matrices for $K^{\pm}p \to K^{*\pm}p$ given in equations (4.2.39) and (4.2.40) compared with the data of reference (90).

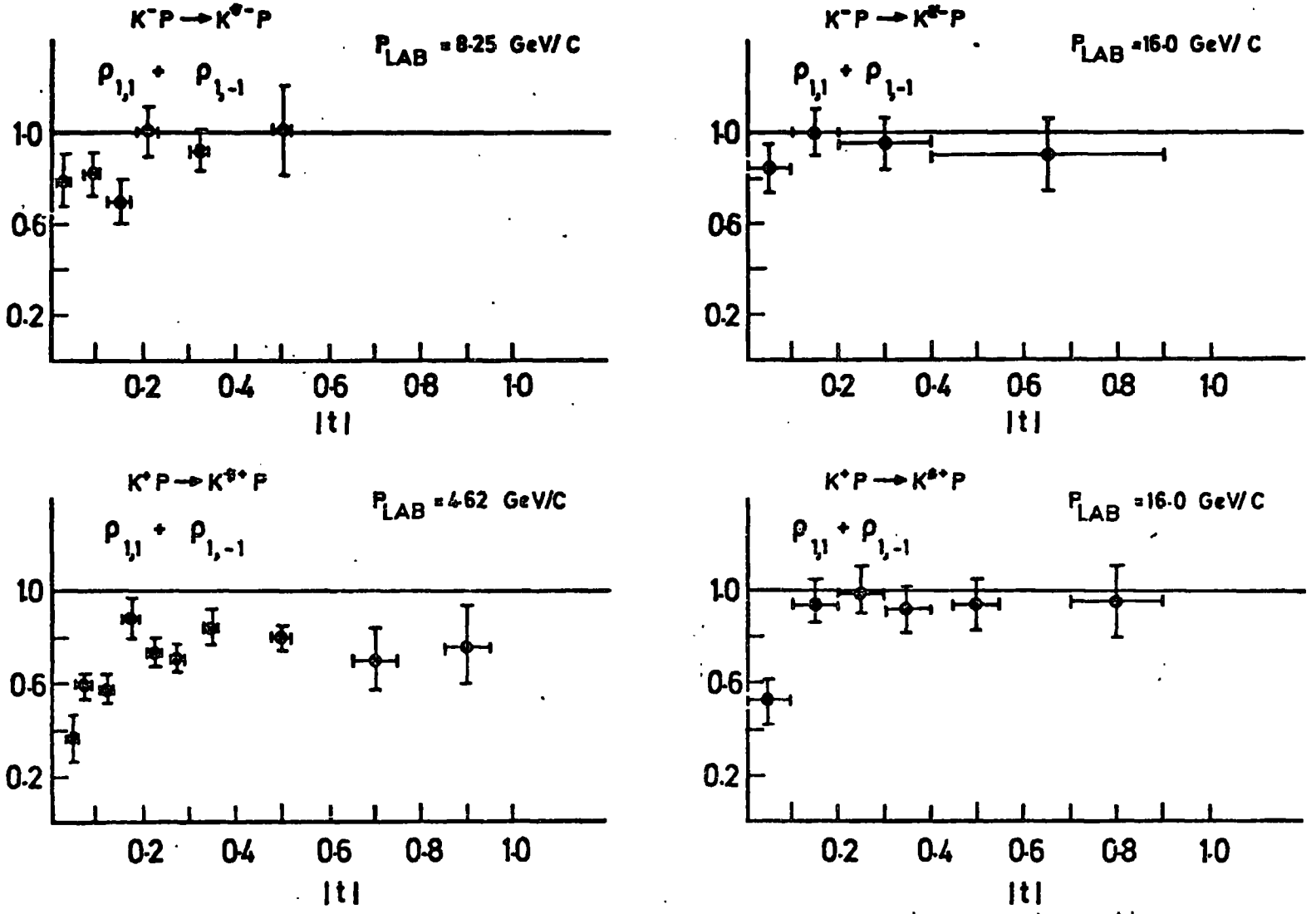

Figure 4.2.7(b): Predictions of the t-channel frame density matrices for $K^{\pm}p \to K^{*\pm}p$ given in equations (4.2.39) and (4.2.40) compared with the data of reference (90).

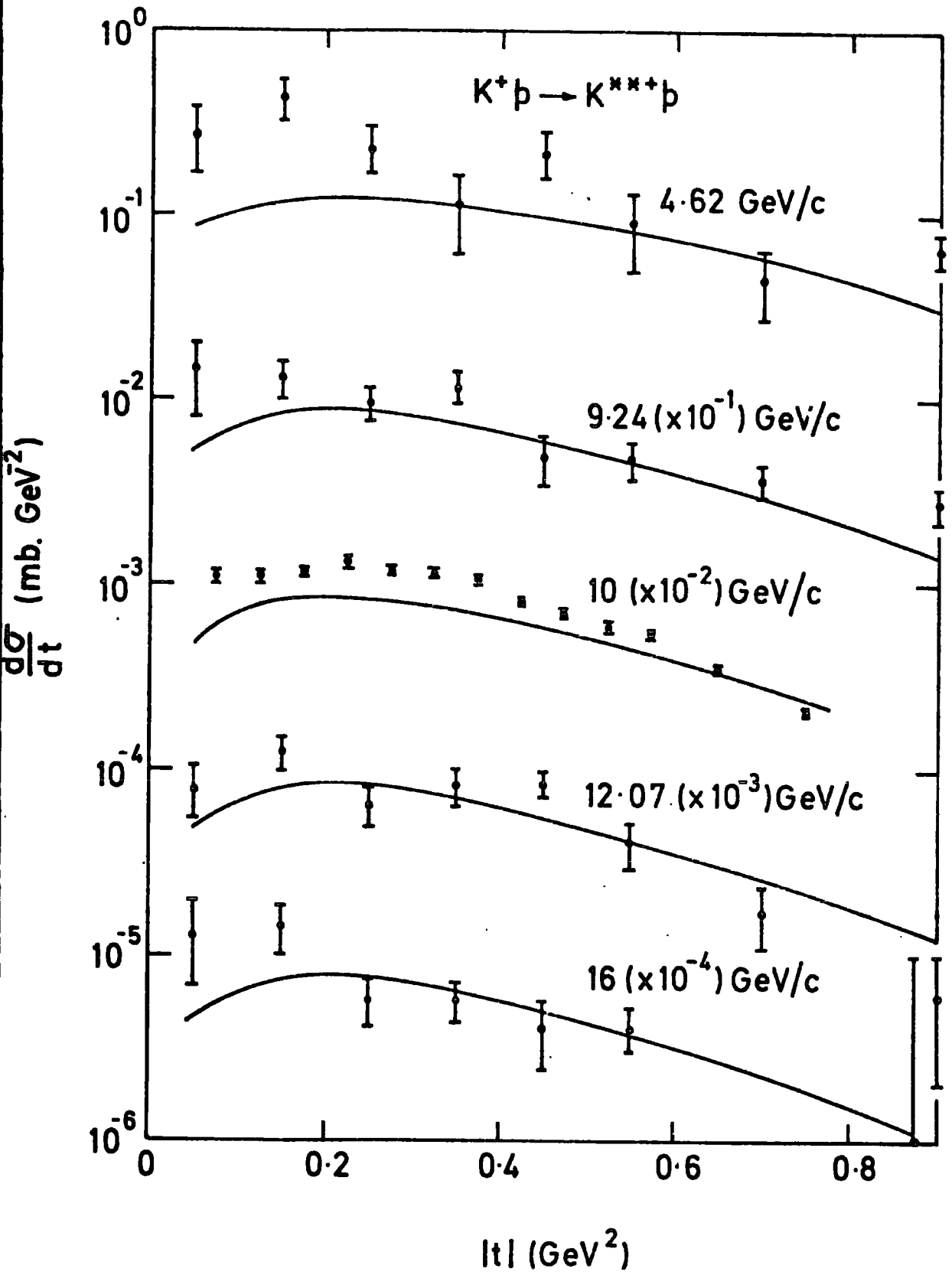

Figure 4.2.8(a): Fit to the differential cross-section $K^+p \rightarrow K^{**+}p$ with data from reference (91).

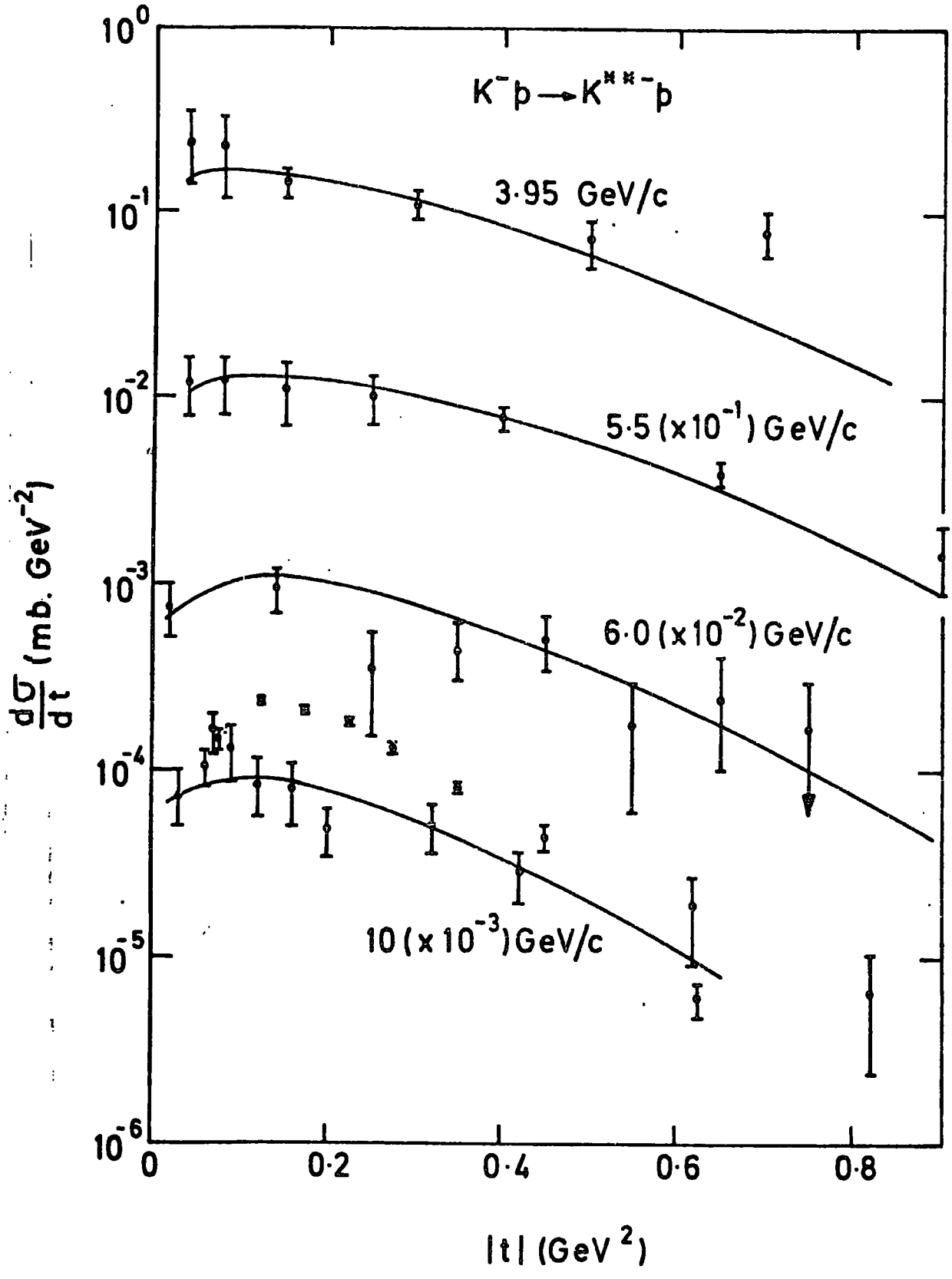

Figure 4.2.8(b): Fit to the differential cross-section $K^- p \rightarrow K^{**-} p$ with data from reference (91).

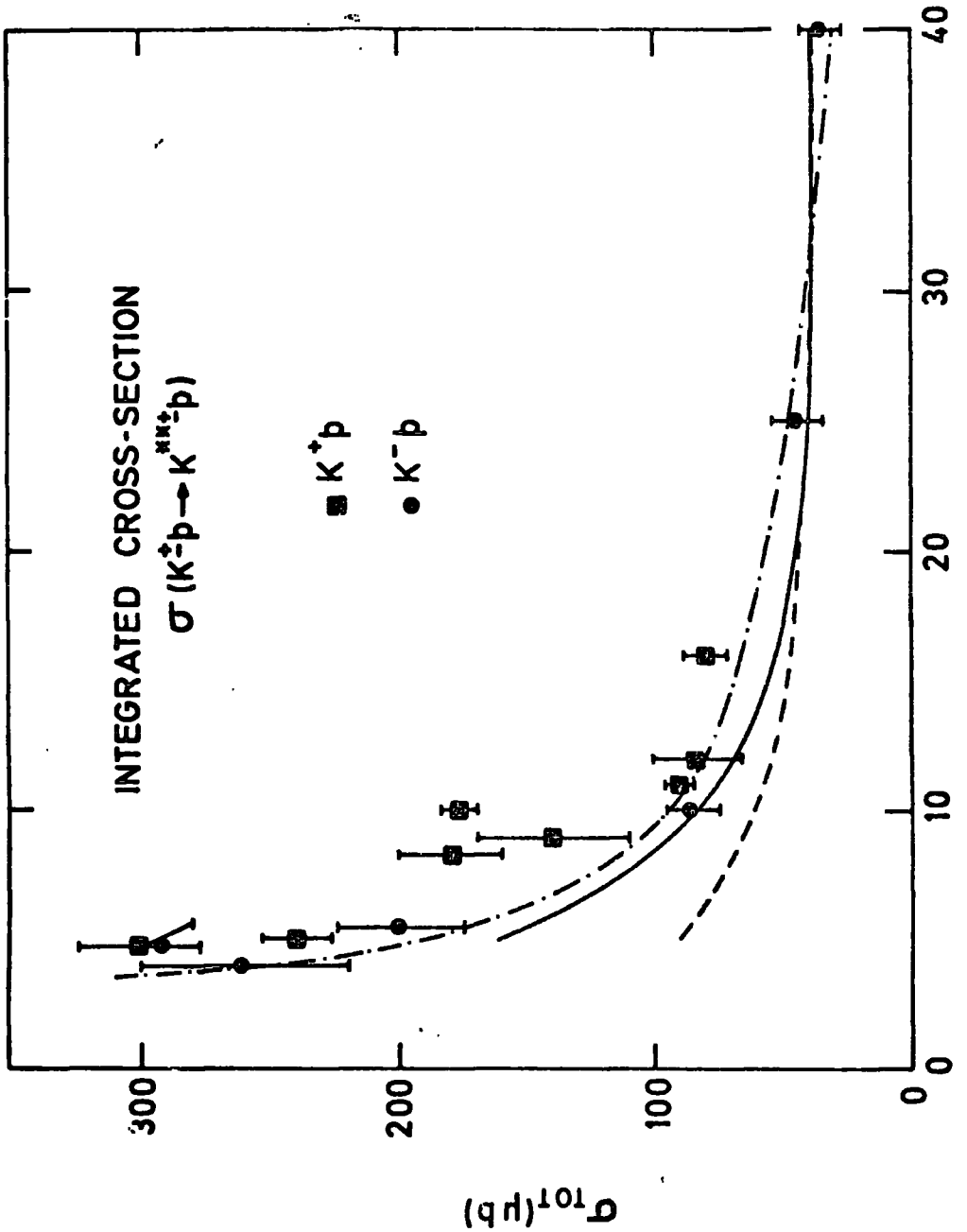

Figure 4.2.9: Our prediction of the integrated cross-section $\sigma(K^{\pm}p \rightarrow K^{**\pm}p)$ compared with the data from references (91, 92). The curves correspond to the conventions of Figures 4.2.3 and 4.2.6.

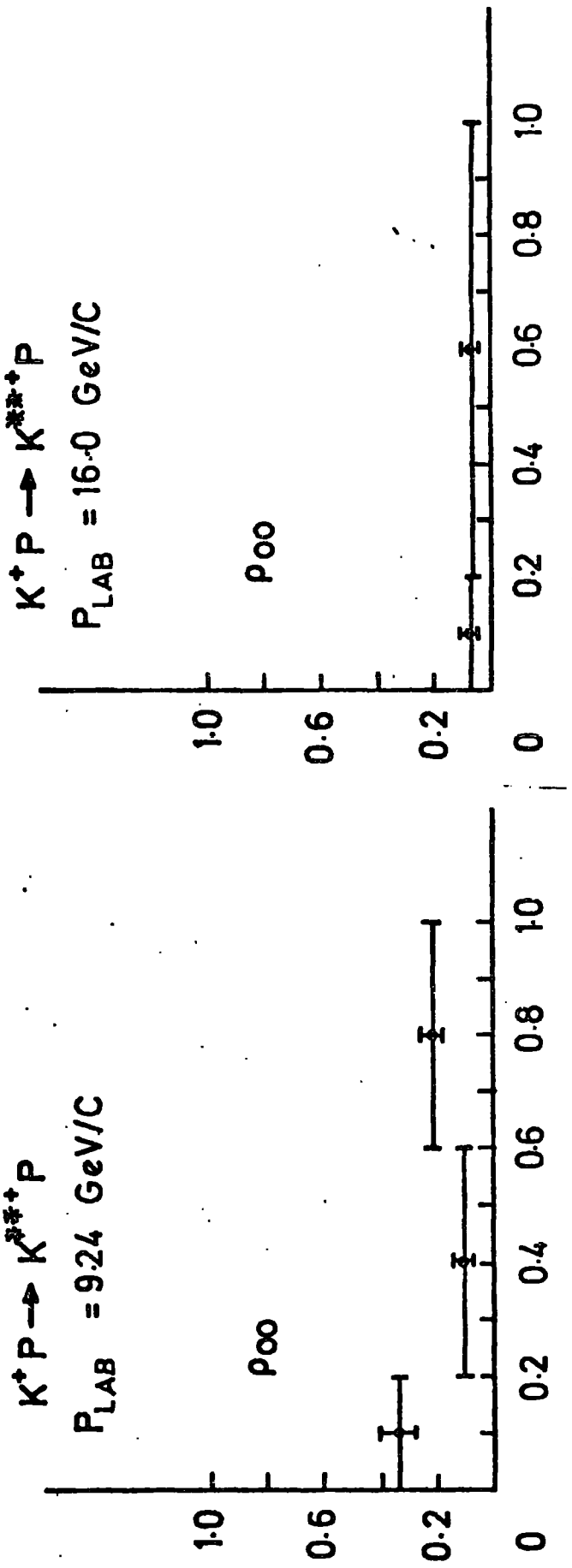

Figure 4.2.10(a): Predictions of the t-channel frame density matrices for $K^{\pm}p \to K^{*\pm}p$ given in equations (4.2.44) and (4.2.45) compared with the data of reference (93).

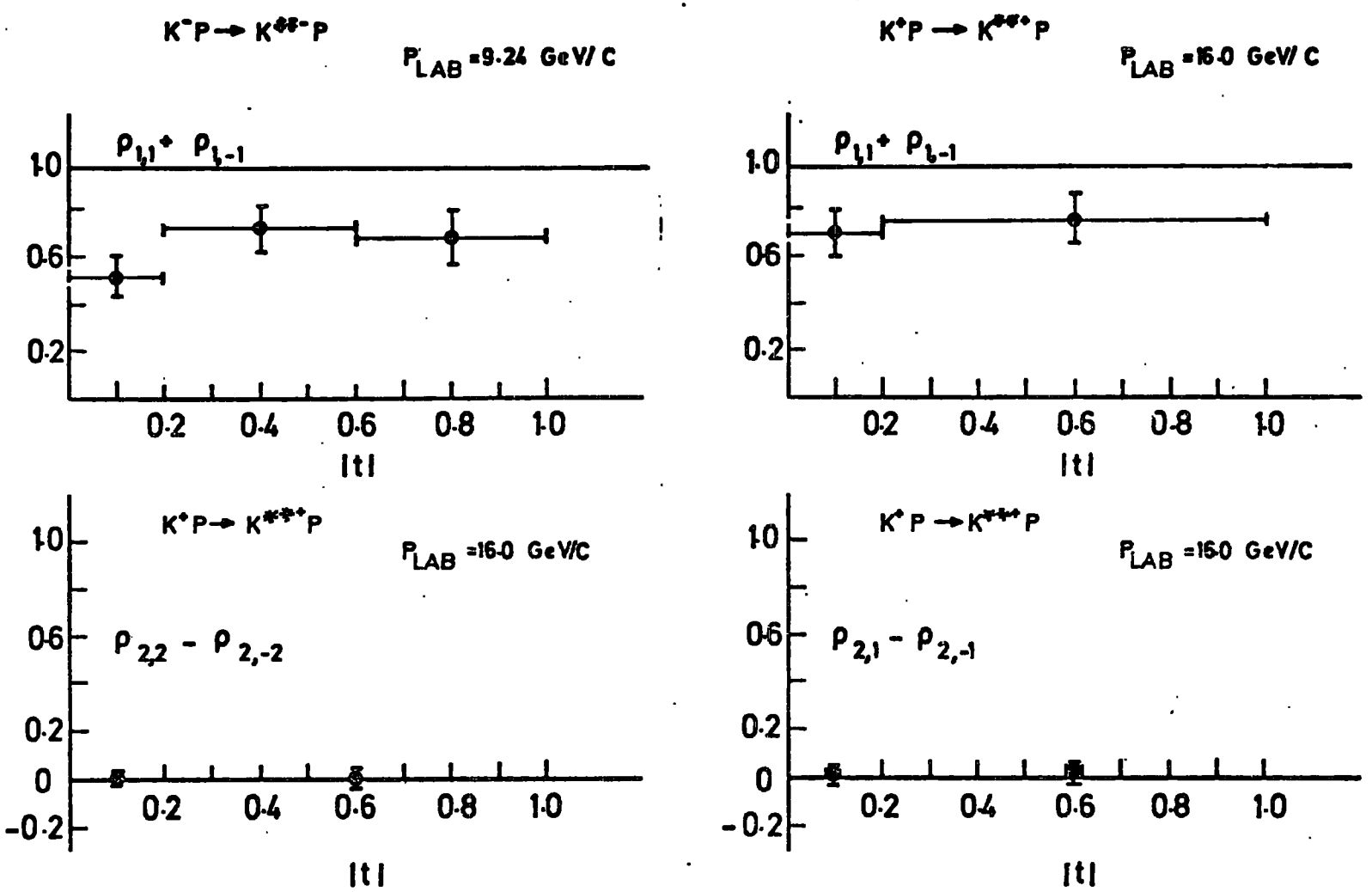

Figure 4.2.10(b) Predictions of the t-channel frame density matrices for $K^{\pm}p \to K^{**\pm}p$ given in equations (4.2.44) and (4.2.45), compared with the data of reference (93).

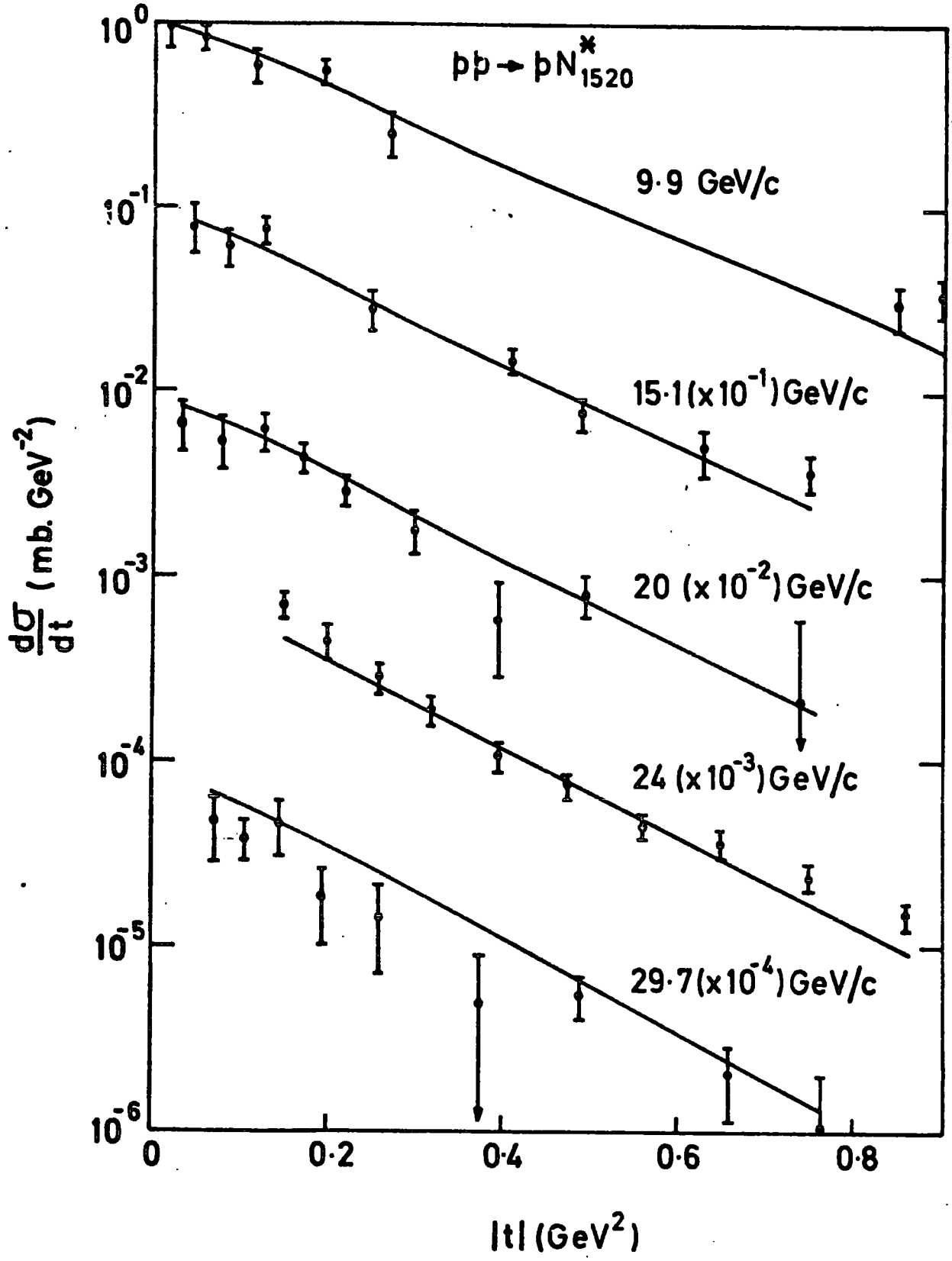

Figure 4.3.1: Our fit to the differential cross-section pp → pN^*_{1520} at small |t| with data from reference (96).

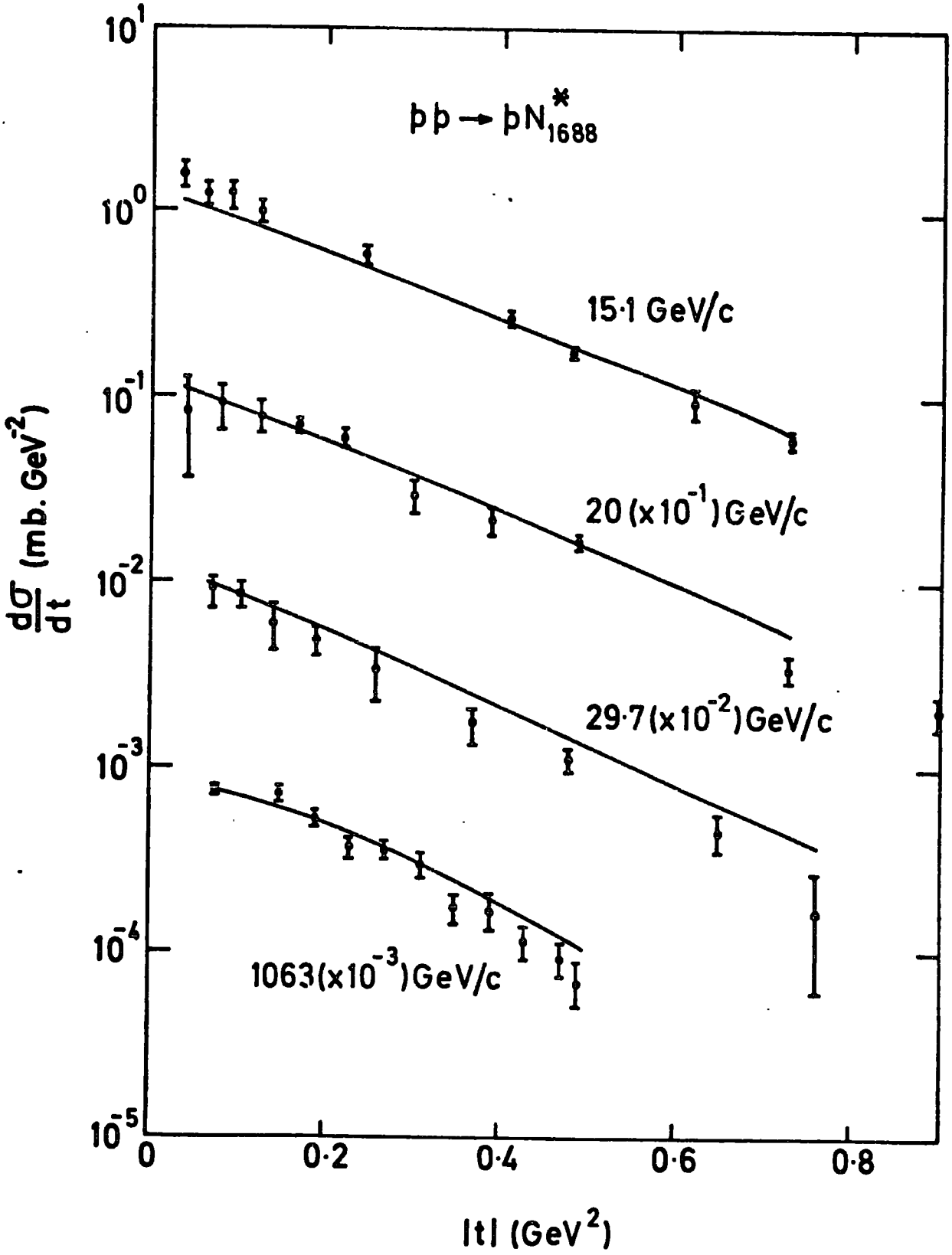

Figure 4.3.2: Our fit to the differential cross-section $pp \to pN^*_{1688}$ at small $|t|$ with data from reference (96).

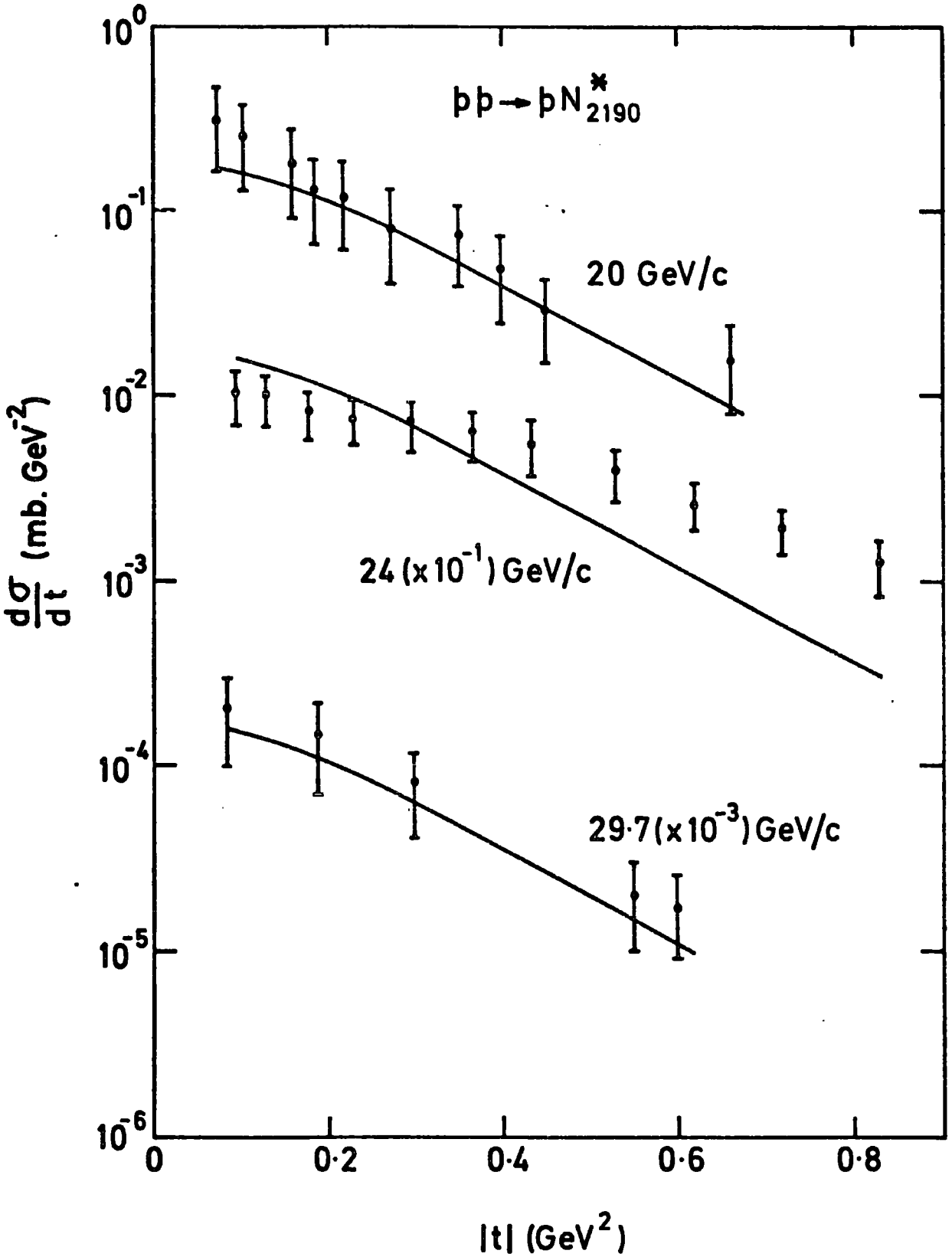

Figure 4.3.3: Our fit to the differential cross-section $pp \to pN^{*}_{2190}$ at small $|t|$ with data from reference (96).

CHAPTER 5

COUPLINGS AND DECAY WIDTHS

5.1 Introduction

In this final chapter we attempt to estimate the decay widths of the resonances ρ, A_2, f, ω etc. (which lie on the exchanged trajectories) by using the meson couplings appearing in our fits. We also estimate the values of g_1^{ℓ} (the orbital angular momentum coupling constants) from resonance decay data by using exchange degeneracy and vector dominance relations. There is however a rather long extrapolation from $t < 0$ (the regge coupling) to $t = M_R^2$ (R ≡ resonance) where the decay coupling is measured. Thus we do not expect a high degree of accuracy from our estimates.

5.2 Resonance Decays into Pseudoscalars

Consider the decay $\rho \to \pi\pi$ as shown in Figure 5.2.1.

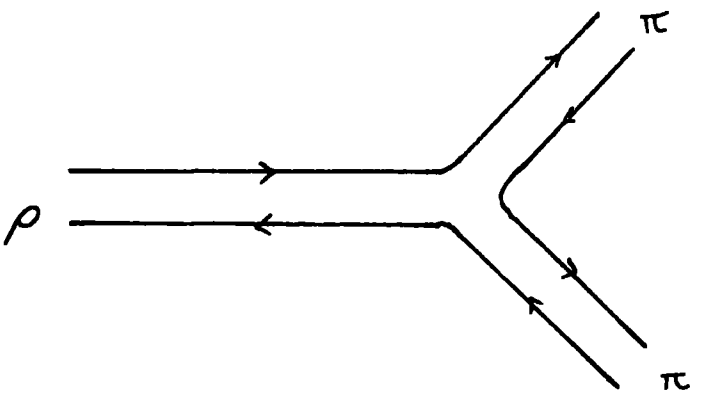

Figure 5.2.1: The decay of the ρ meson into two pions.

Using the VDM hypothesis we can calculate the decay of the ρ into two pions

from Figure 5.2.2.

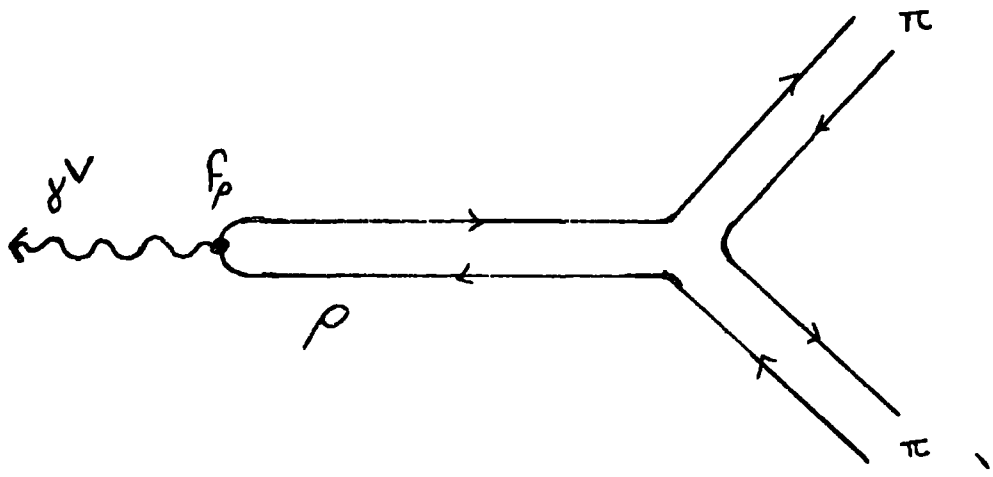

Figure 5.2.2: The decay $\rho \to \pi\pi$ using VDM

From Table 1.5.1, we know the isovector photon coupling to two pions, viz.

$$g^{\gamma V} = 2(g_1^V + g_2^V)e = 2e \tag{5.2.1}$$

and hence, using VDM, the ρ coupling is just

$$2e \cdot \frac{f_\rho}{e} = 2f_\rho \tag{5.2.2}$$

The decay amplitude T_λ^S for the decay $\rho \to \pi\pi$ is

$$T_\lambda^S = T_o^l = \langle \lambda_1 \ldots \lambda_{\ell-j}, jm \mid S, \lambda \rangle \; g_D \left(\frac{q}{M_o}\right)^S \tag{5.2.3}$$

where $S=1$, $\lambda=0$ are the spin and helicity of the decaying resonance, g_D is the decay coupling and q the three momentum. The Clebsch-Gordan

coefficient $\langle\lambda_1 \ldots \lambda_{\ell-j}, jm \,|S,\lambda\rangle$ is the one appropriate for combining ℓ polarization vectors with the quark wave-function ($|j,m\rangle$) to produce the resonance wave- function. In this case (the ρ meson) $\ell = 0$, $j = 1$, $m = 0$, $\lambda = 0$ and thus

$$T_0^1 = 2f_\rho \frac{q}{M_0} \tag{5.2.4}$$

with

$$q = \frac{1}{2M_\rho} \left(\left[M_\rho^2 - (2M_\pi)^2 \right] \left[M_\rho^2 \right] \right)^{\frac{1}{2}} \tag{5.2.5}$$

One can of course arrive at the result (5.2.4) by explicit calculation, that is sandwiching the appropriate coupling $C_{00\alpha}(0,0,1)$ between the initial state (ρ) wave-function and the final state (π) wave-functions and performing the calculation, viz:-

From Appendix 2, the wave-functions are

$$\rho^0 :- \quad \frac{1}{2} \left(u^+(q_u)\, \bar{u}^-(q_u) + u^-(q_u)\bar{u}^+(q_u) + d^+(q_d)\bar{d}^-(q_d) - d^-(q_d)\bar{d}^+(q_d) \right)$$

$$\pi^+ :- \quad \frac{1}{\sqrt{2}} \left(\bar{d}^+(k_d) u^-(k_u) - \bar{d}^-(k_d) u^+(k_u) \right) \tag{5.2.6}$$

$$\pi^- :- \quad \frac{1}{\sqrt{2}} \left(d^+(k'_d)\bar{u}^-(k'_u) - d^-(k'_d)\bar{u}^+(k'_u) \right.$$

with the momenta defined in Figure 5.2.3 below.

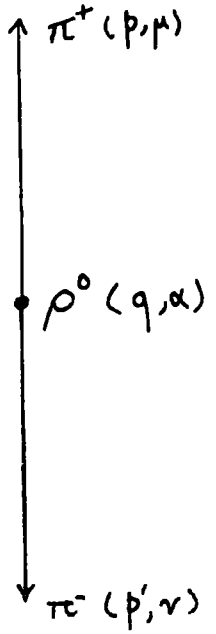

Figure 5.2.3: The decay $\rho \to \pi\pi$ in the rest frame of the ρ-meson. The spin indices are α, μ, ν and the momenta q, p, p' with $q = p + p'$, $q_u + q_d = q$, $k_u + k_d = p$ etc. The decay products travel along the $\pm$ z axes.

From Table 1.4.1 the coupling $C_\alpha(0,0,1)$ is given by

$$\sum_i \left(g_1^i \frac{P_\alpha}{M_o} + g_2^i \gamma_{i\alpha} \frac{M_+}{M_o}\right) \tag{5.2.7}$$

and hence the decay amplitude T_o^1 is

$$T_o^1 = \overline{\rho^o}(q)\ C_\alpha(0,0,1)\ \pi^+(p)\ \pi^-(p') \tag{5.2.8}$$

Since the two pions travel in opposite directions we must choose a particular direction (the + ve z-axis say) and arrange the helicity labels on the pion spinors accordingly. Thus we take the π^+ wave-function to be as given in Appendix 2, and for the π^-, $\frac{1}{\sqrt{2}}(d^{+--+}u^{---+} - d^{---+}u^{+--+}) \to \frac{1}{\sqrt{2}}(d^{---+}u^{+--+} - d^{+--+}u^{---+})$. Hence $\pi^+\pi^-$ is (deleting spinor arguments)

$$\frac{1}{2}(\bar{d}^{+}u^{-}\bar{d}^{--+}u^{---+} - \bar{d}^{+}u^{-}\bar{d}^{+--}u^{+--} - \bar{d}^{--}u^{+}\bar{d}^{---+}u^{---+} + \bar{d}^{--}u^{+}\bar{d}^{+--}u^{+--}) \tag{5.2.9}$$

In the decay $\rho \to \pi\pi$ (as shown in Figure 5.2.1) a $q\bar{q}$ pair is created in order to form the final state. With our definition of the π^+ and π^- wave-functions, we may remove $q\bar{q}$ pairs with opposite spin z-components, that is, terms like $\bar{u}^{+}u^{-}$, $\bar{d}^{-}d^{+}$. Thus the combinations of quarks available to the ρ^o can be contracted to give

$$\frac{1}{2}\,(\bar{d}^{+}d^{-} \;+\; \bar{u}^{-}u^{+} \;+\; \bar{d}^{-}d^{+} \;+\; u^{+}\bar{u}^{-}) \qquad (5.2.10)$$

(The two middle terms of equation (5.2.9) do not contribute since they contain terms like $\bar{d}^{+}d^{+}$, $\bar{u}^{-}u^{-}$).

Referring to equation (5.2.6) we see that the ρ^o wave-function correctly describes the ρ^o quantum numbers, but clearly does not give the correct Lorentz structure since the ρ is a vector particle and hence requires a Lorentz label. Thus we write the ρ^o wave-function as

$$\frac{1}{2}\,(u^{+}\bar{u}^{-} \;+\; u^{-}\bar{u}^{+} \;-\; d^{+}\bar{d}^{-} \;-\; d^{-}\bar{d}^{+})\;\varepsilon^{o}_{\alpha}(q) \qquad (5.2.11)$$

where

$$\varepsilon^{o}_{\alpha}(q) \;=\; (0,0,0,1) \qquad (5.2.12)$$

We then write the decay amplitude T^{1}_{o} as

$$T^{1}_{o} \;=\; \overline{\frac{1}{2}\,(u^{+}\bar{u}^{-} + u^{-}\bar{u}^{+} - d^{+}\bar{d}^{-} - d^{-}\bar{d}^{+})\;\varepsilon^{o*}_{\alpha}(q)\;\sum_{i}\left(g^{i}_{1}\frac{P_{\alpha}}{M_{o}} + g^{i}_{2}\,\gamma_{i\alpha}\frac{M_{+}}{M_{o}}\right)}\;x$$

$$\frac{1}{2}\,(\bar{d}^{+}d^{-} + u^{-}\bar{u}^{+} + \bar{d}^{-}d^{+} + u^{+}\bar{u}^{-}) \qquad (5.2.13)$$

In the rest frame, $\bar{u}_{3}^{\lambda_3}(0)\;\underline{1}\;u_{1}^{\lambda_1}(p) = \delta_{\lambda_3\lambda_1}$ for non-interacting quarks, while for interacting quarks $\bar{u}_{3}^{\lambda_3}(0)\;\underline{1}\;u_{1}^{\lambda_1}(p) = \sqrt{\frac{E_1 + m_1}{2m_1}}$, shown schematically in Figure 5.2.4 below

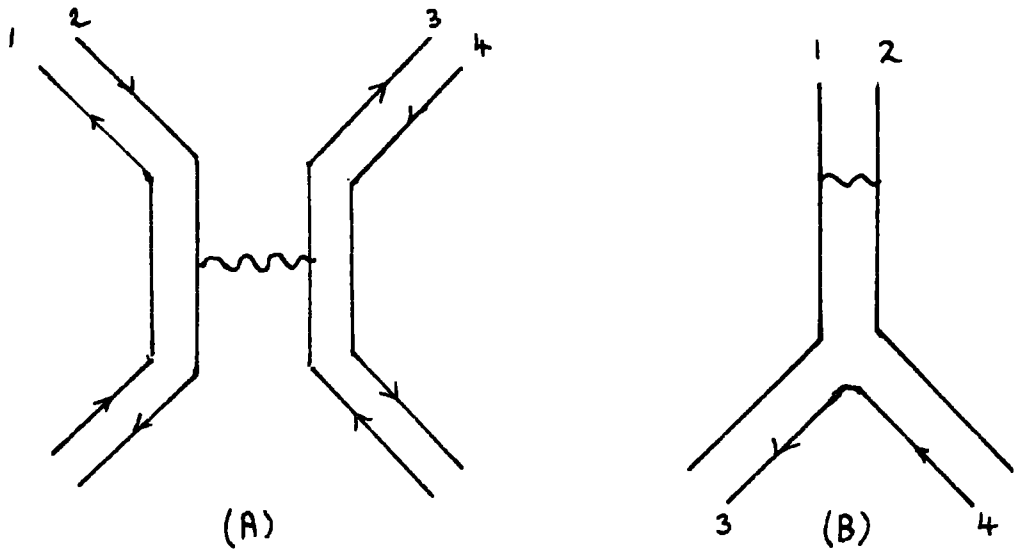

Figure 5.2.4: (A) ρ exchange in $\pi\pi$ scattering, where

$$\bar{u}_4^{\lambda_4} \underline{1}\, u_1^{\lambda_1} = \delta_{\lambda_4\lambda_1} \text{ and}$$

(B) the decay $\rho \to \pi\pi$ where $\bar{u}_2^{\lambda_2} \underline{1}\, u_1^{\lambda_1} = \sqrt{\frac{E_1 + m_1}{2m_1}}$

Using these results

$$T_O^1 = 2g_1^V \varepsilon_\alpha^{o*}(q) \frac{P_\alpha}{M_o} + 2g_2^V \frac{M_+}{M_o} \overline{u^{--+}} \gamma_\alpha . \varepsilon_\alpha^{o*}(q) \bar{u}^{+}u^{-} \qquad (5.2.14)$$

In the ρ's rest frame $P_\alpha = (0,0,0,q)$, where q is given by equation (5.2.5).

Hence,

$$T_O^1 = 2g_1^V \frac{q}{M_o} + 2g_2^V \frac{M_+}{M_o} \overline{u^{--+}} \gamma_\alpha . \varepsilon_\alpha^{o*}(q) \bar{u}^{+}u^{-} \qquad (5.2.15)$$

Further

$$\bar{u}_1^{+} \gamma_\alpha . \varepsilon_\alpha^{o*}(q) \bar{u}_2^{+} = \frac{q}{\sqrt{2m_2}\sqrt{E_2 + m_2}} \qquad (5.2.16)$$

while

$$\bar{u}_1^{+} \underline{1}\, u_2^{+} = \sqrt{\frac{E_2 + m_2}{2m_2}} \qquad (5.2.17)$$

and

$$M_+ = \frac{M_\pi + M_\pi}{2} = M_\pi \qquad (5.2.18)$$

Thus,

$$T_0^1 = -2f_\rho \frac{q}{M_0} + 4f_\rho \frac{q}{M_0} = 2f_\rho \frac{q}{M_0} \qquad (5.2.19)$$

(using Table 1.3.1) which agrees with the result (5.2.4)

With our normalization the decay width is given by

$$\Gamma = \frac{q M_0^2}{8\pi M_R^2} \frac{1}{2S+1} \sum_\lambda \left| T_\lambda^S \right|^2 \qquad (5.2.20)$$

Inserting (5.2.4) and (5.2.5) into (5.2.20) and taking into account the charge states available in the decay $\rho \to \pi\pi$ (see Table 5.2.1), then

$$\Gamma_{\rho \to \pi\pi} = 264 \text{ MeV} \qquad (5.2.21)$$

Final State	I	
	0	1
$\pi\pi$	3	2
$K\bar{K}$	4	4

Table 5.2.1: Charge multiplicity in the mesonic decays of resonances of different isospin.

If we now assume f - ρ exchange degeneracy (that is, the f and ρ couplings to ππ are equal) then the decay $f \to \pi\pi$ is as given in Figure 5.2.2. The decay amplitude is, from (5.2.3)

$$T_0^2 = \sqrt{\frac{2}{3}}\, 2f_\rho \left(\frac{q}{M_0}\right)^2 \qquad (5.2.22)$$

with q given by equation (5.2.5) but $M_\rho \to M_f$. Inserting (5.2.22) into

(5.2.20) and allowing for the charge multiplicity given in Table 5.2.1, we find

$$\Gamma_{f \to \pi\pi} = 117 \text{ MeV} \tag{5.2.23}$$

As a further example, we consider the decay $g \to \pi\pi$. Since the g meson ($j = 1$, $\ell = 2$, $S = 3$) lies on the ρ trajectory, the decay is again given by Figure 5.2.2. The decay amplitude T_o^3 is:-

$$T_o^3 = \sqrt{\frac{6}{15}}\ 2e\ \frac{f_\rho}{e}\ \left(\frac{q}{M_o}\right)^3 \tag{5.2.24}$$

(Note that the Clebsch-Gordan coefficient is the one appropriate for helicity (λ) $0 = 0 + 0 + 0$ where the zeroes on the right hand side are the helicities of the two polarization vectors and the quark wave-function $|1\,0\rangle$. The subsidiary condition $P_\nu \cdot \varepsilon_\nu^{\pm 1}(p) = 0$ for a particle in the rest frame with decay products moving along the $\pm z$ axes (see next section) ensures that terms such as $+1, -1, 0$ appearing in the decay amplitude vanish, leaving only the 0,0,0 term).

Thus,

$$\Gamma_{g \to \pi\pi} = \frac{q^7}{8\pi M_g^2 M_o^4}\ \frac{1}{7}\ \frac{6}{15}\ 4f_\rho^2 \tag{5.2.25}$$

where

$$q = \frac{1}{2M_g}\ \left[(M_g^2 - (2M_\pi)^2)\ (M_g^2)\right]^{\frac{1}{2}} \tag{5.2.26}$$

Thus, using Table 5.2.1

$$\Gamma_{g \to \pi\pi} = 56 \text{ MeV} \tag{5.2.27}$$

Shown in Table 5.2.2 are our predictions of the decay widths of the ρ, ω, A_2, f, ω^*, g and h mesons into pseudoscalars against the data taken from the Particle Data Group's (1978) data compilation (38). As

can be seen from the table, we have given a very reasonable account of the resonance decay widths ($\rho \to \pi\pi$ excepted) despite the fact that we have assumed no extra variation in t of the coupling as we travel from $t < 0$ to $t = M_R^2$ over and above that of the nonsense factors and gamma functions appearing in the exchange amplitudes (see Chapter 2). In fact, we have attempted to estimate the likely variation of the couplings with t using the Veneziano model (see reference (56)) to calculate the change in coupling as we continue from $t \leq 0$ (where the trajectory coupling is measured) to $t = M_R^2$. However, this form of continuation does not give the required variation with t, as can be seen in Table 5.2.2.

Decay	Predicted width (MeV)	Predicted width using Veneziano extrapolation (MeV)	Experimental width (MeV)
$\rho \to \pi\pi$	264	264	155 ± 3
$f \to \pi\pi$	117	234	144 ± 17
$g \to \pi\pi$	56	116	44 ± 16
$h \to \pi\pi$	103	138	∿ 80
$f \to K\bar{K}$	4.4	8.8	5.6 ± 1.4
$A_2 \to K\bar{K}$	5.9	11.9	4.8 ± 0.7
$\omega^*_{1675} \to K\bar{K}$	6.6	13	-
$g \to K\bar{K}$	7.4	15	<<180
$h \to K\bar{K}$	11.3	15	∿ 10

Table 5.2.2: Meson decay widths. Experimental values are taken from reference (38) except for the h decays which are from reference (98).

5.3 Radiative Decays of vector mesons

In this section we estimate the radiative decay widths of the vector mesons ρ, ω and K^*. Since these mesons have $\ell = 0$ their decay amplitudes do not involve the unknown orbital angular momentum coupling constants g_1, g_2 and hence we can make absolute predictions for their decay widths.

We consider first the decay $\rho^+ \to \pi^+\gamma$ as shown in Figure 5.3.1.

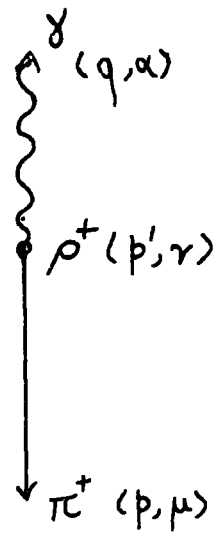

Figure 5.3.1: The radiative decay $\rho^+ \to \pi^+\gamma$ in the ρ's rest frame. The ρ momentum is $p'_\nu = (M_\rho, 0, 0, 0)$ and the photon's momentum is $q_\alpha = (p' - p)_\alpha$. The decay products travel along the $\pm$ z axes.

If we take the photon to be in a helicity = +1 state, the ρ^+ and π^+ wave-functions are (from Appendix 2)

$$\rho^+_+ :- \quad u^+(k'_u)\bar{d}^+(k'_d)$$

$$\pi^+_o :- \quad \frac{1}{\sqrt{2}}\left(\bar{d}^+(k_d)u^-(k_u) - \bar{d}^-(k_d)u^+(k_u)\right) \qquad (5.3.1)$$

$$\gamma :- \quad \varepsilon_\alpha^{+1}(q)$$

and similarly for the photon with $\lambda = -1$, with $\rho^+_+ \to \rho^+_-$. The momenta k_u, k'_u are defined by

$$k'_u + k'_d = p' \tag{5.3.2}$$

with similar relations for k_u, k_d (see Chapter 1). The coupling is given by

$$C_\alpha(1,0,1) = C^\alpha_{qNF} = \sum_i (g^i_1 \frac{P_\alpha}{M_o} + g^i_2 \gamma_{i\alpha} \frac{M_+}{M_o}) \tag{5.3.3}$$

Thus the amplitude for the helicity = + 1 decay $\rho^+ \to \pi^+ \gamma$ is (deleting spinor arguments)

$$T^1_1 = \overline{u^{+-+}\bar{d}} \; (\sum_i g^i_1 \frac{P_\alpha}{M_o} + g^i_2 \gamma_{i\alpha} \frac{M_+}{M_o}) \; \varepsilon^{+1}_\alpha(q) \; \frac{1}{\sqrt{2}} \; (\bar{d}^+ u^- - \bar{d}^- u^+) \tag{5.3.4}$$

Because the decay products travel along the ± z axes, the polarization vectors satisfy the condition

$$\frac{P_\alpha}{M_o} \cdot \varepsilon^{\pm 1}_\alpha(q) = 0 \tag{5.3.5}$$

(See equation (A4.5)) and thus the g^i_1 term in (5.3.4) above vanishes, leaving

$$T^1_1 = \overline{u^{+-+}\bar{d}} \sum_i g^i_2 \, e\gamma_{i\alpha} \frac{M_+}{M_o} \; \varepsilon^{+1}_\alpha(q) \; \frac{1}{\sqrt{2}} \; (\bar{d}^+ u^- - \bar{d}^- u^+) \tag{5.3.6}$$

(where we have inserted e since we are concerned with the photon coupling). Similarly for the helicity = -1 decay amplitude,

$$T^{-1}_{-1} = \overline{u^{---}\bar{d}} \sum_i g^i_2 \, e \, \gamma_{i\alpha} \frac{M_+}{M_o} \; \varepsilon^{-1}_\alpha(q) \; \frac{1}{\sqrt{2}} \; (\bar{d}^+ u^- - \bar{d}^- u^+) \tag{5.3.7}$$

Remembering that $\bar{u}^{\lambda_3}(k'_u) \; \underline{1} \; u^{\lambda_1}(k_u) = \delta_{\lambda_3\lambda_1}$ (see Section 5.2), (5.3.6) gives

$$T_1^1 \; (= T_{-1}^{-1}) = g_2^S \, e \, \frac{1}{\sqrt{2}} \, \frac{M_+}{M_o} \, 2 \, \overline{u^{+-+} d^{+}} \; \gamma_\alpha \cdot \varepsilon_\alpha^{+1}(q) \; \bar{d}^{+} u^{-} \tag{5.3.8}$$

while

$$\overline{u^{+-+} d^{+}} \; \gamma_\alpha \cdot \varepsilon_\alpha^{+1}(q) \; \bar{d}^{+} u^{-} \; \frac{M_+}{M_o} = \frac{\sqrt{2}}{2M_o} \, (M_\rho - M_\pi) \tag{5.3.9}$$

using equations (1.3.7), (1.3.8), (1.3.9) and (1.3.13) .

Thus

$$T_1^1 = \frac{g_2^S}{M_o} \, e \, (M_\rho - M_\pi) \tag{5.3.10}$$

q $(= p' - p)$ is given by

$$q = \frac{1}{2M_\rho} \left(\left[M_\rho^2 - (M_\gamma + M_\pi)^2 \right] \left[M_\rho^2 - (M_\gamma - M_\pi)^2 \right] \right)^{\frac{1}{2}} \tag{5.3.11}$$

$$= \frac{(M_\rho + M_\pi)(M_\rho - M_\pi)}{2M_\rho}$$

Thus

$$T_1^1 = \frac{M_\rho}{M_+} \, \frac{q}{M_o} \, g_2^S \, e = T_{-1}^{-1} \tag{5.3.12}$$

Using equation (5.2.20)

$$\Gamma_{\rho \to \pi\gamma} = \frac{q^3}{8\pi M_\rho^2} \, \frac{2}{3} \left(\frac{M_\rho}{M_+} \right)^2 e^2 \left(g_2^S \right)^2 \tag{5.3.13}$$

and with $\frac{e^2}{4\pi} = \frac{1}{137}$ and $g_2^S = \frac{2}{3}$ (from Table 1.3.1)

$$\Gamma_{\rho \to \pi\gamma} = 0.27 \text{ MeV} .$$

Following a similar procedure for the decay $\omega \to \pi\gamma$ we find

$$\Gamma_{\omega \to \pi\gamma} = 2.5 \text{ MeV}, \quad \text{while} \quad \Gamma_{K^* \to K\gamma} = 0.066 \text{ MeV}.$$

In Table 5.3.1 we compare our predictions of these radiative decays against the available data (38). As can be seen, the agreement is rather poor, especially for the ρ and ω .

Decay	Experimental width (MeV)	Predicted width (MeV)	Predicted width with static Q.M.
$\rho \to \pi\gamma$	0.037 ± 0.012	0.27	0.094
$\omega \to \pi\gamma$	0.88 ± 0.09	2.5	0.87
$K^* \to K\gamma$	0.074 ± 0.043	0.066	0.040

Table 5.3.1: Our predictions of the radiative decay width of the ρ, ω and K^* vector mesons against the data of reference (38).

The naive static quark model (see, for example, Kokkedee (20)) obtains the result (5.3.13) but with $M_+ \ (\equiv \frac{M_\rho + M_\pi}{2}) \to M_\rho$, which would of course be true in the SU(6) limit. If one makes this replacement the predictions for ρ and ω are somewhat improved. Nevertheless, the K^* width becomes smaller, in disagreement with the data, implying that the SU(6) correction employed is only appropriate for the ρ and ω .

5.4 Estimates of g_1^ℓ based on resonance decays

As we have mentioned in Chapter 4, Section 3, the factors g_1^ℓ are free parameters representing orbital angular momentum coupling constants. However, they also represent the couplings appearing in the expressions for the resonance decay widths and hence we may estimate the value of g_1^ℓ directly.

For example, we may calculate the value of g_1^1 from the A_2 decay as follows:-

Consider the decay $A_2 \to \rho\pi$. Using vector dominance we can deduce the decay $A_2 \to \rho\pi$ from $A_2 \to \pi\gamma$ as shown in Figure 5.4.1.

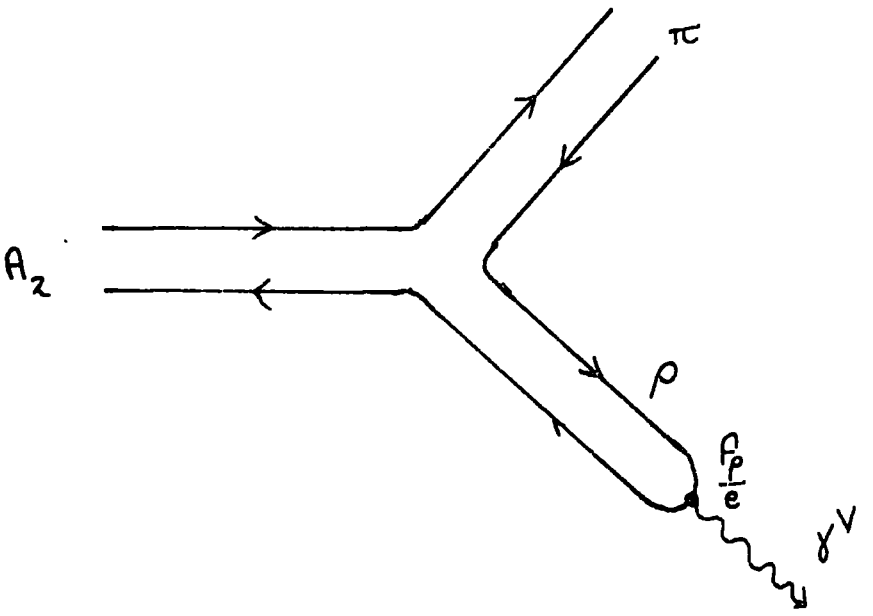

Figure 5.4.1: The decay $A_2 \to \pi\gamma$ using the VDM hypothesis.

In our formalism the decay amplitude for $A_2 \to \pi\gamma$ will be, following the previous section

$$T_\lambda^S = T_1^2 = A_2(p')\ C_{\nu\alpha}\ (2,0,1)\ \pi(p)\ \gamma(q) \qquad (5.4.1)$$

with the labelling defined in Figure 5.4.2.

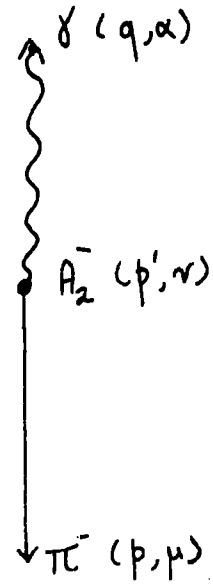

Figure 5.4.2: The decay $A_2 \to \pi\gamma$ in the rest frame of the decaying particle showning the spin indices (α, μ, ν) and momenta (q, p, p') with $q_\alpha = (p - p')_\alpha$ and $p'_\nu = (M_{A_2}, 0, 0, 0))$ of the particles involved As before, the decay products travel along the $\pm$ z axes.

From Appendix 2 the wave-functions are

$$\pi^- :- \quad \frac{1}{\sqrt{2}} \left(d^+(k_d)\bar{u}^-(k_u) \quad - \quad d^-(k_d)\bar{u}^+(k_u)\right)$$

$$A_2^- :- \quad \frac{1}{2} \left(d^+(k'_d)\bar{u}^-(k'_u) + \quad d^-(k'_d)\bar{u}^+(k'_u)\right)\varepsilon_\nu^{+1}(p') \qquad (5.4.2)$$

$$+ \frac{1}{\sqrt{2}} \bar{u}^+(k'_u)\, \bar{d}^+(k'_d)\, \varepsilon_\nu^{o}(p)$$

$$\gamma :- \quad \varepsilon_\alpha^{\pm 1}(q)$$

respectively.

The helicity = + 1 decay amplitude is (deleting, as usual, the spinor arguments)

$$T_1^2 = \frac{1}{\sqrt{2}} \overline{\bar{u}^+ d^+}\, \varepsilon_\nu^{o*}(p') \left[C_{qNF}^{\alpha}\, g_1^1\, e\, \frac{P_\nu}{M_o} + C_{qN}\, g_2^1\, e\, g_{\nu\alpha}\right] \varepsilon_\alpha^{+1}(q)$$

$$\frac{1}{\sqrt{2}} \left(\bar{d}^+ u^- - \bar{d}^- u^+\right) \qquad (5.4.3)$$

where the term in square brackets is the coupling $C_{\nu\alpha}(2,0,1)$ from Table 1.4.1. Similarly, for $\lambda = -1$ the amplitude is

$$T^2_{-1} = \frac{1}{\sqrt{2}} \overline{\bar{u}\bar{d}^-} \, \varepsilon^{o*}_{\nu}(p') \left[C^{\alpha}_{qNF} \, g^1_1 \, e \, \frac{P_\nu}{M_o} + C_{qN} \, g^1_2 \, e \, g_{\nu\alpha} \right] \varepsilon^{-1}_{\alpha}(q)$$

$$\frac{1}{\sqrt{2}} (d^{+--}u^- - d^{--+}u^+) \qquad (5.4.4)$$

Thus

$$T^2_1 = \frac{1}{\sqrt{2}} \overline{\bar{u}^+\bar{d}^+} \, \varepsilon^{o*}_{\nu}(p') \left[e \sum_i (g^i_1 \frac{P_\alpha}{M_o} + g^i_2 \gamma_{i\alpha} \frac{M_+}{M_o}) g^1_1 \frac{P_\nu}{M_o} + \sum_i g^i_1 e g^1_2 g_{\nu\alpha} \right] \varepsilon^{+1}_{\alpha}(q)$$

$$\frac{1}{\sqrt{2}} (d^{+--}u^- - d^{--+}u^+) \qquad (5.4.5)$$

From (5.3.5), $g^i_1 \frac{P_\alpha}{M_o} \cdot \varepsilon^{\pm 1}_{\alpha}(q) = 0$, and $\varepsilon^{o*}_{\nu}(p') \, g_{\nu\alpha} \, \varepsilon^{\pm 1}_{\alpha}(q) = 0$

(since $\varepsilon^{\pm 1}_{\alpha}(q) = \frac{1}{\sqrt{2}} (0, \mp 1, -i, 0)$). Therefore T^2_1 reduces to

$$T^2_1 = \frac{1}{\sqrt{2}} \overline{\bar{u}^+\bar{d}^+} \, \varepsilon^{o*}_{\nu}(p') \, e \sum_i g^i_2 \gamma_{i\alpha} \cdot \varepsilon^{+1}_{\alpha}(q) \frac{M_+}{M_o} g^1_1 \frac{1}{\sqrt{2}} (d^{+--}u^- - d^{--+}u^+) \frac{P_\nu}{M_o}$$

(5.4.6)

Using equations (5.3.9) (from A4.13) and (A4.12)

$$T^2_1 = \frac{e}{2} \, g^V_2 \, g^1_1 \, \frac{q}{2M_o} \, \frac{\sqrt{2}}{M_o} \, \frac{2M_{A_2} \, q}{2M_+} \qquad (5.4.7)$$

where $M_+ = \frac{M_{A_2} + M_\pi}{2}$ and

$$q = \frac{1}{2M_{A_2}} \left[(M^2_{A_2} - (M_\gamma + M_\pi)^2)(M^2_{A_2} - (M_\gamma - M_\pi)^2) \right]^{\frac{1}{2}} \qquad (5.4.8)$$

It is easy to show that

$$T^2_{-1} = -T^2_1 \qquad (5.4.9)$$

According to the vector dominance hypothesis, the rho coupling to πA_2 is just f_ρ times the photon coupling (see (1.2.2)). Thus the decay amplitude T_1^2 for $A_2^- \to \pi^- \rho^o$ is

$$T_1^2 (A_2^- \to \rho^o \pi^-) = \frac{2e}{\sqrt{2}} \frac{f_\rho}{e} g_1^1 \frac{M_{A_2}}{2M_+} \left(\frac{q'}{M_o}\right)^2 \qquad (5.4.10)$$

where $g_2^V = 2e$ (from Table 1.4.1) and q' is given by (5.4.8) above with $M_\gamma (= 0) \to M_\rho$

Using equation (5.2.20) ,

$$\Gamma_{A_2^- \to \rho^o \pi^-} = \frac{q'^5 M_o^2}{8\pi} \frac{2}{(2S+1)} \left(\frac{\sqrt{2} f_\rho g_1^1}{2M_+ M_o^2}\right)^2 \qquad (5.4.11)$$

Since $f_\rho = \frac{f\omega}{3} = 5.7$ (see Chapter 2) and

$\Gamma_{A_2^- \to \rho^o \pi^-} = \frac{1}{2} \Gamma_{A_2 \to \rho\pi} = 0.036 \pm 0.003$ GeV from reference (38) we find $g_1^1 = 2.36 \pm 0.12$, to be compared with our best-fit value of $g_1^1 = 1.1$ from Table 4.4.1.

Using precisely the same arguments we can estimate g_1^1 at the KK** vertex since, by exchange degeneracy ,

$$g_R^{fKK^{**}} = g_R^{\rho KK^{**}} \qquad (5.4.12)$$

The helicity = ±1 decay amplitudes for $K^{**-} \to K^- \rho^o$ are

$$T_1^2 = -T_{-1}^2 = \frac{q'^2 \sqrt{2} g_1^1 f_\rho}{2M_+ M_o^2} M_{K^{**}} \qquad (5.4.13)$$

with

$$M_+ = \frac{M_{K^{**}} + M_K}{2}$$

and

$$q' = \frac{1}{2M_{K^{**}}} \left(\left[M^2_{K^{**}} - (M_\rho + M_K)^2 \right] \left[M^2_{K^{**}} - (M_\rho - M_K)^2 \right] \right)^{\frac{1}{2}} \qquad (5.4.14)$$

Thus

$$\Gamma_{K^{**-} \to K^- \rho^0} = \frac{q'^5}{8\pi} \frac{2}{2S+1} \left(\frac{\sqrt{2}\, f_\rho\, g^1_1}{2M_+ M_o} \right)^2 \qquad (5.4.15)$$

Using the Particle Data Group's (1978) value of

$\Gamma_{K^{**} \to K\rho} = 0.0066 \pm 0.0022$ GeV (so $\Gamma_{K^{**-} \to K^-\rho^0} = 0.003 \pm 0.001$ GeV) we find $g^1_1 = 1.95 \pm 0.35$ compared with our value of 1.16 from the exchange coupling.

And so we can see that our estimated values of g^1_1 based on the decay widths are comparable to our fitted values within a factor of two. Estimates of g^1_1 based on extrapolation of the coupling from $t < 0$ to $t = M^2_R$ using the Veneziano model give values of g^1_1 which are even further from our fitted values than the ones calculated above (see reference (97)). Of course, given that we have found a discrepancy of approximately a factor of 2 between the regge and decay values of g^1_1 indicates that some t-dependence is required. Since the 'decay' products of $\rho \to \pi A_2$ (say) have $\ell > 0$ (to be compared with ρ, f etc... $\to \pi\pi$ where the final state value of $\ell = 0$ and the decay widths are predicted quite accurately without extra t-dependence) it would appear that such t-dependence should in turn depend on the value of ℓ for the final state.

CONCLUSIONS

In this thesis we have explored the consequences of the vector coupling hypothesis and the gamma analogy hypothesis. The former states that all leading normal parity trajectory exchanges (P, f, ω, ρ and A_2) couple to high-spin vertices like vector particles. Thus only helicity changes $\Delta\lambda_t = 0, \pm 1$ are allowed in the t-channel. This means that at least for small $|t|$ the s-channel helicity changes are also restricted approximately to $\Delta\lambda_s = 0, \pm 1$. The latter hypothesis states that the trajectory couplings to quarks are proportional, up to universal t-dependent functions, to the corresponding photon-quark couplings. That is, the P, f and ω couplings are proportional to the isoscalar photon coupling and the ρ and A_2 to the isovector photon coupling.

The principal motivations for these hypothesis are duality, which suggests that the pomeron coupling is proportional to that of the f, which in turn is exchange degenerate with the ω (and the ρ and A_2 are likewise degenerate), and the vector dominance model which relates the couplings of the photon to those of the ω and ρ . Within the context of a naive ideal quark model we have added to these ideas a concrete formalism using the technique of covariant reggeization enabling us to relate form factors and decay couplings to regge exchanges - a covariant formalism being almost essential if we are to relate exchange and decay couplings in a simple manner.

Within this framework our hypotheses have given, for example, s-channel helicity conservation for the P, f and ω trajectories coupling to $N\bar{N}$ while the isovector ρ and A_2 exchanges enjoy predominantly helicity flip couplings to $N\bar{N}$. However, as a major test of our ideas we have used the reggeon-photon coupling analogy (RPCA) to elucidate the nature of the elastic scattering amplitudes and hence describe all the elastic scattering

data. With our ρ , ω-photon coupling hypothesis the ρ, ω electronic decay width coupling constants f_ρ and f_ω set the scale of all our regge couplings. Then, assuming the equality of the nucleon electromagnetic form factors, the t-dependence of the f, ω, ρ and A_2 regge exchanges coupling to $N\bar{N}$ is given just by the nucleon form factor. Since all our couplings factorize the parametrization correctly predicts the difference between $\frac{d\sigma}{dt}$(BB) and $\frac{d\sigma}{dt}$(MB) at small $|t|$ (where B = baryon and M = meson). We have assumed that the pomeron coupling is prescribed by the f-dominated pomeron hypothesis of Carlitz, Green and Zee and thus we have arrived at a 'universal' t-dependent P:f coupling ratio. Then, with only the extra assumption of a small breaking of exchange degeneracy for isoscalar exchange (f,ω) at $N\bar{N}$ vertices, we have fitted the large amount of elastic and total cross-section data as illustrated in Chapter 2.

In Chapter 3 we have shown that our model can make accurate predictions of other cross-sections, $\sigma^{tot}_{\pi\pi}(s)$, $\sigma^{tot}_{\Lambda p}(s)$ for example. Especially encouraging has been our model's ability to predict vector meson-proton differential and total cross-sections and, with the aid of VDM, the photon-proton total cross-section which has recently been measured at high energies.

Having established a reliable set of elastic scattering amplitudes we have applied the model to diffractive boson and baryon production. With our hypothesis we are able to predict, up to one free parameter which serves only to adjust the overall normalization, the differential cross-section for the processes $pp \to pN^*$, $\pi p \to A_2 p$ and $Kp \to K^{**}p$. Because of our quark model input we have been able to give an absolute prediction for the process $Kp \to K^*p$, a prediction which is in good agreement with the data. For the other processes we note that the VCH forbids $\Delta\lambda_t \geq 2$ and hence predicts that the t-channel production density matrices $\rho_{mm'}$, with $|m|$ or $|m'| = 2$ should be negligible - a prediction completely vindicated by the data. Further,

the GAH is quite consistent with the other non-zero production density matrices within the not inconsiderable errors, as we have illustrated in Chapter 4. Moreover, the RPCA has successfully predicted both the energy and t-dependence of all these cross-sections despite the fact that the helicity structure is much richer than, and the t-dependence quite different from, elastic scattering. However, we are aware, as we pointed out in Chapter 4, of the ambiguous and controversial nature of the energy dependence of the A_2 and K^{**} integrated cross-sections.

In the final chapter, we have used the meson couplings determined in our fits to predict mesonic decay widths of resonances lying on the exchanged trajectories, As we demonstrated in Table 5.2.2 our predictions have proved to be in accord with the data. We have also estimated the values of g_1^1 (the orbital angular momentum coupling constant) from meson decays and found agreement with our fitted values to within a factor of 2. Given the rather long extrapolations involved we regard this as satisfactory agreement.

And so with remarkably few free parameters (8 in all) we have been able to account for all the data on elastic scattering. We have successfully extended the ideas to diffractive processes involving high-spin bosons and baryons. A further extension to quantum-number exchange processes involving other trajectories in the same multiplets as f or ω multiplets requires nothing more than the incorporation of the appropriate Clebsch-Gordan coefficients, and at least up to the level of SU(3) appears to work very well (see, for example, reference (99)).

A similar method of relating unnatural parity exchanges to the weak axial current has been developed independently by Irving (100) and Kane (101). Thus it would appear that the reggeon-weakon coupling analogy RWCA (Weakon = γ, w or z) permits one to predict essentially all those features of hadronic scattering which depend just on regge pole (not cut) exchanges.

APPENDIX 1

BASIC CONVENTIONS

(a) Units

Natural units are employed throughout, in which $\hbar = c = 1$ Energies, momenta and masses are expressed in MeV ($= 10^6$ eV) or GeV ($= 10^9$ eV), GeV being the natural unit. Hence 1 natural unit of length $= \frac{\hbar c}{1\,\text{GeV}} = 1.973 \times 10^{-16}$ m. A convenient alternative unit of length is the fermi

$$1\ \text{f} \equiv 10^{-15}\text{m} \simeq 5\ \text{GeV}^{-1} \qquad \text{(A1.1)}$$

Cross-sections are usually measured in millibarns which may be converted to GeV units using

$$\text{GeV}^{-2} = 0.3893\ \text{mb} \qquad \text{(A1.2)}$$

(b) Cross-sections

We use the expressions

$$\sigma^{\text{tot}}(s) = \frac{0.3893}{s}\,\text{Im}A\,(s,t=0) \qquad \text{(A.1.3)}$$

$$\frac{d\sigma}{dt} = \frac{0.3893}{16\pi s^2}\sum_{\lambda}|A_{\lambda}(s,t)|^2 \qquad \text{(A1.4)}$$

(λ = helicity)

and thus our scattering amplitudes are dimensionless.

(c) Dirac matrices and Pauli spinors

The Dirac equation is

$$(\gamma \cdot p - m)\,u(p) = 0 \qquad \text{(A1.5)}$$

where

$$u^{\delta}(p) = \frac{1}{\sqrt{2m}}\,(p_o + m)^{\frac{1}{2}}\left(1 + \frac{i\gamma_5\,\underline{\sigma}\cdot\underline{p}}{(p_o + m)}\right)\phi^{\delta} \qquad \text{(A1.6)}$$

where m = mass and p the four momentum $(p_o, \underline{P})$.

$$\delta = \frac{1}{2} \quad \text{and} \quad \phi^{+\frac{1}{2}} = \begin{pmatrix} 1 \\ 0 \end{pmatrix} , \quad \phi^{-\frac{1}{2}} = \begin{pmatrix} 0 \\ 1 \end{pmatrix}$$

$$\gamma_o = \begin{pmatrix} \underline{1} & 0 \\ 0 & -\underline{1} \end{pmatrix} , \quad \gamma = \begin{pmatrix} 0 & \underline{\sigma} \\ -\underline{\sigma} & 0 \end{pmatrix} , \quad i\gamma_5 = \begin{pmatrix} 0 & \underline{1} \\ \underline{1} & 0 \end{pmatrix}$$

where $\underline{1}$ is the 2 x 2 unit matrix, and $\underline{\sigma}$, the Pauli matrices are defined by

$$\sigma_1 = \begin{pmatrix} 0 & 1 \\ 1 & 0 \end{pmatrix} , \quad \sigma_2 = \begin{pmatrix} 0 & -i \\ i & 0 \end{pmatrix} , \quad \sigma_3 = \begin{pmatrix} 1 & 0 \\ 0 & -1 \end{pmatrix}$$

(d) 4-vectors

Covariant 4-vector $A_\mu = (A_o, A_1, A_2, A_3) = (A_o, \underline{A})$, metric $g_{\mu\nu} = (1, -1, -1, -1)$ with $A^\nu = g_{\mu\nu} A_\mu$ where repeated indices are summed.

4-position $x_\mu = (x_o, \underline{x})$, where x_o is the time and $\underline{x}$ the spatial position.

4-momentum operator $P_\mu = i \partial_\mu = i \frac{\partial}{\partial x_\mu} = \left(i \frac{\partial}{\partial x_o} , - i \underline{\nabla} \right)$.

APPENDIX 2

MESON AND BARYON SU(6) WAVE-FUNCTIONS

The superscript refers to the particle's charge, while the subscript represents the z-component of its spin, m (≡ helicity)

(a) Mesons

Particle	0^- mesons $\|j, m\rangle$
π^+_o	$\frac{1}{\sqrt{2}}(\bar{d}^{+}u^{-} - \bar{d}^{-}u^{+})$
π^-_o	$\frac{1}{\sqrt{2}}(d^{+}\bar{u}^{-} - d^{-}\bar{u}^{+})$
π^o_o	$\frac{1}{2}(\bar{u}^{+}u^{-} - \bar{u}^{-}u^{+} - \bar{d}^{+}d^{-} + \bar{d}^{-}d^{+})$
K^+_o	$\frac{1}{\sqrt{2}}(\bar{s}^{+}u^{-} - \bar{s}^{-}u^{+})$
K^-_o	$\frac{1}{\sqrt{2}}(s^{+}\bar{u}^{-} - s^{-}\bar{u}^{+})$
K^o_o	$\frac{1}{\sqrt{2}}(\bar{s}^{+}d^{-} - \bar{s}^{-}d^{+})$
$\bar{K}^o_o$	$\frac{1}{\sqrt{2}}(s^{-}\bar{d}^{+} - s^{+}\bar{d}^{-})$

1^- mesons

Particle	$\|j, m>$
ϕ^o_{+1}	$s^{+-+}\bar{s}^{+}$
ϕ^o_{-1}	$s^{---}\bar{s}^{-}$
ϕ^o_o	$\frac{1}{\sqrt{2}}\ (s^{+--}\bar{s}^{-} + s^{--+}\bar{s}^{+})$
ω^o_{+1}	$\frac{1}{\sqrt{2}}\ (u^{+-+}\bar{u}^{+} + d^{+-+}\bar{d}^{+})$
ω^o_{-1}	$\frac{1}{\sqrt{2}}\ (u^{---}\bar{u}^{-} + d^{---}\bar{d}^{-})$
ω^o_o	$\frac{1}{2}\ (u^{+--}\bar{u}^{-} + u^{--+}\bar{u}^{+} + d^{+--}\bar{d}^{-} + d^{--+}\bar{d}^{+})$
ρ^+_{+1}	$u^{+-+}\bar{d}^{+}$
ρ^+_{-1}	$u^{---}\bar{d}^{-}$
ρ^+_o	$\frac{1}{\sqrt{2}}\ (u^{+--}\bar{d}^{-} + u^{--+}\bar{d}^{+})$
ρ^o_{+1}	$\frac{1}{\sqrt{2}}\ (u^{+-+}\bar{u}^{+} - d^{+-+}\bar{d}^{+})$
ρ^o_{-1}	$\frac{1}{\sqrt{2}}\ (u^{---}\bar{u}^{-} - d^{---}\bar{d}^{-})$
ρ^o_o	$\frac{1}{2}\ (u^{+--}\bar{u}^{-} + u^{--+}\bar{u}^{+} - d^{+--}\bar{d}^{-} - d^{--+}\bar{d}^{+})$
ρ^-_{+1}	$d^{+-+}\bar{u}^{+}$
ρ^-_{-1}	$d^{---}\bar{u}^{-}$
ρ^-_o	$\frac{1}{\sqrt{2}}\ (d^{+--}\bar{u}^{-} + d^{--+}\bar{u}^{+})$

1^- meson

Particle	$\vert j, m \rangle$
K^{*+}_{+1}	$\bar{s}^{-}u^{+}$
K^{*+}_{-1}	$\bar{s}^{-}u^{-}$
K^{*+}_{o}	$\frac{1}{\sqrt{2}}(\bar{s}^{-}u^{-} + \bar{s}^{-}u^{+})$
K^{*-}_{+1}	$s^{+}u^{+}$
K^{*-}_{-1}	$s^{-}u^{-}$
K^{*-}_{o}	$\frac{1}{\sqrt{2}}(s^{+}u^{-} + s^{-}u^{+})$
K^{*o}_{+1}	$s^{+}\bar{d}^{+}$
K^{*o}_{-1}	$s^{-}\bar{d}^{-}$
K^{*o}_{o}	$\frac{1}{\sqrt{2}}(\bar{s}^{-}d^{-} + \bar{s}^{-}d^{+})$
$\bar{K}^{*o}_{+1}$	$s^{+}\bar{d}^{+}$
$\bar{K}^{*o}_{-1}$	$s^{-}\bar{d}^{-}$
$\bar{K}^{*o}_{o}$	$\frac{1}{\sqrt{2}}(s^{+}\bar{d}^{-} + s^{-}\bar{d}^{+})$

To construct other high-spin meson wave functions we use spin = 1 polarization vectors as described in Chapter 1.

BARYON WAVE-FUNCTIONS

$\frac{1}{2}^+$

Particle	$\lvert j, m \rangle$
$p_+^+ (\equiv p\uparrow)$	$\frac{1}{\sqrt{18}}$ $(2u^+d^-u^+ + 2u^+u^+d^- + 2d^-u^+u^+ - u^+u^-d^+ - u^+d^+u^- - u^-d^+u^+ - d^+u^-u^+ - d^+u^+u^- - u^-u^+d^+)$
$p_-^+ (\equiv p\downarrow)$	$\frac{-1}{\sqrt{18}}$ $(2u^-d^+u^- + 2u^-u^-d^+ + 2d^+u^-u^- - u^-u^+d^- - u^-d^-u^+ - u^+d^-u^- - d^-u^+u^- - d^-u^-u^+ - u^+u^-d^-)$
$n_+^o (\equiv n\uparrow)$	$-\frac{1}{\sqrt{18}}$ $(2d^+u^-d^+ + 2d^+d^+u^- + 2u^-d^+d^+ - u^+d^-d^+ - d^+u^+d^- - d^-u^+d^+ - d^+d^-u^+ - u^+d^+d^- - d^-d^+u^+)$
$n_-^o (\equiv n\downarrow)$	$\frac{1}{\sqrt{18}}$ $(2d^-u^+d^- + 2d^-d^-u^+ + 2u^+d^-d^- - u^-d^+d^- - d^-u^-d^+ - d^+u^-d^- - d^-d^+u^- - u^-d^-d^+ - d^+d^-u^-)$
Λ_+^o	$\frac{1}{\sqrt{12}}$ $(u^+d^-s^+ - u^-d^+s^+ - d^+u^-s^+ + d^-u^+s^+ + s^+u^+d^- - s^+u^-d^+ - s^+d^+u^- + s^+d^-u^+ + d^-s^+u^+ - d^+s^+u^- - u^-s^+d^+ + u^+s^+d^-)$
Λ_-^o	$-\frac{1}{\sqrt{12}}$ $(u^-d^+s^- - u^+d^-s^- - d^-u^+s^- + d^+u^-s^- + s^-u^-d^+ - s^-u^+d^- - s^-d^-u^+ + s^-d^+u^- + d^+s^-u^- - d^-s^-u^+ - u^+s^-d^- + u^-s^-d^+)$

$\frac{3}{2}^+$

Particle	$\|j, m>$
$\Delta^+_{\frac{3}{2}}$	$\frac{1}{\sqrt{3}}$ $(u^+u^+d^+ + u^+d^+u^+ + d^+u^+u^+)$
$\Delta^+_{\frac{1}{2}}$	$\frac{1}{3}$ $(u^+u^+d^- + u^+d^-u^+ + d^-u^+u^+$ $+u^+u^-d^+ + u^-u^+d^+ + u^+d^+u^-$ $+u^-d^+u^+ + d^+u^-u^+ + d^+u^+u^-)$
$\Delta^+_{-\frac{3}{2}}$	$-\frac{1}{\sqrt{3}}$ $(u^-u^-d^- + u^-d^-u^- + d^-u^-u^-)$
$\Delta^+_{-\frac{1}{2}}$	$-\frac{1}{3}$ $(u^-u^-d^+ + u^-d^+u^- + d^+u^-u^-$ $+u^-u^+d^- + u^+u^-d^- + u^-d^-u^+$ $+u^+d^-u^- + d^-u^+u^- + d^-u^-u^+)$

All other particle wave-functions used in this thesis may be derived using the ground state wave-functions tabulated above, in the manner outlined in C.1.

APPENDIX 3

ROTATION OF DENSITY MATRICES

The crossing relation for helicity states(84) is defined by

$$\rho^{H}_{mm'} = \sum_{\mu\mu'} d^{J}_{m\mu}(\beta) \; \rho^{t}_{\mu\mu'} \; d^{J}_{m'\mu'}(-\beta) \qquad \text{(A3.1)}$$

where m, μ etc. are helicity labels, β is the crossing angle defined by (A3.2) below and H and t denote helicity and G.J. frame respectively.

$$\sin\beta = \frac{q_s}{a_3} \sin\theta_s \underset{s\to\infty}{\to} \frac{\sqrt{-t}}{a_3} \qquad \text{(A3.2)}$$

where θ is the c.m.s. scattering angle, q_s the three-momentum and

$$a_3^2 = \left[(t - (M_1 - M_3)^2)\ (t - (M_1 + M_3)^2)\right] \Big/ 4M_3^2 \qquad \text{(A3.3)}$$

The $d^{J}_{mm}(\beta)$ are the rotation matrices defined in Brink and Satchter (85) page 22, equation (2.18), and tabulated for $J = \frac{1}{2}, \frac{3}{2}$, 1 and 2 in Table 1, page 24 of the same reference.

Using the symmetry properties of the d^{J}'s, that is

$$d^{J}_{mm'}(\beta) = (-1)^{m-m'} d^{J}_{m'm}(\beta) = d^{J}_{-m'-m}(\beta) = d^{J}_{m'm}(-\beta) \qquad \text{(A3.4)}$$

Then from (A3.1), for J = 2

$$\rho^H_{1,1} = d^2_{12}(\beta)\,\rho^t_{22}\,d^2_{12}(-\beta) + d^2_{12}(\beta)\,\rho^t_{21}\,d^2_{11}(-\beta) + d^2_{12}(\beta)\,\rho^t_{20}\,d^2_{10}(-\beta)$$
$$+ d^2_{12}(\beta)\,\rho^t_{2-1}\,d^2_{1-1}(-\beta) + d^2_{12}(\beta)\,\rho^t_{2-2}\,d^2_{1-2}(-\beta)$$
$$+ d^2_{11}(\beta)\,\rho^t_{12}\,d^2_{12}(-\beta) + d^2_{11}(\beta)\,\rho^t_{11}\,d^2_{11}(-\beta) + d^2_{11}(\beta)\,\rho^t_{10}\,d^2_{10}(-\beta)$$
$$+ d^2_{11}(\beta)\,\rho^t_{1-1}\,d^2_{1-1}(-\beta) + d^2_{11}(\beta)\,\rho^t_{1-2}\,d^2_{1-2}(-\beta)$$
$$+ d^2_{10}(\beta)\,\rho^t_{02}\,d^2_{12}(-\beta) + d^2_{10}(\beta)\,\rho^t_{01}\,d_{11}(-\beta) + d^2_{10}(\beta)\,\rho^t_{00}\,d^2_{10}(-\beta)$$
$$+ d^2_{10}(\beta)\,\rho^t_{0-1}\,d^2_{1-1}(-\beta) + d^2_{10}(\beta)\,\rho^t_{0-2}\,d^2_{1-2}(-\beta)$$
$$+ d^2_{1-1}(\beta)\,\rho^t_{-12}\,d^2_{12}(-\beta) + d^2_{1-1}(\beta)\,\rho^t_{-11}\,d^2_{11}(-\beta) + d^2_{1-1}(\beta)\,\rho^t_{-10}\,d^2_{10}(-\beta)$$
$$+ d^2_{1-1}(\beta)\,\rho^t_{-1-1}\,d^2_{1-1}(-\beta) + d^2_{1-1}(\beta)\,\rho^t_{-1-2}\,d^2_{1-2}(-\beta)$$
$$+ d^2_{1-2}(\beta)\,\rho^t_{-22}\,d^2_{12}(-\beta) + d^2_{1-2}(\beta)\,\rho^t_{-21}\,d^2_{11}(-\beta) + d^2_{1-2}\,\rho^t_{-20}\,d^2_{10}(-\beta)$$
$$+ d^2_{1-2}(\beta)\,\rho^t_{-2-1}\,d^2_{1-1}(-\beta) + d^2_{1-2}(\beta)\,\rho^t_{-2-2}\,d^2_{1-2}(-\beta)$$

(A3.5)

with a similar expression for $\rho^H_{1,-1}$.

Then, using relation (A3.4), rearranging terms and forming the combination $\rho^H_{11} + \rho^H_{1-1}$ (and dropping the argument of the d^J's, β , and the spin label J) we find

$$\rho^H_{11} + \rho^H_{1,-1} = (\rho^t_{11} + \rho^t_{1-1}) \left[2d_{11}\, d_{1-1} + d_{11}\, d_{11} + d_{1-1} d_{1-1} \right]$$

$$+ (\rho^t_{12} - \rho^t_{1-2}) \left[d_{11}\, d_{12} - d_{1-1} d_{1-2} + d_{11}\, d_{-12} - d_{1-1} d_{-1-2} \right]$$

$$+ (\rho^t_{22} - \rho_{2-2}) \left[d_{12}\, d_{12} + d_{1-2} d_{1-2} + 2 d_{12}\, d_{-12} \right]$$

$$+ (\rho_{21} + \rho_{2-1} \left[d_{12}\, d_{11} - d_{1-2} d_{1-1} + d_{12} d_{-11} - d_{1-2} d_{-1-1} \right]$$

(A3.6)

Then, referring to Table I, page 24, of reference (85)

$$\rho^H_{11} + \rho^H_{1-1} = \sin^2\beta\ (\rho^t_{22} - \rho^t_{2-2}) + \cos^2\beta\ (\rho^t_{11} + \rho^t_{1-1})$$

$$+ \sin\beta \cos\beta\ (\rho^t_{21} + \rho^t_{2-1} + \rho^t_{12} - \rho^t_{1-2})$$

(A3.7)

With the vector coupling hypothesis, only ρ_{11} and ρ_{1-1} survive, hence

$$\rho^H_{11} + \rho^{11}_{1-1} = \cos^2\beta\ (\rho^t_{11} + \rho^t_{1-1}) \qquad \text{(A3.8)}$$

The other relations given in (4.2.27) may be deduced similarly.

APPENDIX 4

THE RADIATIVE DECAY $N^* \to N\gamma$

In order to calculate the decay amplitude for the decay $N^* \to N\gamma$, it is necessary to sandwich the covariant coupling $C_{\mu\nu\alpha}(S_1,S_3,J)$ between wave-functions appropriate for the helicity of the decaying N^* and the decay products N and γ . For simplicity, we consider first the decay of a $S = \frac{3}{2}$ particle (the $N^*(\frac{3}{2}^-, 1520)$, use helicity wave-functions to project out the helicity amplitudes for the decay, and then make use of the relations between wave-functions of different spins to write down the decay amplitudes for an N^* of any spin.

We work in the N^* rest frame, as illustrated in Figure A4.1 and to simplify the notation we fix the photon's helicity at +1 and label the amplitudes by just the N^*'s spin projection on the z-axis, the direction of motion of the decay products. Thus the helicity decay amplitude is denoted by T^S_λ , where S is the spin and λ the helicity of the decaying N^*.

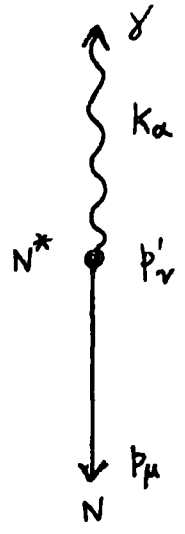

Figure A4.1: The decay $N^* \to N\gamma$ in the N^*'s rest frame. The N^* momentum is $p'_\nu = (M_{N^*}, 0, 0, 0)$ and the photon's momentum is $k_\alpha = (p' - p)_\alpha$. The photon has helicity $\lambda_\gamma = +1$, so the N^* helicity states $\frac{3}{2}, \frac{1}{2}$ produce nucleons with helicities $\pm\frac{1}{2}$ respectively.

Referring to Table 1.4.1, the reduced coupling $C_{\nu\alpha}(\frac{1}{2}, \frac{3}{2}, 1)$ is given by

$$C_{\nu\alpha}(\tfrac{1}{2}, \tfrac{3}{2}, 1) = C^{\alpha}_{qNF}\, g_1^1 \frac{P_\nu}{M_o} + C_{qN}\, g_2^1\, g_{\nu\alpha} \qquad \text{(A4.1)}$$

where

$$C^{\alpha}_{qNF} \equiv \sum_i \left(g_1^i \frac{P_\alpha}{M_o} + g_2^i \gamma_{i\alpha} \frac{M_+}{M_o} \right), \quad C_{qN} = \sum_i g_1^i \qquad \text{(A4.2)}$$

The $J = \frac{3}{2}$ N^* wave-functions are

$$\bar{\psi}^{\frac{3}{2}}(p') = \bar{P}\uparrow(p')\ \varepsilon_\nu^{+1*}(p') \qquad \text{(A4.3)}$$

$$\bar{\psi}^{\frac{1}{2}}(p') = \sqrt{\tfrac{1}{3}}\ \bar{P}\downarrow(p')\ \varepsilon_\nu^{+1*}(p') + \sqrt{\tfrac{2}{3}}\ \bar{P}\uparrow(p')\ \varepsilon_\nu^{o*}(p')$$

while that of the photon is $\varepsilon_\alpha^{+1}(k)$, and that of the nucleon $P\uparrow(p)$. (Where we have used the shorthand notation $\bar{P}\uparrow(p')$ (see Appendix 2) for the quark part of the N^* wave-function, the notation implying that with our model, the $N^*(\frac{3}{2}^-, 1520)$ is a proton with one unit of orbital angular momentum, denoted by $\varepsilon_\nu^{+1*}(p')$). Thus, the decay amplitude $T^{\frac{3}{2}}_{\frac{3}{2}}$ is given by

$$T^{\frac{3}{2}}_{\frac{3}{2}} = \bar{P}\uparrow(p')\ \varepsilon_\nu^{+1*}(p') \left[\sum_i \left(g_1^i \frac{P_\alpha}{M_o} + g_2^i\, \gamma_{i\alpha} \frac{M_+}{M_o} \right) \frac{P_\nu}{M_o}\ g_1^1 \right. \qquad \text{(A4.4)}$$

$$\left. + \sum_i g_1^i\, g_2^1\, g_{\nu\alpha} \right] P\uparrow(p)\ \varepsilon_\alpha^{+1}(k)$$

Because of the subsidiary condition 1.3.14, then

$$\frac{P_\nu}{M_o} \cdot \varepsilon_\nu^{+1*}(p') = \frac{1}{2M_o}(p + p')_\nu\, \varepsilon_\nu^{+1*}(p') = \frac{1}{2M_o}\, p_\nu \cdot \varepsilon_\nu^{+1*}(p') = 0 \qquad \text{(A4.5)}$$

because p_ν is along the z-axis, so only the g_2^1 term of A4.4 will contribute to the decay. In the rest frame, the matrix elements of $\bar{u}^{\lambda}1(p') \underline{1} u^{\lambda}3(p)$ (where $\underline{1}$ is the unit matrix) are just $\delta_{\lambda',\lambda}$, and hence it is easy to show that

$$\bar{P}\uparrow(p') \sum_i g_1^i \; P\uparrow(p) = 3g_1^S \tag{A4.6}$$

while

$$\varepsilon_\nu^{+1*}(p') \; g_{\nu\alpha} \; \varepsilon_\alpha^{+1}(k) = -1 \tag{A4.7}$$

Hence,

$$T^{\frac{3}{2}}_{\frac{3}{2}} = -3g_1^S \; g_2^1 \tag{A4.8}$$

$$\begin{aligned} T^{\frac{3}{2}}_{\frac{1}{2}} = &\sqrt{\tfrac{1}{3}} \; \bar{P}\downarrow(p') \; \varepsilon_\nu^{+1*}(p') \sum_i \left(g_1^i \frac{P_\alpha}{M_o} + g_2^i \gamma_{i\alpha} \frac{M_+}{M_o}\right) \frac{P_\nu}{M_o} g_1^1 \; P\downarrow(p) \; \varepsilon_\alpha^{+1}(k) \\ &+ \sqrt{\tfrac{1}{3}} \; \bar{P}\downarrow(p') \; \varepsilon_\nu^{+1*}(p') \sum_i g_1^i \; g_2^1 \; g_{\nu\alpha} \; P\downarrow(p) \; \varepsilon_\alpha^{+1}(k) \\ &+ \sqrt{\tfrac{2}{3}} \; \bar{P}\uparrow(p') \; \varepsilon_\nu^{o*}(p') \sum_i \left(g_1^i \frac{P_\alpha}{M_o} + g_2^i \gamma_{i\alpha} \frac{M_+}{M_o}\right) \frac{P_\nu}{M_o} g_1^1 \; P\downarrow(p) \; \varepsilon_\alpha^{+1}(k) \\ &+ \sqrt{\tfrac{2}{3}} \; \bar{P}\uparrow(p') \; \varepsilon_\nu^{o*}(p') \sum_i g_1^i \; g_2^1 \; g_{\nu\alpha} \; P\downarrow(p) \; \varepsilon_\alpha^{+1}(k) \end{aligned} \tag{A4.9}$$

From equation (A4.5), we see that the first term in (A4.9) above is zero, while the second term (from (A4.6)) is just

$$-\frac{3}{\sqrt{3}} \; g_1^S \; g_2^1 \tag{A4.10}$$

Using $\bar{P}\uparrow(p') \underline{1} P\downarrow(p) = 0$, the third term equals

$$\sqrt{\tfrac{2}{3}} \; \bar{P}\uparrow(p') \; g_2^S \; \varepsilon_\alpha^{+1}(k) \cdot \gamma_\alpha \; P\downarrow(p) \; \varepsilon_\nu^{o*}(p') \frac{P_\nu}{M_o} g_1^1 \frac{M_+}{M_o} \tag{A4.11}$$

while the 4th term gives zero since $\varepsilon_{\nu}^{o*}(p')\ g_{\nu\alpha}\ \varepsilon_{\alpha}^{+1}(k) = 0$.

[remember,

$$\varepsilon_{\mu}^{\pm 1}(p) = \frac{1}{\sqrt{2}}\ (0, \mp 1, -i, 0)$$

$$\varepsilon_{\mu}^{o}(p) = \frac{1}{M}\ (p_z, 0, 0, p_o)\ ]$$

From equations (1.5.14), with $t = (p' - p)^2 = k^2 = 0$

$$\frac{p_\nu}{M_o}\ \varepsilon_{\nu}^{o*}(p') = \frac{1}{2M_o}\ p_\nu \cdot \varepsilon_{\nu}^{o*}(p') = \frac{1}{4M_{N^*}M_o}\ (M_{N^*}^2 - M_N^2) \qquad \text{(A4.12)}$$

(where M_N = mass of nucleon)

while

$$\bar{u}^{\frac{1}{2}}(p')\ \gamma_\alpha \cdot\ \varepsilon_{\alpha}^{+1}(k)\ g_2^S\ u^{-\frac{1}{2}}(p)\ \frac{M_+}{M_o} = \frac{\sqrt{2}}{2M_o}\ (M_{N^*} - M_N)\ g_2^S \qquad \text{(A4.13)}$$

using equations (1.3.7), (1.3.8), (1.3.9) and (1.3.13). Thus, it is easy to show that

$$\bar{P}\uparrow(p')\ \gamma_\alpha \cdot\ \varepsilon_{\alpha}^{+1}(k)\ g_2^S\ P\downarrow(p)\ \frac{M_+}{M_o} = \frac{\sqrt{2}}{2M_o}\ (M_{N^*} - M_N)\ g_2^S \qquad \text{(A4.14)}$$

Inserting (A4.12) and (A4.14) in (A4.11) yields

$$\frac{1}{\sqrt{3}}\ \sqrt{2}\ \sqrt{2}\ \frac{1}{2M_o}\ (M_{N^*} - M_N)\ g_2^S\ g_1^1\ \frac{1}{4M_{N^*}M_o}\ (M_{N^*}^2 - M_N^2) \qquad \text{(A4.15)}$$

Combining (A4.15) with (A4.10) gives

$$\sqrt{3}\ T_{\frac{1}{2}}^{\frac{3}{2}} = -3g_1^S\ g_2^1 + \frac{(M_{N^*} - M_N)}{M_o^2}\ g_2^S\ \frac{1}{4M_{N^*}}\ (M_{N^*}^2 - M_N^2)\ g_1^1 \qquad \text{(A4.16)}$$

From Table 1.3.1, $-3g_1^S = 2g_2^S$, so

$$\sqrt{3}\, T^{\frac{3}{2}}_{\frac{1}{2}} = g^S_2 \left[2g^1_2 + (M_{N^*} - M_N)^2 \frac{M_+}{2M_{N^*}M_o^2}\, g^1_1 \right] \qquad \text{(A4.17)}$$

Using the properties of Clebsch-Gordan coefficients (see reference (33)) we can show that

$$T^S_{\frac{1}{2}} = -F(S)\,(S - \tfrac{1}{2})^{\frac{1}{2}}\, g^S_2 \left[2g^1_2 + g^1_1 \frac{M_+ (M_{N^*} - M_N)^2}{2M_{N^*} M_o^2} \right]$$

$$T^S_{\frac{3}{2}} = -F(S)\,(S + \tfrac{3}{2})^{\frac{1}{2}}\, 3g^S_2\, g^1_2 \qquad \text{(A4.18)}$$

where

$$F(S) = \left(\frac{M^2_{N^*} - M^2_N}{2\sqrt{2}\, M_{N^*} M_o} \right)^{S-\frac{3}{2}} \left[\frac{(S + \frac{1}{2})!\,(S - \frac{3}{2})!}{(2S)!} \right]^{\frac{1}{2}} \qquad \text{(A4.19)}$$

Empirically it is found that the $T^S_{\frac{1}{2}}$ decay is much suppressed relative to $T^S_{\frac{3}{2}}$. This is certainly true for $N^*(\frac{5^+}{2}, 1688)$ and seems also to be the case for $N^*(\frac{3^-}{2}, 1520)$. Setting $T^S_{\frac{1}{2}} = 0$, we find from (A4.17)

$$\left[2g^1_2 + \frac{(M_{N^*} - M_N)^2 (M_{N^*} + M_N)}{4M_{N^*} M_o^2}\, g^1_1 \right] = 0 \qquad \text{(A4.20)}$$

and thus

$$\frac{g^1_2}{g^1_1} = - \frac{(M_{N^*} + M_N)(M_{N^*} - M_N)^2}{8M_{N^*} M_o^2} \qquad \text{(A4.21)}$$

This is the result used in our fits to $pp \to pN^*$ in Chapter 4, setting $M_o^2 = 1\ \text{GeV}^2$.

REFERENCES

1. T.T. Chou and C.N. Yang, Phys. Rev. 170 (1965) 1591; 175 (1968) 1832
   F. Ravendal, Phys. Letters 37B (1971) 300
2. H.D.I. Abarbanel, S.D. Drell and F.J. Gilman, Phys. Rev. Letters 20,280 (1968), Phys. Rev. 177 (1969) 2458
3. P.D.B. Collins, F.D. Gault and A. Martin, Phys. Letters 47B (1973) 171
4. J.J. Sakurai, Ann. of Phys. 11 (1960) 1
5. R. Carlitz, M.B. Green and A. Zee, Phys. Rev. D4 (1971) 3439
6. P.D.B. Collins, Phys. Reports 1 (1971) 451
7. A. Silverman, Proc. 7th Int. Symp. on lepton and photon interactions at high energies (Stanford, 1975)
8. F.D. Gault, G.R. Coldstein and H.F. Jones, Nuovo Cimento 27A (1975) 174
9. V. Barger, Proc. 17th Int. Conf. on high energy physics (London, 1974)
10. R.L. Jaffe, Phys. Rev. D15 (1977) 267, 281
11. G. Zweig, Cern Report No. TH-402 (1964) (unpublished)
12. J. Harari, Phys. Rev. Letters 20 (1968) 1395
13. Chan Hong-Mo, J. Paton and Tsou Sheung Tsu, Nucl. Phys. B86 (1975) 479
14. T. Inami and R.G. Roberts, Nucl. Phys. B93 (1975) 497
15. C. Quigg and E. Rabinovici, Phys. Rev. D13 (1976) 2525
16. B.T. Feld, "Models of Elementary Particles", (Ginn/Blaisdell, Massachusetts, (1969))
17. H. Pilkuhn, "The interactions of Hadrons", (North-Holland, Amsterdam (1967)).
18. W. Thirring, Acta. Phys. Austriaca, Suppl. II (1965) 205
19. P. Csonka, M. Moravcsik and M.D. Scadron, Ann. Phys. (N.Y.) 40 (1966) 100
20. J.J.J. Kokkedee, "The Quark Model", (Benjamin (1969)).
21. M.D. Scadron, Phys. Rev. 165 (1968) 1640
22. H.F. Jones and M.D. Scadron, Nucl. Phys. B4 (1968) 267, Phys. Rev. 171 (1968) 1809

23. P.M. Osborne and J.C. Taylor, Nucl. Phys. B10 (1969) 213

24. J.C. Taylor, Nucl. Phys. B3 (1967) 504

25. J.C. Taylor, Nucl. Phys. B4 (1969) 201

26. V. De Alfaro, S. Fubini and C. Rossetti, Ann. of Phys. 44 (1967) 165

27. F.D. Gault and M.D. Scadron, Nucl. Phys. B15 (1970) 442

28. F.D. Gault and H.F. Jones, Nucl. Phys. B30 (1971) 68

29. L. Durand, Phys. Rev. Letters 18 (1967) 58

30. F.D. Gault, J. Phys. A4 (1971) 38

31. F.D. Gault and P.J. Walters, Nucl. Phys. B49 (1972) 273

32. F.D. Gault and P.J. Walters, Nuovo Cimento Letters 4 (1972) 461

33. P.D.B. Collins and F.D. Gault, Nucl. Phys. B112 (1976) 483

34. P.D.B. Collins, "An Introduction to Regge Theory and High Energy Physics", (Cambridge University Press (1977))

35. M. Jacob and G.C. Wick, Ann. of Phys. 7 (1959) 404

36. C.J. Bebek et al; Phys. Rev. D13 (1976) 25

37. P. Lehmann et al; Phys. Rev. 126 (1962) 1163
L.E. Price et al; Phys. Rev. D 4 (1971) 45

38. Particle Data Group, Phys. Letters 75B (1978)

39. P.D.B. Collins and E.J. Squires, "Regge Poles in Particle Physics", (Springer, Berlin (1968))

40. P.D.B. Collins and F.D. Gault, Phys. Letters 73B (1978) 330

41. C.N. Akerlof et al; Phys. Rev. D14 (1976) 2864

42. R.G. Roberts, R.V. Gavai and D.P. Roy, Nucl. Phys. B133 (1978) 285

43. F. Halzen and C. Michael, Phys. Letters 36B (1971) 367

44. V. Barger and F. Halzen , Phys. Rev. D6 (1972) 1918

45. A.D. Martin et al; Phys. Letters T.B.P. (1978)
R. Baldi et al; Phys. Letters T.B.P. (1978)

46. P.D.B. Collins and A. Fitton, Nucl. Phys. B91 (1975) 332

47. D. Bugg et al; Phys. Rev. 146 (1966(980

K.J. Foley et al; Phys. Rev. Letters 19 (1967) 857

S.P. Denisov et al; Phys. Letters 36B (1971) 415, 528

A.S. Carroll, Phys. Letters 61B (1976) 303

U. Amaldi et al; Phys. Letters 44B (1973) 112

S.R. Amendolia et al; Phys. Letters 44B (1973) 119

S.P. Denisov et al; Phys. Letters 34B (1971) 167

W. Galbraith et al; Phys. Rev. 138 (1965) 913

J.V. Allaby et al; Phys. Letters 30B (1969) 500

W.F. Baker et al; Phys. Rev. 129 (1963) 2285

V. Dardel et al; Phys. Rev. Letters 8 (1962) 173

K.J. Foley et al; Phys. Rev. Letters 14 (1967) 330

48. S.L. Kramer et al; Argonne preprint ANLHEP PR77.74 (Nov. 1977)

49. P. Baillon et al; Nucl. Phys. B107 (1976) 189

O. Dumbrais, University of Helsinki, preprint HU-TFT-78-15 (1978)

J. Lach, Fermilab-Conf.-77/38. Invited talk presented at the XIIth Recontre de Moriond, March 1977

R.J. De Boer et al. Nucl. Phys. B106 (1976) 125

K.J. Foley et al; Phys. Rev. 181 (1969) 1775

V.D. Apokin et al; Nucl. Phys. B106 (1976) 413

I.M. Geshov et al; Phys. Rev. D13 (1976) 1846

U. Amaldi et al; Phys. Letters 43B (1973) 231, 66B (1977) 390

G.G. Begnogikh et al; Phys. Letters 39B (1972) 411

V. Bartenov et al; Phys. Rev. Letters 31 (1973) 1367

K.J. Foley et al; Phys. Rev. Letters 19 (1967) 857

L.F. Kirillova et al; J.E.T.P. 23 (1966) 52

50. G.B. Yodh, to be published in the Proceedings of the Brookhaven Symposium on Prospects of Strong Interactions at Isabelle, April 1977.

51. H.J. Lipkin, Phys. Rev. D17 (1978) 366

52. O.I. Dahl et al; Phys. Rev. Letters 37 (1976) 80

V.N. Bolotov et al;, Nucl. Phys. B73 (1974) 387

M.A. Wahlig et al;. Phys. Rev. 168 (1968) 1515

53. P. Sonderegger et al; Phys. Letters 20 (1966) 75

M.A. Wahlig et al; Phys. Rev. 168 (1968) 1515

V.N. Bolotov et al; Nucl. Phys. B73 (1974) 387

A.V. Barnes et al; Phys. Rev. Letters 37 (1976) 76

54. V. Barger, Proceedings of the 17th Conference on High Energy Physics, London 1974

55. P.D.B. Collins and F.D. Gault, Nucl. Phys. B113 (1976) 34

56. P.D.B. Collins and A.D.M. Wright, J. Phys. To be published

57. J.L. Hartmann et al; Phys. Rev. Letters 39 (1977) 975

H. Dekerret et al; Phys. Letters 62B (1976) 363, 68B (1977) 374

J.V. Allaby et al; Nucl. Phys. B52 (1973) 316

J.V. Allaby et al; Phys. Letters 28B (1968) 67

C.W. Akerlof et al; Phys. Rev. D14 (1976) 2864

N. Kwak et al; Phys. Letters 58B (1975) 233

G. Barbiellini et al; Phys. Letters 39B (1972) 663

D. Birnbaum et al; Phys. Rev. Letters 23 (1969) 663

Y.M. Antipov et al; Nucl. Phys. B57 (1973) 333

K.J. Foley et al; Phys. Rev. Letters 11 (1963) 425

S. Brandt et al; Phys. Rev. Letters 10 (1963) 413

K.J. Foley et al; Phys. Rev. Letters 15 (1965) 45

J. Orear et al; Phys. Rev. 152 (1966) 1162

K.J. Foley et al; Phys. Rev. Letters 11 (1963) 503

W.F. Baker et al; Nucl. Phys. B25 (1971) 385

58. M. Borghini et al; Phys. Letters 36B (1971) 493, 501

P. Grannis et al; Phys. Rev. 148 (1966) 1297

59. A.C. Irving, Nucl. Phys. B101 (1975) 263

60. D.O. Caldwell et al; Phys. Rev. D7 (1973) 1362

D.O. Caldwell et al; Phys. Rev. Letters 40 (1978) 1222

61. J. Hanlon et al; Phys. Rev. Letters 37 (1976) 967

H. Abramowicz et al; paper submitted to the Budapest Conference, July 1977

62. S. Gjesdal et al; Phys. Letters 40B (1972) 152

63. M. Davier et al; Phys. Rev. D1 (1968) 790

J. Ballam et al; Phys. Rev. D5 (1972) 545

J. Ballam et al; Phys. Letters 30B (1969) 421

M. Davier et al; Phys. Rev. Letters 21 (1968) 841

G. McClellan et al; Phys. Rev. Letters 22 (1969) 347

Y. Eisenberg et al; Phys. Rev. Letters 22 (1969) 669

W.G. Jones et al; Phys. Rev. Letters 21 (1968) 586

W. Struczinski et al; Nucl. Phys. B108 (1976) 45

J. Park et al; Nucl. Phys. B36 (1972) 404

R. Anderson et al; Phys. Rev. D1 (1970) 27

Y. Eisenberg et al; Phys. Rev. D5 (1972) 15

M. Davier et al; Phys. Letters 28B (1969) 619

J. Ballam et al; Phys. Rev. D7 (1973) 3150

C. Berger et al; Phys. Letters 39B (1972) 659

R.L. Anderson et al; Phys. Rev. Letters 30 (1973) 149

R. Erbe et al: Phys. Rev. 175 (1968) 1669

G. McClellan et al; Phys. Rev. Letters 26 (1971) 1593

H.J. Behrend et al; Phys. Letters 56B (1975) 408

H. Alvensleben et al; Phys. Rev. Letters 28 (1972) 66

U. Camerini et al; Phys. Rev. Letters 35 (1975) 483

R.L. Anderson et al; Phys. Rev. Letters 38 (1977) 263

64. J. Ballam et al; Phys. Rev. D7 (1973) 3150

65. A. Silverman, Proc. of 1975 International Symposium on Lepton and Photon interactions at High Energies (Stanford)

66. U. Camerini et al; Phys. Rev. Letters 35 (1975) 483

67. A. Bradley and F.D. Gault, Nucl. Phys. B128 (1977) 313

68. G.J. Gournaris, Phys. Letters 72B (1977) 91

69. J.J. Sakurai, Phys. Letters 46B (1973) 207

70. D.R. Yennie, Phys. Rev. Letters 34 (1975) 239

71. F.E. Close, D.M. Scott and D. Sivers, Phys. Letters 62B (1976) 213

F.E. Close, D.M. Scott and D. Sivers, Nucl. Phys. B117 (1976) 134

72. B. Margolis, Fermilab-Pub-77171 THY August 1977

J.P. Cumalat and B. Margolis, paper submitted to the 1977 International Symposium on Lepton and Bhoton interactions at High Energies.

73. Review of particle properties, Rev. Mod. Phys. 48 (1976) No.2

A. Silverman, Proc. of 1975 International Symposium on Lepton and Hadron Interactions at High Energies (Stanford)

F. Laplance, Proc. of 1977 International Symposium on Photon Interactions at High Energies (Hamburg)

C. Bemporad, Proc. of 1977 International Symposium on Photon Interactions at High Energies (Hamburg)

G. Bassompierre et al; Phys. Letters 65B (1976) 397

B.H. Wiik and G. Wolf, Lectures at Les Houches Summer School, 1976

V. Siderov, rapporteur talk at the 1976 Tblisi Conference

S.N. Herb et al; Phys. Rev. Letters 39 (1977) 252

L. Lederman, Proc. of 1977 International Symposium on Photon Interactions at High Energies (Hamburg)

74. V.N. Gribov, Sov. J. Nucl. Phys. 5 (1967) 138

D.R.O. Morrison, Phys. Letters 25B (1967) 238

75. M. Kisslinger, Caltech. report CALT-68-341 (1971) unpublished

76. G.C. Fox and A.J.G. Hey, Nucl. Phys. B56 (1973) 386

77. Yu. M. Antipov et al; Nucl. Phys. B63 (1973) 153

H.A. Gordon et al; Phys. Rev. Letters 33 (1974) 603

G. Ascoli et al; Phys. Rev. Letters 33 (1974) 610

G. Grayer et al; Phys. Letters 34B (1971) 330

K.J. Foley et al; Phys. Rev. D6 (1972) 747

M. Margulies et al; Phys. Rev. D14 (1976) 667

M. Alston-Garnjost, Phys. Letters 34B (1971) 156

M. Anderholz et al; Nucl. Phys. B8 (1968) 45

G. Thompson et al; Phys. Rev. D9 (1974) 560

78. Y.M. Antipov et al; Nucl. Phys. B63 (1973) 153

79. A.C. Irving, Nucl. Phys. B121 (1977) 176

80. A.D. Martin et al; Paper submitted to Nuclear Physics

81. M. Margulies et al; Phys. Rev. D14 (1976) 667

82. G. Ascoli et al; Phys. Rev. Letters 33 (1974) 610

83. A.D. Martin, Private Communication

84. J.D. Jackson, Nuovo Cimento 34 (1964) 748

85. D.M. Brink and G.R. Satchler, "Angular Momentum", Oxford University Press (1962)

86. S. Gasiorowicz, "Elementary Particle Physics", Wiley, New York (1966)

87. E. Zevgolatakos et al; Nucl. Phys. B55 (1974) 15

M. Anderholz et al; Nucl. Phys. B5 (1968) 567

B. Chaurand et al; Phys. Letters 38B (1972) 253

M. Deutschmann et al; Nucl. Phys. B81 (1973) 1

Y.M. Antipov et al; Nucl. Phys. B63 (1973) 202

J.N. Carney et al; Nucl. Phys. B107 (1976) 381

M. Spiro et al; Nucl. Phys. B125 (1977) 162

P. Estabrooks et al; Phys. Rev. D17 (1978) 658

88. J.N. Carney et al; Nucl. Phys. B107 (1976) 381

89. P. Estabrooks et al; Phys. Rev. D17 (1978) 658

90. J.N. Carney et al; Nucl. Phys. B107 (1976) 381

M. Spiro et al; Nucl. Phys. B125 (1977) 162

91. A. Rouge et al; Nucl. Phys. B46 (1972) 29

R. Engelmann et al; Phys. Rev. D5 (1972) 2162

D.C. Colley et al; Nuovo Cimento 53A (1968) 552

M. Anderholz et al; Nucl. Phys. B7 (1968) 111

J.N. Carney et al; Nucl. Phys. B107 (1976) 381

92. M. Spiro et al; Nucl. Phys. B125 (1977) 162

93. M. Deutschmann et al; Nucl. Phys. B36 (1972) 373

R. Engelmann et al; Phys. Rev. D5 (1972) 2162

J.N. Carney et al; Nucl. Phys. B107 (1976) 381

94. M. Deutschmann et al; Nucl. Phys. B36 (1972) 373, B81 (1974) 1

95. P.D.B. Collins and F.D. Gault, Nucl. Phys. B113 (1976) 34

96. J.V. Allaby et al; Nucl. Phys. B52 (1973) 316

R.M. Edelstein et al; Phys. Rev. D5 (1972) 1073

R. Webb et al; Phys. Letters B55 (1975) 331, 336

97. P.D.B. Collins, F.D. Gault and A.D.M. Wright, J. Phys. G. 4 (1978) 471

98. G. Hentschel, Max Planck Institute Munich Thesis (1976)

99. A.C. Irving and R.P. Worden, Physics Reports (to be published)

100. A.C. Irving, Phys. Letters 59B (1975) 451

101. H.E. Haber and G.L. Kane, Nucl. Phys. B129 (1977) 429